IntechOpen

Basic Concepts Viewed from Frontier in Inorganic Coordination Chemistry

Edited by Takashiro Akitsu

BASIC CONCEPTS VIEWED FROM FRONTIER IN INORGANIC COORDINATION CHEMISTRY

Edited by **Takashiro Akitsu**

Basic Concepts Viewed from Frontier in Inorganic Coordination Chemistry
http://dx.doi.org/10.5772/intechopen.76741
Edited by Takashiro Akitsu

Contributors

Muhammad Adnan Iqbal, Hina Hayat, Alexandra R Fernandes, Ataf Ali Altaf, Amin Badshah, Sumbal Naz, Ming-Der Su, Jia-Syun Lu, Ming-Chung Yang, Emmanuel Etim, Usman Lawal, Govinda Khanal, Idaresit Mbakara, Tanja V. Soldatovic, Takashiro Akitsu

Notice

First published in London, United Kingdom, 2018 by IntechOpen
eBook (PDF) Published by IntechOpen, 2019
IntechOpen is the global imprint of INTECHOPEN LIMITED, registered in England and Wales, registration number: 11086078, The Shard, 25th floor, 32 London Bridge Street
London, SE19SG – United Kingdom
Printed in Croatia

British Library Cataloguing-in-Publication Data
A catalogue record for this book is available from the British Library

Additional hard and PDF copies can be obtained from orders@intechopen.com

Basic Concepts Viewed from Frontier in Inorganic Coordination Chemistry
Edited by Takashiro Akitsu

p. cm.

Print ISBN 978-1-78984-864-9

Online ISBN 978-1-78984-865-6

eBook (PDF) ISBN 978-1-83881-835-7

Meet the editor

Takashiro Akitsu, PhD, has been a full professor in the Department of Chemistry, Faculty of Science Division II at Tokyo University of Science, since 2016. He completed his undergraduate school training (chemistry) at Osaka University in 1995, and his graduate school training (physical and inorganic chemistry, especially coordination, crystal and bioinorganic chemistry) at Osaka University in 2000. Dr. Akitsu has published many articles in journals working at Osaka University (2000–2002), Keio University2002–2008), and Tokyo University of Science2008–present). He has been a peer reviewer of many journals and is a member of the organizing committees of several international conferences. His research interest is absorption of light by chiral metal complexes and their hybrid materials.

Contents

Preface

This book is both a review of current research and an undergraduate textbook for inorganic chemistry at university level. In university undergraduate lectures, basic concepts are mainly explained and added examples of frontier research are optional. However, in many cases, frontier research is more interesting for students than basic studies. This book is aimed at undergraduates in inorganic chemistry. Each author introduces or reviews "frontier research topics" of inorganic coordination chemistry. Their application examples are indicated with "basic concepts" as found in textbooks on this subject. The chapters' topics are structured as "frontier research topics" but also "related items" or concept in a typical standard textbook of inorganic chemistry.

Takashiro Akitsu
Department of Chemistry
Faculty of Science
Tokyo University of Science, Japan

Chapter 1

Introductory Chapter: Concepts in Textbook and a Study on Schiff Base Metal Complexes

Takashiro Akitsu

Additional information is available at the end of the chapter

http://dx.doi.org/10.5772/intechopen.81684

1. Introduction

The reason to propose the concept of this book is that some graduate students could not think their own researches in laboratory with related things learned in undergraduate textbooks. In order to overcome this issue, chapters in this book mention basic things of inorganic chemistry as well as frontier research topics on purpose.

In a conference [1], for example, we have recently reported the results of Z-scan NLO measurements for the analogous achiral organic ligands and metal complexes shown in **Figure 1**. As a promising renewable energy, a dye-sensitized solar cell (DSSC) is developing to improve performance of each materials and systems. From the view point of dye of metal complexes (or extended organic compounds), we have reported chiral Schiff base (salen-type) metal complexes. Induced CD from chiral Schiff base metal complexes containing azo-group has been also investigated for Au or TiO_2 nanoparticles using their optical interaction so far.

Probably, the disagreement between researches and textbook may come from deviation (explained in brackets) from typical cases of definition (description) of terms (bold fonts). In this case, related things in basic inorganic chemistry are as follows:

Four-coordinated complexes (coordination numbers): A complex of four-coordinated coordination structure adopts two structures, tetrahedral type and square planar type. In tetrahedral type, metal atoms are steric repulsion such as large ligand is larger than electron factor (The complex in **Figure 1** is a square planar one having chelate ligand.)

Multidentate (chelate) ligands: Ligands in which two or more atoms can simultaneously form two electrons (lone-pair) donor bonding to the same metal ion are called "multidentate" ligands in contrast to monodentate ligand. These ligands are also called as "chelate" ligands

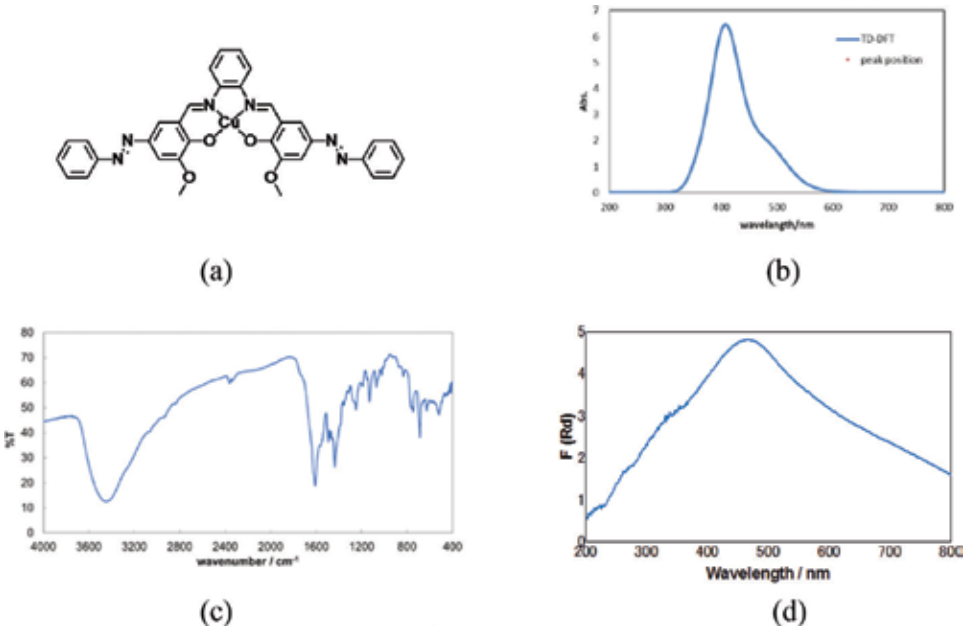

Figure 1. (a) Molecular structure, (b) simulated UV-vis spectrum (DFT), (c) IR spectrum, and (d) diffuse reflectance UV-vis spectrum of a Schiff base Cu(II) complex.

and include bidentate, tridentate, tetradentate, etc. and various coordination sites. For example, ethylenediamine has (N,N) coordination atoms (The complex in **Figure 1** has a tetradentate (N,N,O,O) Schiff base ligand.)

Electronic spectra (d-d transition): In order for the electronic state of a molecule to cause optical transition between d orbitals, the following "selection rule" exists. The d-d transitions occurring according to the selection rule are called allowed transitions, and the rest ones are called forbidden transitions. However, even for forbidden transitions, transitions may occur due to perturbation by vibration modes within the molecule. In **Figure 1**, UV-vis and IR spectra are exhibited. However, the intense bands in UV-vis spectrum are π-π* band due to organic ligands.

In this way, it is a wish of the editor to master basic concepts [2] in advanced researches [3–5] mainly for graduate students.

Author details

Takashiro Akitsu

Address all correspondence to: akitsu@rs.kagu.tus.ac.jp

Department of Chemistry, Faculty of Science, Tokyo University of Science, Tokyo, Japan

References

[1] Akitsu T, Sato H, Kunitake F, Beppu I, Haraguchi T, Joe IH. Z-scan NLO of Schiff base metal complexes having azobenzene. In: 8th International Science Conference; 21-23 November 2018; India: Jadavpur University

[2] Akitsu T. Lecture Notes: D,f-Block Inorganic Chemistry. Riga, Latvia: Scholars' Press; 2018. ISBN: 978-620-2-30609-6

[3] Akitsu T, editor. Integrating Approach to Photofunctional Hybrid Materials for Energy and the Environment. NY, USA: Nova Science Publishers, Inc.; 2013. ISBN: 978-1-62417-638-8

[4] Akitsu T, editor. Descriptive Inorganic Chemistry Researches of Metal Compounds. Rijeka, Croatia: InTech; 2017. ISBN: 978-953-51-3397-1

[5] Akitsu T, editor. Symmetry (Group Theory) and Mathematical Treatment in Chemistry. Rijeka, Croatia: InTech; 2018. ISBN: 978-1-78923-315-5

Chapter 2

Modern Techniques in Synthesis of Organometallic Compounds of Germanium

Hina Hayat and Muhammad Adnan Iqbal

Additional information is available at the end of the chapter

http://dx.doi.org/10.5772/intechopen.79985

Abstract

Germanium is one of the most significant semiconductors to be used for electronic devices due to small bandgap and high intrinsic mobility of holes and electrons. Germanium has received a large attention due to its extraordinary reactivity and properties. It is commonly used in fluorescent lamps and as catalyst as well to produce various types of plastic. Germanium nanomaterials have broad range of applications from photovoltaic devices to phase-change memory materials. Germanium forms complexes by reacting with numerous elements such as carbon, oxygen, nitrogen, hydrogen, and phosphorous as a part of several organic compounds. Germanium coordinates with these elements by single, double, and triple linkages. Interestingly, all such reactions occur at ambient temperature usually in tetrahydrofuran under vacuum. Germanium may also react directly with primary and secondary nitrogen in the presence of a suitable base, whereas with tertiary nitrogen, it may react directly even in the absence of a base. Nevertheless, this chapter describes the modern techniques in synthesis of organometallic compounds of germanium.

Keywords: germylene, organometallic germanium, germanium coordination

1. Introduction

Organometallic compounds may be defined as *the compounds having at least one metal-carbon bond in a molecule*. This bond may be covalent in nature as in tetraethyl lead, $Pb(C_2H_5)_4$; pi-dative as in chromocene, $Cr(\eta^5\text{-}C_5H_5)_2$; ionic as in potassium cyclopentadienyl, $K^+(C_5H_5)^-$; and more interestingly, coordinate covalent as in silver(I)-*N*-heterocyclic carbene, $Ag(NHC)_2$ (**Figure 1**). However, the mentioned definition is not limited to metal-carbon bond only; there are several other examples where metal-nitrogen, metal-boron, metal-hydrogen, metal-oxygen,

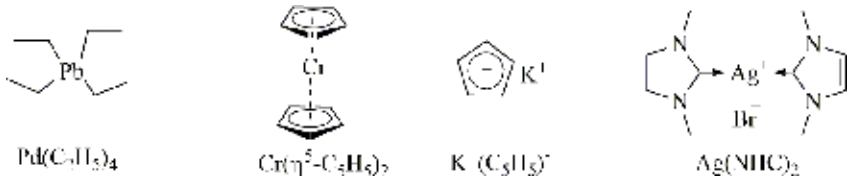

Figure 1. Different types of organometallic compounds having metal-carbon bonds.

metal-sulfur, etc. bonds are also included in organometallic chemistry. Nevertheless, their bonding way is uniquely different than in coordination compounds, which makes them organometallic compounds instead of coordination compounds. For instance, just keep in mind that metal-carbon bond-containing compounds are organometallic in nature.

The current chapter describes organometallic compounds of germanium. Germanium was exposed by Clemens Winkler in 1886, and its initial wide application was in the formation of point-contact Schottky diodes for radar response during WWII. Germanium is a conventional electronic material. The history of element germanium is at the closely same era as the story of transition from physics of dirt to beginning of recent semiconductor physics. The revelation of point-contact transistor of germanium by J. Bardeen and W. Brattain on Christmas Eve 1947 was followed by the discovery of germanium junction transistor by W. Shockley that represents the establishment of semiconductor age. The years succeeding the findings of germanium did not show any main scientific conclusion and technological applications for this expensive, brittle, rare, and metal-like element. F.W. Aston found three reasonably stable isotopes, namely, ^{70}Ge, ^{72}Ge, and ^{74}Ge in 1923. In the 1930s, germanium was supposed to be a bad conducting metal [1].

Germanium is one of the most significant semiconductors used for electronics due to small bandgap and high intrinsic mobility of holes and electrons. Germanium oxides are hygroscopic and water soluble. GeO_2 is thermally unstable and it is transformed into volatile germanium monoxide (GeO) [2]. Germanium compounds have great importance due to their distinctive applications in electronic field. Geranium films also gained attention due to their use in phase-change random access memory (PRAM) devices. They have fascinating great deal of interest due to high endurance, nonvolatility, and higher programming speed. GST ($Ge_2Sb_2Te_5$) mainly is a well-liked phase-change substance for phase-change random access memory devices [3]. Group 14 elements have extensive variety of application from photovoltaic devices to PRAM material [4].

Group 14 elements usually have wide significance because of their unusual properties. In recent times, surprising application of alkoxy germylenes has been described. Alkoxy germylene has been used as precursors of nanomaterials. Hypermetallyl germylenes may be appropriate for the preparation of nanomaterial alloys because hypermetallyl germylenes contain good leaving substituent and a low coordinate atom of group 14. Hypergermyl ligands demonstrate limitations of steric shielding for stabilization of low coordinate species [5].

In earlier period, germylene compounds were used for transition metals as ligands due to their potential. Germylenes have been paying interest in organic chemistry. Germylenes are highly reactive derivatives and can be stabilized by sterically challenging substituent [6].

Germanium monocations may demonstrate both nucleophilic and electrophilic properties. Aminotroponiminate GeII monocation was synthesized by elimination of chloride from particular chlorogermylene using (η^5-C_5H_5) $ZrCl_3$ as a halide scavenger [7]. Germanium monocations may demonstrate both nucleophilic and electrophilic properties. Aminotroponiminate GeII monocation was synthesized by elimination of chloride from particular chlorogermylene using (η^5-C_5H_5) $ZrCl_3$ as a halide scavenger [7].

2. Germanium complexes involving bonding through carbon (C)

C1 (cholorogermyliumylidene) was obtained by reacting 1 equivalent of **L1** (a free bis-NHC) with $GeCl_2$-dioxane in dry tetrahydrofuran (THF) at room temperature under an inert atmosphere (**Scheme 1**). The reaction mixture was stirred overnight to isolate **C1** as white precipitates. Single crystals of **C1** were grown by slow evaporation at 4°C in acetonitrile. NHC-Ge bond was confirmed by ^{13}C NMR by obtaining a chemical shift at δ166.3 ppm. **C1** was further reacted with a dark green solution of sodium naphthalene in THF very carefully. According to the reported procedure, 1 equivalent of naphthalene was stirred in THF overnight with 1 equivalent of sodium metal to obtain sodium naphthalenide. A suspension of half equivalent of **C2** in THF (at −30°C) was added to the sodium naphthalenide solution at −30°C, and the mixture was stirred to bring the reaction mixture temperature up to 0°C in about 3 h.

The volatilities were removed under vacuum, and the residue was washed with cold THF during filtration. Single dark red-colored crystals, suitable for X-ray crystallography, of **C2** were obtained by a concentrated solution of C_2 in THF at −20°C (cooling method). The formation

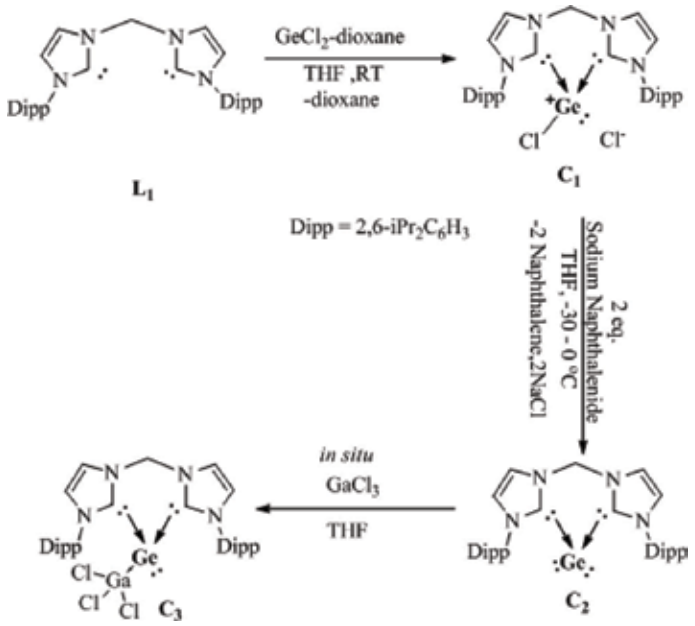

Scheme 1. Synthesis of Ge compounds involving bonding through carbon.

of NHC-Ge bond was confirmed by ^{13}C NMR where the respective chemical shift appeared at δ 196.1 ppm, which is interestingly much downfield compared to **C1** [8]. Compound **C3** can be prepared through *in situ* path, adding 1 equivalent of $GaCl_3$ in a solution of **C2** in THF at room temperature and stirring the reaction mixture for about 2 h. The volatilities are removed under vacuum, and the product can be extracted by THF. The single crystals of **C3** suitable for X-ray crystallography were obtained by cooling a concentrated solution of it in acetonitrile to 4°C. The ^{13}C NMR showed chemical shift of NHC-Ge at δ 174.16 ppm. This upfield movement of chemical shift might be because of electron drift from gallium toward NHC.

Synthesis of another NHC-Ge adduct **C4** was achieved by adding a dropwise solution of 1 equivalent of **L2** (NHC-$GeCl_2$) in 1 equivalent of $Mg[Ge(SiCH_3)_3]_2$.2THF in THF at −60°C (**Scheme 2**). The solution was then stirred at room temperature for 2 days to obtain the required product as precipitates. At the end, volatile components were removed under reduced pressure to obtain red residue, washed with pentane, and orange red product was isolated in 45% yield. ^{13}C NMR indicated the formation of NHC-Ge bond by showing a chemical shift at δ 173.9 ppm for the bonded carbene carbon [5]. The synthesis of derivative **C5** from **L2** can be achieved by adding a THF solution of 1 equivalent of $Mg[Sn(SiCH_3)_3]_2$.2THF into a THF solution of **L2** at −78°C, and the mixture is slowly warmed to room temperature in 12 h with consistent stirring. The solvent and other volatilities were removed from the reaction mixture under vacuum, and the residue was extracted with pentane, which was filtered and the filtrate was evaporated to obtain **C5** as orange red powder. Single crystals of orange color were obtained by slow evaporation of saturated solution of **C5** in pentane at −24°C. ^{13}C NMR indicated the NHC-Ge chemical shift at δ 175.5 ppm, whereas 119Sn NMR indicated the chemical shift for bonded tin at δ −589.7 ppm [5].

C6 was formed by dissolving **L3** to a solution of $GeCl_2$ at 0°C. After stirring the reaction mixture at 0°C for 15 min, the cooling bath was removed and mixture was kept stirred continuously at room temperature for 1 h. Yellow solid was obtained after removing all solvent in vacuum. The mixture (yellow solid) was treated with precooled toluene at 0°C with the addition of $Li[CpMo(CO)_3]$ and again stirred continuously for next 2.5 h (**Scheme 3**). The mixture was warmed at room temperature and solution color changed from yellow to brown

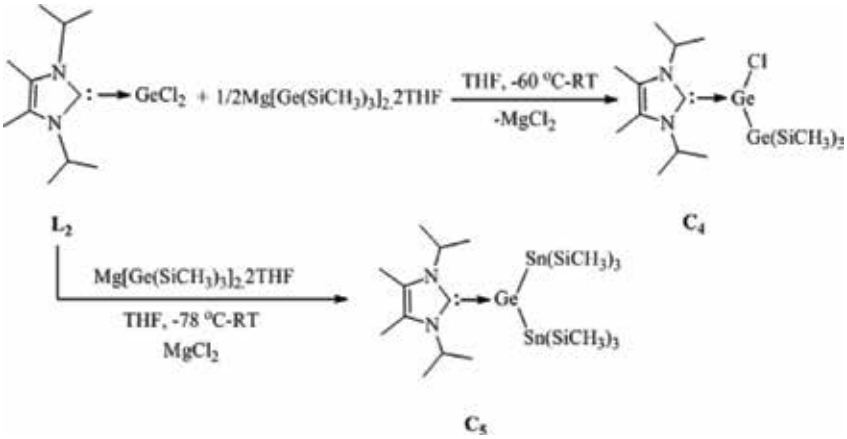

Scheme 2. Synthesis of NHC-stabilized hypermetallyl germylene.

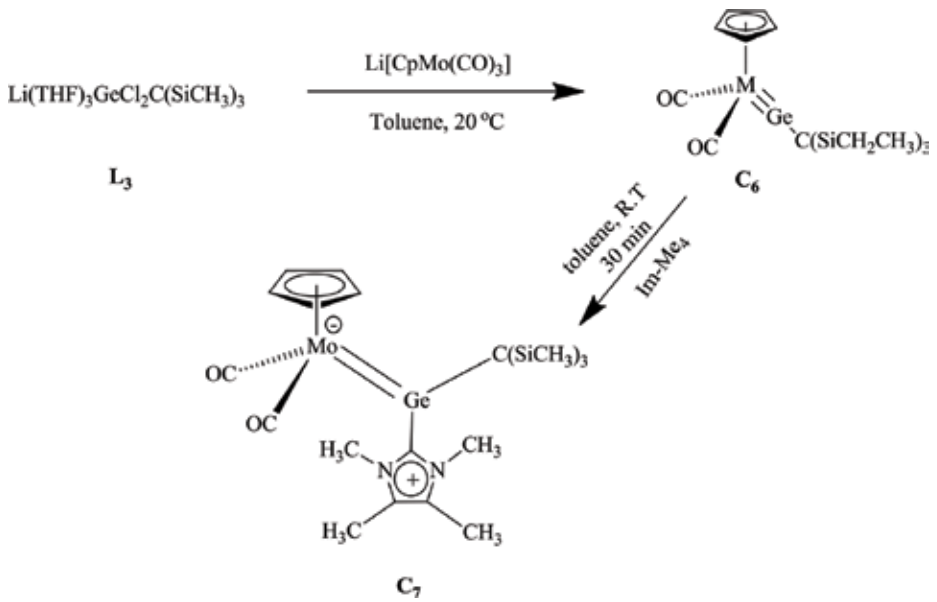

Scheme 3. Synthesis of $[Cp(CO)_2Mo{\cdot}GeC(SiCH_3)_3]$ complex, **C7**.

and then red. The product was obtained with hexane and the extract was stored at −30°C for 16 h. At −30°C, mother liquor was removed by filtration of mixture. At room temperature, precipitate was dried in vacuum for 1 h. End product was extracted as orange red crystalline material in 73% yield. Melting point of the extracted product was 85°C. Production of **C7** was achieved when an Im-Me_4 (tetramethyl imidazolium salt) solution was added slowly in **C6** at room temperature. The solution color changed from red orange to red brown during addition of Im-Me_4. Solution was stirred continuously for 30 min. All volatiles were removed under vacuum, and the residue was dissolved in toluene-hexane mixture for the purpose of extracting the required material. The extract was concentrated and few drops of n-hexane were added on it, and then it was cooled to −60°C and stored for 16 h at the same temperature to isolate the red-brown crystals of **C7** from mother liquor in 69% yield [9].

3. Germanium complexes involving bonding through nitrogen (N)

C8 (chlorogermyliumylidene) was formed by reacting **L4** (1,8-bis (tributylphosphazenyl)-naphthalene) with $GeCl_2$-dioxane in 60% isolated yield (**Scheme 4**). The addition of $GeCl_2$-dioxane into a solution of **L8** in toluene at ambient temperature generates white precipitates of the desired ionic species, which can be filtered from the reaction medium [8, 10].

C9 [(ButNacnac)Ge:] was obtained by mixing **L5** solution in toluene with $[(^{Mes}Nacnac)Mg]_2$ in toluene at −80°C for 5 min (**Scheme 5**). The mixture was then warmed slowly for 6 h at 0°C, and during this period of time, the mixture turned deep red colored. The residue was extracted into cold hexane at 0°C, and volatiles were removed in vacuum. The product was stored at −30°C overnight. At the end, purple-red crystals were formed in 38% isolated yield [11].

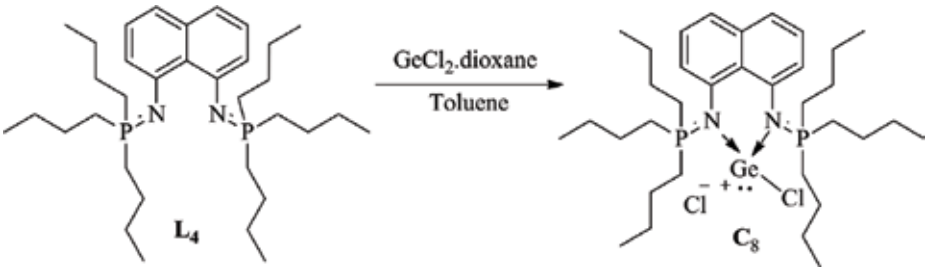

Scheme 4. Synthesis of β-diketiminate germanium complex.

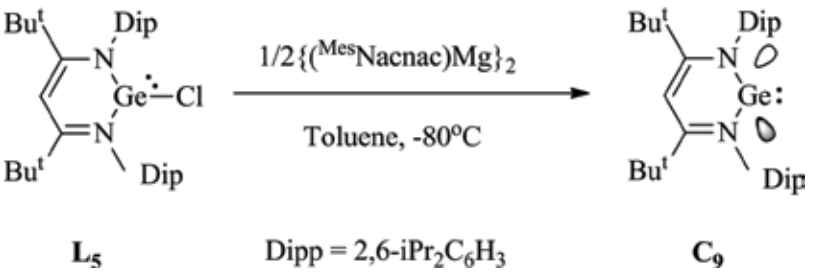

Scheme 5. Synthesis of [(ButNacnac)Ge:] complex.

C10 was formed when a colored solution of **L6** in diethyl ether was added into $[RhCl(cod)]_2$ solution in diethylether at −78°C (**Scheme 6**). The solution was placed at room temperature for 45 min. Then, the solution was stirred continuously for another 45 min. After filtration, the solvent was concentrated under reduced pressure. Yellow crystals were obtained in 49% isolated yield. Melting point of the product was 91°C. Reaction was occurred in dry and oxygen-free atmosphere of argon by using glove box techniques. Synthesis of **C11** was carried out in NMR tube. A solution of **C10** in deuterated tetrahydrofuran was contacted with carbon monoxide atmosphere at −80°C. The ligand exchange reaction was completed in less than 10 min as per monitoring by ^1H NMR [12].

C12.$[BF_4]$ was formed by reacting amino(imino)germylene in toluene with $BF_3{\cdot}OEt_2$ at −78°C (**Scheme 7**). The reaction mixture was stirred for 12 h, and during this course of time, it was allowed to slowly warm to the room temperature. Evaporation of solvent and washing residual material with diethyl ether provided the required compound as a yellow powder, which in turn provided compound as colorless crystals suitable for X-ray diffraction on recrystallization by THF. **C12** was formed via the intermediate fluorogermylene dimer $[FGeNIPr]_2$ as suggested by DFT calculations. The boron tetrafluoride played the role of fluorination reagent as well as fluoride abstraction agent. Multinuclear NMR spectroscopy was used to confirm the formulation of **C12** $[BF_4]$. The researchers found a highly disordered germanium-bonded fluorine atom by single crystal X-ray structure analysis, which possesses 50% site occupancy factor at each of the two germanium atoms [7].

C13 was formed when a dark green solution of **L13** was added to a suspension of selenium powder in THF at 0°C (**Scheme 8**). Reaction can occur in the absence of light. A yellow solution was formed when mixture was stirred continuously at room temperature for 2 days. The residue was extracted with toluene and hexane, and volatiles were removed under vacuum.

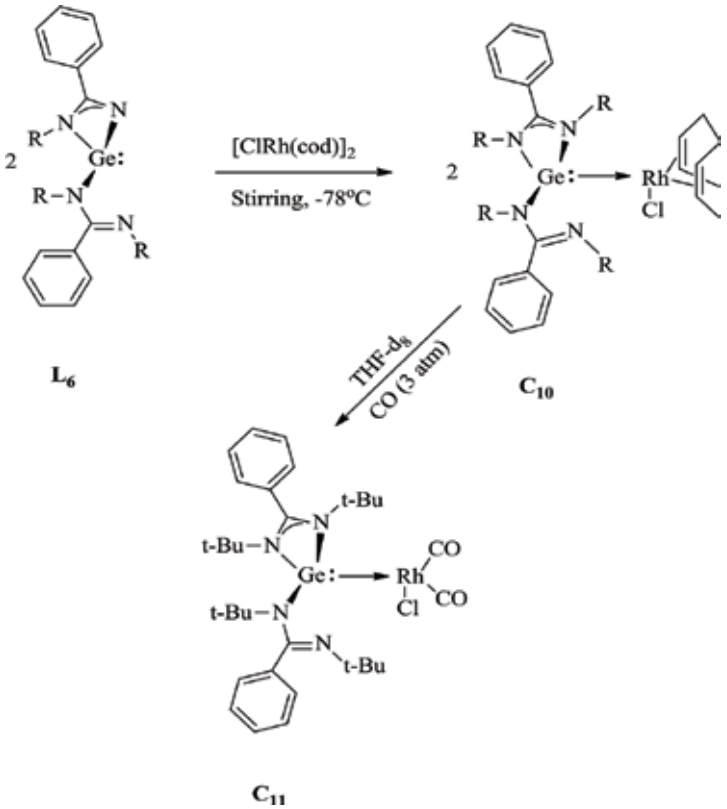

Scheme 6. Synthesis of the germylenedicarbonylrhodium(I) complex, **C11**.

The resulting product was separated as yellow crystals in 67.5% isolated yield. Melting point of the resulting product was 206.5°C [13].

C14 was formed when slurry of tellurium suspended in toluene was added dropwise in 1-Cy solution (**Scheme 9**). Mixture was continuously stirred at ambient temperature for 24 h, meanwhile mixture color changed from purple to red. After filtration, the reaction mixture was concentrated under vacuum. Mixture was stored for 24 h at −27°C to obtain red crystals of the product [4].

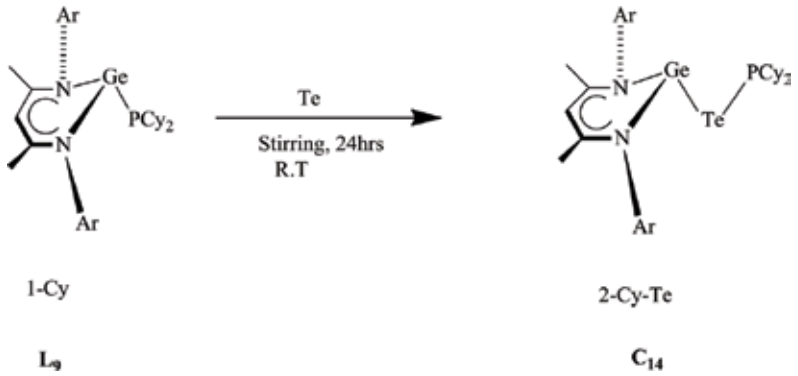

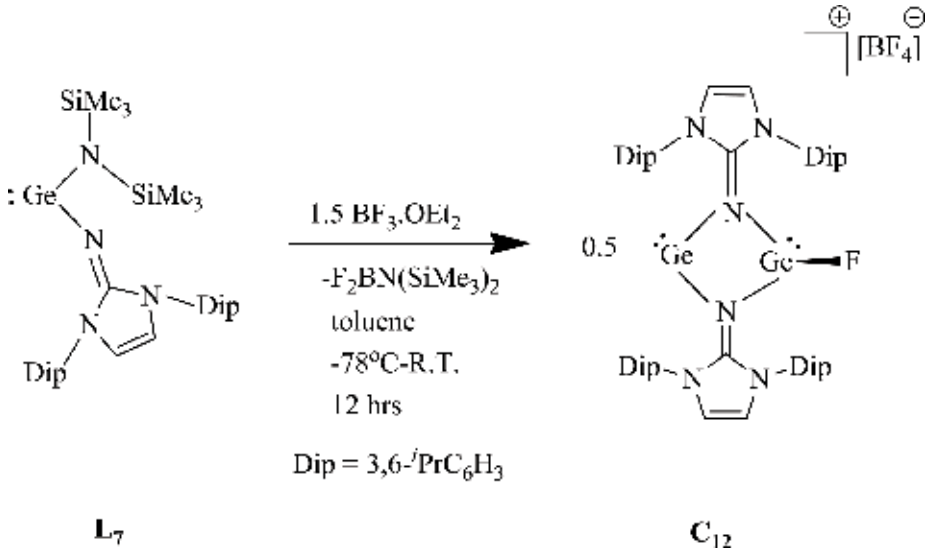

Scheme 7. Synthesis of germyliumylidene salt **C12**.[BF_4].

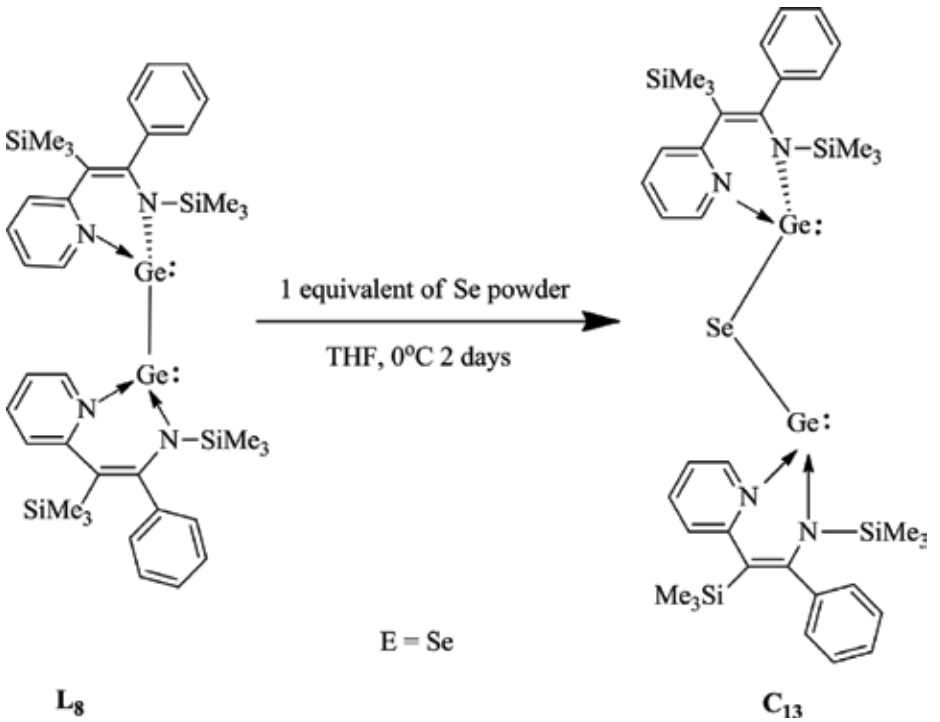

Scheme 8. Synthesis of bis(germylene)selenide.

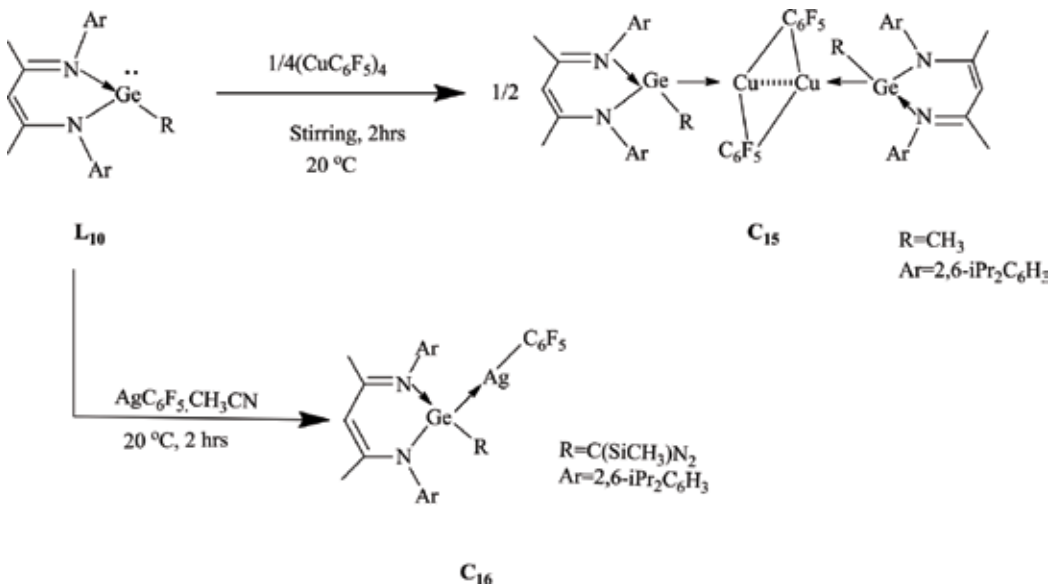

Scheme 9. β-Diketiminate germylene-supported pentafluorophenylcopper(I) and -silver(I) complexes.

4. Germanium complexes involving bonding through carbon and nitrogen (C, N)

C15 was formed when a solution of $(CuC_6F_5)_4$ in toluene was added to a solution of **L10** in toluene using a glove box with a consistent stirring. A quick color change was observed from orange red to light yellow. The mixture was further stirred continuously for next 2 h. After filtration, the filtrate was kept unattended at −20°C. After 5 days, crystals grew and the mixture was filtered and light yellow crystals of **C15** were obtained in 81% isolated yield. The X-ray crystallography showed that complex carries two toluene molecules packed during crystal growth. Melting point of the crystal was 206°C [14]. One more product was formed by mixing **L10** with $AgC_6F_5{\cdot}CH_3CN$ in a brown vial in the presence of toluene. For half an hour, the mixture was stirred and toluene was continuously added until all solids dissolved. After filtration, the filtrate was overlayered with n-hexane and placed unattended at −20°C for 2 days. After 48 h, light yellow crystals of **C16** were collected by filtration in 71% isolated yield. Melting point of the crystals was 156°C [14].

C17 was synthesized by mixing n-butyl lithium dropwise to a solution of **L11** in THF at −78°C (**Scheme 10**). After 3 h stirring of mixture, $GeCl_2{\cdot}$dioxane was added to reaction mixture at −78°C. The resulting product was reddish brown. The reddish brown solution was warmed gradually at room temperature and stirred overnight. The residue was extracted with dichloromethane, and solvent was removed under vacuum. Lithium chloride was filtered off, and the filtrate was concentrated. Orange crystals of **C17** were obtained in 47% isolated yield.

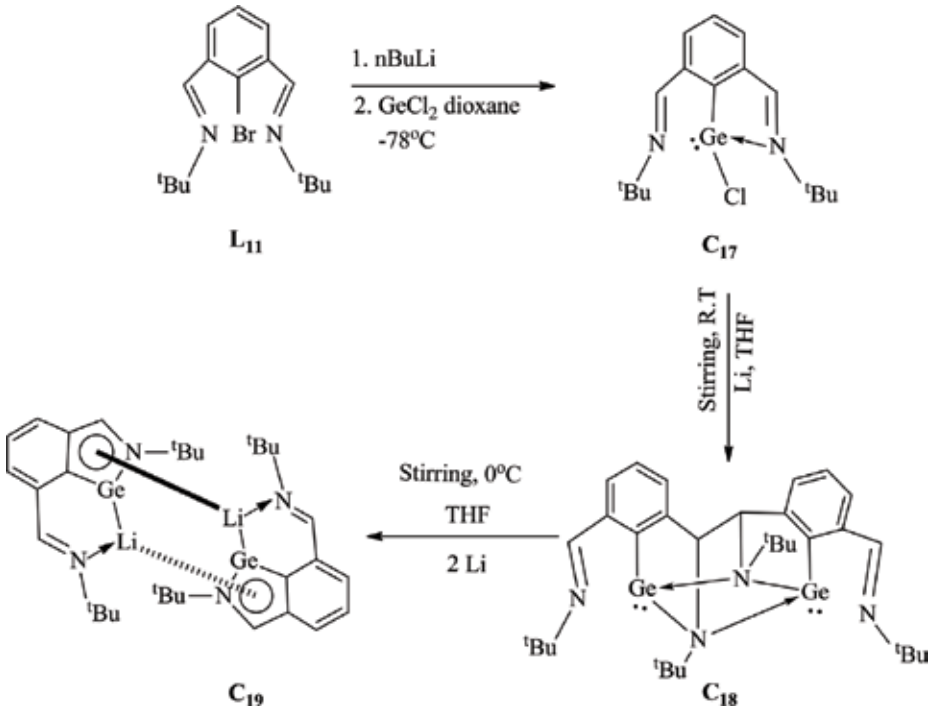

Scheme 10. Preparation of a germylidenide anion from the C▬C bond activation of a bis(germylene).

Melting point of the product was 163°C [15]. **C18** was formed when THF was added to a mixture of **C17** and Li metal at 0°C. The resulting mixture was warmed at room temperature and stirred for 15 h. The dark green residue was extracted with diethyl ether, and lithium chloride was filtered off. The resulting green solution was stirred at room temperature for 2 h. After filtration, the solution was concentrated affording dark green crystals of **C18** in 49% isolated yield. Melting point of the product was 218°C [15]. **C18** was further used to synthesize **C19** by adding THF into **C18** mixture and Li granules at 0°C. Dark green solution was formed when resulting red mixture was warmed at room temperature and stirred continuously for 15 h. The end product was obtained after removing the solvent under vacuum [15].

C20 was formed when in a solution of **L12** in THF was added sodium cyclopentadienyl in THF dropwise at 0°C (**Scheme 11**). Yellowish orange solution was obtained, which was warmed at room temperature with continuous stirring for 12 h. The mixture was extracted with diethyl ether, and volatiles were removed under reduced pressure. At the last, yellow crystals were extracted in 74% isolated yield. Melting point of the product was 128°C [16].

C21 was prepared by adding dropwise a solution of $[RhCl(cod)_2Cl]_2$ in THF in a stirred solution of **L13** in THF at room temperature (**Scheme 12**). The mixture was filtered after 16 h stirring. Dark purple crystals were obtained by concentrating the mixture. Melting point of the end product was 194°C [17]. **C22** was prepared by adding $[RhCl(cod)]_2$ solution dropwise in a stirred solution of **L22** in toluene at room temperature. After 16 h stirring, the reaction mixture was filtered and then concentrated. At the end, the resulting product was obtained as an orange-colored transparent crystalline solid in 85.7% yield. Melting point of the end product was 225°C [17].

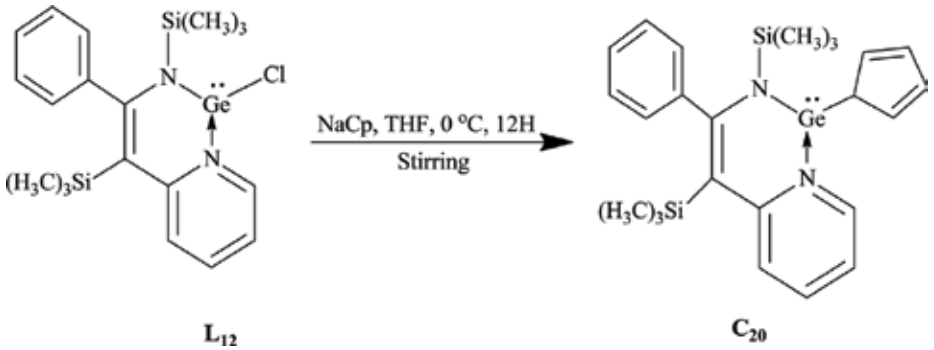

Scheme 11. Metallogermylenes, Cp-substituted germylene.

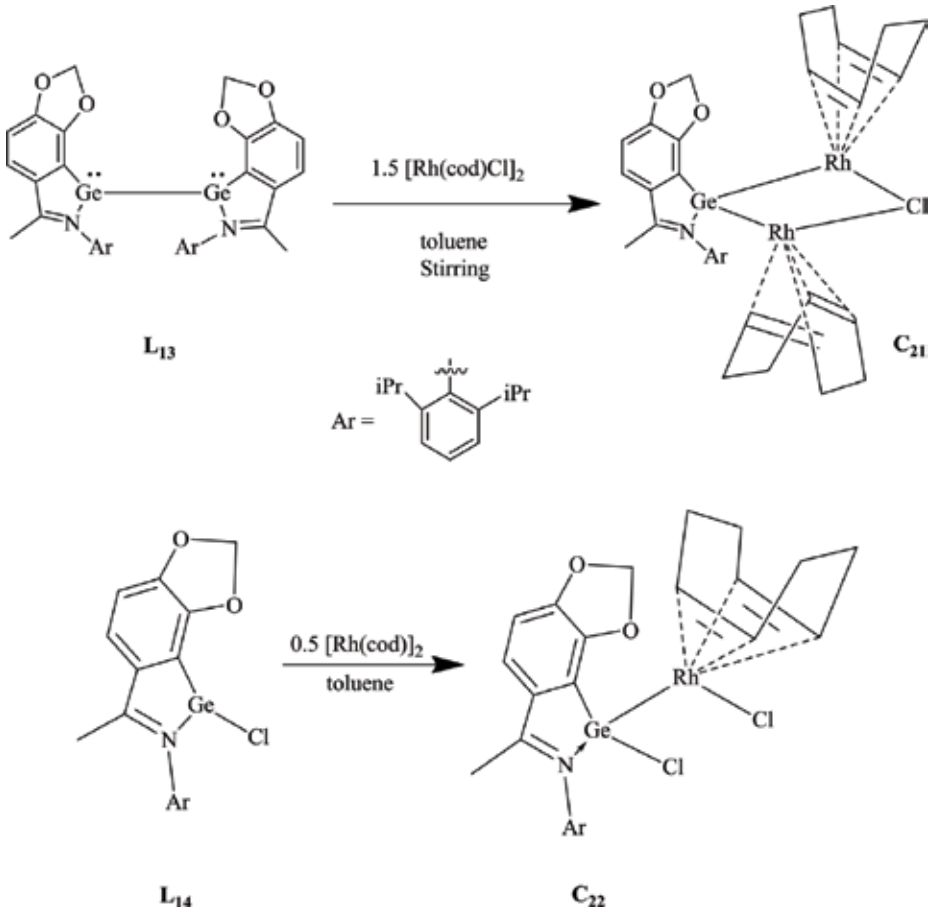

Scheme 12. Synthesis of germanium(I) dimer.

C23 was formed by reacting **L15** with P ≡ CBu^t at 20°C in toluene (**Scheme 13**). The reaction mixture was warmed at 35°C and stirred continuously for 15 h. During stirring, the color of reaction mixture was changed into deep red. The residue was extracted by using hexane. All

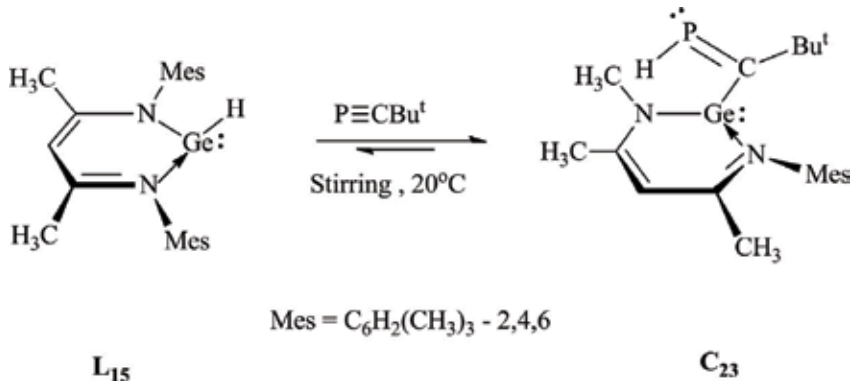

Scheme 13. Synthesis of *N*-heterocyclic germanium(II) hydride.

volatiles were removed in vacuum. After filtration, the filtrate was stored at 30°C overnight. The end product was obtained as dark red crystals in 67% isolated yield. Melting point of the end product was 142°C [18].

5. Germanium complexes involving bonding through nitrogen and hydrogen (N, H)

Three products were prepared from **L16** (diarylgermylene) by addition of different compounds such as hydrazoic acid, hydrogen cyanide, and anhydrous hydrazine in presence of toluene at room temperature (**Scheme 14**). First, an ethereal solution of hydrazoic acid was formed when methanol was added into $[(CH_3)_3Si]N_3$ solution in diethyl ether. After stirring of solution for 5 min, this colorless solution was added to a stirred solution of **L16** at room temperature. Purple solution became colorless when reaction mixture was stirred continuously overnight. The resulting product (white solid) was washed with pentane and mixed with small amount of hot hexane. Then, the solution was slowly cooled to 6°C and temperature was sustained overnight. **C24** was obtained as colorless blocks in 79% isolated yield [19]. These colorless blocks were suitable for single X-ray diffraction. Melting point of the end product was 177–183°C. Second, hydrogen cyanide was prepared by adding methanolic solution of $(CH_3Si)CN$ in diethyl ether. Colorless solution was stirred for 30 min. After stirring, it was added to stirred $Ge(Ar^{Me6})_2$ solution in toluene at room temperature. The purple solution became colorless when solution was stirred continuously overnight. **C25** was obtained as white solid product, which was washed with small amount of pentane, and all volatile materials were removed under reduced pressure. Third, **C26** was formed when stoichiometric amount of anhydrous hydrazine was added to a stirred solution of **L16** in toluene. The mixture was stirred continuously overnight, and deep purple color changed to colorless during stirring. The resulting microcrystalline white solid was washed by using small amount of hexane and dried under reduced pressure. The microcrystalline solid was stored at 20°C for 1 week after dissolving the solid in toluene. The colorless end product was obtained in 86% isolated yield [20].

http://dx.doi.org/10.5772/intechopen.79985

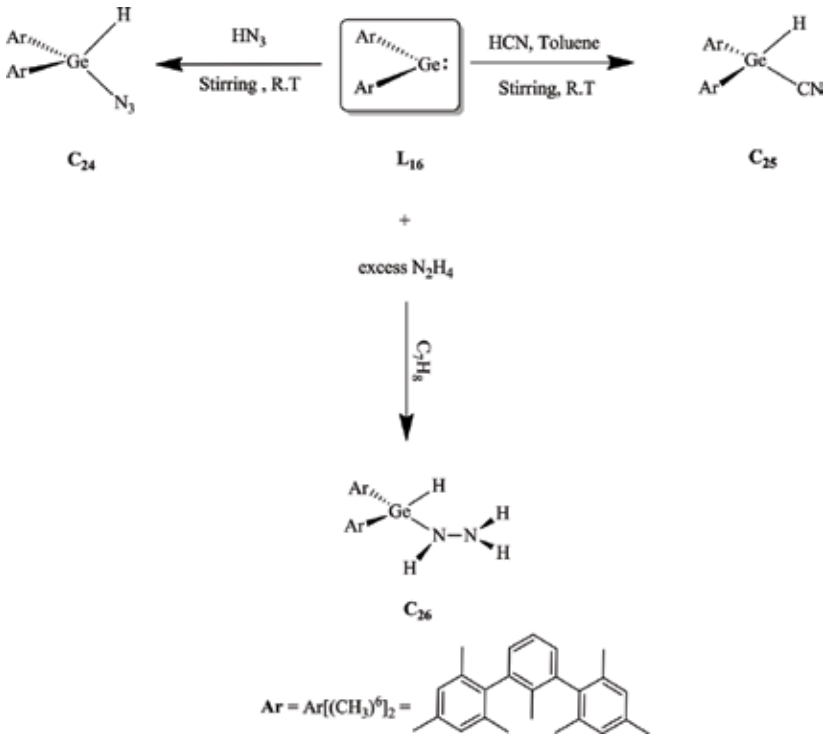

Scheme 14. Synthesis of germylene complexes from diaryl germylene complexes.

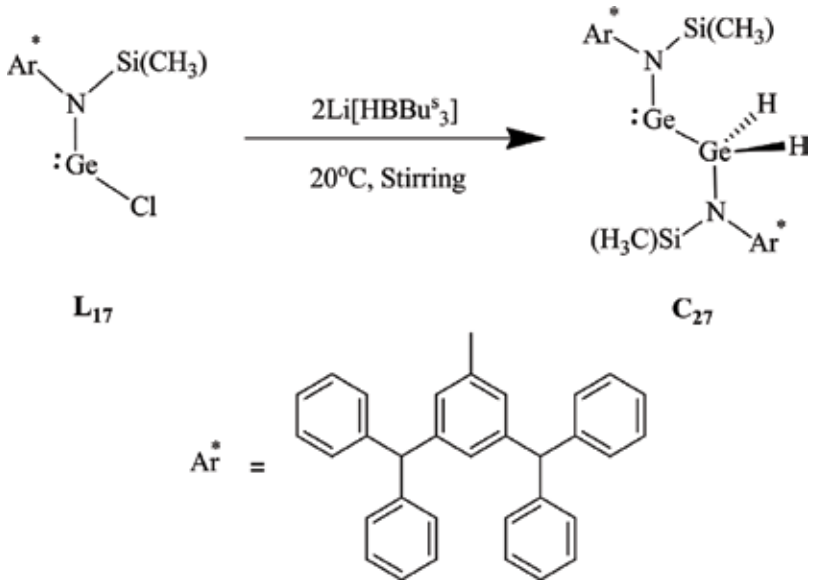

Scheme 15. Synthesis of digermylene complexes with a Ge▬Ge single bond.

C27 was formed when a solution of **L17** in toluene left in Youngs Schlenk flask at 20°C under 1 atmospheric pressure of highly pure H_2 (**Scheme 15**). The reaction mixture was stirred continuously for 30 min. All volatiles were removed under vacuum. Pale orange solid was obtained as end product. By recrystallization, solid single crystals of complex were obtained from minimum volume of diethyl ether, which remained suitable for X-ray crystallography. Melting point of the end product was 190–194°C [21].

6. Germanium complexes involving bonding through carbon and oxygen (C, O)

C28 was formed when n-butyl lithium was added slowly to a solution of **L18** (bis-sulfone) in toluene at 40°C (**Scheme 16**). The solution color changed into deep red, and this solution was further stirred continuously for 20 min at 40°C. Then, the reaction mixture was added over a suspension of $GeCl_2$-dioxane in toluene at 0°C. The reaction mixture was heated to room temperature and stirred for 18 h. After stirring, all volatiles were removed and the residue was washed with CH_2Cl_2. White solid was obtained in 58% isolated yield. Melting point of the white solid was 260°C. Colorless crystals of **C28** were obtained by slow diffusion of pentane in CH_2Cl_2. **C29** was formed by adding a solution of $Fe_2(CO)_9$ into germylene solution in THF at −20°C. Then, the mixture was warmed slowly at room temperature and stirred for 24 h. All volatiles were evaporated. The product was extracted with diethyl ether. Colorless product was obtained at room temperature for X-ray crystallographic analysis [22].

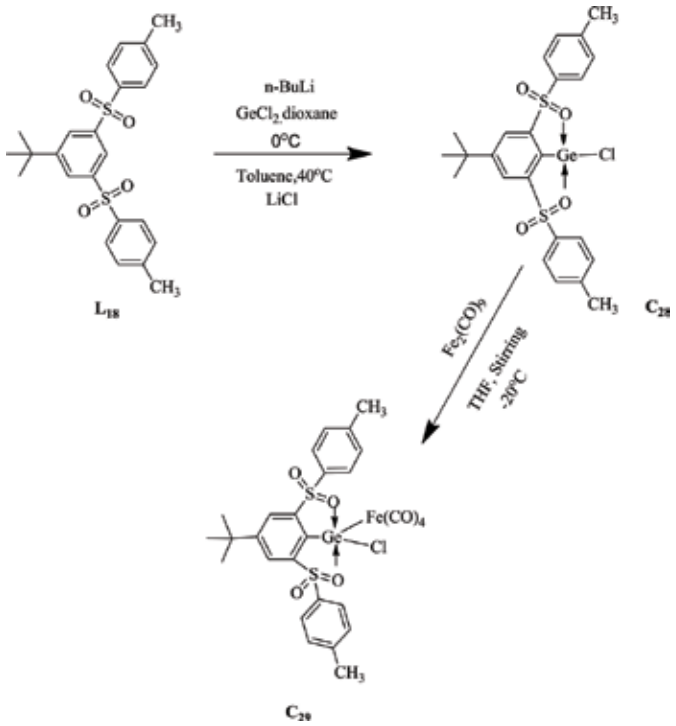

Scheme 16. Synthesis of bis-sulfonyl O,C,O-chelated germylenes.

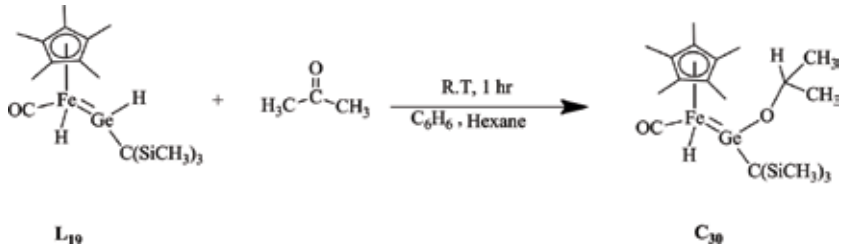

Scheme 17. Synthesis of iron germylene complex having Fe-H and Ge-H bonds.

C30 was formed when a solution of **L19** in hexane was dissolved into acetone (**Scheme 17**). The reaction mixture was stirred continuously at room temperature for 1 h. All volatiles were removed under vacuum. The end product was obtained as a greasy solid. Pure red crystals were obtained by recrystallization of the greasy solid in hexane at 30°C in 42% isolated yield [23].

7. Germanium complexes involving bonding through carbon and hydrogen (C, H)

A red solution of **L20** was added into K[HB(s-Bu)$_3$] in THF at room temperature and stirred continuously (**Scheme 18**). The color of reaction mixture changed immediately into yellow. After 1 h, all volatiles were removed under vacuum. B(s-Bu)$_3$, the by-product, was removed away with n-pentane. Colorless crystals of **C31a** were obtained in THF solutions at −20°C in 91% isolated yield. Melting point of the end product was 270°C. $[Ph_3C]^+[B(C_6F_5)_4]^-$ and toluene

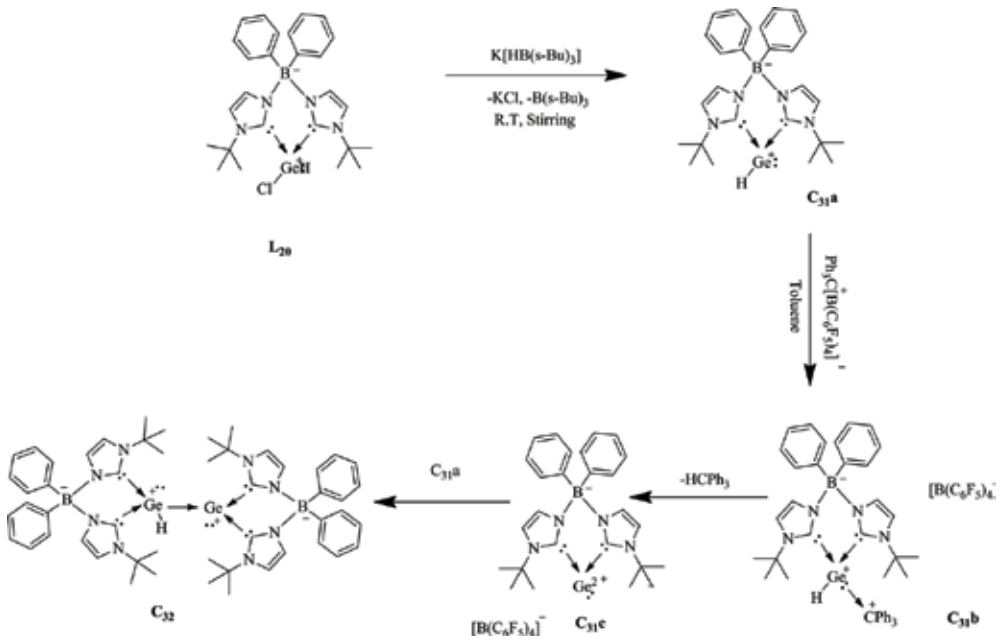

Scheme 18. Synthesis of germyliumylidene hydride [:GeH]$^+$ stabilized by a bis(NHC) borate ligand.

were added into **C31a** at room temperature and the mixture was stirred. Two phases were formed immediately when the mixture was stirred continuously. After 3 h, ^{1}H NMR indicated the formation of **C32** and $HCPh_3$ (a by-product). The formation of the by-product was indicated by a singlet at δ = 5.58 ppm for $HCPh_3$. All volatiles were removed under vacuum. Ph_3CH, a by-product, was removed by using n-pentane. The residue was dissolved in acetonitrile, and **C32** was first crystallized in the form of yellowish rods at 4°C in 57% isolated yield. When the solution was further concentrated, the yellowish product changed into orange rods and was collected in 25% isolated yield. Melting point of the end product was 201°C [24].

8. Germanium complexes involving bonding through nitrogen and oxygen (N, O)

C33 was prepared by mixing a solution of **L21** in toluene at −80°C and was placed under an atmosphere of dry CO_2 gas (**Scheme 19**). The orange red reaction mixture was allowed to heat toward ambient temperature with consistent stirring. At about −30°C, the reaction mixture turned colorless. However, it was allowed to heat till room temperature. The resulting reaction mixture was concentrated toward saturation using rotary evaporator. The saturated solution was layered with n-hexane. Colorless crystals of **C34** were obtained in 75% isolated yield. Melting point of the product was 175–178°C [18].

C34 was formed by dissolving diethyl ether and $Ge[N(SiCH_3)_2]_2$ in **L22** (**Scheme 20**). In reaction mixture, n-pentane was added slowly. Then, mixture was stirred at ambient temperature for 5 min. After filtration of reaction mixture, a solid material was obtained and was dried in vacuum to obtain colorless crystalline solid. The product was recrystallized to obtain colorless crystals of **C34** in 85% isolated yield [25].

Spirocyclic compounds (**C35a–C35c**) were synthesized by adding n-butyl lithium in n-hexane into a solution of 2-(phenylaminomethyl)phenol in diethyl ether (**Scheme 21**). The reaction mixture was stirred at ambient temperature for 2 h. After filtration, the reaction mixture was washed with n-pentane and was then dried under low pressure. The solid was dispersed in toluene and $GeCl_4$ was added dropwise with the help of syringe. Then, the solution was stirred at ambient temperature for 16 h. The solution was filtered using celite 545 and was

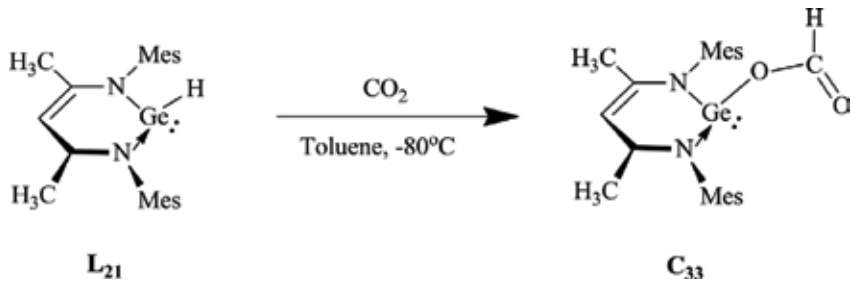

Scheme 19. Synthesis of *N*-heterocyclic germanium(II) hydride.

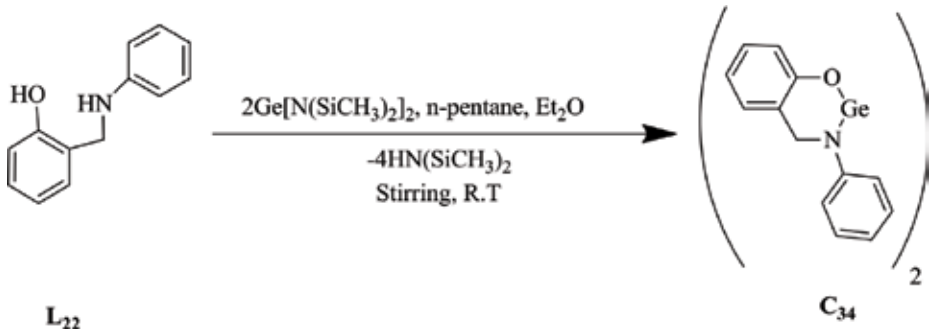

Scheme 20. Synthesis of amido alkoxide of germanium.

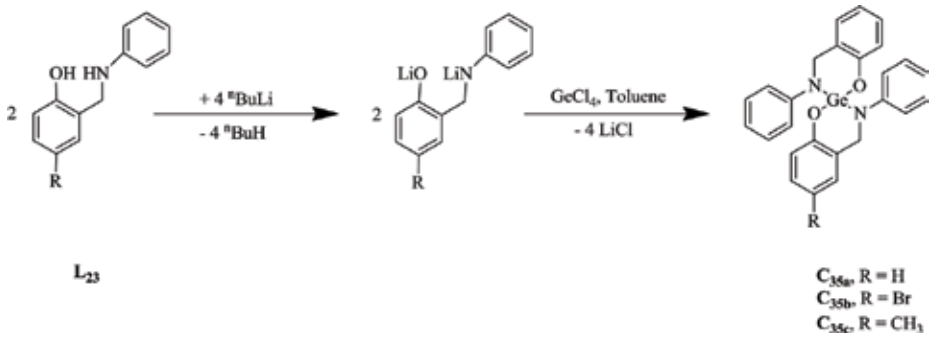

Scheme 21. Synthesis of spirocyclic compounds of germanium bonded through "N" and "O".

concentrated in vacuum and hence finally gave solids, which were crystallized from an appropriate solvent. The end product was obtained in 82% isolated yield. For single X-ray diffraction, colorless crystal was grown from n-hexane at 18°C [25].

C36a–C36c were formed when a suspension of KOR (R = ^{i}Pr, ^{t}Bu, ^{s}Bu) was added into $GeCl_4$·dioxane solution in THF at ambient temperature (**Scheme 22**). The reaction mixture was stirred for 3 days at ambient temperature. All volatiles were removed using rotary evaporator. The orange crude product was extracted with toluene, and the solution was filtered through celite 545. The filtered material was evaporated to obtain a solid. Recrystallization of this solid was carried out by n-hexane through an overnight period at −27°C. The end product was obtained as orange crystals in 76% isolated yield [26].

C37 was formed when solution of sodium bis(trimethylsilyl)amide and $GeCl_4$ in THF was stirred and refluxed for 96 h (**Scheme 23**). All volatiles were removed under low pressure. The residue was extracted three times by pentane. The pentane solution was concentrated and was kept in glove box at −40°C overnight. The white solid was washed with cold n-pentane, and the product was dried in vacuum. The end product was obtained as white powder in 65% isolated yield [27].

Synthesis of **C38** was carried out when a solution of **L26** and $Ge[N(SiCH_3)_2]_4$.(THF) was mixed and stirred for 10 min at room temperature. After removing solvent from reaction mixture, the

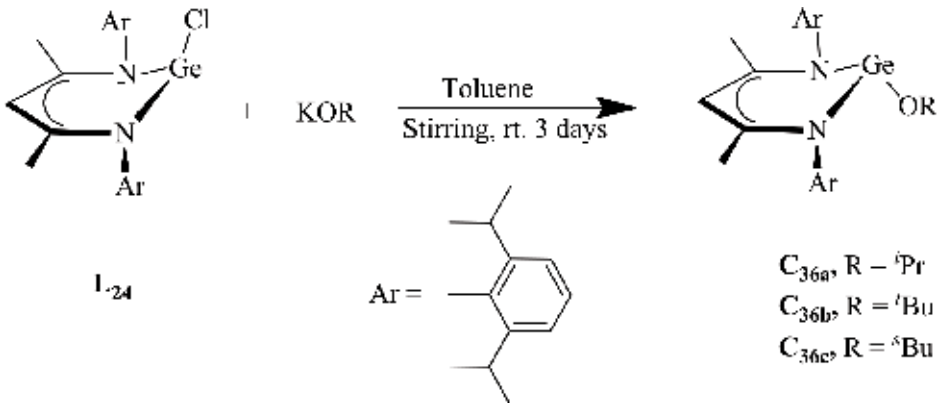

Scheme 22. Synthesis of germanium alkoxide complexes.

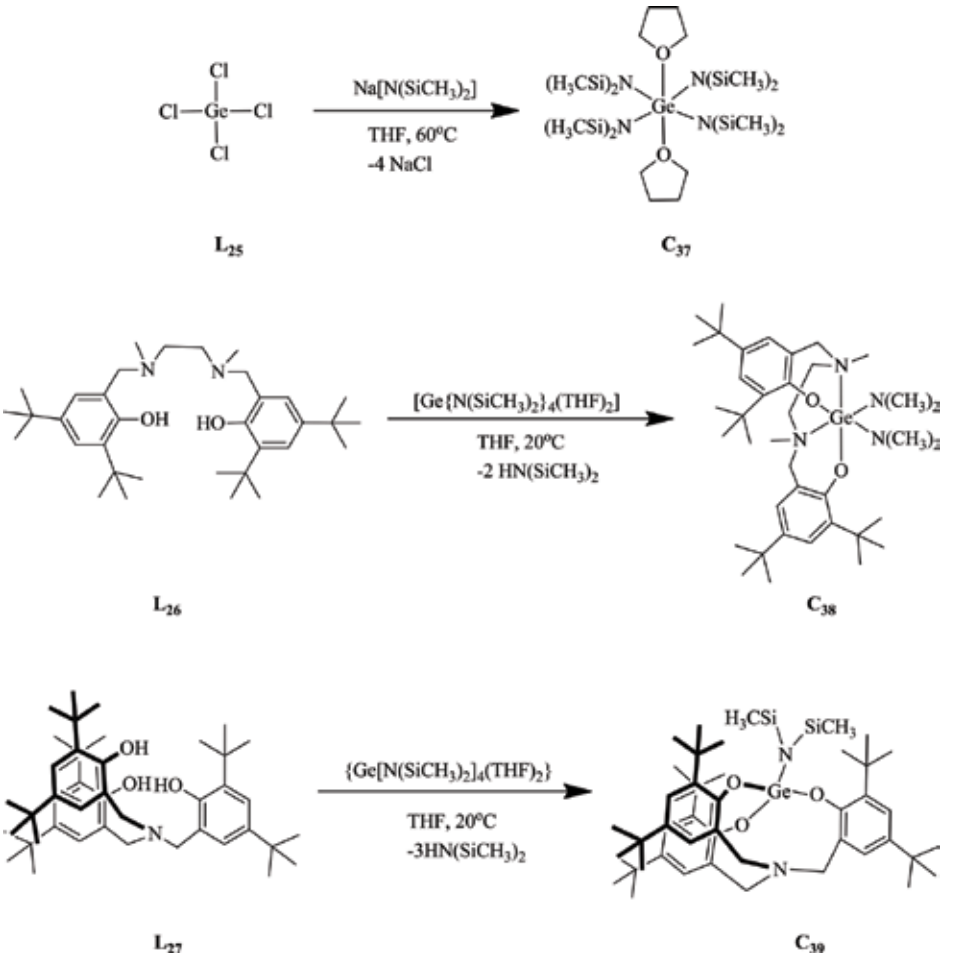

Scheme 23. Synthesis of germanium complexes involving bonding through "N" and "O".

solid residue was dissolved in n-pentane. Then, n-pentane solution was kept in a glove box at −40°C overnight. A white crystalline solid was extracted out from solution and was washed with clean and cold n-pentane. The extracted product was dried in vacuum. The end product was obtained as white powder in 90% isolated yield [27]. Similarly, **C39** was formed when **L27** was added to a stirred solution of $Ge[N(SiCH_3)_2]_4.(THF)_2$ in toluene at room temperature. The reaction mixture was stirred for 10 min at room temperature. All volatiles were removed under vacuum. The extracted residue was washed several times by n-pentane and was dried under vacuum. The end product was obtained as white powder in 85% isolated yield [27].

C40 was synthesized in two steps (**Scheme 24**). Firstly, $GeCl_2$·dioxane was added slowly into a solution of Na(dmamp), where dmamp = 1-dimethylamino-2-methyl-2-propanolate, in THF. The reaction mixture was stirred continuously at room temperature overnight. The reaction mixture was filtered to remove sodium chloride salt as by-product. After filtration, the filtrate was concentrated in vacuum to obtain $Ge(dmamp)_2$ as crude product. The end product was obtained as colorless liquid by distillation in 81% isolated yield. Sulfur powder was then added slowly into a solution of $Ge(dmamp)_2$ in toluene. The reaction mixture was stirred at room temperature overnight. **C40** was obtained as a white solid after removing all the volatiles from the reaction mixture. Recrystallization of the crude product from an ethereal solution of it gave the pure product as colorless crystals in 82% [28].

C41 $[(^tBu)_2ATI]GeO^tBu$ was formed by adding **L29** solution in hexane into KO^tBu at −40°C (**Scheme 25**). The reaction mixture was stirred at room temperature for 12 h. After filtration, hexane was removed and **C41** was obtained as red solid in 97% isolated yield. Melting point of the end product was 78°C. **C42** was formed when elemental sulfur was added into **L28** solution in THF at room temperature. The reaction mixture was stirred at room temperature for 2 h. All volatiles were removed under reduced pressure. The residue was washed with n-hexane and was dried to get the product as yellow solid in 98% isolated yield. Single

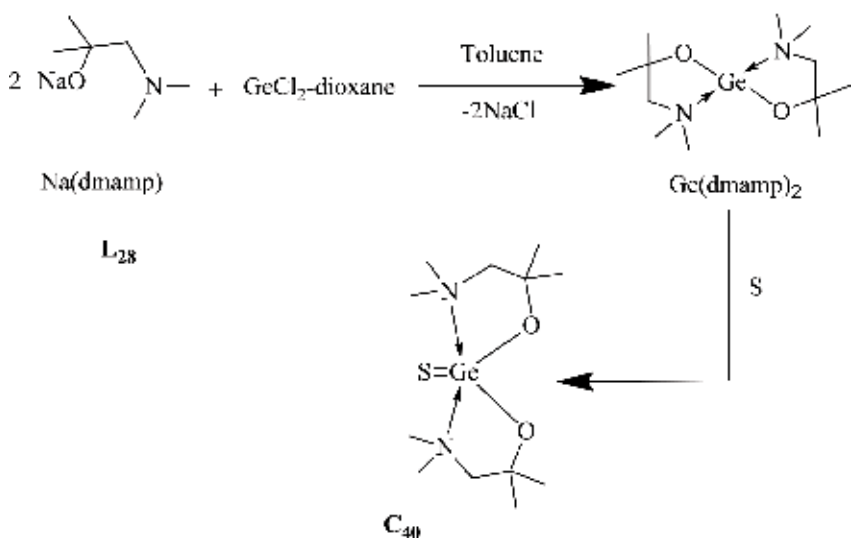

Scheme 24. Synthesis of germanium complex containing Ge═S double bond.

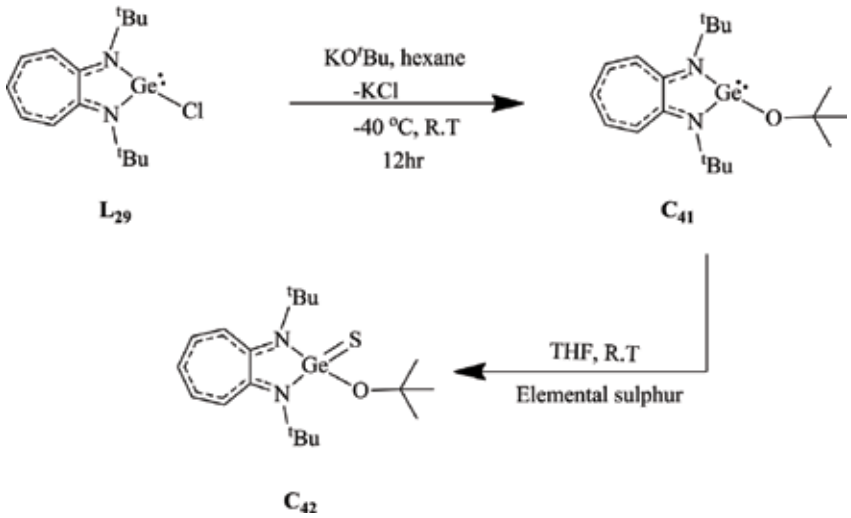

Scheme 25. Synthesis of aminotroponiminatogermylenealkoxide complexes.

crystals of **C42** were obtained by the slow evaporation of solvent from its chloroform solution. Crystals of **C42** were remained suitable for X-ray crystallographic studies. Melting point of the end product was 178°C [29].

n-BuLi was added into a cold solution of 4,6-di-ter-butylresorcinol of dry diethyl ether at −30°C (**Scheme 26**). After mixing, immediately a milky solid suspension was observed. Cooling bath was removed and reaction material was again stirred for 3 h at ambient temperature. The reaction mixture was then cooled and N,N-di-tert-butylchloro(phenylamidinate)-germanium(II) was added dropwise in the reaction mixture. After complete addition, the reaction mixture was maintained at ambient temperature overnight. All volatile solvents were removed in vacuum. **C43** was extracted with the addition of hot hexane in reaction mixture *via* cannula filtration. The reaction mixture was concentrated and cooled at −3°C, which led

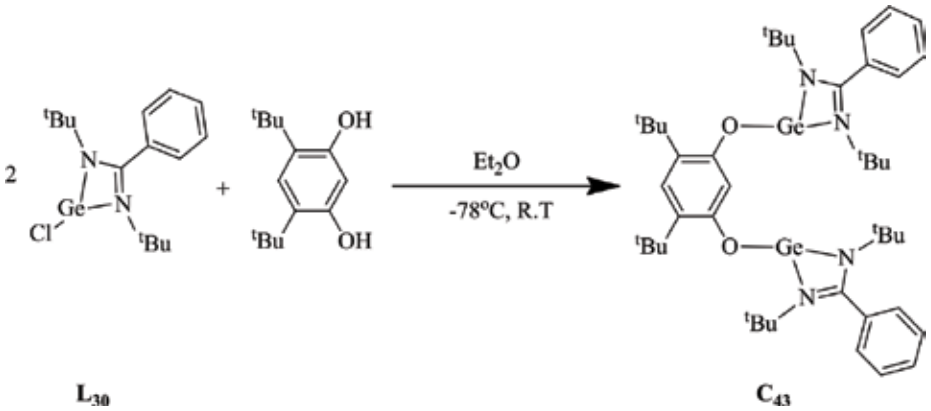

Scheme 26. Synthesis of $GeC_{aromatic}Ge$-type pincer for further coordination with iridium.

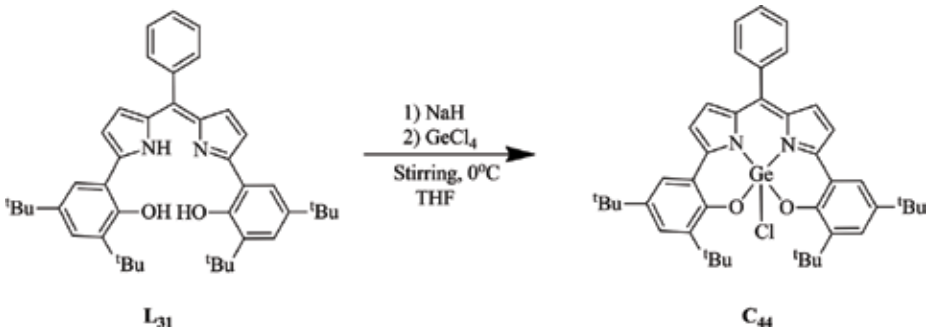

Scheme 27. Synthesis of salophene-like germanium complex.

to the crystallization of product overnight. Product was dried in vacuum for 2 h. The end product was obtained as yellowish crystalline product in 83% isolated yield [30].

C44 was synthesized by mixing NaH and $GeCl_4$ with **L31** (**Scheme 27**). The solution was stirred for 1 h at ambient temperature. After filtration, the filtrate was placed in Schlenk tube and the tube was taken outside the glove box. $GeCl_4$ was added dropwise in the reaction mixture at 0°C. After stirring of solution for 25 min at same temperature, the reaction mixture was warmed at room temperature for another 1 h and was concentrated under reduced pressure. The residue was filtered through syringe filter in a glove box by using Et_2O. The resulting residue was redissolved in pentane and was concentrated to remove uncoordinated THF. The end product was obtained as green solid in 98% isolated yield [31].

9. Three linkages

9.1. Germanium complexes involving bonding through carbon, nitrogen, and oxygen (C, N, O)

C45 was synthesized when iodine was added to a solution of **L32** (**Scheme 28**). Pale yellow precipitates were formed when the reaction mixture was stirred for a period of 12 h. Then, precipitates were washed several times with n-pentane and the end product was obtained as a dark orange powder in 92% isolated yield. Dark red crystals were produced by storing the saturated solution of **C45** in THF/C_6H_5F mixture at −27°C for 7 days [26].

C46 was formed by mixing **L33** with $ZnCl_2$ in THF (**Scheme 29**). The reaction mixture was stirred for 4 h at ambient temperature. All volatiles were removed using rotary evaporator. Yellow solid product was washed with toluene and was dried in vacuum. Single crystals of **C46** were grown from its hot acetonitrile solution for X-ray diffraction studies. The end product was obtained as yellow solid in 94% isolated yield. Melting point of the end product was 152°C [32]. **C47** was synthesized when a solution of **L34** was transferred into $GeCl_2$ solution in THF at room temperature, and the reaction mixture was stirred for 4 h. All volatiles were removed using rotary evaporator. The yellow solid was washed with n-hexane and was

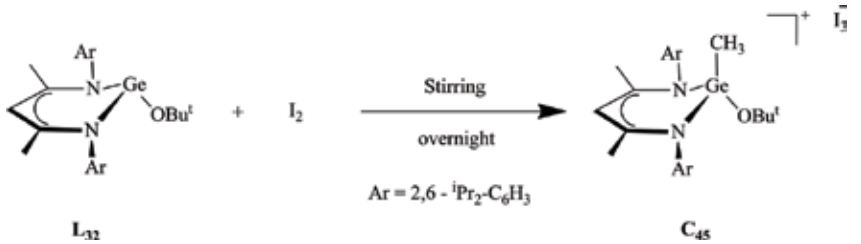

Scheme 28. Synthesis of germanium alkoxide complex.

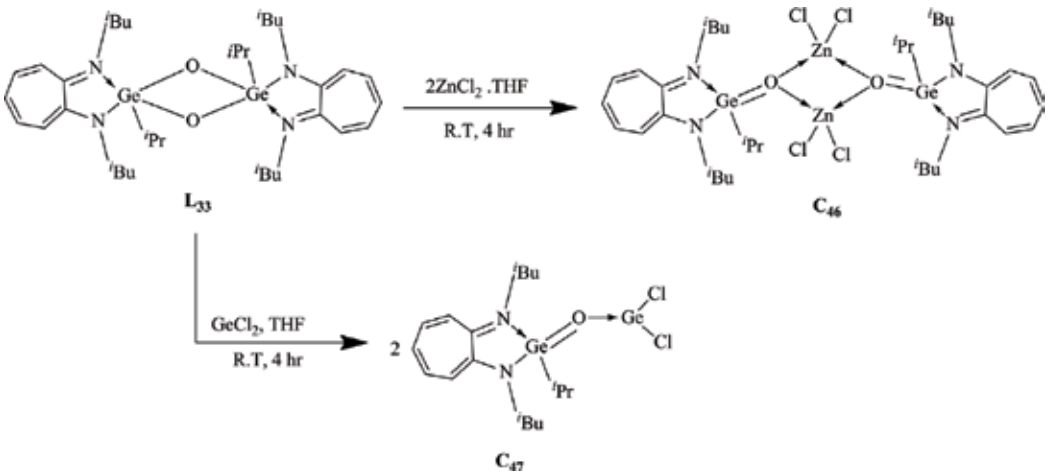

Scheme 29. Synthesis of germanone from a germanium-μ-oxo dimer.

dried in vacuum to obtain pure sample of **C47** as yellow solid. Single crystals of complex were grown from its solution in THF and hexane at −40°C, which remained suitable for X-ray diffraction studies. The end product was obtained as yellow solid in 94% isolated yield. Melting point of the end product was 110°C [32].

L34 in CH_3CN was placed in a round bottom flask under an inert atmosphere using argon gas (**Scheme 30**). Triethyleneamine (NEt_3) and $GeCl_4$ were added in the reaction medium. The reaction mixture was then stirred at room temperature for 15 min and passed through a short pad of silica gel column (C-200, CH_2Cl_2). Separation through silica gel column (C-300, n-hexane: CH_2Cl_2 = 2:1) gave **C48** as a second fraction. All volatiles were removed. The end product was obtained as dark brown solid in 76% isolated yield [33].

9.2. Germanium complexes involving bonding through nitrogen, oxygen, and sulfur/selenium (N, O, S/Se)

C49 was formed when elemental sulfur was added into a solution of **L35** in THF at room temperature (**Scheme 31**). The reaction mixture was stirred at room temperature for 2 h. All volatiles were removed using rotary evaporator. The residue was washed with n-hexane and dried to obtain product as yellow solid. Single crystals of complex were obtained

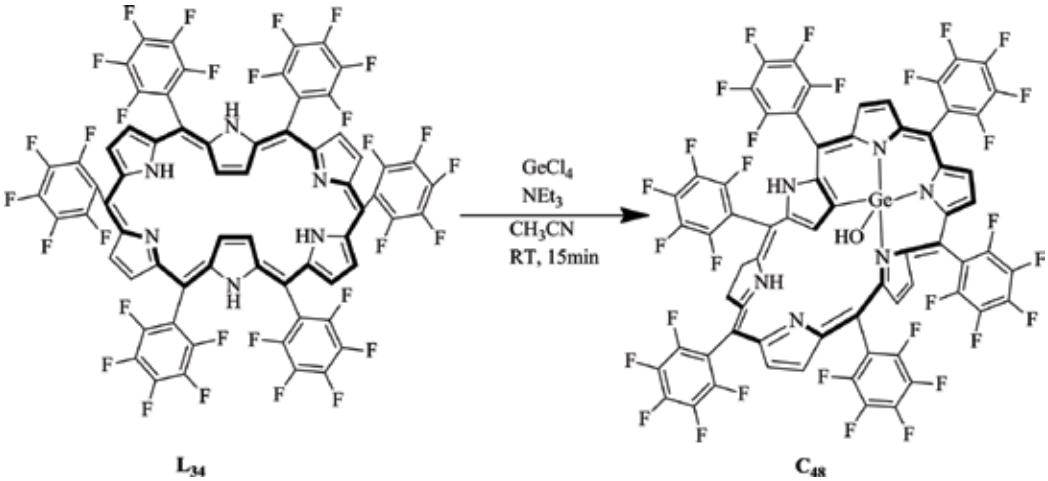

Scheme 30. Synthesis of aromatic [28]hexaphyrin germanium(IV) complex.

Scheme 31. Synthesis of sulfur-bonded germaester complex.

by evaporation method. According to this method, a slow evaporation of solvent from its saturated solution in chloroform was managed to obtain crystals suitable for X-ray diffraction study. The end product was obtained as yellow solid in 98% isolated yield. Melting point of the end product was 178°C [29].

C50 was obtained when selenium powder was added slowly into a $Ge(dmampS)_2$ solution in toluene (**Scheme 32**). The reaction mixture was stirred at room temperature overnight. All volatiles were removed from reaction mixture under vacuum. The product was obtained as yellow solid. The pure product was synthesized by recrystallization of yellow solid from an ether solution. At the end, yellow crystals were obtained in 89% isolated yield [28].

9.3. Germanium complexes involving bonding through nitrogen, phosphorus, carbon (N, P, C)

C51 was synthesized by adding **L37** solution in THF slowly into phenyl lithium at −80°C (**Scheme 33**). The reaction mixture was warmed slowly at room temperature and stirred continuously for 2 h. All volatiles were removed in vacuum. The product was extracted twice with n-pentane. The major diastereomer as **C51** was obtained in pure form from a concentrated

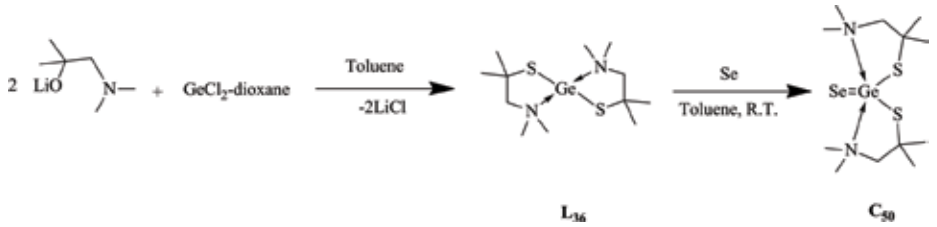

Scheme 32. Synthesis of selenium-bonded germaester complex.

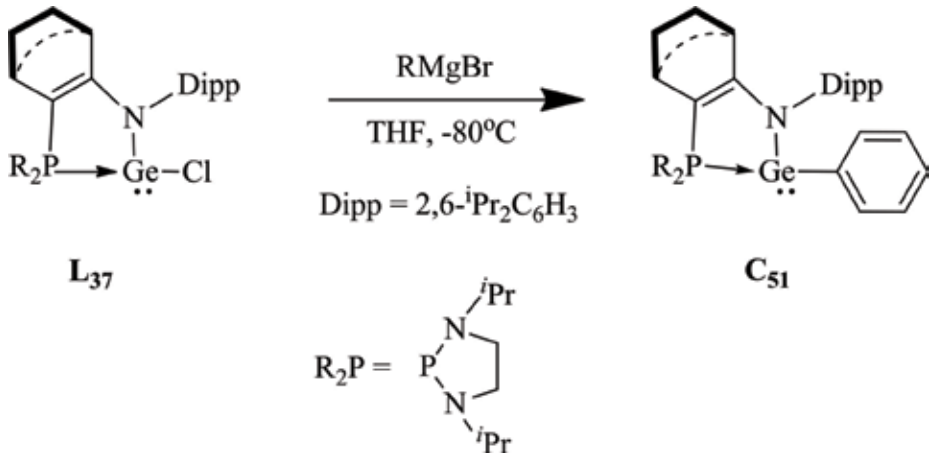

Scheme 33. Synthesis of phosphine-stabilized germylene complex.

solution of n-pentane at −30°C. At the end, pale yellow crystals were obtained in 45% isolated yield. Melting point of the end product was 25°C [6].

9.4. Germanium complexes involving bonding through nitrogen, carbon, manganese (N, C, Mn)

C52 was formed when a solution of **L38** was added dropwise to a stirred suspension of $Mn_2(CO)_{10}$ in toluene at room temperature (**Scheme 34**). The reaction mixture was refluxed overnight. After filtration, the filtrate was concentrated. The end product was obtained as dark red crystals in 46.3% isolated yield. Melting point of the end product was 261°C [17].

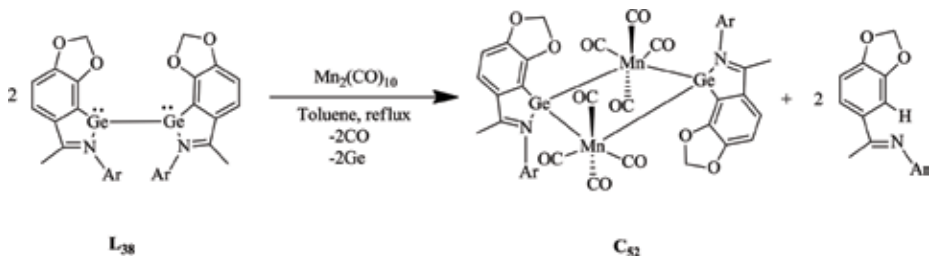

Scheme 34. Synthesis of germanium(I) dimer stabilized by dimanganese decacarbonyl.

10. Miscellaneous

10.1. Germanium complexes involving bonding through oxygen

C53 was formed when N-methoxypropanamide was added dropwise to a stirring diethyl ether solution of **L39** (**Scheme 35**). After reaction mixture was placed overnight at room temperature, volatiles were removed in vacuum and crude product was distilled at 10^{-1} torr to afford pure complex. The resulting pure complex was obtained as a colorless liquid at 120°C in 33% isolated yield [3].

10.2. Germanium complexes involving bonding through phosphorus (P)

L40 was dissolved in THF and n-butyl lithium was added into reaction mixture through a syringe (**Scheme 36**). The resulting white suspension was stirred for 30 min at room temperature. $GeCl_2$ was added as a solid, and dark yellow solution was formed. The dark yellow solution was stirred for 3 h at room temperature. All volatiles were removed under vacuum. n-Pentane was added in residue, which was then filtered to remove LiCl. n-Pentane solution was concentrated and cooled at 25°C. The end product was obtained as yellow rod-like crystals in 6% isolated yield. Melting point of the end product was 110–112°C [34].

10.3. Germanium complexes involving bonding through carbon and sulfur (C, S)

C55 was synthesized when superhydride was added into the solution of naphthol in THF (**Scheme 37**). The reaction mixture was stirred continuously for 30 min. $(CH_3)_2GeCl_2$ was added and the reaction mixture was stirred overnight. All volatiles were removed under vacuum. The product was dissolved in DCM and filtered through celite. The product was washed with hexane. The end product was obtained as cream crystalline solid in 25% isolated yield. Melting point of the end product was 79–80°C [35].

10.4. Germanium complexes involving bonding through nitrogen and boron (N, B)

C56 was formed by adding **L42** solution into a solution of $B(C_6F_5)_3$ in Et_2O at 0°C (**Scheme 38**). The resultant yellow reaction mixture was warmed at room temperature and stirred for 24 h. All volatiles were removed under vacuum and were extracted with toluene. The end product was obtained as yellow crystals in 60% isolated yield. Melting point of the end product was 157°C [16].

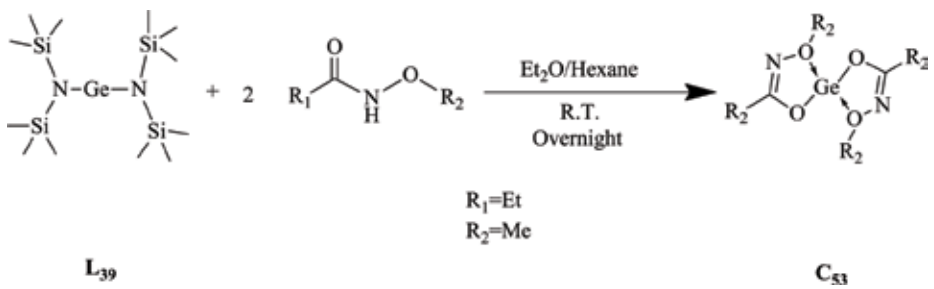

Scheme 35. Synthesis of *N*-alkoxy carboxylamide-stabilized germanium(II) complexes.

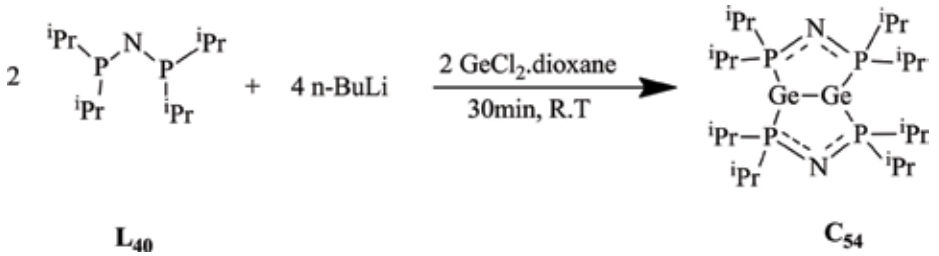

Scheme 36. Synthesis of bicyclic low-valent germanium complex bridged by bis(diisopropylphosphino)amine.

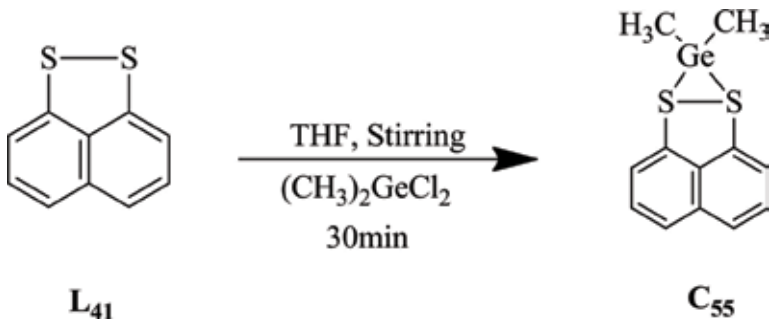

Scheme 37. Complexation of aromatic dichalcogen ligands to germanium.

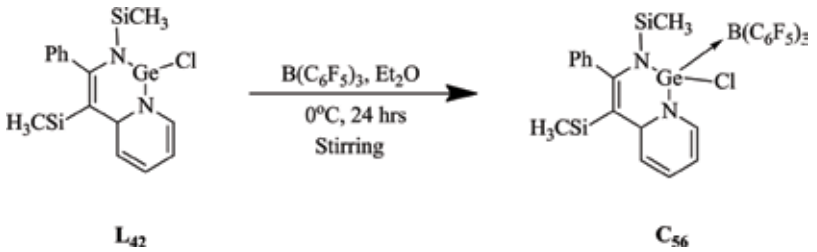

Scheme 38. Synthesis of boron-substituted metallogermylenes.

10.5. Germanium complexes involving bonding through nitrogen and phosphorous (N, P)

C57 was formed when a suspension of TPH was added to a mixture of LGeCl (**L43**) in presence of free NHC in Et_2O at −18°C (**Scheme 39**). After stirring for 12 h, all volatiles were removed using rotary evaporator to get an oily paste. n-hexane was layered on this paste. The n-hexane-layered oily paste was stored at room temperature for 1 week. The end product was obtained as dark red crystals in 38% isolated yield. Melting point of the end product was 198°C [36].

10.6. Germanium complexes involving bonding through nitrogen and sulfur (N, S)

C58 was formed when CS_2 was added in **L44** solution in toluene at −70°C (**Scheme 40**). The reaction mixture was warmed at room temperature and was further stirred for 18 h. All

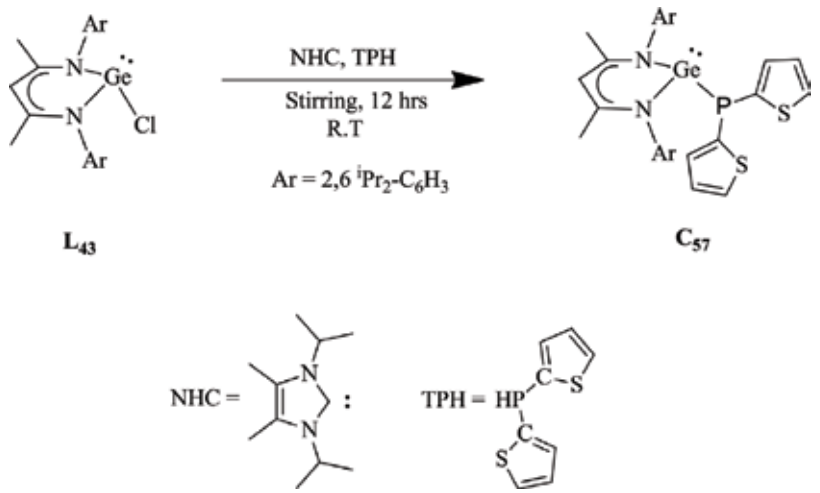

Scheme 39. Synthesis of β-diketiminate germanium(II) complex.

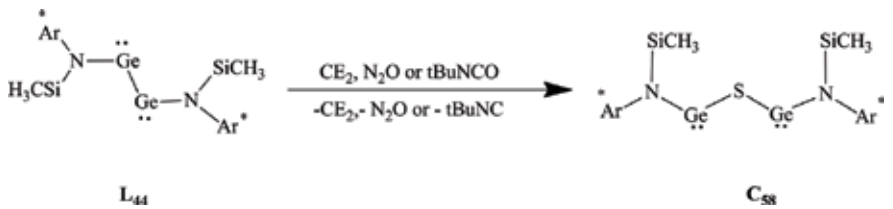

Scheme 40. Synthesis of digermyne with a Ge-Ge single-bonded compounds.

volatiles were removed under vacuum. Pure pale yellow crystals of **C58** were obtained in 93% isolated yield by recrystallization of compound using diethyl ether. Melting point of the end product was 146–150°C [37].

10.7. Germanium complexes involving bonding through phosphorus and carbon (P, C)

C59 was synthesized by mixing **L45** and NaOCP·dioxane in toluene at room temperature (**Scheme 41**). The solution was stirred for 2 h. At that time, the reaction flask was wrapped

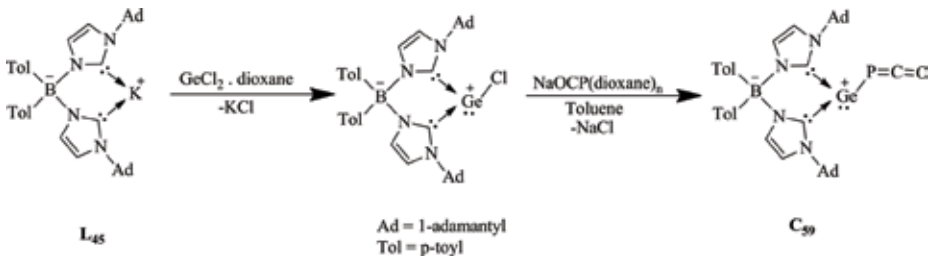

Scheme 41. Synthesis of the bis-NHC chlorogermyliumylidene borate.

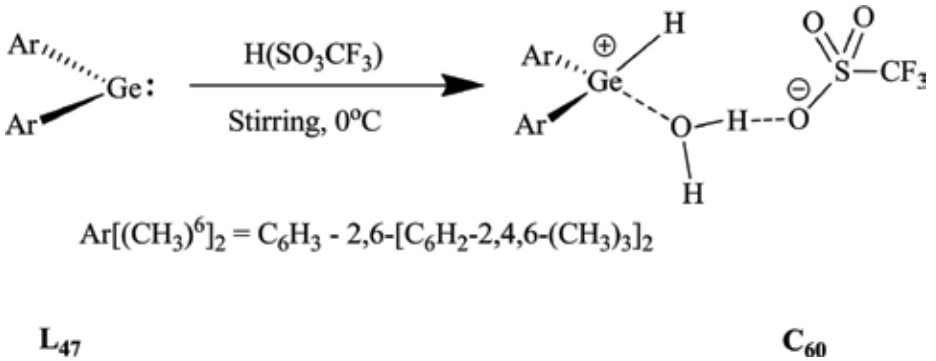

Scheme 42. Synthesis of functionalized germanium complex.

with aluminum foil to protect day light. The precipitate of NaCl was separated from reaction mixture through centrifugation. All volatiles were removed under reduced pressure. Then, the residue was washed with n-hexane and extracted with diethyl ether. The end product was crystallized as yellow rods in 67% isolated yield. Melting point of the end product was 190°C [38].

10.8. Germanium complexes involving bonding through oxygen and hydrogen (O, H)

C60 was formed when HSO_3CF_3 was added to a stirred solution of **L46** in toluene at 0°C (**Scheme 42**). The color of reaction mixture changed immediately into pale yellow. The reaction mixture was further stirred for 2 h, and volume of solution is reduced under vacuum. After addition of n-hexane in flask, the reaction mixture was cooled slowly. The reaction mixture was placed unattended at −20°C overnight. The end product was obtained as colorless blocks in 83% isolated yield [19].

Author details

Hina Hayat[1] and Muhammad Adnan Iqbal[1,2]*

*Address all correspondence to: adnan.iqbal@uaf.edu.pk

1 Department of Chemistry, University of Agriculture, Faisalabad, Pakistan

2 Organometallic & Coordination Chemistry Laboratory, Department of Chemistry, University of Agriculture, Faisalabad, Pakistan

References

[1] Haller E. Germanium: From its discovery to SiGe devices. Materials Science in Semiconductor Processing. 2006;**9**(4-5):408-422

[2] Svarnas P, Botzakaki M, Skoulatakis G, Kennou S, Ladas S, Tsamis C, et al. Controllable growth of stable germanium dioxide ultra-thin layer by means of capacitively driven radio frequency discharge. Thin Solid Films. 2016;**599**:49-53

[3] George SM, Nam JH, Lee GY, Han JH, Park BK, Kim CG, et al. N-alkoxy carboxamide stabilized tin (II) and germanium (II) complexes for thin-film applications. European Journal of Inorganic Chemistry. 2016;**2016**(36):5539-5546

[4] Harris LM, Tam EC, Cummins SJ, Coles MP, Fulton JR. The reactivity of germanium phosphanides with chalcogens. Inorganic Chemistry. 2017;**56**(5):3087-3094

[5] Katir N, Matioszek D, Ladeira S, Escudié J, Castel A. Stable N-heterocyclic carbene complexes of hypermetallyl germanium (II) and tin (II) compounds. Angewandte Chemie International Edition. 2011;**50**(23):5352-5355

[6] García JM, Ocando-Mavárez E, Kato T, Coll DS, Briceño A, Saffon-Merceron N, et al. Synthesis and characterization of rhodium complexes with phosphine-stabilized germylenes. Inorganic Chemistry. 2012;**51**(15):8187-8193

[7] Ochiai T, Szilvási T, Franz D, Irran E, Inoue S. Isolation and structure of germylene-germyliumylidenes stabilized by N-heterocyclic imines. Angewandte Chemie. 2016; **128**(38):11791-11796

[8] Yao S, Xiong Y, Driess M. A new area in main-group chemistry: Zerovalent monoatomic silicon compounds and their analogues. Accounts of Chemical Research. 2017; **50**(8):2026-2037

[9] Filippou AC, Stumpf KW, Chernov O, Schnakenburg G. Metal activation of a germylenoid, a new approach to metal–germanium triple bonds: Synthesis and reactions of the germylidyne complexes [Cp (CO) 2M Ge–C (SiMe3) 3](M= Mo, W). Organometallics. 2012;**31**(2):748-755

[10] Xiong Y, Yao S, Inoue S, Berkefeld A, Driess M. Taming the germyliumylidene [CIGe:]+ and germathionium [CIGe=S]+ ions by donor-acceptor stabilization using 1,8-bis (tributylphosphazenyl)naphthalene. Chemical Communications. 2012;**48**(100):12198-12200. DOI: 10.1039/C2CC36926E

[11] Woodul WD, Carter E, Müller R, Richards AF, Stasch A, Kaupp M, et al. A neutral, monomeric germanium (I) radical. Journal of the American Chemical Society. 2011;**133**(26): 10074-10077

[12] Matioszek D, Saffon N, Sotiropoulos J-M, Miqueu K, Castel A, Escudié J. Bis (amidinato) germylenerhodium complexes: Synthesis, structure, and density functional theory calculations. Inorganic Chemistry. 2012;**51**(21):11716-11721

[13] Leung W-P, Chan Y-C, So C-W, Mak TC. Reactivity study of a pyridyl-1-azaallylgermanium (I) dimer: Synthesis of heavier ether and Ester analogues of germanium. Inorganic Chemistry. 2016;**55**(7):3553-3557

[14] Zhao N, Zhang J, Yang Y, Zhu H, Li Y, Fu G. β-diketiminate germylene-supported pentafluorophenylcopper(I) and -silver(I) complexes $[LGe(Me)(CuC_6F_5)_n]_2$ (n = 1, 2), $LGe[C(SiMe_3)N_2]AgC_6F_5$, and $\{LGe[C(SiMe_3)N_2](AgC_6F_5)_2\}_2$ (L = HC[C(Me)N-2,6-*i* $Pr_2C_6H_3]_2$): Synthesis and structural characterization. Inorganic Chemistry. 2012;**51**(16): 8710-8718

[15] Seow C, Xi H-W, Li Y, So C-W. Synthesis of a germylidenide anion from the C–C bond activation of a bis (germylene). Organometallics. 2016;**35**(8):1060-1063

[16] Leung W-P, Chiu W-K, Mak TC. Synthesis and structural characterization of metallogermylenes, Cp-substituted germylene, and a germanium (II)-borane adduct from pyridyl-1-azaallyl germanium (II) chloride. Organometallics. 2012;**31**(19):6966-6971

[17] Ismail MLB, Liu F-Q, Yim W-L, Ganguly R, Li Y, So C-W. Reactivity of a base-stabilized germanium (I) dimer toward group 9 metal (I) chloride and dimanganese decacarbonyl. Inorganic Chemistry. 2017;**56**(9):5402-5410

[18] Choong SL, Woodul WD, Schenk C, Stasch A, Richards AF, Jones C. Synthesis, characterization, and reactivity of an N-heterocyclic germanium (II) hydride: Reversible hydrogermylation of a phosphaalkyne. Organometallics. 2011;**30**(20):5543-5550

[19] Brown ZD, Erickson JD, Fettinger JC, Power PP. Facile, high-yield functionalization of germanium and tin by oxidative insertion of tetrelenes into the E–H bonds of inorganic acids (E = C, N, O, F): Arene elimination versus oxidative addition and formation of a germanium cation–water complex. Organometallics. 2013;**32**(2):617-622. DOI: 10.1021/om301121x

[20] Brown ZD, Guo J-D, Nagase S, Power PP. Experimental and computational study of auxiliary molecular effects on the mechanism of the addition of hydrazines to a low-valent germanium complex. Organometallics. 2012;**31**(9):3768-3772

[21] Li J, Schenk C, Goedecke C, Frenking G, Jones C. A digermyne with a Ge–Ge single bond that activates dihydrogen in the solid state. Journal of the American Chemical Society. 2011;**133**(46):18622-18625

[22] Deak N, Petrar PM, Mallet-Ladeira S, Silaghi-Dumitrescu L, Nemeş G, Madec D. Bis-sulfonyl O, C, O-chelated metallylenes (Ge, Sn) as adjustable ligands for iron and tungsten complexes. Chemistry—A European Journal. 2016;**22**(4):1349-1354

[23] Dhungana TP, Hashimoto H, Tobita H. An iron germylene complex having Fe-H and Ge-H bonds: Synthesis, structure and reactivity. Dalton Transactions. 2017;**46**:8167-8179

[24] Xiong Y, Szilvási T, Yao S, Tan G, Driess M. Synthesis and unexpected reactivity of germyliumylidene hydride [: GeH]+ stabilized by a bis (N-heterocyclic carbene) borate ligand. Journal of the American Chemical Society. 2014;**136**(32):11300-11303

[25] Dannenberg F, Thiele G, Dornsiepen E, Dehnen S, Mehring M. Synthesis, structure and thermolysis of oxazagermines and oxazasilines. New Journal of Chemistry. 2017; **41**:4990-4997

[26] Ferro L, Hitchcock PB, Coles MP, Fulton JR. Reactivity of divalent germanium alkoxide complexes is in sharp contrast to the heavier tin and lead analogues. Inorganic Chemistry. 2012;**51**(3):1544-1551

[27] Guo J, Haquette P, Martin J, Salim K, Thomas CM. Replacing tin in lactide polymerization: Design of highly active germanium-based catalysts. Angewandte Chemie International Edition. 2013;**52**(51):13584-13587

[28] Kim H-S, Jung EA, Han SH, Han JH, Park BK, Kim CG, et al. Germanium compounds containing Ge=E double bonds (E= S, Se, Te) as single-source precursors for germanium chalcogenide materials. Inorganic Chemistry. 2017;**56**(7):4084-4092

[29] Siwatch RK, Nagendran S. Germaester complexes with a Ge (E) O t-Bu moiety (E= S or Se). Organometallics. 2012;**31**(8):3389-3394

[30] Brück A, Gallego D, Wang W, Irran E, Driess M, Hartwig JF. Pushing the σ-donor strength in iridium pincer complexes: Bis (silylene) and Bis (germylene) ligands are stronger donors than Bis (phosphorus (III)) ligands. Angewandte Chemie International Edition. 2012;**51**(46):11478-11482

[31] Nakano K, Kobayashi K, Nozaki K. Tetravalent metal complexes as a new family of catalysts for copolymerization of epoxides with carbon dioxide. Journal of the American Chemical Society. 2011;**133**(28):10720-10723

[32] Sinhababu S, Yadav D, Karwasara S, Sharma MK, Mukherjee G, Rajaraman G, et al. The preparation of complexes of germanone from a germanium μ-Oxo dimer. Angewandte Chemie International Edition. 2016;**55**(27):7742-7746

[33] Izawa M, Kim T, Si I, Tanaka T, Mori T, Kim D, et al. Möbius aromatic [28] hexaphyrin germanium (IV) and tin (IV) complexes: Efficient formation of triplet excited states. Angewandte Chemie International Edition. 2017;**56**(14):3982-3986

[34] Miller CJ, Chadha U, Ulibarri-Sanchez JR, Dickie DA, Kemp RA. Structure and Lewis-base reactivity of bicyclic low-valent germanium and tin complexes bridged by bis (diisopropylphosphino) amine. Polyhedron. 2016;**114**:351-359

[35] Meigh CB, Nejman PS, Slawin AM, Woollins JD. Complexation of aromatic dichalcogen ligands to germanium. Inorganica Chimica Acta. 2017;**456**:120-127

[36] Yang Y, Zhao N, Wu Y, Zhu H, Roesky HW. Synthesis and characterization of β-diketiminate germanium (II) compounds. Inorganic Chemistry. 2012;**51**(4):2425-2431

[37] Li J, Hermann M, Frenking G, Jones C. The facile reduction of carbon dioxide to carbon monoxide with an amido-digermyne. Angewandte Chemie International Edition. 2012;**51**(34):8611-8614

[38] Xiong Y, Yao S, Szilvási T, Ballestero-Martínez E, Grützmacher H, Driess M. Unexpected photodegradation of a phosphaketenyl-substituted germyliumylidene borate complex. Angewandte Chemie International Edition. 2017;**56**(15):4333-4336

Chapter 3

Inorganic Coordination Chemistry: Where We Stand in Cancer Treatment?

Pedro Pedrosa, Andreia Carvalho,
Pedro V. Baptista and Alexandra R. Fernandes

Additional information is available at the end of the chapter

http://dx.doi.org/10.5772/intechopen.80233

Abstract

Metals have unique characteristics such as variable coordination modes, redox activity, and reactivity being indispensable for several biochemical processes in cells. Due to their reactivity, their concentration is tightly regulated inside the cells, and abnormal concentrations are associated with many disorders, such as cancer. As such metal complexes turned out to be very attractive as potential anticancer agents. The discovery of cisplatin was a crucial moment, which prompted the interest in Pt(II) and other metal complexes as potential anticancer agents. This chapter highlights the state of the art on metal complexes in cancer therapy, highlighting their uptake mechanisms, biological targets, toxicity, and drug resistance. Finally, based on the importance of selective target of cancer cells, drug delivery systems will also be discussed.

Keywords: cancer therapy, metal complexes, mechanism of action, clinical trials, platinum, ruthenium, copper

1. Introduction

Metal compounds are of undeniable importance to medicine, either for their toxicity or for their effectiveness in disease treatment. In ancient Egypt, copper was used to reduce inflammation and iron to treat anemia [1]. In modern medicine, noticeable discoveries of metal-based compounds marked the last centuries such as $K[Au(CN)_2]$, by Robert Koch, at around 1890, to treat tuberculosis; arsphenamine developed in the 1910s to cure syphilis; and Cisplatin discovered by Barnett Rosenberg in the late 1960s as an anticancer agent [2]. The latter marked a milestone in drug discovery for inorganic complexes, revolutionizing cancer

treatment and shifting focus to rational design to improve metal-based drugs, where other coordination compounds (e.g., gold, ruthenium, titanium, and copper) were also explored with some reports of (pre)clinical and clinical candidates [3, 4].

Transition metals, such as zinc, iron, and copper, are involved in several biological processes, from electron transfer to enzyme cofactors meaning that their intracellular concentration is tightly regulated, otherwise it can lead to the development of various pathological disorders such as Menkes and Wilson diseases associated with copper impairment and accumulation, respectively [4]. A common characteristic of these metals is their ability to form reactive oxygen species (ROS), which are a part of cellular redox balance and fundamental in cell metabolism, signal transduction for proliferation, differentiation, and cell death, among others [3]. Redox homeostasis is controlled by compartmentalizing reactions in the cell in subcellular units such as mitochondria and peroxisomes [3]. It is therefore understandable the great impact that metal complexes can have on such redox balance. Disturbing the oxidant-antioxidant balance promotes an oxidizing environment leading to oxidative stress. When ROS are formed inside the cells, they can induce the lipid peroxidation of cell membranes, disrupt the mitochondrial membrane potential promoting membrane depolarization, induce DNA single-strand breaks, and oxidize the cysteine residues resulting in protein structural changes [3]. Cancer cells are known to have a different redox metabolism from normal cells, with augmented levels of intracellular ROS, mostly due to increased metabolic activity and hypoxia, especially in the core of solid tumors [4]. Metal complexes, due to their redox properties, have been shown to disturb cellular redox homeostasis resulting in enhanced levels of oxidative stress prompting cancer cell death [4–8].

DNA is the main intracellular target for a high number of anticancer metal complexes (e.g., cisplatin, carboplatin, and oxaliplatin); however, several other targets are known (**Figure 1**) [4].

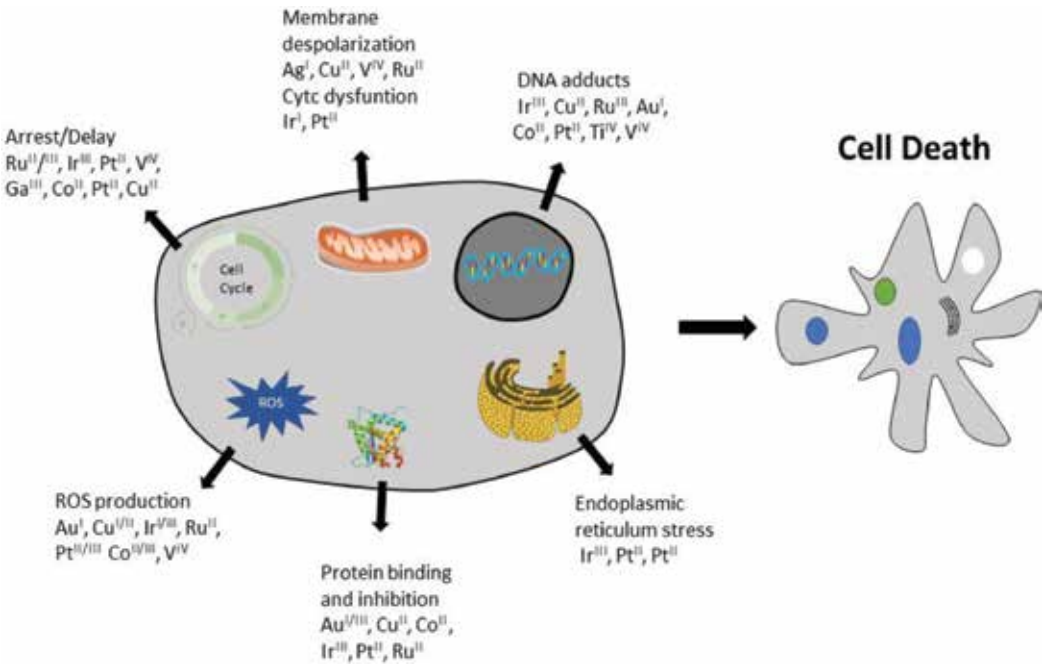

Figure 1. Schematics of metal complex mechanisms of action that promotes cell death.

In the following sections, we will summarize the current knowledge on Pt, Au, Ru, Ti, Pd, Ir Cu, V, Co, Ga, and Os complexes, highlighting their uptake mechanisms, biological targets, toxicity, and drug resistance mechanisms and elucidating how far they are from translation to the clinics in cancer therapy.

1.1. Platinum

Platinum-containing complexes revolutionized cancer treatment since the introduction of cisplatin. Synthesized in 1844, it was used for the first time, more than 100 years later to treat patients with testicular cancer with survival rates over 90% [9]. Since then, more than 3000 platinum derivatives were synthesized and tested for antiproliferative potential against cancer cells. Today, there are six platinum drugs approved in cancer treatment, three of them—cisplatin, carboplatin, and oxaliplatin—by Food and Drug Administration (FDA) and used worldwide and the other three approved in specific countries—nedaplatin in Japan, lobaplatin in Korea, and heptaplatin in China [10]. Platins are the first-line therapeutics in several cancers either alone, in combination with radiotherapy, or with other antitumor or antiangiogenic drugs [9, 11, 12]. Their cellular effects result from four main steps: (i) internalization, (ii) aquation, (iii) formation of DNA adducts, and (iv) cell response (either survival or apoptosis) [13]. Once inside the cells, the ligands (chloride in cisplatin, dicarboxylate in carboplatin, and oxalate in oxaliplatin) are substituted by water molecules that interact with nucleophilic centers on purine bases of DNA, promoting not only cross-linking of the N7 sites of adjacent guanine nucleobases, but also interstrand crosslinks, inducing severe structural distortion of the double helix. This stalls DNA transcription and arrests the cell cycle at the G2/M transition. DNA repair machinery is recruited, and if unable to repair, cells trigger apoptotic cell death [13]. However, some cells enhance their DNA repair activity becoming resistant to cisplatin that have been associated with patient's relapse [14, 15]. Other DNA damage-independent processes have been proposed such as destabilization of redox homeostasis by increasing the intracellular levels of ROS. Cisplatin metabolism is in part performed by glutathione leading to its decrease, affecting NADPH pools, resulting in dysfunctional mitochondrial redox status, and causing ROS [16]. For all FDA approved platins, the mechanism of action is believed to be very similar, with incremental variations [17, 18]. Carboplatin has less toxicity than cisplatin because 1,1-cyclobutanedicarboxylate is a poorer leaving group than chloride lowering its potency being primarily used for ovarian cancer treatment [19]. Oxaliplatin was the latest approved platinum drug and is a part of the first-line treatment for colorectal cancer. In contrast to cisplatin and carboplatin, oxaliplatin features a quelating nonleaving group, 1,2-diaminocyclohexane (DACH) in place of the two monodentate amine ligands. It also features a bidentate chelating oxalate leaving group ligand [19]. Oxaliplatin does not form adducts as efficient as cisplatin, but the hydrophobicity and size of the DACH group make it more efficient in inhibiting DNA polymerization and repair [3]. Oxaliplatin cellular uptake is active and through copper transporters 1 and 2 and organic cation transporters (OCTs) 1 and 2; the latter explains its efficacy against colorectal cancer (with OCTs overexpression) [9]. Nedaplatin features *cis* ammine nonleaving group ligand (glycolate), associated with its greater water solubility. It has less toxicity than cisplatin and less nephrotoxic and is mainly used in combination therapy to manage urological tumors [20].

Heptaplatin features malonate as a chelating leaving group ligand and a chelating 2-(1-methylethyl)-1,3-dioxolane-4,5-dimethanamine nonleaving group ligand, which forms a seven-membered chelate ring. It is used for gastric cancer, but its advantage over cisplatin

has controversial results in clinical trials [11]. Lobaplatin, a derivative of heptaplatin, fuses a cyclobutene ring to the seven-membered chelate ring instead of a dioxolane with an S-lactate as a leaving group ligand. It was originally approved to manage patients with chronic myelogenous leukemia, small-cell lung cancer, and metastatic cancer showing noncross-resistance to cisplatin [21]. Phase I clinical trial is undergoing to expand its use in combination therapy in solid tumors [22].

Currently, there are other platinum drugs in clinical trials: satraplatin, picoplatin, and two polymer/liposomal-based platinum drugs—ProLindac and Lipoplatin. Satraplatin, bis-(acetato) -ammine-dichloro-(cyclohexylamine) platinum(IV), was enrolled in several Phase I, II and III clinical trials mainly in conjunction with other drugs (e.g., docetaxel, paclitaxel, and capecitabine), but all have been recently terminated or concluded. Satraplatin was administered orally, absorbed by the gastrointestinal mucosa, and reduced in the bloodstream into more than six different Pt(II) complexes of which cis ammine dichloride(cyclohexylamine)-platinum(II) is the most important and showed anticancer activity against platinum sensitive and resistant cell lines. One of the most relevant Phase III trials evaluated a combination of satraplatin and prednisone against hormone refractory prostate cancer who had progressed after initial chemotherapy. In this study, 40% of patients had reduced risk of prostate cancer progression [23].

Picoplatin, cis-ammine-dichloride(2-methylpyridine) platinum(II), has a pyridine ring nearly perpendicular to the platinum plane, thus positioning the ligand's methylpyridine in a position that protects the metal center from nucleophilic attacks, specially by thiols. It has shown ability to overcome platinum drug resistance [23]. In Phase I clinical trials, picoplatin showed some side effects such as neutropenia, thrombocytopenia, nausea, and vomiting; however, no neuro- or nephrotoxicity was observed, and in three different Phase II clinical trials, it showed reduced efficacy as first- and second-line therapy. It is currently undergoing Phase I and Phase II studies as a combination therapy for colorectal cancer [24, 25].

Lipoplatin is a liposomal nanoparticle formulation of cisplatin with dipalmitoyl phosphatidyl glycerol (DPPG), soy phosphatidyl choline (SPC-3), cholesterol, and methoxy polyethylene glycol (mPEG2000)-distearoyl phosphatidylethanolamine (DSPE). The PEG allows cisplatin to evade the immune system increasing the circulation time. Lipoplatin fuses with cancer cells through DPPG, a fusogenic lipid embedded in the lipid bilayer allowing the release of cisplatin inside the cytoplasm of tumor cells [26]. It has successfully finished Phase III clinical trials showing superior effects when in combination with paclitaxel compared to cisplatin. Due to enhanced permeability and retention (EPR) effect, the nanoparticles are concentrated inside the tumor with 40- to 200-fold higher platinum concentration than healthy tissues [26].

ProLindac is a nanopolymer composed of [Pt(R,R-dach)], the active group of oxaliplatin, bound to an hydrophilic biocompatible polymer [hydroxypropylmethacrylamide (HPMA)] to better increase tumor targeting by EPR. The polymer segments are connected by amidomalonate chelating group and a triglycine spacer. The amidomalonate-platinum chelate bond breaks at low pH for releasing platinum complex in the hypoxic tumor microenvironment. ProLindac showed activity against cisplatin resistant cell lines [27]. Clinical trials showed no acute significant adverse effects. ProLindac has currently finished Phase II in combination with paclitaxel in the second-line treatment of pretreated advanced ovarian cancer with 66% of all patients achieving disease stabilization [27].

Despite all advances, platinum complexes still suffer from severe side effects as well as intrinsic or acquired multidrug drug resistance (MDR), limiting its applications. To surpass this, novel strategies are being explored. Some examples include the "rule-breaking" platinum compounds: complexes with glucose ligands, complexes that display trans geometries [28], positively charged molecules, Pt(IV) prodrugs that become reduced to Pt(II) inside the cells, and photoactive molecules, among others [6, 29]. Of those we will highlight three approaches, first the tentative to vectorize Pt(II) to cancer cells through glucose as a ligand. Cancer cells overexpress glucose transporters making them an ideal target for active therapy [29]. Patra and coworkers showed that this is a viable conjugation with increased accumulation of platinum in tumor cells and comparable efficacy *in vivo* with oxaliplatin [29]. Later, Lippard et al. described a Pt(IV)-(D)-1methyltryptophan conjugate coupled with an indoleamine-2,3-dioxygenase (IDO) ligand. IDO is an inhibitory immune checkpoint target that enhances antitumor immune response, thus increasing the efficacy of common chemotherapeutics and radiotherapy. This prodrug killed hormone-dependent, cisplatin resistant, and human ovarian cancer cells, by deregulating the autocrine-signaling loop IDO-AHR-IL6 and paving the way to new platinum immune-chemotherapy [30]. A photoactive platinum(IV) anticancer complex trans-$[Pt(N_3)_2(OH)_2(Py)_2]$ was used in photodynamic therapy. Upon irradiation with blue light, it binds to amino acid residues of thioredoxin, a multifunctional enzyme that regulates gene transcription, redox signaling, and cell growth, inhibiting cell apoptosis, overexpressed in several cancers, leading to an increase oxidative stress persistent for more than 48 h *in vitro*, with a potent antiproliferative activity. The complex might be suitable for treatment of peripheral cancers such as bladder and esophageal [10, 31].

1.2. Ruthenium

Ruthenium complexes are already recognized as an effective alternative to platinum complexes, providing different mechanisms of action, different spectrum of activities, and potential to overcome platinum associated MDR [32]. Ruthenium has numerous properties: (i) they can exist in multiple oxidation states (II, III, and IV), all accessible under physiologic conditions, an advantage in the reducing environment of cancer tissues; (ii) they have the ability to coordinate ligands that can modulate their activity and have the same kinetics of ligand substitution in aqueous medium as that of Pt(II) complexes [33]; (iii) they have the possibility of occupying a large number of spatial positions due to its octahedral coordination geometry allowing to explore more and different ligands compared to platinum complexes; (iv) they reduced toxicity compared to platinum compounds and attributed to their ability to mimic iron binding to serum transferrin [34, 35] with higher selectivity for their targets due to selective uptake by the tumor compared with healthy tissues [36].

In the last year, several ruthenium compounds have been synthetized, and their antiproliferative activities and mechanism of action against several tumors characterized [8, 37–39], where cell membrane changes, cell death due to intrinsic apoptosis pathway and/or autophagic pathway, ROS induction, inhibition of topoisomerase I and II might be the cause of their cytotoxicity/antiproliferative activities [8, 39–44]. KP1019, trans-$[Ru(In)_2Cl_4]$ [InH] (In = indazole), is known to bind transferrin and causes apoptosis through the mitochondrial pathway promoting the formation of ROS [45]. $[Ru(bpy)(phpy)(dppz)]^+$ has found to be very cytotoxic against cancer cell line, the high affinity that presents for DNA leads to damages in the transcription

factor NF-κB [46]. DW1/2 inhibits PI3K and GSK3-β, which leads to apoptosis mediated by the mitochondrial and p53 pathways [34]. Several Ru(II) complexes demonstrate high-binding affinity to DNA [47–49]. Some of these complexes appear to act by intercalation in the tumor cells, although in some cases it has been demonstrated that they can operate by DNA photocleavage [50–52]. Ruthenium complexes with polypyridine ligands such as 2,2-bipyridine (bpy), 1,10-phenanthroline (phen), and 2,2′:6,2″-terpyridine (terpy) ligands have been largely explored as molecular DNA probes due to their photophysical properties and the ability of polypyridyl ligands to intercalate with DNA [35, 38, 53–55]. This type of ligands stabilizes the ruthenium metal ion in the oxidation state (II), resulting in solution-stable complexes of aqueous solution. Polypyridine ligands can confer photoluminescent properties to Ru(II) complexes, through a charge transfer between the metal and the ligand [56].

Cellular uptake of ruthenium complexes may occur through two mechanisms, energy dependent (endocytosis and active transport) and energy independent (facilitated diffusion and passive diffusion) [40]. For example, the complex $[Ru(phen)_2(mitatp)]^{2+}$ exhibited significant antitumor activity against several tumor cells, and flow cytometry experiments showed that the ruthenium compounds penetrate the cell membrane and accumulate in the nucleus, leading to cell cycle arrest and apoptosis [57]. The ruthenium compound $[Ru(DIP)_2(dppz)]^{2+}$ showed cellular uptake through an energy-independent process [58]. Transferrin is used to transport iron centers into the cell, where the cancer cells have a high number of transferrin receptors compared to healthy cells [59]. Ruthenium complexes are transported by transferrin into cells by binding to two ruthenium centers. Upon entry into cells, the complex is released at acidic pH. For example, KP1019 can use iron transport systems to locate itself inside the cell, binding to the DNA with a preference shown for G and A residues [36].

Several other ruthenium(II) metal complexes have been described in the literature that offers the possibility of designing molecules suitable for binding to specific biological targets, due to the fact that they exhibit a wide range of coordination numbers and possible geometries that allow the spatial organization of the different anions and organic ligands (for a review, See [60–64]). Examples with *in vitro* and *in vivo* antitumor activities are ruthenium(II) (η^6-arene) complexes, such as [Ru (η^6-C_6H_6) (dien)] Cl (dien = ethylenediamine), and RAPTA, ruthenium(II)-arene complexes with the monodent ligand PTA (PTA = 1,3,5-triaza-7-phosphoadamantene) [46–48]. Stable bidentate chelating ligands (e.g., dien), more hydrophobic arene ligand (tetrahydroanthracene), and chloride ligand were associated with complexes with increased activity [65]. The RAPTA family comprises a monodent ligand PTA and the η6-arene ligand. Recently, the RAPTA-C complex has been shown to reduce the growth of primary tumors in preclinical models in ovarian and colorectal carcinomas through an antiangiogenic mechanism [66]. RAPTA-C binds selectively to the nucleus of the histone protein in the chromatin, resulting in the chloride binding of the ligands, and the inhibition of moderate growth in primary tumors *in vivo* is translated [67]. Sadler and coworkers studied ruthenium complexes (II)-arene with dien ligands ([Ru (n-6-arene) Cl (dien)] and demonstrated to be stable and soluble in water, exhibiting anticancer activity both *in vitro* and *in vivo*, including activity against cisplatin-resistant cancer cells. The dien ligand was used because of the similarities presented with the ammonium ligands in cisplatin, which are thought to contribute for cytotoxicity, forming a hydrogen bond with the DNA [68].

Of the numerous ruthenium complexes with antitumor action studied, only five Ru(III) complexes have entered clinical trials: trans-[$RuCl_4$ (DMSO) (Im)] [ImH] (NAMI-A, Im = imidazole), KP1019, NKP-1339 (KP1019 sodium salt), KP1339, and Ru(II)-based therapeutic TLD1433 [35, 69]. NAMI-A is an antimetastatic compound that reduces the metastases and prevents the spread of secondary tumors [70, 71], whereas KP1019 is a cytotoxic compound effective against primary tumors [72]. NAMI-A and KP1019 are prodrugs that are activated *in vivo* by reduction to Ru(II) and well tolerated in clinical applications. The exact mode of action of both complexes is not clear, but it is known that they interact with DNA. NAMI-A and KP1019 successfully completed Phase I clinical trials; however, NAMI-A was recently withdrawn after Phase II due to its poor efficacy [69, 73]. In addition, the combination of gemcitabine with NAMI-A allows entry into a new Phase II [70], but the combination was not well tolerated by patients and did not continue to Phase III [73]. KP1019 demonstrated low solubility that limited further development. NKP-1339 is a GRP78-targeted ruthenium-based anticancer compound and administered intravenously with promising results in solid tumors, such as colorectal carcinoma and neuroendocrine tumors [74]. The results obtained so far in clinical trials with some of these Ru(III) drug candidates fostered the increased interest in Ru(II) candidates for cancer therapy [40]. Recently, TLD1433, a mixed ligand Ru(II)-polypyridyl compound, entered Phase I of clinical trials for nonmuscle invasive bladder cancer treatment with photodynamic therapy (PDT) [75].

The interaction between the compounds and the plasma proteins is recognized as a crucial step in the access to bioavailability of metal complexes [32, 76, 77]. Serum albumin is the major protein in blood plasma acting as the carrier and distributor of many drugs because of its ability to bind reversibly to a variety of exogenous compounds [78, 79]. Their binding may increase solubility and prolong the *in vivo* half-life of the compounds, with a specific drug release at the target [77, 79, 80]. The interaction between compounds and proteins is usually analyzed by electronic absorption and fluorescence quenching. As various drugs bind to proteins in plasma, there has been an increasing investigation in the field of plasma protein binding (PPB). Ru(II) compounds bind preferentially to human serum albumin (HSA) and serum transferrin (Tf). These binding affinities showed that HSA appears to be the better partner [81]. KP1019 is known to strongly bind to serum proteins and hamper P-glycoprotein-mediated efflux, making this ruthenium therapeutic attractive for multidrug-resistant tumor therapy [82]. RAPTA-C has shown a binding affinity to thioredoxin reductase and cathepsin B [83].

More recently, nanotechnology has provided numerous nanoplatforms that may act as vehicles for the active and more specific deliver of ruthenium(II) complexes toward cancer cells, namely Ru(II)—selenium nanoparticles, Ru(II)—gold nanomaterials, and Ru(II)—silica composite [39, 78–80]. Recently, Ru(II)-polypyridyl/thiol-selenium nanoparticles were found to be a powerful theranostic system, acting simultaneously as an imaging agent while fostering cancer cell death [84]. Chen and collaborators described a nanoparticle/Ru(II) polypyridyl system that is able to release a DNA-binding agent $[Ru(bpy)_2(H2O)_2]^{2+}$ upon laser irradiation [85]. In this sight, this nanosystem might improve ruthenium complex stability, distribution, and delivery specifically toward cancer cells providing a new avenue as a future therapeutic strategy [86].

1.3. Copper

Copper is an essential element in the organism, important for the function of enzymes and proteins involved in energy metabolism, respiration, and DNA synthesis [87]. This metal acts as a catalytic cofactor in several enzymes and is involved in hemoglobin formation, xenobiotics, catecholamines biosynthesis, collagen crosslinking, and oxidation-reduction reactions in which it reacts with molecular oxygen for the production of free radicals [87]. Copper-dependent enzymes, such as cytochrome C oxidase, superoxide dismutase, ferroxidases, monoamine oxidase, and dopamine b-monooxygenase, are involved in ROS neutralization. In addition, efflux of anticancer drugs such as cisplatin employs specific copper efflux transporters ATP7A and ATP7B, together with multidrug efflux pumps belonging to the ABC superfamily [e.g., P-glycoprotein (Pgp, ABCB1) and multidrug resistance protein 2 (MRP2, ABCC2)] [88, 89].

Copper complexes are the most studied transition metal complexes for their antitumor properties because endogenous metal ions may lead to less systemic toxicity. The properties of the copper complexes are determined by the nature of their ligands, which themselves may exhibit antiproliferative activity [87]. Several Cu(II) complexes with a variety of ligands containing N, S, or O have been developed, demonstrating different mechanisms for their antitumor activity [6, 90, 91]. The ligands neutralize the electrical charge of the copper ion and facilitate the transport of the complex through the cell membrane, interacting noncovalently with proteins or intercalating into the DNA molecule [92]. Copper complexes are capable of inducing DNA breaks through hydrolytic or oxidative cleavages [93–97]. Recently, a copper(II) complex $[Cu(C_{20}H_{22}NO_3)_2]\cdot H_2O$ was synthesized, and its mechanism of action evaluated by spectroscopic methods, showing that the complex binds to calf-thymus DNA through a partial intercalation and presents a static quenching process as binding mechanism. The cytotoxicity evaluation in cancer cell lines showed an enhanced cytotoxicity compared with the Schiff base ligand; thus, a positive synergetic effect may be occurring [98]. Horman et al. developed functionalized Cu(II) cyclen complexes with three (2-anthraquinonyl)methyl substituents that efficiently inhibited DNA and RNA syntheses resulting in high cytotoxicity accompanied by DNA condensation/aggregation phenomena [99]. Sigman et al. reported the first set of copper complexes with phen ligand with good cytotoxic activities [100]. The complex with two phen ligands is capable of cleaving the DNA by binding to the deoxyribose units, acting as a chemical nuclease [101]. Trejo-Solis et al. synthesized a class of Cu(II) complexes having the general formula [Cu (NN) (AA)] NO_3, wherein NN is phen or bipy, and AA is a nitrogen-oxygen donor or oxygen-oxygen donor ligand that is capable of inducing autophagy and programmed cell death cells by activation of ROS and JNK in glioma cells [102]. Another study demonstrated the antitumor properties of phen Cu(II) complexes with different alkyl chains. One of them showed a promising anticancer activity as well as antimetastatic and antiangiogenic potential, evidencing the versatility of Cu(II) complexes for cancer therapy [103].

A complex of Topo-I inhibitors, [Cu (N) L] Cl (N = phen, bipy or 5,50-dimethyl-2,20-bipyridine; L = doubly 5-triphenylphosphonium-methyl)-salicylaldehyde deprotonated hyde-benzoyl hydrazone, exhibits good cytotoxic activity against human lung and prostate adenocarcinoma cell lines [104], with the most active compound of this family being the one containing the fen motif.

Proteasome inhibition is another mechanism by which copper complexes exercise their antitumor activity. For example, Cu(II) complexes containing phen, 8-hydroxyquinolinate, pyrrolidine

dithiocarbamate, or (pyridine-2-ylmethylamino)-methylphenolate have been shown to induce apoptosis by proteasome inhibition [105].

Copper complexes with thiosemicarbazone ligands have antitumor activity by inhibiting enzymatic activity and inducing cell apoptosis [106]. A Cu pro-drug derived from thiosemicarbazone based on the His146 residue in the IB subdomain of palmitic acid (PA)-modified human serum albumin (HSA-PA) was able to kill cancer cell by targeting DNA and proteins. Also, the efficient delivery of the Cu pro-drug was improved when the leaving group was replaced with His146 and coordinated with Cu^{2+} to form the HSA − PA complex. The HSA-PA complex showed better tolerance and a higher drug accumulation in the tumor, a stronger capacity for inhibiting tumor growth, and a lower toxicity in other tissues [107].

Casiopeína IIgly, one of the most promising drugs, shows a strong inhibition of cell proliferation against a glioma C6 cell line, *in vivo* as well as *in vitro*. This drug promotes cell death by an increase of ROS, with the consequence mitochondria damage followed by apoptosis caused through, caspase dependent and caspase independent pathways. Cas IIgly prevents malignant cells to continue with their life cycle, by inhibiting estrogen-mediated G1/S cell cycle progression [108, 109]. Currently, Cas IIIia is in Phase I clinical trials in Mexico, and experimental evidences demonstrated that the main mechanism of action is related to generation of ROS and DNA damage, through intercalation process [110].

Copper complexes are normally water insoluble. Therefore, the use of polymers/nanoparticles with suitable size can increase cellular internalization, distribution, and targeting of tumor cells with reduced toxicity in healthy cells. Intramolecular copper containing amphiphilic hyperbranched polytriazoles (mPEGhb-S-S-PTAs) was synthesized via Cu(I)-catalyzed azide-alkyne cycloaddition (CuAAC) reaction, forming copper-triazole coordination polyprodrugs that were used to delivery copper and for label-free cellular bioimaging, a novel theranostic (diagnostic and therapy simultaneously) application toward cancer therapy [111].

1.4. Vanadium

The major molecular targets for anticancer effects of vanadium compounds are the breakdown of cellular metabolism through the generation of ROS, GSH depletion, changes in cellular organelles, some pathways of signal transduction, and caspases, which can lead to cell cycle arrest and cell death. Pombeiro et al. synthesized two water-soluble heterometallic potassium-dioxidovanadium(V) complexes, with an antiproliferative potential toward human colorectal carcinoma, lung, and breast adenocarcinoma cell lines. They demonstrate that the complex has a very high cytotoxic potential in the HCT116 cell line, a positive trait for future *in vivo* studies [112].

Vanadocene is a metallocene with a metal ion sandwiched between two cyclopentadienyl rings. Vanadocene dichloride, $[VCp_2Cl_2]$, was the first vanadocene that showed interesting results in preclinical studies [113]. This complex showed a strong activity *in vitro* against several tumor cells. In addition, *in vivo* studies demonstrated antitumor properties with vanadocene dichloride [114]. Some vanadocene derivatives present cytotoxic effect against T-lymphocytic leukemia cells, where the mechanism used evolves the DNA damage and p53 activation [115]. On the other hand, vanadocenes are effective agents against human testicular

cell lines [36]. Vanadocenes containing fen ligands are promising anticancer agents, due to their high anticancer activity, solubility, and stability [37]. Currently, there are two complexes under preclinical trial [VCp_2Cl_2] and Metvan, bis(4,7-dimethyl-1,10-phenanthroline) sulfatooxovanadium(IV). Metvan induces cell damage through apoptosis in several cell lines, with a special cytotoxic in ovarian and testicular cancer cell resistant to cisplatin. *In vivo* models, Metvan shows a promising anticancer activity on glioblastoma and breast cancer [116]. Cortizo et al. developed a delivery system of vanadium(IV) with aspirin (VOAspi) functionalized with poly(beta-propiolactone) (PbetaPL) films. VOAspi-PbetaPL film inhibited cell proliferation of UMR106 osteosarcoma cells in a dose-response manner [117].

1.5. Iridium

Iridium complexes are emerging as a class of anticancer agents. Novohradsky et al. studied the mechanisms of new cytotoxic iridium(III) complex in cancer cells. A half-sandwich cyclometallated Ir(III) complex [(η^5-Cp*)(Ir)(7,8-benzoquinoline)Cl] bearing a C^N chelating ligand was designed and studied its uptake in ovarian cancer cells [118]. The temperature dependence and the coincubation with different substrates (such as ouabain, 2-deoxy-D-glucose and oligomycin, verapamil, reversan, and buthionine sulfoximine) indicate that an energy-independent passive diffusion and an energy-dependent transport play a partial role in the complex accumulation. Moreover, the competition experiments with $CuCl_2$ suggested an involvement of Ctr1 pathway in the compound's uptake. The authors highlighted the importance of ATP-dependent processes and transport proteins, such as Na/K-ATPase for accumulation of Ir complexes. The iridium complexes may exert anticancer efficacy through various mechanisms including modulation of cellular redox reactions and inhibition of protein kinases. Recently, the cyclometalated iridium(III) complexes have gained increasing attention in bioimaging and biosensing applications due to their luminescence properties, for example, large Stokes shifts, long-lived luminescence, high quantum yields, and cell permeability [119].

1.6. Titanium

Since the 1970s, when the first titanium complex arises, a series of complexes containing titanium, Ti, as a metal center have been synthesized and characterized, and some of them were shown to possess a wide spectrum of antitumor properties. Indeed, titanium complexes such as titanocene dichloride and octahedral species budotitane are promising anticancer results being translated to (pre)- and clinical trials. Preclinical trials had shown efficacy in a broad of tumors [113, 120]. Budotitane was investigated in Phase I trial, and pharmacokinetic study administered as i.v. infusion twice weekly with a starting dose of 100 mg/m^2. However, no response was observed, but 17 of 18 patients have been resistant as they had received prior chemotherapy [121]. Titanocene dichloride showed promising results in Phase I trials with patients suffering from various cancer types. In one study, 40 patients with refractory solid malignancies the titanocene dichloride revealed a two minor responses (in bladder carcinoma and in nonsmall cell lung cancer), with dose-limiting toxicity side effect was nephrotoxicity [122]. Phase II trials were conducted at 270 mg/m^2 every 3 weeks with 14 patients suffering from metastatic renal-cell carcinoma [123]. However, no significant response was noted, and the effectiveness of the treatment was limited in both cases. The instability under physiological

condition and low solubility in aqueous media were the reasons of low activity in Phase II trials [124]. On the other hand, it was found that titanocene dichloride binds to DNA through the phosphate backbone, inhibiting DNA synthesis and leading to cell death [125]. The binding studies allowed to conclude that the cellular uptake of titanocene dichloride can be mediated by the iron transferrin transporter protein [126].

1.7. Gallium

The biological activity of gallium(III) arises from chemical similarity with iron(III). They have similar ionic radius, ionization potential, and electronic affinity [127]. However, the principal difference is that Ga(III) is nonreducible, whereas Fe(III) is reduced to Fe(II) under physiological condition [63].

Clinical Phase I and Phase II studies were performed on gallium nitrate, gallium chloride, and gallium maltolate. The first-generation gallium nitrate demonstrated, in several clinical trials, efficacy against bladder cancer and urothelium carcinoma, but these studies were discontinued due to ocular toxicity. The most promising results, come from the combination with vinblastine and ifosfamide, in a Phase II trial GA were effective in metastatic urothelial carcinomas at a dose of 300 mg/m^2/24 h for 5 consecutive days. However, the duration of the responses was short at 20 weeks. This was associated with a high toxicity, and 11 of 27 patients had anemia and renal function alteration [128]. Oral gallium chloride seems to potentiate the action of cisplatin and etoposide. Oral gallium maltolate demonstrated higher bioavailability than gallium chloride. Preclinical studies have demonstrated synergy between Ga and paclitaxel [129]/gemcitabine [130]. Currently, two compounds are in clinical trials, gallium tris-8-quinolinolate (KP46) and gallium tris-maltolate. KP46 contains the metal chelating agent 8-hydroxyquinoline and has an inhibitory effect in cell growth proliferation *in vitro* and *in vivo* superior to gallium salt. An oral formulation of KP46 demonstrates a pattern of cytotoxicity with synergism across a broad range of antitumor agents targeting the endoplasmic reticulum in multiple tumor types [131, 132]. Gallium maltolate, (3-hydroxy-2-methyl-4H-pyran-4-onato) gallium, is an oral formulation for therapeutic use. This compound entry in Phase I demonstrated an oral bioavailability of about 27–47%. At doses as high as 3500 mg/day for 28-day cycles, no dose-limiting toxicity or drug-related adverse effects were observed [133]. However, this study was discontinued, and no new results were published. The mechanism of action of gallium(III) has been studied, and Ga^{3+} ions normally compete with Fe^{3+} for binding transferrin. Analyzing the biological pathways of gallium(III), it seems that its mechanism of action is associated with the inhibition of ribonucleotide reductase (RR). The enzyme RR produces during the transition from G1 to S phase of the cell cycle and catalyzes the conversion of ribonucleotides to deoxyribonucleotides [63].

1.8. Osmium

Osmium(II) complexes are the heavier congeners of ruthenium, exhibit slower kinetic than ruthenium, and are substitution-inert (Os(II) and Os(III) complexes). In addition, they offer a more complex interaction with double-helical DNA. However, the reactivity of the Os(II)-arene complexes can be adjusted by the chemistry of the aqueous solution. Sadler et al. synthesized

and developed osmium(II) arene complexes and proved their anticancer properties by systematically varying the chelating ligand in kinetics and thermodynamic reaction of the complexes [134, 135]. These series of N,O-chelates ligands are important choices in the stability and cancer toxicity [134, 136]. DNA-binding studies on a series of complexes of the type osmium(II)-arene have shown that these complexes bind to polymeric DNA, where some coordinate with guanine and others undergo quantitative reaction with DNA [137].

Recent work from Sadler and coworkers showed the distribution of osmium in cancer cells treated with relevant doses of Os^{II} arene azopyridine complex by using X-ray fluorescence nanoprobe. This analysis shows localization of Os in mitochondria and not in nucleus and mobilization of calcium from endoplasmic reticulum [138]. Osmium compounds have been extensively exploited because they are capable to induce the formation of ROS, targeting mitochondria, and oxidize NADH to NAD^+ that lead to interference in the redox signaling pathways in cancer cells and are capable to interfere with cell cycle [69, 139]. In the last year, osmium analogs of the ruthenium anticancer agents, such as RAPTA-C, NAMI-A, and KP1019, have been developed. Therefore, osmium complexes demonstrated a good stability and inertness toward hydrolysis or ligand substitution. These are promising results for a future understanding of the mechanism of action of osmium compounds [134].

1.9. Gold

Gold in its elemental form is stable in an extensive range of conditions. Gold oxidation states range from −1 to +5, but I and III are the most relevant. The coordination geometry of gold(I) complexes is not only generally linear accepting two ligands, but it can also coordinate three (trigonal) or four (tetragonal) ligands. Au(I) prefers to bind with thiolates, cyanides, phosphines, and soft halides [140]. Mainly due to the success of platinum compounds, and that gold(III) is isoelectronic with platinum(II) and forms similar square-planar complexes, a large number of gold(I) and gold(III) compounds have been studied for their anticancer activity [6]. Till now, auranofin [tetra-O-acetyl-b-D-(glucopyranosyl)thio](triethylphosphine) is the only gold compound ever approved. Used since 1985 as oral drug for the treatment of rheumatoid arthritis, its side effects, and restricted efficacy, it is only used for severe cases [141]. Some studies proposed its use as anticancer drug, and it is currently under several Phase I and II clinical trials to treat chronic lymphocytic leukemia (NCT01419691), lung cancer (NCT01737502), and glioblastoma (Glioblastoma).

The mode of action of auranofin is still not clear, and it is thought to be related with inhibition of thioredoxin reductase (TrxR). As gold has a high affinity for thiol and selenol groups, it tends to bind to amino acid residues, forming stable, irreversible adducts. TrxR is an essential enzyme in many cellular processes, mainly in balancing the redox homeostasis, controlling the level of ROS, and preventing DNA damage. As cancer cells tend to overexpress redox enzymes, they are mostly affected by auranofin. Selenoproteins, such as TrxR, when inhibited by auranofin compromise the mitochondria, leading to production of ROS that cause cellular oxidative stress and ultimately intrinsic apoptosis [141]. Several reports show the effect of auranofin against several tumors *in vitro*, including cisplatin resistant tumors [141]. Aurothiomalate is another gold compound, which is currently investigated in Phase I clinical trials to treat patients with advanced nonsmall cell lung cancer (NCT00575393). Its mechanism of action seems to be linked with protein kinase Ciota, which is overexpressed in

nonsmall cell lung cancer, ovarian, and pancreatic cancers, playing a critical role in oncogenesis. Aurothiomalate has been shown to inhibit PKCiota signaling having potent antitumor activity in preclinical studies [142, 143]. Using the same mechanism, aurothioglucose also showed antitumor efficacy *in vitro* against nonsmall cell lung cancer cells [144]. For the cellular uptake, it was proposed that Au(I) enters the cell through albumin bond or through other thiol metabolites [144]. A recent study by Mármol proposes an alkynyl gold(I) complex [Au(C ≡ C-2-NC_5H_4)(PTA)] to treat colorectal carcinoma. In their study, using Caco-2 cells, gold complex enters the mitochondria and disrupts its normal function, triggering the necroptosis. Necrose-inducing compounds are mainly interesting as they are an alternative chemotherapy for apoptosis resistance tumors [145].

1.10. Other complexes

Cobalt complexes have normally two accessible oxidation states. Co(III) is kinetically inert, whereas Co(II) is labile. Some studies demonstrated that Co(III) complexes can act as carriers for selective delivery of drugs [69]. However, when Co(III) is reduced to Co(II), the molecule is released in its active form and can kill cancer cells [146]. Hexacarbonyl dicobalt and alkynes exhibit a promising activity of antitumor activity [147]. The activity is most pronounced when the alkyne is the propargyl ester of aspirin (CoASS), which inhibits the cyclooxygenase enzymes COX-1 and COX-2 [147, 148]. It was shown that CoASS itself inhibits COX-1 and COX-2 more strongly than ASA alone and enhanced the cytotoxicity against breast cancer cell line [148]. The development of new complexes bearing different types of pyrazole-based ligands demonstrated the potential use of these complexes as antiproliferative agents [149].

A new compound $CoCl(H_2O)(phendione)_2][BF_4]$ (phendione = 1,10-phenanthroline-5,6-dione) (TS265) was demonstrated to induce cell cycle arrest in S phase with a subsequent cell death by apoptosis and high cytotoxicity against colorectal carcinoma cell [76]. Fernandes et al. evaluated the efficiency of two metal compounds $[Zn(DION)_2]Cl$ (TS262, DION = 1,10-phenanthroline-5,6-dione) and TS265 and the application of AuNPs as a drug delivery system to improve the anticancer efficacy of these compounds in a new canine mammary tumor (FR37-CMT) [150]. The same group formulated a multifunctional nanovectorization system using gold nanoparticles to enhance cytotoxic of TS265. This nanoformulation efficient delivered the cytotoxic cargo in a controlled selective manner [151]. Two mononuclear Ni^{II} and Mn^{II} compounds with a "scorpionate" type precursor demonstrated to induce damage in ovarian cancer cells through ROS accumulation. In addition, the mononuclear Ni^{II} compound induced mitochondria dysfunction and autophagy cell death [5].

Although the intensive study of transition metals is focused on a specific biomolecular target, some complexes are developed for other purposes. For example, palladium-porphyrin complex (TOOKAD-soluble) acts as a photosensitizer and has progressed to Phase III clinical trial for the photodynamic treatment of prostate cancer (NCT01875393). Phase II clinical trials were evaluated the efficacy and safety of a single dose of the drug and light dosage combination of TOOKAD® Soluble in the focal treatment of patients with localized prostate cancer, 6 months after treatment. Positive results obtained at 6-month negative biopsies were acquire. This complex has a dual role; that is, it provides the ideal photophysical properties to the porphyrin and is inert enough not to be displaced during therapy (**Table 1**) [152].

Name	Description	Target cancer	Approved/clinical trial	Refs.
Platinol	Cisplatin	Metastatic testicular, ovarian and bladder cancers	FDA approval	[153]
Paraplatin	Carboplatin	Advanced ovarian cancer	FDA approval	[153]
Eloxatin	Oxaliplatin	Advanced colorectal cancer in combination with 5-FU and leucovorin	FDA approval	[153]
Aqupla	Nedaplatin	Urological tumors	Approved in Japan	[153]
Lobaplatin	1,2-Diammino-l-methylcyclobutane-platinum(II)-lactate	Inoperable metastatic breast and small cell lung cancer	Approved in China	[153]
Heptaplatin	Cisplatin analogs	Gastric cancer	Approved in Korea	[154]
Picoplatin	2-Methylpyridine analog of cisplatin	Colorectal cancer in combination with 5-FU and leucovorin	Phase II	[11]
Satraplatin	Bis-(acetate)-ammine dichloro-(cyclohexylamine) platinum(IV)	Colorectal cancer in combination with 5-FU and leucovorin/prostate cancer in combination with docetaxel	Phase II/III	[153]
Lipoplatin	Liposomal form of cisplatin	Locally advanced gastric cancer/squamous cell carcinoma of head and neck	Phase II/III	[155]
ProLindac	Oxaliplatin with hydrophilic polymer	Ovarian cancer/head and neck cancer	Phase II/III	[153]
NAMIA-A	$RuCl_4$ (DMSO) (Im)	Metastatic tumor (lung, colorectal, melanoma, ovarian, and pancreatic) in combination with gemcitabine	Phase II	[156]
KP1019	Trans-[Ru(In)$_2$ Cl$_4$] [InH]	Advanced colorectal cancer	Phase I	[157]
NKP-1339	KP1019 sodium salt	Colorectal carcinoma and neuroendocrine tumors	Phase I	[74]
TLD1433	Ru(II)-polypyridyl compound	Nonmuscle invasive bladder cancer treatment with photodynamic therapy (PDT)	Phase I	[75]
Aurothiomalate	Gold compound	Advanced nonsmall cell lung cancer	Phase I	[158]
Auranofin	TetraO-acetyl-b-D-(glucopyranosyl)thio] (triethylphosphine)	Chronic lymphocytic leukemia, lung cancer, and glioblastoma	Phase I/II	[141]
CasII-gly	Casiopeína	Cervical cancer cell	Phase I in Mexico	[159]
KP46	Gallium tris-8-quinolinolate	Solid tumors	Phase I	[132]

Name	Description	Target cancer	Approved/clinical trial	Refs.
TOOKAD® Soluble	Palladium-porphyrin complex	palladium-porphyrin complex	Phase III	[152]
Gallium tris-maltolate	(3-Hydroxy-2-methyl-4H-pyran-4-onato) gallium	Hepatocellular carcinoma	Phase I	[160]

Table 1. Clinical approved/undergoing clinical trials and metal compounds for anticancer therapeutic application.

2. Conclusion

Since the discovery of cisplatin, coordination complexes have been widely used in cancer therapy. Thirty years after its approval as a chemotherapeutic agent by the FDA, cisplatin remains to be one of the best-selling anticancer agents. Thousands of metal compounds have been described since then with only a few passing for clinical trials and even less getting approval. Both the high costs translating a promising drug to the clinic and the focus of pharma to go for new targeted therapies with minimum side effects instead of new cytotoxic agents can explain the current stall in the discovery of novel metal anticancer drugs. Despite the significant efforts in cancer treatment to increase efficacy without promoting side effects and/or resistance by cancer cells, cancer remains one of the major causes of death worldwide. To overcome this fatality, the identification of unique cellular and biochemical features of each tumor and the knowledge of the molecular mechanisms and biological targets of anticancer agents have, together, brought up the necessity for both synthesis and evaluation of new compounds with more promising antiproliferative potential with specific intracellular targets in cancer cells. The success of clinical treatment sparked interest in platinum compounds and other complexes (Ru, Cu, Au, and Co) containing metal ions to be used as anticancer agents. Well-established *in vitro* and *in vivo* studies, such as those shown in this chapter, are extremely important because the interest of a better quality of treatment is increasingly demanded. In addition to the development of more effective drugs, novel nanoscale drug delivery systems showing improved pharmacokinetic and pharmacodynamic properties, such as increased bioavailability, have emerged in the last decade as promising solutions for the required therapeutic efficacy. Combination of new metal complexes with known chemotherapeutic agents already in the market targeting different cellular pathways in a nanostructure may provide a new avenue and the future for cancer therapy.

Acknowledgements

This work was supported by the Unidade de Ciências Biomoleculares Aplicadas-UCIBIO, which is financed by national funds from FCT/MEC (UID/Multi/04378/2013) and cofinanced by the ERDF under the PT2020 Partnership Agreement (POCI-01-0145-FEDER-007728). PP also acknowledges FCT-MCTES grant PD/BD/105734/2014.

Conflict of interest

Authors declare no conflict of interests.

Author details

Pedro Pedrosa†, Andreia Carvalho†, Pedro V. Baptista and Alexandra R. Fernandes*

*Address all correspondence to: ma.fernandes@fct.unl.pt

UCIBIO, Department of Life Sciences, Faculty of Science and Technology, NOVA University of Lisbon, Caparica, Portugal

† Both authors contributed equally

References

[1] Wenjie M, Qiong W. Applications of metal nanoparticles in medicine/metal nanoparticles as anticancer agents. In: Metal Nanoparticles [Internet]. Weinheim: Wiley-Blackwell; 2017. pp. 169-190. Available from: https://onlinelibrary.wiley.com/doi/abs/10.1002/9783527807093.ch7

[2] Pricker SP. Medical uses of gold compounds: Past, present and future. Gold Bulletin [Internet]. 1996;**29**(2):53-60. DOI: 10.1007/BF03215464

[3] Jungwirth U, Kowol CR, Keppler BK, Hartinger CG, Berger W, Heffeter P. Anticancer activity of metal complexes: Involvement of redox processes. Antioxidants & Redox Signaling. Aug 2011;**15**(4):1085-1127

[4] Frezza M, Hindo S, Chen D, Davenport A, Schmitt S, Tomco D, et al. Novel metals and metal complexes as platforms for cancer therapy. Current Pharmaceutical Design. Jun 2010; **16**(16):1813-1825

[5] Das K, Beyene BB, Datta A, Garribba E, Roma-Rodrigues C, Silva A, et al. EPR and electrochemical interpretation of bispyrazolylacetate anchored Ni(ii) and Mn(ii) complexes: Cytotoxicity and anti-proliferative activity towards human cancer cell lines. New Journal of Chemistry [Internet]. 2018;**42**(11):9126-9139. DOI: 10.1039/C8NJ01033A

[6] Maron A, Czerwinska K, Machura B, Raposo L, Roma-Rodrigues C, Fernandes AR, et al. Spectroscopy, electrochemistry and antiproliferative properties of Au(iii), Pt(ii) and Cu(ii) complexes bearing modified 2,2[prime or minute]:6[prime or minute],2[prime or minute][prime or minute]-terpyridine ligands. Dalton Transactions [Internet]. 2018;**47**(18): 6444-6463. DOI: 10.1039/C8DT00558C

[7] Martins M, Baptista PV, Mendo AS, Correia C, Videira P, Rodrigues AS, et al. *In vitro* and *in vivo* biological characterization of the anti-proliferative potential of a cyclic trinuclear organotin(iv) complex. Molecular BioSystems [Internet]. 2016;**12**(3):1015-1023. Available from: http://www.ncbi.nlm.nih.gov/pubmed/26842219

[8] Lenis-rojas OA, Roma-rodrigues C, Fernandes AR, Marques F, Pe D, Ferna A. Dinuclear RuII(bipy)2 derivatives: Structural, biological, and in vivo zebrafish toxicity evaluation. Inorganic Chemistry. 2017;**56**(12):7127-7144

[9] Johnstone TC, Suntharalingam K, Lippard SJ. The next generation of platinum drugs: Targeted Pt(II) agents, nanoparticle delivery, and Pt(IV) prodrugs. Chemical Reviews [Internet]. Mar 9, 2016;**116**(5):3436-3486. DOI: 10.1021/acs.chemrev.5b00597

[10] Johnstone TC, Park GY, Lippard SJ. Understanding and improving platinum anticancer drugs—Phenanthriplatin. Anticancer Research. Jan 2014;**34**(1):471-476

[11] Wheate NJ, Walker S, Craig GE, Oun R. The status of platinum anticancer drugs in the clinic and in clinical trials. Dalton Transactions. Sep 2010;**39**(35):8113-8127

[12] Ndagi U, Mhlongo N, Soliman ME. Metal complexes in cancer therapy—An update from drug design perspective. Drug Design, Development and Therapy. 2017;**11**:599-616

[13] Johnstone TC, Suntharalingam K, Lippard SJ. Third row transition metals for the treatment of cancer. Philosophical Transactions of The Royal Society A Mathematical Physical and Engineering Sciences. Mar 2015;**373**(2037):20140185

[14] Shen D-W, Pouliot LM, Hall MD, Gottesman MM. Cisplatin resistance: A cellular self-defense mechanism resulting from multiple epigenetic and genetic changes. Pharmacological Reviews. Jul 2012;**64**(3):706-721

[15] Crul M, Schellens JHM, Beijnen JH, Maliepaard M. Cisplatin resistance and DNA repair. Cancer Treatment Reviews [Internet]. 1997;**23**(5):341-366. Available from: http://www.sciencedirect.com/science/article/pii/S0305737297900323

[16] Chen HHW, Kuo MT. Role of glutathione in the regulation of cisplatin resistance in cancer chemotherapy. Metal-Based Drugs [Internet]. Sep 14, 2010;**2010**:430939. Available from: http://www.ncbi.nlm.nih.gov/pmc/articles/PMC2946579/

[17] Shanta D, Lippard SJ. Current status and mechanism of action of platinum-based anticancer drugs. In: Bioinorganic Medicinal Chemistry [Internet]. Weinheim: Wiley-Blackwell; 2011. pp. 79-95. Available from: https://onlinelibrary.wiley.com/doi/abs/10.1002/9783527633104.ch3

[18] Hall MD, Amjadi S, Zhang M, Beale PJ, Hambley TW. The mechanism of action of platinum (IV) complexes in ovarian cancer cell lines. Journal of Inorganic Biochemistry [Internet]. 2004;**98**(10):1614-1624. Available from: http://www.sciencedirect.com/science/article/pii/S0162013404001916

[19] Sousa de GF, Wlodarczyk SR, Monteiro G. Carboplatin: Molecular mechanisms of action associated with chemoresistance. Brazilian Journal of Pharmaceutical Sciences [Internet]. 2014;**50**:693-701. Available from: http://www.scielo.br/scielo.php?script=sci_arttext&pid=S1984-82502014000400693&nrm=iso

[20] Nakamura T, Ueda T, Oishi M, Nakanishi H, Fujihara A, Naya Y, et al. Salvage combined chemotherapy with paclitaxel, ifosfamide and nedaplatin for patients with advanced germ cell tumors. International Journal of Urology. Mar 2015;**22**(3):288-293

[21] McKeage MJ. Lobaplatin: A new antitumour platinum drug. Expert Opinion on Investigational Drugs [Internet]. Jan 1, 2001;**10**(1):119-128. DOI: 10.1517/13543784.10.1.119

[22] Peng Y, Liu Y-E, REN X-C, Chen X-J, Su H-L, Zong J, et al. A phase I clinical trial of dose escalation of lobaplatin in combination with fixed-dose docetaxel for the treatment of human solid tumours that had progressed following chemotherapy. Oncology letters [Internet]. Jan 5, 2015;**9**(1):67-74. Available from: http://www.ncbi.nlm.nih.gov/pmc/articles/PMC4246893/

[23] Sternberg CN, Whelan P, Hetherington J, Paluchowska B, Slee PHTJ, Vekemans K, et al. Phase III trial of satraplatin, an oral platinum plus prednisone vs. prednisone alone in patients with hormone-refractory prostate cancer. Oncology. 2005;**68**(1):2-9

[24] Hamilton G, Olszewski U. Picoplatin pharmacokinetics and chemotherapy of non-small cell lung cancer. Expert Opinion on Drug Metabolism & Toxicology [Internet]. Oct 1, 2013;**9**(10):1381-1390. DOI: 10.1517/17425255.2013.815724

[25] Eckardt JR, Bentsion DL, Lipatov ON, Polyakov IS, Mackintosh FR, Karlin DA, et al. Phase II study of picoplatin as second-line therapy for patients with small-cell lung cancer. Journal of Clinical Oncology. Apr 2009;**27**(12):2046-2051

[26] Boulikas T. Clinical overview on lipoplatin: A successful liposomal formulation of cisplatin. Expert Opinion on Investigational Drugs. Aug 2009;**18**(8):1197-1218

[27] Nowotnik DP, Cvitkovic E. ProLindac™ (AP5346): A review of the development of an HPMA DACH platinum polymer therapeutic. Advanced Drug Delivery Reviews [Internet]. 2009;**61**(13):1214-1219. DOI: 10.1016/j.addr.2009.06.004

[28] Silva J, Sebastião A, Videira PA, Lasri J, Januário A, Pombeiro AJL, et al. Characterization of the antiproliferative potential and biological targets of a trans ketoimine platinum complex. Inorganica Chimica Acta [Internet]. 2014;**423**:156-167. DOI: 10.1016/j.ica.2014.07.067

[29] Patra M, Johnstone TC, Suntharalingam K, Lippard SJ. A potent glucose-platinum conjugate exploits glucose transporters and preferentially accumulates in cancer cells. Angewandte Chemie (International Ed. in English). Feb 2016;**55**(7):2550-2554

[30] Awuah SG, Zheng Y-R, Bruno PM, Hemann MT, Lippard SJ. A Pt(IV) pro-drug preferentially targets indoleamine-2,3-dioxygenase, providing enhanced ovarian cancer immunochemotherapy. Journal of the American Chemical Society [Internet]. Dec 2, 2015;**137**(47): 14854-14857. DOI: 10.1021/jacs.5b10182

[31] Du J, Wei Y, Zhao Y, Xu F, Wang Y, Zheng W, et al. A photoactive platinum(IV) anticancer complex inhibits thioredoxin–Thioredoxin reductase system activity by induced oxidization of the protein. Inorganic Chemistry [Internet]. May 7, 2018;**57**(9):5575-5584. DOI: 10.1021/acs.inorgchem.8b00529

[32] Demoro B, Almeida R, Marques F, Matos C, Otero L, Pessoa C, et al. Screening organometallic binuclear thiosemicarbazone ruthenium complexes as potential anti-tumour agents: Cytotoxic activity and human serum albumin binding mechanism. Dalton Transactions. 2013;**42**:7131-7146

[33] Muhammad N, Guo Z. Metal-based anticancer chemotherapeutic agents. Current Opinion in Chemical Biology [Internet]. 2014;**19**(1):144-153. DOI: 10.1016/j.cbpa.2014.02.003

[34] Bergamo A, Gaiddon C, Schellens JHM, Beijnen JH, Sava G. Approaching tumour therapy beyond platinum drugs: Status of the art and perspectives of ruthenium drug candidates. Journal of Inorganic Biochemistry [Internet]. 2012;**106**(1):90-99. DOI: 10.1016/j.jinorgbio.2011.09.030

[35] Motswainyana WM, Ajibade PA. Anticancer activities of mononuclear ruthenium(II) coordination complexes. Advances in Chemistry. 2015;**2015**:21

[36] Clarke MJ, Zhu F, Frasca DR. Non-platinum chemotherapeutic metallopharmaceuticals. Chemical Reviews. Sep 1999;**99**(9):2511-2534

[37] Côrte-Real L, Mendes F, Coimbra J, Morais TS, Tomaz AI, Valente A, et al. Anticancer activity of structurally related ruthenium(II) cyclopentadienyl complexes. Journal of Biological Inorganic Chemistry. 2014;**19**(6):853-867

[38] Chen J, Li G, Peng F, Jie X, Dongye G, Zhong Y, et al. Investigation of inducing apoptosis in human lung cancer A549 cells and related mechanism of a ruthenium(II) polypyridyl complex. Inorganic Chemistry Communications [Internet]. 2016;**69**:35-39. Available from: http://linkinghub.elsevier.com/retrieve/pii/S1387700316301228

[39] Lenis-Rojas OA, Fernandes AR, Roma-Rodrigues C, Baptista PV, Marques F, Pérez-Fernández D, et al. Heteroleptic mononuclear compounds of ruthenium(II): Synthesis, structural analyses, in vitro antitumor activity and in vivo toxicity on zebrafish embryos. Dalton Transactions [Internet]. 2016;**45**(47):19127-19140. Available from: http://xlink.rsc.org/?DOI=C6DT03591D

[40] Zeng L, Gupta P, Chen Y, Wang E, Ji L, Chao H, et al. The development of anticancer ruthenium(ii) complexes: From single molecule compounds to nanomaterials. Chemical Society Reviews [Internet]. 2017;**46**(19):5771-5804. DOI: 10.1039/C7CS00195A

[41] Thota S, Vallala S, Yerra R, Rodrigues DA, Raghavendra NM, Barreiro EJ. Synthesis, characterization, DNA binding, DNA cleavage, protein binding and cytotoxic activities of Ru(II) complexes. International Journal of Biological Macromolecules [Internet]. 2016;**82**:663-670. Available from: http://www.sciencedirect.com/science/article/pii/S0141813015006601

[42] Ratanaphan A, Nhukeaw T, Hongthong K, Dyson PJ. Differential cytotoxicity, cellular uptake, apoptosis and inhibition of BRCA1 expression of BRCA1-defective and sporadic breast cancer cells induced by an anticancer ruthenium(II)-arene compound, RAPTA-EA1. Anti-Cancer Agents in Medicinal Chemistry. 2017;**17**(2):212-220

[43] Popolin CP, Reis JPB, Becceneri AB, Graminha AE, Almeida MAP, Correa RS, et al. Cytotoxicity and anti-tumor effects of new ruthenium complexes on triple negative breast cancer cells. PLoS One. 2017;**12**(9):e0183275

[44] Grozav A, Balacescu O, Balacescu L, Cheminel T, Berindan-Neagoe I, Therrien B. Synthesis, anticancer activity, and genome profiling of thiazolo arene ruthenium complexes. Journal of Medicinal Chemistry [Internet]. Nov 12, 2015;**58**(21):8475-8490. DOI: 10.1021/acs.jmedchem.5b00855

[45] Li W, Jiang G-B, Yao J-H, Wang X-Z, Wang J, Han B-J, et al. Ruthenium(II) complexes: DNA-binding, cytotoxicity, apoptosis, cellular localization, cell cycle arrest, reactive oxygen species, mitochondrial membrane potential and western blot analysis. Journal of Photochemistry and Photobiology. B. Nov 2014;**140**:94-104

[46] Huang H, Zhang P, Yu B, Chen Y, Wang J, Ji L, et al. Targeting nucleus DNA with a cyclometalated dipyridophenazineruthenium(II) complex. Journal of Medicinal Chemistry [Internet]. Nov 13, 2014;**57**(21):8971-8983. DOI: 10.1021/jm501095r

[47] Putta VR, Chintakuntla N, Mallepally RR, Yaswanth VVN, Prakasham RS, Surya SS. Synthesis and evaluation of in vitro DNA/protein binding affinity, antimicrobial, antioxidant and antitumor activity of mononuclear Ru(II) mixed polypyridyl complexes. Journal of Fluorescence. 2015;**26**(1):225-240

[48] Busto N, Valladolid J, Martínez-Alonso M, Lozano HJ, Jalón FA, Manzano BR, et al. Anticancer activity and DNA binding of a bifunctional Ru(II) arene aqua-complex with the 2,4-diamino-6-(2-pyridyl)-1,3,5-triazine ligand. Inorganic Chemistry [Internet]. Sep 3, 2013;**52**(17):9962-9974. DOI: 10.1021/ic401197a

[49] Su W, Qian Q, Li P, Lei X, Xiao Q, Huang S, et al. Synthesis, characterization, and anticancer activity of a series of ketone-N4-substituted thiosemicarbazones and their ruthenium(II) arene complexes. Inorganic Chemistry [Internet]. Nov 4, 2013;**52**(21):12440-12449. DOI: 10.1021/ic401362s

[50] Liu Y, Li Z, Liang C, Yao J-H, Huang H-L. Cytotoxicity, apoptosis, cellular uptake, cell cycle arrest, photocleavage, and antioxidant activity of 1, 10-phenanthroline ruthenium(II) complexes 1. DNA and Cell Biology. 2011;**30**(10):839-848

[51] Wachter E, Heidary DK, Howerton BS, Parkin S, Glazer EC. Light-activated ruthenium complexes photobind DNA and are cytotoxic in the photodynamic therapy window. Chemical Communications. 2012;**48**:9649-9651

[52] Qian C, Wang J, Song C, Wang L, Ji L, Chao H. The induction of mitochondria-mediated apoptosis in cancer cells by ruthenium(II) asymmetric complexes. The Royal Society of Chemistry. 2013;**5**:844-854

[53] Han W, Dyson PJ. Classical and non-classical ruthenium-based anticancer drugs: Towards targeted chemotherapy. European Journal of Inorganic Chemistry. 2006;**20**:4003-4018

[54] Reddy MR, Reddy VP, Kumar PY, Srishailam A, Nambigari N, Satyanarayana S. Synthesis, characterization, DNA binding, light switch "On and Off", docking studies and cytotoxicity, of ruthenium(II) and cobalt(III) polypyridyl complexes. Journal of Fluorescence. 2014;**24**:803-817

[55] Brabec V, Nováková O. DNA binding mode of ruthenium complexes and relationship to tumor cell toxicity. Drug Resistance Updates. 2006;**9**:111-122

[56] Medici S, Peana M, Marina V, Lachowicz JI, Crisponi G, Antonietta M. Noble metals in medicine: Latest advances. Coordination Chemistry Reviews [Internet]. 2014;1-22. DOI: 10.1016/j.ccr.2014.08.002

[57] Yu H-J, Chen Y, Yu L, Hao Z, Zhou L. Synthesis, visible light photocleavage, antiproliferative and cellular uptake properties of ruthenium complex [Ru(phen)2(mitatp)]$^{2+}$. European Journal of Medicinal Chemistry. Sep 2012;**55**:146-154

[58] Puckett CA, Barton JK. Mechanism of cellular uptake of a ruthenium polypyridyl complex. Biochemistry. Nov 2008;**47**(45):11711-11716

[59] Allardyce CS, Dyson PJ. Ruthenium in medicine: Current clinical uses and future prospects. Platinum Metals Review. 2001;**45**(2):62-69

[60] Alama A, Tasso B, Novelli F, Sparatore F. Organometallic compounds in oncology: Implications of novel organotins as antitumor agents. Drug Discovery Today. 2009;**14**:500-507

[61] Martins P, Marques M, Coito L, Pombeiro AJL, Baptista PV, Fernandes AR. Organometallic compounds in cancer therapy: Past lessons and future directions. Anti-Cancer Agents in Medicinal Chemistry [Internet]. 2014;**14**(9):1199-212. Available from: http://www.ncbi.nlm.nih.gov/pubmed/25173559

[62] Han W, Casini A, Sava G, Dyson PJ. Organometallic ruthenium-based antitumor compounds with novel modes of action. Journal of Organometallic Chemistry [Internet]. 2011; **696**(5):989-998. DOI: 10.1016/j.jorganchem.2010.11.009

[63] Van Rijt SH, Sadler PJ. Current applications and future potential for bioinorganic chemistry in the development of anticancer drugs. Drug Discovery Today. 2009;**14**(December): 1089-1097

[64] Sadler PJ, Habtemariam A, Melchart M, Fernandez R, Parsons S, Oswald IDH, et al. Structure–activity relationships for cytotoxic ruthenium(II) arene complexes containing N,N–, N,O–, and O,O– chelating ligands. Journal of Medicinal Chemistry. 2006;49:6858-6868

[65] Kostova I. Ruthenium complexes as anticancer agents. Current Medicinal Chemistry. 2006;**13**:1085-1107

[66] Weiss A, Berndsen RH, Dubois M, Muller C, Schibli R, Griffioen A, et al. In vivo anti-tumor activity of the organometallic ruthenium(II)-arene complex [Ru(h6-p-cymene)-Cl2(pta)] (RAPTA-C) in human ovarian and colorectal carcinomas. Chemical Science. 2014;**5**:4742-4748

[67] Adhireksan Z, Davey GE, Campomanes P, Groessl M, Clavel CM, Yu H, et al. Ligand substitutions between ruthenium-cymene compounds can control protein versus DNA targeting and anticancer activity. Nature Communications. Mar 2014;**5**:3462

[68] Morris RRE, Aird RE, del Socorro MP, Chen H, Cummings J, Hughes ND, et al. Inhibition of cancer cell growth by ruthenium(II) arene complexes. Journal of Medicinal Chemistry. 2001;**44**(22):3616-3621

[69] Zhang P, Sadler PJ. Redox-active metal complexes for anticancer therapy. European Journal of Inorganic Chemistry. 2017;**2017**(12):1541-1548

[70] Gransbury GK, Kappen P, Glover CJ, Hughes JN, Levina A, Lay PA, et al. Comparison of KP1019 and NAMI-A in tumour-mimetic environments. Metallomics. 2016;**8**:762-773. DOI: 10.1039/C6MT00145A

[71] Clavel CM, Paunescu E, Nowak-sliwinska P, Griffioen AW, Scopelliti R, Dyson PJ. Modulating the anticancer activity of ruthenium(II)-arene complexes. Journal of Medicinal Chemistry. 2015;**58**(8):3356-3365

[72] Bergamo A, Masi A, Jakupec MA, Keppler BK, Sava G. Inhibitory effects of the ruthenium complex KP1019 in models of mammary cancer cell migration and invasion. Metal-Based Drugs. 2009;**2009**:681270

[73] Leijen S, Burgers SA, Baas P, Pluim D, Tibben M. Phase I/II study with ruthenium compound NAMI-A and gemcitabine in patients with non-small cell lung cancer after first line therapy. Investigational New Drugs. 2015;**33**:201-214

[74] Flocke LS, Trondl R, Jakupec MA. Molecular mode of action of NKP-1339—a clinically investigated ruthenium-based drug—involves ER- and ROS-related effects in colon carcinoma cell lines. Investigational New Drugs [Internet]. 2016;**34**:261-268. DOI: 10.1007/s10637-016-0337-8

[75] Abid M, Shamsi F, Azam A. Ruthenium complexes: An emerging ground to the development of metallopharmaceuticals for cancer therapy. Mini-Reviews in Medicinal Chemistry [Internet]. 2016;**16**(10):772-786. Available from: http://www.ncbi.nlm.nih.gov/pubmed/26423699

[76] Luis D V, Ana S, Tomaz I, De Almeida RFM, Silva TFS, Borralho PM, et al. Insights into the mechanisms underlying the antiproliferative potential of a Co(II) coordination compound bearing 1, 10-phenanthroline-5, 6-dione: DNA and protein interaction studies. Journal of Biological Inorganic Chemistry 2014;**19**(6):787-803

[77] Pessoa JC, Tomaz I. Transport of therapeutic vanadium and ruthenium complexes by blood plasma components. Clujul Medical. 2010;**1019**(17):3701-3738

[78] Tian Z, Zang F, Luo W, Zhao Z, Wang Y, Xu X, et al. Spectroscopic study on the interaction between mononaphthalimide spermidine (MINS) and bovine serum albumin (BSA). Journal of Photochemistry and Photobiology B: Biology [Internet]. 2015;**142**:103-109. DOI: 10.1016/j.jphotobiol.2014.10.013

[79] Li D, Zhu M, Xu C, Ji B. Characterization of the baicalein e bovine serum albumin complex without or with Cu 2 þ or Fe 3 þ by spectroscopic approaches. European Journal of Medicinal Chemistry [Internet]. 2011;**46**(2):588-599. DOI: 10.1016/j.ejmech.2010.11.038

[80] Topala T, Bodoki A, Oprean L, Oprean R. Bovine serum albumin interactions with metal complexes. Clujul Medical. 2014;**87**(4):215-219

[81] Canovic P, Simovic AR, Radisavljevic S, Bratsos I, Demitri N, Mitrovic M, et al. Impact of aromaticity on anticancer activity of polypyridyl ruthenium(II) complexes: Synthesis, structure, DNA/protein binding, lipophilicity and anticancer activity. Journal of Biological Inorganic Chemistry. Oct 2017;**22**(7):1007-1028

[82] Heffeter P, Bock K, Atil B, Reza Hoda MA, Korner W, Bartel C, et al. Intracellular protein binding patterns of the anticancer ruthenium drugs KP1019 and KP1339. Journal of Biological Inorganic Chemistry. Jun 2010;**15**(5):737-748

[83] Casini A, Gabbiani C, Sorrentino F, Rigobello MP, Bindoli A, Geldbach TJ, et al. Emerging protein targets for anticancer metallodrugs: Inhibition of thioredoxin reductase and cathepsin B by antitumor ruthenium(II)-arene compounds. Journal of Medicinal Chemistry. 2008;**51**(Ii):6773-6781

[84] Sun D, Liu Y, Yu Q, Zhou Y, Zhang R, Chen X, et al. The effects of luminescent ruthenium(II) polypyridyl functionalized selenium nanoparticles on bFGF-induced angiogenesis and AKT/ERK signaling. Biomaterials. Jan 2013;**34**(1):171-180

[85] Chen Y, Jiang G, Zhou Q, Zhang Y, Li K, Zheng Y, et al. An upconversion nanoparticle/Ru(ii) polypyridyl complex assembly for NIR-activated release of a DNA covalent-binding agent. RSC Advances [Internet]. 2016;**6**(28):23804-23808. DOI: 10.1039/C6RA03396B

[86] Coimbra J, Mota C, Santos S, Baptista PV, Fernandes AR. Inorganic compounds going NANO. Annals of Medicinal Chemistry and Research. 2015;**2**(1):1010

[87] Marzano C, Pellei M, Tisato F, Santini C. Copper complexes as anticancer agents. Anti-Cancer Agents in Medicinal Chemistry. Feb 2009;**9**(2):185-211

[88] Samimi G, Katano K, Holzer AK, Safaei R, Howell SB. Modulation of the cellular pharmacology of cisplatin and its analogs by the copper exporters ATP7A and ATP7B. Molecular Pharmacology. Jul 2004;**66**(1):25-32

[89] Leslie EM, Deeley RG, Cole SPC. Multidrug resistance proteins: Role of P-glycoprotein, MRP1, MRP2, and BCRP (ABCG2) in tissue defense. Toxicology and Applied Pharmacology [Internet]. 2005;**204**(3):216-237. Available from: http://www.sciencedirect.com/science/article/pii/S0041008X0400482X

[90] Sutradhar M, Rajeshwari -, Roy Barman T, Fernandes AR, Paradinha F, Roma-Rodrigues C, et al. Mixed ligand aroylhydrazone and N-donor heterocyclic Lewis base Cu(II) complexes as potential antiproliferative agents. Journal of Inorganic Biochemistry. Oct 2017;**175**:267-275

[91] Czerwinska K, Machura B, Kula S, Krompiec S, Erfurt K, Roma-Rodrigues C, et al. Copper(ii) complexes of functionalized 2,2[prime or minute]:6[prime or minute],2[prime or minute][prime or minute]-terpyridines and 2,6-di(thiazol-2-yl)pyridine: Structure, spectroscopy, cytotoxicity and catalytic activity. Dalton Transactions [Internet]. 2017;**46**(29):9591-9604. DOI: 10.1039/C7DT01244F

[92] Iakovidis I, Delimaris I, Piperakis SM. Copper and its complexes in medicine: A biochemical approach. Molecular Biology International. 2011;**2011**:1-13

[93] Rajendiran V, Karthik R, Palaniandavar M, Stoeckli-Evans H, Periasamy VS, Akbarsha MA, et al. Mixed-ligand copper(II)-phenolate complexes: Effect of coligand on enhanced DNA and protein binding, DNA cleavage, and anticancer activity. Inorganic Chemistry [Internet]. 2007;**46**(20):8208-8221. Available from: http://www.ncbi.nlm.nih.gov/pubmed/17784750

[94] Li X-W, Zheng Y-J, Li Y-T, Wu Z-Y, Yan C-W. Synthesis and structure of new bicopper(II) complexes bridged by N-(2-aminopropyl)-N′-(2-oxidophenyl)oxamide: The effects of terminal ligands on structures, anticancer activities and DNA-binding properties. European Journal of Medicinal Chemistry. Sep 2011;**46**(9):3851-3857

[95] Chen Q-Y, Fu H-J, Zhu W-H, Qi Y, Ma Z-P, Zhao K-D, et al. Interaction with DNA and different effect on the nucleus of cancer cells for copper(II) complexes of N-benzyl di(pyridylmethyl)amine. Dalton Transactions. May 2011;**40**(17):4414-4420

[96] Gup R, Gokce C, Akturk S. Copper(II) complexes with 4-hydroxyacetophenone-derived acylhydrazones: Synthesis, characterization, DNA binding and cleavage properties. Spectrochimica Acta. Part A, Molecular and Biomolecular Spectroscopy. Jan 2015;**134**: 484-492

[97] Barilli A, Atzeri C, Bassanetti I, Ingoglia F, Dall'Asta V, Bussolati O, et al. Oxidative stress induced by copper and iron complexes with 8-hydroxyquinoline derivatives causes paraptotic death of HeLa cancer cells. Molecular Pharmaceutics. Apr 2014;**11**(4):1151-1163

[98] Shokohi-Pour Z, Chiniforoshan H, Momtazi-Borojeni AA, Notash B. A novel Schiff base derived from the gabapentin drug and copper(II) complex: Synthesis, characterization, interaction with DNA/protein and cytotoxic activity. Journal of Photochemistry and Photobiology B: Biology [Internet]. 2016;**162**:34-44. DOI: 10.1016/j.jphotobiol.2016.06.022

[99] Hormann J, Malina J, Lemke O, Hülsey MJ, Wedepohl S, Potthoff J, et al. Multiply intercalator-substituted Cu(II) cyclen complexes as DNA condensers and DNA/RNA synthesis inhibitors. Inorganic Chemistry. 2018;**57**(9):5004-5012

[100] Sigman DS, Graham DR, D'Aurora V, Stern AM. Oxygen-dependent cleavage of DNA by the 1,10-phenanthroline . cuprous complex. Inhibition of *Escherichia coli* DNA polymerase I. The Journal of Biological Chemistry. Dec 1979;**254**(24):12269-12272

[101] Pivetta T, Cannas MD, Demartin F, Castellano C, Vascellari S, Verani G, et al. Synthesis, structural characterization, formation constants and in vitro cytotoxicity of phenanthroline and imidazolidine-2-thione copper(II) complexes. Journal of Inorganic Biochemistry. Mar 2011;**105**(3):329-338

[102] Trejo-Solis C, Jimenez-Farfan D, Rodriguez-Enriquez S, Fernandez-Valverde F, Cruz-Salgado A, Ruiz-Azuara L, et al. Copper compound induces autophagy and apoptosis of glioma cells by reactive oxygen species and JNK activation. BMC Cancer. Apr 2012;**12**:156

[103] Shi X, Chen Z, Wang Y, Guo Z, Wang X. Hypotoxic copper complexes with potent anti-metastatic and anti-angiogenic activities against cancer cells. Dalton Transactions. 2018; **47**(14):5049-5054

[104] Chew ST, Lo KM, Lee SK, Heng MP, Teoh WY, Sim KS, et al. Copper complexes with phosphonium containing hydrazone ligand: Topoisomerase inhibition and cytotoxicity study. European Journal of Medicinal Chemistry. Apr 2014;**76**:397-407

[105] Hindo SS, Frezza M, Tomco D, Heeg MJ, Hryhorczuk L, McGarvey BR, et al. Metals in anticancer therapy: Copper(II) complexes as inhibitors of the 20S proteasome. European Journal of Medicinal Chemistry [Internet]. 2009;**44**(11):4353-4361. Available from: http://www.sciencedirect.com/science/article/pii/S0223523409003122

[106] Tisato F, Marzano C, Porchia M, Pellei M, Santini C. Copper in diseases and treatments, and copper-based anticancer strategies. Medicinal Research Reviews. Jul 2010;**30**(4): 708-749

[107] Qi J, Zhang Y, Gou Y, Zhang Z, Zhou Z, Wu X, et al. Developing an anticancer copper(II) pro-drug based on the His146 residue of the human serum albumin carrier IIA subdomain. Molecular Pharmaceutics. 2016;**13**(5):1501-1507

[108] Hernandez-Esquivel L, Marin-Hernandez A, Pavon N, Carvajal K, Moreno-Sanchez R. Cardiotoxicity of copper-based antineoplastic drugs casiopeinas is related to inhibition of energy metabolism. Toxicology and Applied Pharmacology. Apr 2006;**212**(1):79-88

[109] Alemon-Medina R, Brena-Valle M, Munoz-Sanchez JL, Gracia-Mora MI, Ruiz-Azuara L. Induction of oxidative damage by copper-based antineoplastic drugs (Casiopeinas). Cancer Chemotherapy and Pharmacology. Jul 2007;**60**(2):219-228

[110] Ruiz-Azuara L, Bastian G, Bravo-Gómez ME, Cañas RC, Flores-Alamo M, Fuentes I, et al. Abstract CT408: Phase I study of one mixed chelates copper(II) compound, Casiopeina CasIIIia with antitumor activity and its mechanism of action. Cancer Research [Internet]. 2014;**74**(19 Supplement): CT408-CT408. Available from: http://cancerres.aacrjournals.org/content/74/19_Supplement/CT408

[111] Ban Q, Du J, Sun W, Chen J, Wu S, Kong J. Intramolecular copper-containing hyperbranched polytriazole assemblies for label-free cellular bioimaging and redox-triggered copper complex delivery. 2018;**1800171**:1-6

[112] Sutradhar M, Fernandes AR, Silva J, Mahmudov KT, da Silva MFC, Pombeiro AJL. Water soluble heterometallic potassium-dioxidovanadium(V) complexes as potential antiproliferative agents. Journal of Inorganic Biochemistry [Internet]. 2016;**155**:17-25. DOI: 10.1016/j.jinorgbio.2015.11.010

[113] Harding MM, Mokdsi G. Antitumour metallocenes: Structure-activity studies and interactions with biomolecules. Current Medicinal Chemistry. Dec 2000;**7**(12):1289-1303

[114] Havelek R, Siman P, Cmielova J, Stoklasova A, Vavrova J, Vinklarek J, et al. Differences in vanadocene dichloride and cisplatin effect on MOLT-4 leukemia and human peripheral blood mononuclear cells. Medicinal Chemistry. Jul 2012;**8**(4):615-621

[115] Aubrecht J, Narla RK, Ghosh P, Stanek J, Uckun FM. Molecular genotoxicity profiles of apoptosis-inducing vanadocene complexes. Toxicology and Applied Pharmacology [Internet]. 1999;**154**(3):228-235. Available from: http://www.sciencedirect.com/science/article/pii/S0041008X98985921

[116] Narla RK, Dong Y, Klis D, Uckun FM. Bis(4,7-dimethyl-1,10-phenanthroline) sulfatooxovanadium(I.V.) as a novel antileukemic agent with matrix metalloproteinase inhibitory activity. Clinical Cancer Research. Apr 2001;**7**(4):1094-1101

[117] Cortizo MS, Alessandrini JL, Etcheverr SB, Cortizo AM. A vanadium/aspirin complex controlled release using a poly(beta-propiolactone) film. Effects on osteosarcoma cells. Journal of Biomaterials Science. Polymer Edition. 2001;**12**(9):945-959

[118] Novohradsky V, Liu Z, Vojtiskova M, Sadler PJ, Brabec V, Kasparkova J. Mechanism of cellular accumulation of an iridium(III) pentamethylcyclopentadienyl anticancer complex containing a C,N-chelating ligand. Metallomics. Mar 2014;**6**(3):682-690

[119] Lo KK-W, Chan BT-N, Liu H-W, Zhang KY, Li SP-Y, Tang TS-M. Cyclometalated iridium(iii) polypyridine dibenzocyclooctyne complexes as the first phosphorescent bioorthogonal probes. Chemical Communications [Internet]. 2013;**49**(39):4271-4273. DOI: 10.1039/C2CC36907A

[120] Caruso F, Rossi M. Antitumor titanium compounds. Mini Reviews in Medicinal Chemistry. Jan 2004;**4**(1):49-60

[121] Schilling T, Keppler KB, Heim ME, Niebch G, Dietzfelbinger H, Rastetter J, et al. Clinical phase I and pharmacokinetic trial of the new titanium complex budotitane. Investigational New Drugs. 1996;**13**(4):327-332

[122] Korfel A, Scheulen ME, Schmoll HJ, Grundel O, Harstrick A, Knoche M, et al. Phase I clinical and pharmacokinetic study of titanocene dichloride in adults with advanced solid tumors. Clinical Cancer Research. Nov 1998;**4**(11):2701-2708

[123] Lummen G, Sperling H, Luboldt H, Otto T, Rubben H. Phase II trial of titanocene dichloride in advanced renal-cell carcinoma. Cancer Chemotherapy and Pharmacology. 1998; **42**(5):415-417

[124] Melendez E. Titanium complexes in cancer treatment. Critical Reviews in Oncology/ Hematology. Jun 2002;**42**(3):309-315

[125] Guo M, Guo Z, Sadler PJ. Titanium(IV) targets phosphoesters on nucleotides: Implications for the mechanism of action of the anticancer drug titanocene dichloride. Journal of Biological Inorganic Chemistry. Sep 2001;**6**(7):698-707

[126] Timerbaev AR, Hartinger CG, Aleksenko SS, Keppler BK. Interactions of antitumor metallodrugs with serum proteins: advances in characterization using modern analytical methodology. Chemical Reviews [Internet]. Jun 1, 2006;**106**(6):2224-2248. DOI: 10.1021/cr040704h

[127] Chitambar CR. Gallium-containing anticancer compounds. Future Medicinal Chemistry. 2012;**4**(10):1257-1272

[128] Senderowicz AM, Reid R, Headlee D, Abornathy T, Horti J, Lush RM, et al. A phase II trial of gallium nitrate in patients with androgen-metastatic prostate cancer. Urologia Internationalis. 1999;**63**(2):120-125

[129] Hata Y, Sandler A, Loehrer PJ, Sledge GWJ, Weber G. Synergism of taxol and gallium nitrate in human breast carcinoma cells: Schedule dependency. Oncology Research. 1994; **6**(1):19-24

[130] Myette MS, Elford HL, Chitambar CR. Interaction of gallium nitrate with other inhibitors of ribonucleotide reductase: Effects on the proliferation of human leukemic cells. Cancer Letters. Jul 1998;**129**(2):199-204

[131] Hofheinz RD, Dittrich C, Jakupec MA, Drescher A, Jaehde U, Gneist M, et al. Early results from a phase I study on orally administered tris(8-quinolinolato)gallium(III) (FFC11, KP46) in patients with solid tumors—A CESAR study (Central European Society for Anticancer Drug Research—EWIV). International Journal of Clinical Pharmacology and Therapeutics. Dec 2005;**43**(12):590-591

[132] Valiahdi SM, Heffeter P, Jakupec MA, Marculescu R, Berger W, Rappersberger K, et al. The gallium complex KP46 exerts strong activity against primary explanted melanoma cells and induces apoptosis in melanoma cell lines. Melanoma Research. Oct 2009;**19**(5):283-293

[133] Bernstein LR, Tanner T, Godfrey C, Noll B. Chemistry and pharmacokinetics of gallium maltolate, a compound with high oral gallium bioavailability. Metal-Based Drugs. 2000;**7**(1):33-47

[134] Peacock AFA, Sadler PJ. Medicinal organometallic chemistry: Designing metal arene complexes as anticancer agents. Chemistry, An Asian Journal. Nov 2008;**3**(11):1890-1899

[135] Peacock AFA, Habtemariam A, Fernández R, Walland V, Fabbiani FPA, Parsons S, et al. Tuning the reactivity of osmium(II) and ruthenium(II) arene complexes under physiological conditions. Journal of the American Chemical Society [Internet]. Feb 1, 2006; **128**(5):1739-1748. DOI: 10.1021/ja055886r

[136] Peacock AFA, Parsons S, Sadler PJ. Tuning the hydrolytic aqueous chemistry of osmium arene complexes with N,O-chelating ligands to achieve cancer cell cytotoxicity. Journal of the American Chemical Society [Internet]. Mar 1, 2007;**129**(11):3348-3357. DOI: 10.1021/ja068335p

[137] Kostrhunova H, Florian J, Novakova O, Peacock AFA, Sadler PJ, Brabec V. DNA Interactions of monofunctional organometallic osmium(II) antitumor complexes in cell-free media. Journal of Medicinal Chemistry [Internet]. Jun 1, 2008;**51**(12):3635-3643. DOI: 10.1021/jm701538w

[138] Sanchez-Cano C, Romero-Canelon I, Yang Y, Hands-Portman IJ, Bohic S, Cloetens P, et al. Synchrotron X-ray fluorescence nanoprobe reveals target sites for organo-osmium complex in human ovarian cancer cells. Chemistry. Feb 2017;**23**(11):2512-2516

[139] Hanif M, Babak MV, Hartinger CG. Development of anticancer agents: Wizardry with osmium. Drug Discovery Today. Oct 2014;**19**(10):1640-1648

[140] Nobili S, Mini E, Landini I, Gabbiani C, Casini A, Messori L. Gold compounds as anticancer agents: Chemistry, cellular pharmacology, and preclinical studies. Medicinal Research Reviews. May 2010;**30**(3):550-580

[141] Roder C, Thomson MJ. Auranofin: Repurposing an old drug for a golden new age. Drugs in R&D [Internet]. Mar 20, 2015;**15**(1):13-20. Available from: http://www.ncbi.nlm.nih.gov/pmc/articles/PMC4359176/

[142] Trani M, Sorrentino A, Busch C, Landström M. Pro-apoptotic effect of aurothiomalate in prostate cancer cells. Cell Cycle [Internet]. Jan 15, 2009;**8**(2):306-313. DOI: 10.4161/cc.8.2.7596

[143] Regala RP, Thompson EA, Fields AP. Atypical protein kinase C iota expression and aurothiomalate sensitivity in human lung cancer cells. Cancer Research. Jul 2008;**68**(14):5888-5895

[144] Stallings-Mann M, Jamieson L, Regala RP, Weems C, Murray NR, Fields AP. A novel small-molecule inhibitor of protein kinase Ciota blocks transformed growth of non-small-cell lung cancer cells. Cancer Research [Internet]. 2006;**66**(3):1767-1774. Available from: http://cancerres.aacrjournals.org/content/66/3/1767

[145] Mármol I, Virumbrales-Muñoz M, Quero J, Sánchez-de-Diego C, Fernández L, Ochoa I, et al. Alkynyl gold(I) complex triggers necroptosis via ROS generation in colorectal carcinoma cells. Journal of Inorganic Biochemistry [Internet]. 2017;**176**:123-133. Available from: http://www.sciencedirect.com/science/article/pii/S0162013417304130

[146] Munteanu CR, Suntharalingam K. Advances in cobalt complexes as anticancer agents. Dalton Transactions [Internet]. 2015;**44**(31):13796-13808. DOI: 10.1039/C5DT02101D

[147] Ott I, Kircher B, Dembinski R, Gust R. Alkyne hexacarbonyl dicobalt complexes in medicinal chemistry and drug development. Expert Opinion on Therapeutic Patents [Internet]. Mar 1, 2008;**18**(3):327-337. DOI: 10.1517/13543776.18.3.327

[148] Trudu F, Amato F, Vaňhara P, Pivetta T, Peña-Méndez EM, Havel J. Coordination compounds in cancer: Past, present and perspectives. Journal of Applied Biomedicine [Internet]. 2015;**13**(2):79-103. Available from: http://www.sciencedirect.com/science/article/pii/S1214021X15000095

[149] Silva TFS, Martins LMDRS, Guedes da Silva MFC, Fernandes AR, Silva A, Borralho PM, et al. Cobalt complexes bearing scorpionate ligands: Synthesis, characterization, cytotoxicity and DNA cleavage. Dalton Transactions. 2012;**41**(41):12888-12897

[150] Raposo LR, Roma-Rodrigues C, Jesus J, Martins LMDRS, Pombeiro AJ, Baptista PV, et al. Targeting canine mammary tumours via gold nanoparticles functionalized with promising Co(II) and Zn(II) compounds. Veterinary and Comparative Oncology. 2017;**15**(4):1537-1542

[151] Fernandes AR, Jesus J, Martins P, Figueiredo S, Rosa D, Martins LMRDRS, et al. Multifunctional gold-nanoparticles: A nanovectorization tool for the targeted delivery of novel chemotherapeutic agents. Journal of Controlled Release. 2017;**245**:52-61

[152] Azzouzi AR, Barret E, Bennet J, Moore C, Taneja S, Muir G, et al. TOOKAD(R) soluble focal therapy: Pooled analysis of three phase II studies assessing the minimally invasive ablation of localized prostate cancer. World Journal of Urology. Jul 2015;**33**(7):945-953

[153] Monneret C. Platinum anticancer drugs. From serendipity to rational design. Annales Pharmaceutiques Françaises [Internet]. 2011;**69**(6):286-295. DOI: 10.1016/j.pharma.2011.10.001

[154] Choi CH, Cha YJ, An CS, Kim KJ, Kim KC, Moon SP, et al. Molecular mechanisms of heptaplatin effective against cisplatin-resistant cancer cell lines: Less involvement of metallothionein. Cancer Cell International. 2004;**4**:1-12

[155] Apps MG, Choi EHY, Wheate NJ. The state-of-play and future of platinum drugs. Endocrine-Related Cancer. Aug 2015;**22**(4):R219-R233

[156] Alessio E. Thirty years of the drug candidate NAMI-A and the myths in the field of ruthenium anticancer compounds: A personal perspective. European Journal of Inorganic Chemistry. 2017;**2017**(12):1549-1560

[157] Alessio E, Messori L. The deceptively similar ruthenium(III) drug candidates KP1019 and NAMI-A have different actions. What did we learn in the past 30 years? Metal Ions in Life Sciences. Feb 2018;**18**:141-171

[158] Mansfield AS, Fields AP, Jatoi A, Qi Y, Adjei AA, Erlichman C, et al. Phase I dose escalation study of the PKCiota inhibitor aurothiomalate for advanced non-small-cell lung cancer, ovarian cancer, and pancreatic cancer. Anti-Cancer Drugs. Nov 2013;**24**(10):1079-1083

[159] Espinal-Enríquez J, Hernández-Lemus E, Mejía C, Ruiz-Azuara L. Network analysis shows novel molecular mechanisms of action for copper-based chemotherapy. Frontiers in Physiology. 2016;**6**(Jan):1-13

[160] Bernstein LR, van der Hoeven JJM, Boer RO. *Hepatocellular carcinoma* detection by gallium scan and subsequent treatment by gallium maltolate: Rationale and case study. Anti-Cancer Agents in Medicinal Chemistry [Internet]. 2011;**11**(6):585-590. Available from: http://www.ncbi.nlm.nih.gov/pubmed/21554205

Chapter 4

Coordination Chemistry of Networking Materials

Ataf Ali Altaf, Sumbal Naz and Amin Badshah

Additional information is available at the end of the chapter

http://dx.doi.org/10.5772/intechopen.80864

Abstract

The coordination chemistry explains the chemistry, physical properties, structure, bonding, and other properties of the compounds of d-block elements. In the current chapter, we have discussed the coordination chemistry of networking complexes of d-block elements. The networking complexes of d-block elements comprise of metal organic frameworks (MOF) also known as coordination polymers. In this context, the geometry around central metal atom of MOFs has been discussed to explain their different properties. Different theoretical approaches (like hybridization, valance bond theory, molecular orbital theory, and crystal field theory) have been utilized to explain the properties of some selected exemplary compounds, e.g., $[Ag(1,4\text{-pyrazine})_{1.5}CF_3SO_3]$, $[[Cu(3,4\text{-Hpdc})_2\ (H_2O)_2]\cdot 2dmso]_n$, and $[Zn(II)(SEPCPU)]_n$.

Keywords: coordination chemistry, networking materials, metal organic frameworks, geometries, properties of MOF

1. Introduction

The coordination chemistry mention to a versatile branch of which flourishes depends upon inorganic chemistry. The foundation of coordination chemistry breaks down the boundaries of physical, organic, and inorganic chemistry and it alters to joint part of various chemical fields. Coordination chemistry forms an assured achievement in research and practical applications due to its different properties. Theories that explain bonds in coordination compounds are valence bond theory (VBT), crystal field theory (CFT), and ligand field theory (LFT). Properties of coordination chemistry enter into microscale from macrolevel. It accentuates the study on microlevel such as study of the internal structure of molecule. Latest coordination chemistry follows different mathematical models to turn the qualitative description of compounds into quantitative way [1].

Due to higher valency of transition metals, the solution of bonding was expected by Alfred Werner.Werner's analysis provided the basis for field of transition metal complexes in coordination chemistry [2]. Werner, the beginner of coordination chemistry, granted his concepts of metal ligand complexes in his book in 1905 and his book was translated into another language like English in 1911 [3]. According to Webster, coordinate means to convey into proper order of molecules. Coordination chemistry provides important conceptual basics and chemical content of chemistry. In this chemical branch, some important concepts of chemistry were developed like stereochemistry of compounds of higher coordination numbers, bonding in d orbital systems, and mechanism of reactions [4]. The control of molecular conformation in solid materials is the significant motif of modern chemistry. For proper molecular organization, there is preference to use directional bonds (coordinate covalent bond and hydrogen bond) [5]. Coordination compounds are formed by dual aggregation of metal and multidentate ligands. In these coordination compounds, molecules and atoms may be considered as specific points. In these, network is connected, and metal and ligand are connected with each other to form a coordination compound. If inferred impulsions are applied to coordination number of metal through beating its coordination sphere by its counterions, then prediction of formation of final network should increase. The chorography of coordination network is expected to follow from geometry of its constituent parts [6]. The connection of ligand toward metal atom is controlled by covalent synthesis. The prophecy of network structure depends upon coordination properties of metal atom. The coordination of metal is effected by counter ion, duplicity of ligand, and solvent [7].

2. Coordination polymers

Polymers can be described as molecules of high molecular weight which are formed by repetition of their monomeric subunits connected by covalent bonds [8]. However, coordination polymers are formed by central metal atom connected with organic ligands via coordination bonds and weak chemical bonds. These compounds are also named as metal organic frameworks [9]. The organization of different factors in coordination polymers exists in solid form most of the time [10]. Coordination polymers are completely regular in shape, having high porosity and designable frameworks. Synthesis of these networks is done under mild conditions by using discrete subunits and this method is commonly known as bottom-up method. Components of these polymers are blocking ligands, counteranions, and template molecules. Transition metal ions are often used as functional connectors in the formation of coordination polymers. Variable geometries of a polymer can be formed by varying reaction conditions like solvents, ligands, and counteranions, etc. [11].

3. Examples of coordination polymers

3.1. [Ag(1,4-pyrazine)$_{1.5}$CF$_3$SO$_3$] complex

In a clean glass vial, a solution of silver triflate in acetone was added to a solution of 1,4-pyrazine in acetone covered by Teflon cap. Precipitates of white color are formed. For production of clear solution, heat this vial on hot water bath at 85°C. The resultant mixture was filtered at the same time to remove water by using Whatman No. 50 filter paper. On cooling, the clear solution becomes

turbid. The resulting mixture was heated in oven at 70°C and homogeneous mixture was cooled at room temperature; colorless long needle-like structures were formed for XRD analysis.

Stoichiometry of complex of silver as a central metal atom and 1,4-pyrazine as a ligand is $ML_{1.5}$. The structure of complex contains endless chains of cyclical 1,4-pyrazine molecules and metal ions to form ladder-like structure. This ladder-like structure was formed by alternation of 1,4-pyrazine and metal ions. The pyrazine subunits on chain are at a distance of about 3.55. The plane of pyrazine units is 77.8° toward plane of poles of ladder structure. The crystallization solvent of this complex is acetone. Silver is four-coordinated metal bonding to one oxygen atom of triflate and three nitrogen atoms of 1,4-pyrazine. Silver adopts sawhorse geometry. The N-Ag(1) bond distances are 2.246 (N1), 2.312 (N2), and 2.460 Å (N3) and the N-Ag(1)-N bond angles are 173.2 and 87.3°. The Ag(1)-O bond distance is 2.590 Å [7] (**Figure 1**).

Hybridization of given complex can be explained on the basis of VBT. In this complex, charge on Ag is +1, its magnetic moment indicates that paired electrons are present per atom and one electron is lost from 5s orbital, no electron loss from d orbital, one of d orbital electrons may participate in bonding by acting as lone pair to cause lone pair-bond pair repulsion.

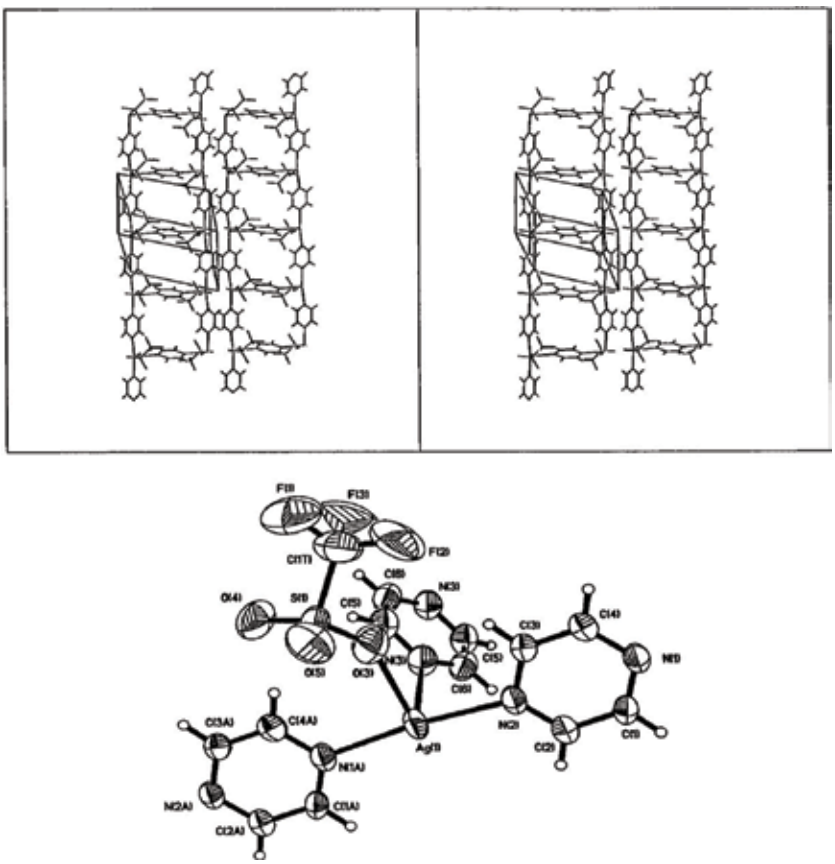

Figure 1. In the $[Ag(1,4\text{-pyrazine})_{1.5}CF_3SO_3]$ complex, chains that run along an axis (at top of figure). This figure indicating the coordination sphere of silver(I) in the $[Ag(1,4\text{-pyrazine})_{1.5}CF_3SO_3]$ complex in which geometry of silver(I) is sawhorse geometry with specified bond lengths and bond angles (at the bottom of figure).

Due to presence of repulsion, this complex showed sawhorse geometry instead of tetrahedral geometry having dsp^3 hybridization in which one d orbital, one s orbital, and three p orbitals of almost same energy of same shell are involved, such type of complexes are known as spin paired complexes. Magnetic moment indicates that this complex is diamagnetic in nature because all electrons present in d orbital are paired. After intermixing of these orbitals, this complex gives five dsp^3 hybrid orbitals.

3.2. $[[Cu(3,4\text{-}Hpdc)_2\ (H_2O)_2]\cdot 2dmso]_n$

Formula weight of this compound is 588.05 g M^{-1} and density is 1.607 g cm^{-3}. Its crystal system is monoclinic. To synthesize this complex, 3,4-pyridinedicorboxlic acid was dissolved in DMSO, and this mixture was added in ethanol solution of $CuCl_2.6H_2O$ by diffusion method. Elemental analysis shows that ratio of metal and ligand is 1:2 in this complex [12]. The resultant mixture becomes green; after 3 weeks, the color of the solution has changed to blue. Blue crystals were suitable for XRD analysis; these crystals were collected by filtration and washed by using DMSO.

XRD analysis indicates that crystals which are formed are monoclinic in nature with space group P_{21}/n. In given complex, central metal atom is coordinated to two nitrogen and two oxygen atoms of 3,4-$Hpdc^-$ ligands and two molecules of water leads to six coordination with octahedral geometry. Each 3,4-$Hpdc^-$ molecule is deprotonated partially, with only one carboxylate ion involving in coordination toward metal center due to the presence of vibrational frequency of CO and (COO^-). No any basic material was added into reaction mixture and the reaction was carried out under optimum conditions to obtain partially protonated material. The bond distance of Cu-O_5 (2.467(3) Å) is much larger than that of Cu-O_4 and Cu-$N1^{ii}$ are (1.977(2) Å) and (2.006(2) Å) [13, 14]. In two-dimensional sheet of polymer, Cu···Cu distance is about 8.781 Å [15].

Thermal analysis indicates that this complex polymer molecule has coordinated molecules of water and DMSO molecule in the resulting network. Two hydrogen bonds involved in

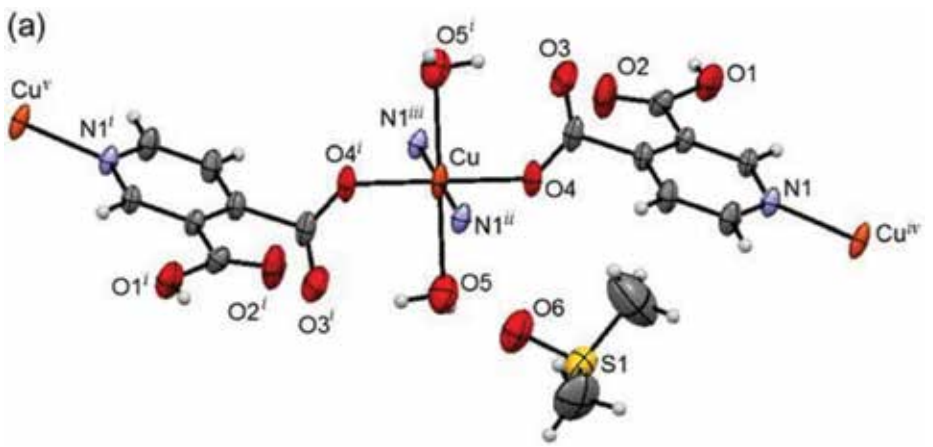

Figure 2. Three-dimensional diagram of complex $\{[Cu(3,4\text{-}Hpdc)_2\ (H_2O)_2]\cdot 2dmso\}_n$ with only one lattice molecule of DMSO with different symmetry codes showing distorted octahedral geometry.

coordinated water molecules—one with DMSO molecule and another with carboxylate ion—are observed [16] (**Figure 2**).

Hybridization of this complex polymer molecule can be explained on the basis of VBT. The charge on central metal atom is Cu^{2+}. Its magnetic moment indicates that complex is paramagnetic because one unpaired electron was left in one of 3d orbitals. The vacant $4dx^2$-y^2 and $4dz^2$ orbitals are hybridized with vacant 4s and 4p orbitals to give six sp^3d^2 hybrid orbitals. All water and 3,4-Hpdc$^-$ can donate two electrons to one of sp^3d^2hybrids [17].

3.3. [PVA-Ni(II)]$_n$ complex

These polymer metal complexes were prepared by using template method. A solution of polyvinyl alcohol is dissolved in water and the given solution was stirred magnetically and was heated at specific temperature on hot plate. One mole of metal chloride was diffused in water; this mixture was added dropwise into solution of polymer, again stirred and heated on hot plate approximately for 1 h. Complexes were precipitated by using acetone and filtered, then washed with acetone and then dried in oven. Complexes of polyvinyl alcohol are not soluble in water. Elemental analysis showed polymer and metal ratio of about 126:1. These complexes are not prepared in the form of tablets and pellets due to its springy nature [18, 19]. These complex polymers are diamagnetic and show square planar geometry [20]. No electronic bands were formed due to insolubility of these polymers in water; these metal complex polymers show rubber-like structure. This polymer exhibited about 17% of rubber naturally. Due to its rubber-like structure, stress-strain experiments of these complex materials were performed. This complex polymer molecule has breaking strain value of about 83%. These stress-strain values are due to hydroxyl group (**Figure 3**).

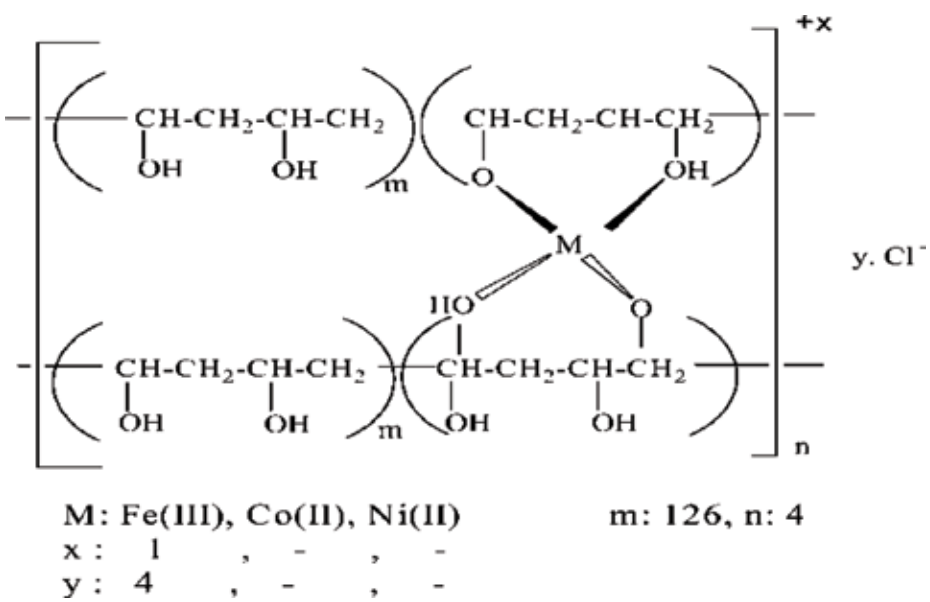

Figure 3. Structure of PVA-metal complex polymer.

This complex polymer is square planar polymer resulting from dsp^2 hybridization; in this, one d, one s, and two p orbitals of same energy of same shell are involved; charge on central metal atom is Ni^{2+}. Magnetic moment of this polymer complex indicated that this complex polymer is diamagnetic because all electrons are paired in 3d orbitals of central metal atom. Color of this complex is green. Polyvinyl alcohol donates two electrons to one of dsp^2 hybrid orbitals [20].

3.4. [Zn(II)(SEPCPU)]n

The name of ligand in this complex polymer is sebacoylbis-p-chlorophenyl urea. This ligand was prepared by condensation of 0.1 mmol of sebacoyl dichloride (prepared by sebacic acid and double-distilled thionyl chloride) and 0.2 mmol of p-chlorophenyl urea (prepared by p-chloroaniline and glacial acetic acid and sodium cyanate solution) in sodium-dried benzene for almost 5 h. Coordination polymer by using this ligand was formed by mixing ligand and metal acetate in minimum amount of hot dimethylformamide separately. Both solutions of ligand and metal acetate were filtered and then mixed under hot conditions. Reaction mixture was refluxed on oil bath for 5–6 h at 135–145°C. The colored products obtained were filtered and washed first with hot DMF and then with ethanol and acetone for elimination of unreacted reactants if present and finally dried in oven. This complex polymer is insoluble in water completely. Normal method of characterization is proton NMR and electronic spectra cannot be attained in solution.

IR sharp band appears at 1656 cm^{-1} due to C═O stretching vibrations; this band disappears in coordination polymers due to enolization and coordination of metal atom. This coordination polymer is diamagnetic in nature and shows tetrahedral geometry. This complex polymer is white in color. All coordination polymers are thermally stable and show insolubility in all organic solvents and due to their thermal stability, they can be used as powder coating materials (**Figure 4**).

This complex is tetrahedral resulted from sp^3 hybridization. In this type of hybridization, one s and three p orbitals of same shell having same energy are involved; charge on central metal atom is Zn^{2+}. Magnetic moment of this complex polymer indicates that this complex

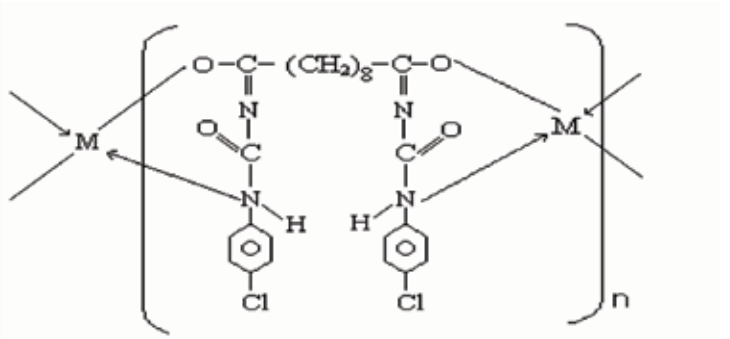

Figure 4. Structure of $[Zn(II)(SEPCPU)]_n$ complex polymer.

is diamagnetic due to the presence of paired electrons in 3d orbitals. Color of this complex polymer is white. O and N atoms of ligand can donate two electrons to one of four sp^3 hybrid orbitals [21].

3.5. $([Cu(L)(CF_3COO)]_2)_n$

In this polymer complex, ligand is Schiff base ((E)-2-((pyridin-2-yl)methyleneamino)-5-chlorobenzoic acid) which was prepared by reflux condensation of 0.536 g, 5 mmol of 2-pyridinecarboxaldehyde, and 0.858 g, 5 mmol of 2-amino-5-chlorobenzoic acid in 50 ml solution of methanol for 1 h approximately. The resulting solution is orange red in color. Performed TLC of this solution indicates the presence of Schiff base ligand. This product was separated by performing column chromatography by using mixture of ethyl acetate and light petroleum in a ratio of 1:1. Then, evaporation of this content yields pure ligand [22].

The copper complex with this ligand was prepared by using 10 ml of methanolic solution; 0.261 g, 1 mmol of Schiff base was added to another methanolic solution of 0.290 g, 1 mmol of copper trifluoroacetate with slow stirring on hot plate for almost half an hour. The resulting mixture was blue in color and was filtered; the filtrate was kept undisturbed for 7 days. A plate-shaped blue-colored crystal of this complex was obtained.

In this complex, every cupric center is penta-coordinated in a distorted square planar geometry, where Schiff base ligands act as tridentate ligand toward one cupric center; in fact, they are tetradentate ligand. The basal plane of Cu1 is provided by nitrogen of pyridine and imine

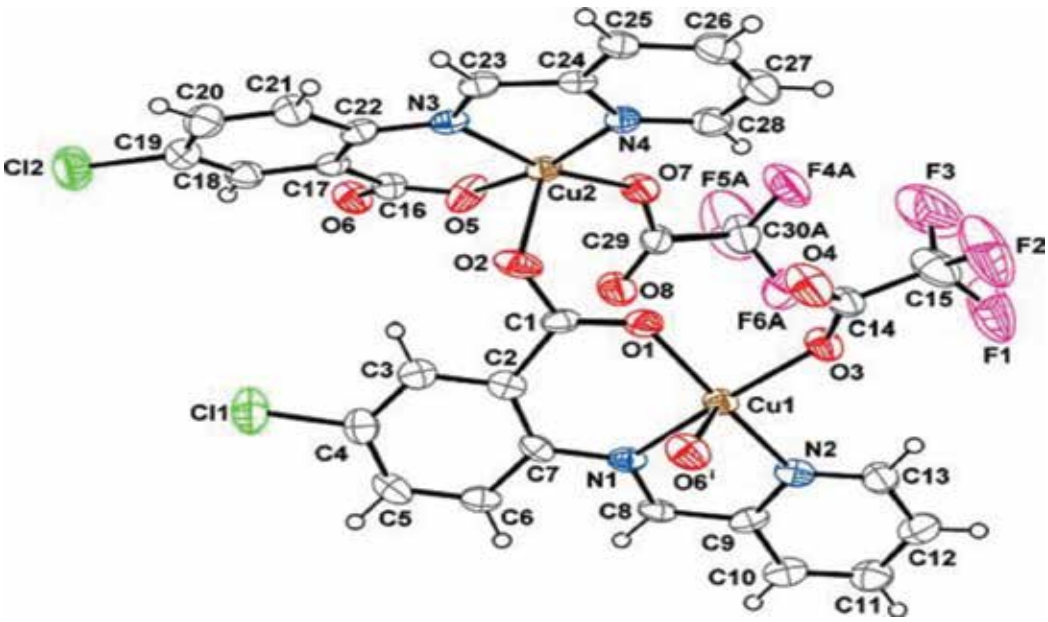

Figure 5. This figure showed the ORTEP view of asymmetric unit of complex polymer. Its bond lengths are described below.

and one carboxylate oxygen atom and one oxygen atom of monodentate triflouroacetate group and apical position of the complex are occupied by symmetry-related ligand. In the same way, the basal plane of Cu2 is clocked up by N_4, N_3, O_5, O_7 and apical position is clocked up by O_2 atom of Schiff base coordinated to Cu1 (**Figure 5**).

Bond lengths in this complex molecule are Cu_1-O_1, Cu_2-O_2, Cu_1-O_3, Cu_2-O_5, Cu_1-N_1, Cu_2-O_7, Cu_1-N_2, Cu_2-N_3, Cu_1-O_6, and Cu_2-N_4 1.904, 2.162, 1.941, 1.895, 2.011, 1.939, 2.006, 2.017, 2.178, 2.008 Å, respectively [23].

The geometry of this complex polymer is square pyramidal. Hybridization of this polymer is sp^3d^2 which involves one s and three p orbitals of same shell and outer two d orbitals of fourth shell. Charge on central metal atom is Cu^{2+}; its magnetic moment indicates that this complex polymer is paramagnetic in behavior because one unpaired electron was left in one of 3d orbitals. And ligands show interactions toward metal center through sp^3d^2 orbitals by donation of two electrons.

4. Examples of transition metal compounds

4.1. [Ni(D)(G)]: D = dimethylglyoxime, G = N-acetylglycine

An ethanolic solution of potassium hydroxide of dimethylglyoxime and of N-acetylglycine was added to aqueous solution of metal salts after some stirring on water bath; precipitates of product are formed and immediately filtered and washed by mixture of ethanol and water in ratio of 1:3, and finally dried in oven at 60°C. The metal complexes which are formed are solids and completely insoluble in organic solvents showing complete solubility in DMF. IR spectra of DMG showed absorption bands at 3400, 2931, 1570, 1141, and 756 cm^{-1} which are accounted for ν(OH), ν(C—H), ν(C = N), ν(N—O), and ν(C = N—O), respectively. In metal ligand complexes, these bands shifted toward lower frequencies.

IR band of N-acetylglycine was appeared at 3380 cm^{-1}; on complexation, this band shifted toward lower value. Electronic spectra of Ni(II) complex show absorption bands at 445 nm.

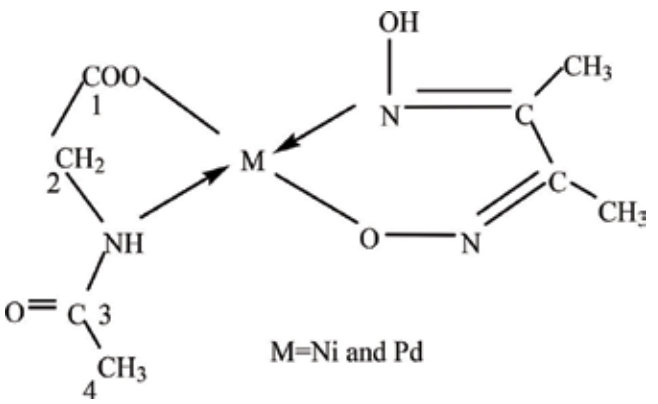

Figure 6. Square planar structure of the complex.

IR study and electronic spectra indicated that dimethylglyoxime and N-acetylglycine were coordinated to metal by N and O atoms (**Figure 6**).

All metal complexes are insoluble in water as well as in most organic solvents but soluble in DMF and DMSO. They are nonelectrolytes. The electronic spectra of this complex indicate d^8 system showing absorption bands at 445 and 514 nm in visible region showing electronic transitions at A_1g-A_2g, etc. Such type of transitions of these complexes indicates that structure of this complex is square planar.

This complex is resulted from dsp^2 hybridization. In this type of hybridization, one d, one s, and two p orbitals of same shell having same energy are involved. Charge on central metal atom is Ni^{2+}. Its magnetic moment indicates that two electrons of five 3d orbital are unpaired which become paired by using strong ligands such as dimethylglyoxime and N-acetylglycine; as a result, complex becomes diamagnetic in character and shows pink color. Due to dsp^2 hybridization, its geometry is square planar [24]

4.2. $RuCl_2[P(C_6H_5)_3]_3$

This complex is five-coordinated and d^6 system. This complex was prepared by Vaska by using $(NH_4)_2RuBr_6$ with triphenylphosphine in 2-methoxyethanol at 25°C. From magnetic moment, molecular weight of complex and its conductivity measurements show that such type of complexes is diamagnetic and monomeric. Compounds of Os and Ru are isomorphs of each other and their crystal structure is monoclinic. This complex can be distorted square pyramidal when Ru occupied the position of center of gravity.

This complex molecule consists of only 68% by weight of carbon; so the structure of this complex is based on Ru, P, and Cl atoms. Bond distances of Ru-P_1, Ru-P_2, Ru-P_3, Ru-Cl_1, and Ru-Cl_2 are 2.374, 2.412, 2.230, 2.387, and 2.388 Å, respectively. In present case, vacant octahedral site of complex is occupied by phenyl ring especially by phenyl hydrogen. Ru and Os complexes of Vaska are slightly soluble in most solvents. In this complex, color change occurs

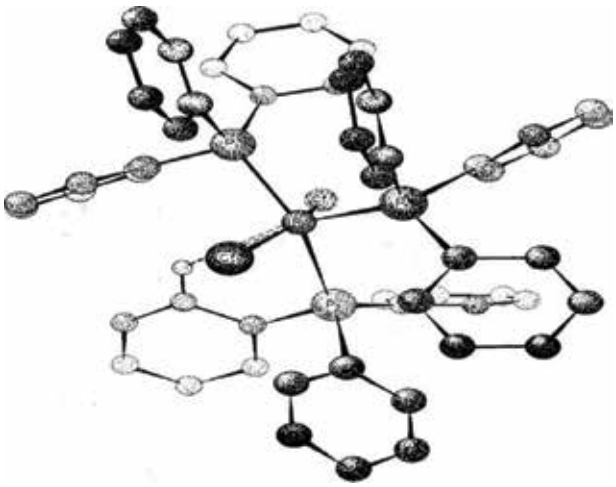

Figure 7. The structure of $RuCl_2[P(C_6H_5)_3]_3$, in which only hydrogen atoms are shown which block the unused octahedral position.

due to rotation of phenyl ring. Preferable geometry for this complex is square pyramidal or octahedral. But stability of this complex may arise by blocking of unused octahedral site by rotation of phenyl ring [25] (**Figure 7**).

This complex resulted from d^2sp^3 hybridization. Charge on central metal atom is Ru (+2). Magnetic moment of this complex showed that electrons are paired per Ru^{2+} atom. The $3dx^2$-y^2 and $3dz^2$ orbitals, one s, and three p orbitals of same energy of same shell are involved in d^2sp^3 hybridization. Triphenylphosphine is the strong ligand force pairing of all electrons of Ru. This complex is diamagnetic in behavior and may be known as spin paired complex and forms octahedral geometry.

4.3. Zinc(4-amino-5-pyridyl-4H-1,2,4-triazole-3-thiol)$_2$

In ethanol, a mixture of isonicotinic acid from potassium hydroxide was dissolved; when fluxing or dissipation was complete, carbon disulfide was added slowly to this mixture. And then, it was stirred on hot plate for almost 10 h; dried ether was added to this content resulting in precipitates of yellow color; the precipitates are filtered and washed by using ether and dried. Then, these yellow precipitates were added into excess amount of hydrazine hydride and were refluxed along with stirring until estimation of hydrogen sulfide was done. This process was stopped by using lead acetate paper; after cooling, this mixture was filtered and then acidified by using hydrochloric acid to yield product of white color. That is the ligand used in this complex formation.

Ethanolic solution of metal salt zinc acetate dihydrate was added into ethanolic solution of ligand in metal to ligand ratio of about 1:2 and refluxed for 2 h; crystalline colored precipitates were appeared at room temperature and washed by hot methanol and left for drying and recrystallized by using ethanol.

FTIR spectra showed some specific vibrations of ligand at 3250 and 3213, 2736, 1645, 673, 529, 432 cm^{-1} due to NH_2, S—H, C=N, M—N, and M—S of triazole ring and metal ligand complex, and the last one is due to stretching of C—S bond, respectively. Tautomeric form of triazole could be responsible for deprotonation of ligand before complexation; after complexation, ligand can attach to metal ion either through N atom or through S atom of thioamide group; bonding at S atom is more preferable because this gives more stable chelate. Electronic spectra of ligand exhibit three bands at 263, 302, 309 nm due to (π-π*), (π-π*), (n-π*) intraligand transitions. The given complex is diamagnetic in behavior due to completely filled d-orbitals, so no any d-d transitions can be possible in visible region [26] (**Figure 8**).

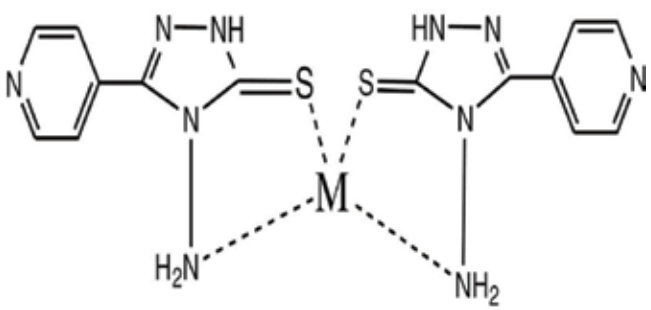

Figure 8. Structure of zinc(4-amino-5-pyridyl-4H-1,2,4-triazole-3-thiol)$_2$ complex.

The hybridization of this complex is sp^3, in which one s and three p orbitals are involved. Magnetic measurement of this complex indicates that this complex is diamagnetic because its all d orbital electrons are paired, electrons lose only from s orbital of Zn due to charge on Zn^{2+} and no magnetic moment was observed and ligand attaches to metal atom via s and p orbitals of metal atom and exhibited tetrahedral geometry.

4.4. [Cu(acac)(Me_2bipy)(NCS)]

Ligands have been prepared by dissolving 2 mmol Me_2bipy in 20 ml of ethanol and other ligand has been prepared by 2 mmol acetylacetone. Stoichiometric quantity of Hacac on LiOH was added over 25 ml of aqueous solution of 2 mmol $Cu(ClO_4)_2$ rapidly. The slow process of evaporation of this mixture gives brown-colored crystals of complex [Cu(acac)(Me_2bipy)](ClO_4) which is square planar in geometry having sp^3 hybridization. Perchlorate ion is not involved in geometry.

The above complex has been prepared by reaction of ethanolic solution of 0.5 mmol [Cu(acac)(Me_2bipy)](ClO_4) and aqueous solution of 10 ml of 0.5 mmol KCNS. The slow process of evaporation of this mixture leads to green-colored crystals. These crystals are monoclinic form. The resultant complex has square pyramidal geometry. The bond distance of Cu—O is shorter than that of Cu—N such as [1.882(3); 1.896(3) Å] and s [1.981(3); 1.984(3) Å] and the bond angles of O-Cu-O and N-Cu-N are 94.74(11) and 81.44(11), respectively.

The insertion of another ligand to complex of Cu which acts as bridging ligand leads to square pyramid. Reaction of [Cu(acac)(Me_2bipy)](ClO_4) and KCNS gives mononuclear complex with isothiocyanato ligand coordinated to copper in apical position. In this complex, two ligands overlap in face-to-face manner with interplanar distances of about 3.09–3.37 Å and 3.50–3.57 Å

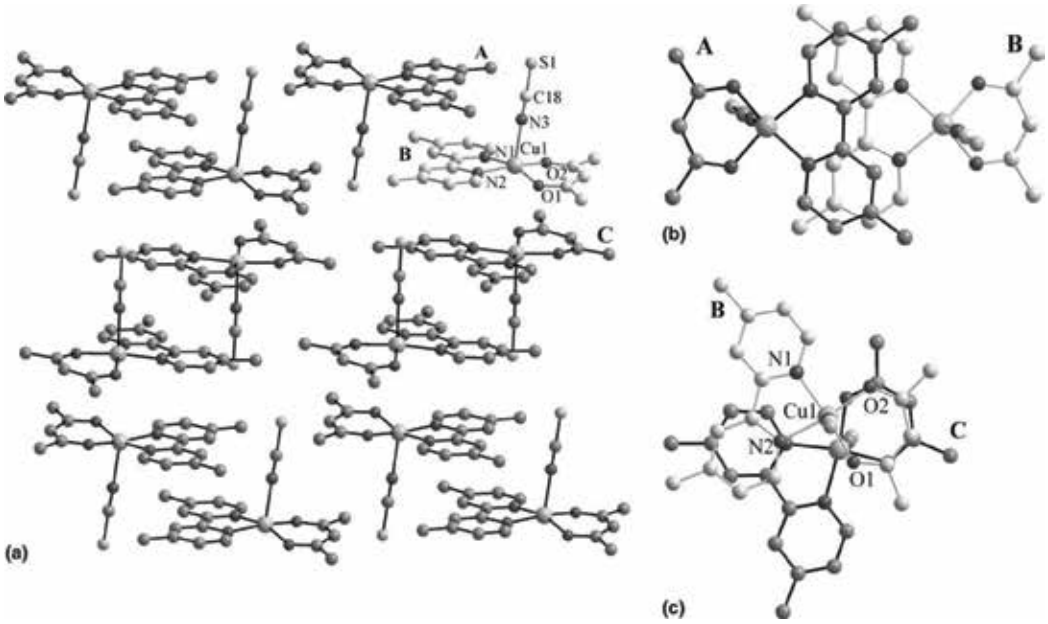

Figure 9. Crystal structure of complex [Cu(acac)(Me2bipy)(NCS)] (a) numbering scheme of atoms and its packing diagram, (b) stacking interaction among ligand molecules, and (c) stacking interaction among Me2bipy ligand and acac ligands.

for acac and Me_2bipy ligands, respectively and give dimmers. Within dimer structures, distance between Cu(II) ions is 3.920 Å [27] (**Figure 9**).

The hybridization of this complex is sp^3d^2 resulted by the involvement of one s, three p, and two d orbitals. Magnetic moment of this complex indicates that this complex is diamagnetic because all electrons are paired in 3d orbitals; electrons are lost from 3s orbital due to Cu^{2+} charge. The ligands are coordinated toward metal ion via one s, three p, and two 4d orbitals leading to square pyramidal geometry.

4.5. $[Co(H_2O)(EDTAH)].2H_2O$

A 0.291 g of $Co(No_3)_2.6H_2O$ was mixed with 0.416 g of sodium salt of EDTA in distilled deionized water at room temperature. On disintegration of these two reactants, 3% solution of hydrogen peroxide was added with constant stirring until changing in color was complete. The volume of water reduced slowly by evaporation over a period of several days. Crystals of compound were left. Purity of product and quality of crystals depend on the rate of reaction. The fast rate of reaction would lead to the impurity formation and mixture of products.

The structure of this complex is distorted pentagonal bipyramidal. Cobalt is attached to nitrogen atom and oxygen atoms of three acetate groups and one acetic acid group of $EDTAH^{-3}$ and one oxygen atom of water molecule. Axial positions of the complex were being occupied by two oxygen atoms of different acetate groups, and pentagonal plane of this molecule was being occupied by two nitrogen donors, one oxygen of $EDTAH^{-3}$, one oxygen atom of acetato group, and one oxygen atom of water molecule.

Bond distance of carbon and oxygen for protonated O(4) is 1.294 Å. The bond distance of coordinated O(3)-C(4) is 1.215 Å. Bond lengths of attached ligand molecule are longer than

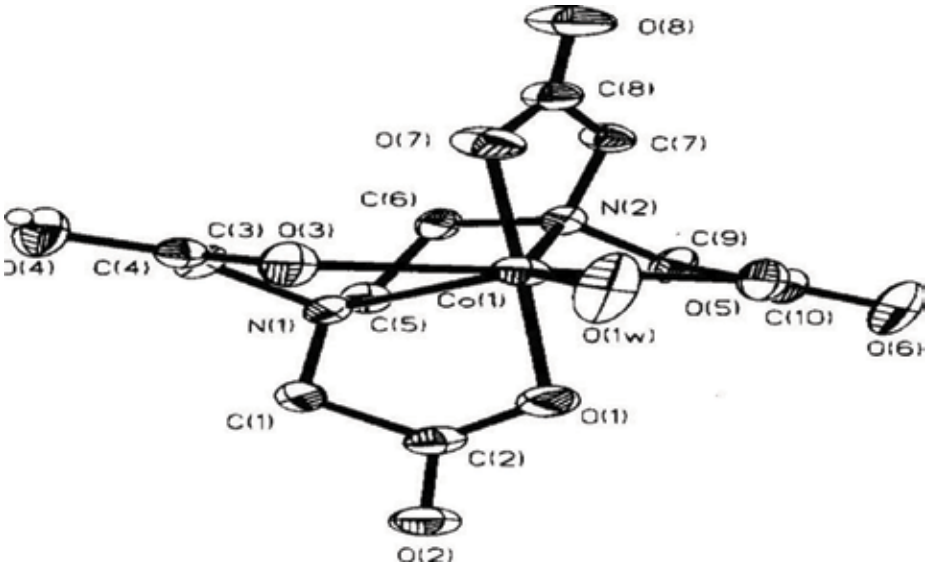

Figure 10. Structure of Co(EDTAH)(H_2O) complex which indicates the distortion in pentagonal plane.

that of Co-EDTA complex. The bond lengths of Co(1)-O(1), Co(1)-O(5), Co(1)-O(3), Co(1)-O(1W), Co(1)-O(7), Co(1)-N(2), Co(1)-N(1) are 2.124, 2.272, 2.465, 2.073, 2.078, 2.229, and 2.256 Å, respectively. Bond lengths and bond angles suggest that geometry of this complex is pentagonal bipyramidal [28] (**Figure 10**).

The hybridization of this complex molecule is dsp^3d^2 due to involvement of one s, three p, and three d orbitals intermixed to give seven hybrid orbitals of dsp^3d^2 which are arranged in pentagonal bipyramidal symmetry. Charge on central metal atom is Co (+3); its magnetic moment indicates that this complex is diamagnetic in behavior because all electrons present in 3d orbitals become paired favored by EDTA ligand. Ligand showed interaction toward central metal atom via one d, one s, and three p orbitals of third shell and two $d_{(x2-y2)}$ and d_{z2} resulting in seven dsp^3d^2 hybrid orbitals.

5. Conclusion

This chapter is focused on coordination chemistry of metal organic frameworks and compounds of transition metals. Bonding and hybridization in these compounds was explained by valence bond theory and molecular orbital theory; specific distortions due to the presence of lone pair of electrons were explained via crystal field theory. Magnetic behavior, color of compounds described above, space groups, crystal shapes, and geometry of the complex compounds were also explained.

Author details

Ataf Ali Altaf[1]*, Sumbal Naz[1] and Amin Badshah[2]

*Address all correspondence to: atafali.altaf@uog.edu.pk

1 Department of Chemistry, University of Gujrat, Gujrat, Pakistan

2 Department of Chemistry, Quaid-i-Azam University, Islamabad, Pakistan

References

[1] Zhang Y. On study of new progress and application of coordination chemistry in chemistry and chemical industry in recent years. In: IOP Conference Series: Earth and Environmental Science. IOP Publishing; 2017

[2] Bowman-James K. Alfred Werner revisited: The coordination chemistry of anions. Accounts of Chemical Research. 2005;**38**(8):671-678

[3] Busch DH. The complete coordination chemistry-one practioner's perspective. Chemical Reviews. 1993;**93**(3):847-860

[4] Werner A. Neuere Anschauungen auf dem Gebiete der anorganischen chemie. Vol. 8. F. Vieweg und Sohn; 1920

[5] Zaworotko MJ. Coordination polymers. NATO ASI Series C Mathematical and Physical Sciences-Advanced Study Institute. 1999;**539**:383-408

[6] Fujita M et al. Self-assembled molecular ladders. New Journal of Chemistry. 1998;**22**(2): 189-191

[7] Venkataraman D et al. Coordination networks based on multitopic ligands and silver (I) salts: A study of network connectivity and topology as a function of counterion. Chemistry of Materials. 1996;**8**(8):2030-2040

[8] Bailar J Jr. Coordination Polymers. Vol. 1. New York: Interscience; 1964. pp. 1-25

[9] Janiak C. Engineering coordination polymers towards applications. Dalton Transactions. 2003;(14):2781-2804

[10] Robin AY, Fromm KM. Coordination polymer networks with O-and N-donors: What they are, why and how they are made. Coordination Chemistry Reviews. 2006;**250**(15-16): 2127-2157

[11] Kitagawa S, Kitaura R, Noro Si. Functional porous coordination polymers. Angewandte Chemie International Edition. 2004;**43**(18):2334-2375

[12] Yan S-H et al. Self-assembly and characterization of copper 3,4-pyridinedicarboxylate complexes based on a variety of polynuclear hydroxo clusters. Dalton Transactions. 2011;**40**(8): 1758-1767

[13] Fu ZY et al. Three novel polymeric frameworks assembled from CdII, CoII, and MnII with the mixed organic ligands 3,4-pyridinedicarboxylate, 1,3-bis(4-pyridyl) propane, or 1,2-bis(4-pyridyl)ethane. European Journal of Inorganic Chemistry. 2003;**2003**(14): 2670-2677

[14] Yan S, Li X, Zheng X. Effect of the carboxyl groups on the assembly of copper pyridinedicarboxylate complexes. Journal of Molecular Structure. 2009;**929**(1):105-111

[15] Blatov V. TOPOS-version 4.0 professional (Beta evaluation), Samara State University, Samara, Russia, 2006 search PubMed; (b) VA Blatov, AP Shevchenko and VN Serezhkin. Journal of Applied Crystallography. 2000;**33**:1193

[16] Steed JW, Atwood JL. Supramolecular Chemistry. 2nd Edition. USA: John Wiley & Sons; 2013

[17] Scaldini FM et al. 2-D coordination polymers of copper and cobalt with 3,4-pyridinedicarboxylic acid: Synthesis, characterization, and crystal structures. Journal of Coordination Chemistry. 2014;**67**(18):2967-2982

[18] El-Sonbati A, Al-Shihri A, El-Bindary A. Polymer complexes. XLIII. EPR, spectra, and stereochemical versatility of novel copper (II) polymer complexes. Journal of Inorganic and Organometallic Polymers. 2003;**13**(2):99-108

[19] Arafa I, El-Ghanem H, Al-Shalabi R. Formation, characterization and electrical conductivity of polycarbosilazane-Cu(II),-Ni(II) and-Cr(III) chloride metallopolymers. Journal of Inorganic and Organometallic Polymers. 2003;**13**(2):69-86

[20] Sari N et al. Synthesis of some polymer-metal complexes and elucidation of their structures. Journal of Macromolecular Science Part A: Pure and Applied Chemistry. 2006; **43**(8):1227-1235

[21] Bonde A et al. Synthesis, spectral and thermal studies of coordination polymers of sebacoyl bis-P-chlorophenyl urea. RASAYAN Journal of Chemistry. 2011;**4**(4):838-843

[22] Shit S et al. Crystal structure, characterization and magnetic properties of a 1D copper (II) polymer incorporating a Schiff base with carboxylate side arm. Journal of Chemical Sciences. 2016;**128**(6):913-920

[23] Shit S et al. Syntheses, structural variations and fluorescence studies of two dinuclear zinc (II) complexes of a Schiff base ligand with an extended carboxylate side arm. Journal of Molecular Structure. 2016;**1108**:475-481

[24] Shaker SA. Preparation and spectral properties of mixed-ligand complexes of VO(IV), Ni(II), Zn(II), Pd(II), Cd(II) and Pb(II) with dimethylglyoxime and N-acetylglycine. Journal of Chemistry. 2010;**7**(S1):S580-S586

[25] La Placa SJ, Ibers JA. A five-coordinated d6 complex: Structure of dichlorotris (triphenylphosphine) ruthenium(II). Inorganic Chemistry. 1965;**4**(6):778-783

[26] Haddad R, Yousif E, Ahmed A. Synthesis and characterization of transition metal complexes of 4-amino-5-pyridyl-4H-1,2,4-triazole-3-thiol. Springerplus. 2013;**2**(1):510

[27] Madalan AM et al. Chemistry at the apical position of square-pyramidal copper (II) complexes: Synthesis, crystal structures, and magnetic properties of mononuclear Cu(II), and heteronuclear Cu(II)-Hg(II) and Cu(II)-Co(II) complexes containing [Cu (AA)(BB)] + moieties (AA = acetylacetonate, salicylaldehydate; BB = 1,10-phenanthroline, Me 2 bipy = 4,4′-dimethyl-2,2′-bipyridine). Inorganica Chimica Acta. 2004;**357**(14):4151-4164

[28] Zubkowski JD et al. A seven coordinate co-EDTA complex. Crystal and molecular structure of aquo (ethylenediaminetriacetatoacetic acid) cobalt (III) dihydrate. Inorganic Chemistry. 1995;**34**(25):6409-6411

Chapter 5

The Triply Bonded Al≡Sb Molecules: A Theoretical Prediction

Jia-Syun Lu, Ming-Chung Yang and Ming-Der Su

Additional information is available at the end of the chapter

http://dx.doi.org/10.5772/intechopen.78412

Abstract

The effect of substitution on the potential energy surfaces of RAl≡SbR (R = F, OH, H, CH_3, SiH_3, $SiMe(Si\mathit{t}Bu_3)_2$, Si*i*PrDis$_2$, Tbt, and Ar*) is investigated using density functional theories (M06-2X/Def2-TZVP, B3PW91/Def2-TZVP, and B3LYP/LANL2DZ + dp). The theoretical results demonstrated that all the triply bonded RAl≡SbR compounds with small substituents are unstable and can spontaneously rearrange to other doubly bonded isomers. That is, the smaller groups, such as R = F, OH, H, CH_3 and SiH_3, neither kinetically nor thermodynamically stabilize the triply bonded RAl≡SbR compounds. However, the triply bonded R′Al≡SbR′ molecules that feature bulkier substituents (R′ = SiMe(Si*t*Bu3)2, Si*i*PrDis2, Tbt, and Ar*) are found to possess the global minimum on the singlet potential energy surface and are both kinetically and thermodynamically stable. In particular, the bonding characters of the R′Al≡SbR′ species agree well with the valence-electron bonding model (model) as well as several theoretical analyses (the natural bond orbital, the natural resonance theory, and the charge decomposition analysis). That is to say, R′Al≡SbR′ molecules that feature groups are regarded as R′—Al≡Sb—R′. Their theoretical evidence shows that both the electronic and the steric effects of bulkier substituent groups play a decisive role in making triply bonded R′Al≡SbR′ species synthetically accessible and isolable in a stable form.

Keywords: aluminum, antimony, group 13 elements, group 13 elements, triple bond

1. Introduction

The chemical synthesis and structural characterization of molecules that feature triple bonds [2] between heavier group 14 elements (E14 = Si, Ge, Sn and Pb) are of interest because of their interesting structural chemistry and their potential applications in organic and inorganic synthesis [1–10]. Although understanding of these RE14≡E14R molecules that feature heavier

group 14 atoms has increased during the last two decades, the understanding of the RE13≡E15R compounds, which are isoelectronic to acetylene from a valence electron viewpoint, is still limited. The reason for this limited knowledge of acetylene analogues, RE13≡E15R, could be due to the fact that there has been limited preparation and the isolation of these species in a stable form [11, 12]. Theoretical methods allow a theoretical design of the RE13≡E15R molecules to be made that increases understanding of their potential properties.

The III-V semiconductors that contain antimony have several important applications in optoelectronic devices that operate in the infrared region and in high-speed devices, which has prompted widespread studies of promising precursor systems for these materials [13]. In particular, the chemical synthesis and structural characterization of AlSb single-source precursors of the type R3Al-SbR′3 has attracted much attention, owing to their importance in CVD procedures [14], which is a developing industry for the production of thin films of the corresponding semiconducting materials [15]. As far as the authors are aware, only a handful of group 13 antimonides that contain Al—Sb σ-bonds have been discovered [16], No triply bonded RAl≡SbR species, which is isoelectronic to HC≡CH, has been reported both experimentally and theoretically.

Density functional theory (DFT) is sued to determine the structures, the kinetic stability and bonding properties of various RAl≡SbR triply bonded forms on the singlet ground state, in order to obtain a better understanding of aluminum≡antimony triple bonds. This work reports the possible existence of triply bonded RAl≡SbR molecules, from the viewpoint of the effect of substituents, using DFT [17]. That is, M06-2X/Def2-TZVP, B3PW91/Def2-TZVP

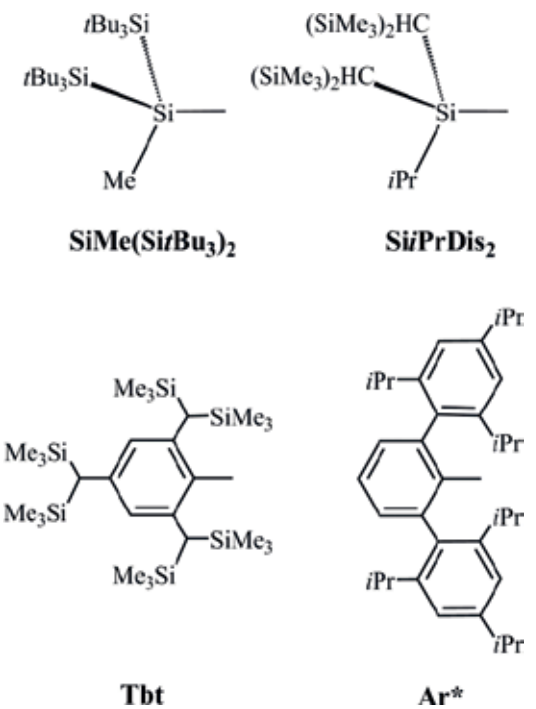

Scheme 1. Four bulky ligands, which are SiMe(Si*t*Bu$_3$)$_2$, Si*i*PrDis$_2$, Tbt, and Ar*.

and B3LYP/LANL2DZ + dp are used for small substituents (R = H, F, OH, CH_3, and SiH_3) and M06-2X/Def2-TZVP [18] for large substituents (R = SiMe(Si*t*Bu3)2, Si*i*PrDis2, Tbt, and Ar*; see **Scheme 1**) [19].

2. General considerations

The valence-bond bonding model is a well-known satisfactory method, which is an approximate theory to explain the electron pair or chemical bond by quantum mechanics, for predicting molecular geometries [20]. Two valence-bond bonding models (**Figure 1**) are thus used to interpret the bonding properties of triply bonded RAl≡SbR species. In model [1], the RAl≡SbR molecule is partitioned into two units: a singlet R—Al and a singlet R—Sb. In model [2], the RAl≡SbR compound is divided into two moieties: a triplet R—Al and a triplet R—Sb.

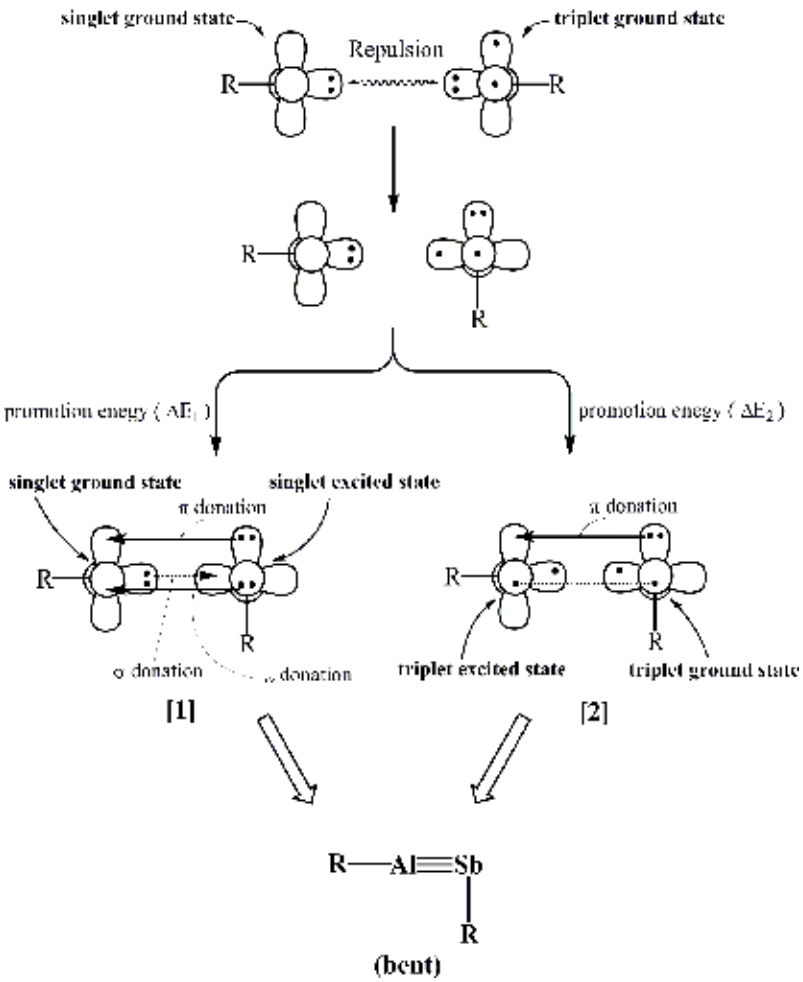

Figure 1. The valence-bond bonding models [1, 2] for the triply bonded RAl≡SbR molecule.

As a result, the choice of the bonding model that is used to explain the bonding characters of RAl≡SbR depends on the promotion energies ($\Delta E_{ST} = E_{triplet} - E_{singlet}$) of the R—Al and R—Sb fragments. According to current theoretical calculations (see below), it is known that R—Al occupies the singlet ground state, but R—Sb occupies the triplet ground state. In consequence, if the value of ΔE_{ST} for R—Al is much larger than that for R—Sb, the latter easily jumps to the singlet excited state. Hence, model [1] can be used to explain the bonding nature of the RAl≡SbR molecule. In contrast, if the value of ΔE_{ST} for R—Al is smaller than that for R—Sb, the former is readily promoted to the excited triplet state. Therefore, model [2] is used to interpret the bond constitutions of the RAl≡SbR compound.

Two points are worthy of note. The first is that since aluminum and antimony respectively belong to group 13 and group 15 and both elements have different atomic radii (covalent radii: 118 pm and 140 for Al and Sb, respectively) [20], the overlapping populations between Al and Sb should not be strong. The second is that the lone pairs of both aluminum and antimony feature the valence s character. This, in turn, makes the overlap integrals between the lone pair orbital and the pure p orbital small. These two factors mean that the triple bond between aluminum and antimony is weak, unlike the traditional triple bond in acetylene.

Bearing the above bonding analyses in mind, theoretical evidences are given in the following sections.

3. Results and discussion

3.1. Small ligands on substituted RAl≡SbR

Five small substituents (R = F, OH, H, CH_3 and SiH_3) are chosen, which include electronegative and electropositive groups, to determine their stability and bonding properties on the triply bonded RAl≡SbR molecules using the three types of DFT calculations (i.e., M06-2X/Def2-TZVP, B3PW91/Def2-TZVP and B3LYP/LANL2DZ + dp). **Figure 2** shows the potential energy surfaces of the intra-molecular 1,2-migration reactions for five triply bonded RAl≡SbR compounds that feature small substituents. That is to say, the triply bonded RAl≡SbR species can undergo a 1,2-shift to give either R2Al=Sb: or: Al=SbR2 doubly bonded isomers.

As seen in **Figure 2**, the three DFT computational results demonstrate that the triply bonded RAl≡SbR species that feature small substituents are all both kinetically and thermodynamically unstable on the intra-molecular 1,2-migration reaction potential energy surfaces. In other words, once the triply bonded RAl≡SbR with small substituents is formed, it can easily proceed along the 1,2-migration to give the thermodynamically stable doubly bonded isomer, either R2Al=Sb: or: Al=SbR2. The theoretical findings give strong evidence that the triply bonded RAl≡SbR molecules that feature the small ligands are highly unlikely to be detected experimentally.

Although current theoretical observations show that the formation of RAl≡SbR involving small ligands is not likely, some of their physical properties, which are shown in **Table 1**, must be theoretically determined in order to design much more stable aluminum≡antimony acetylene analogues.

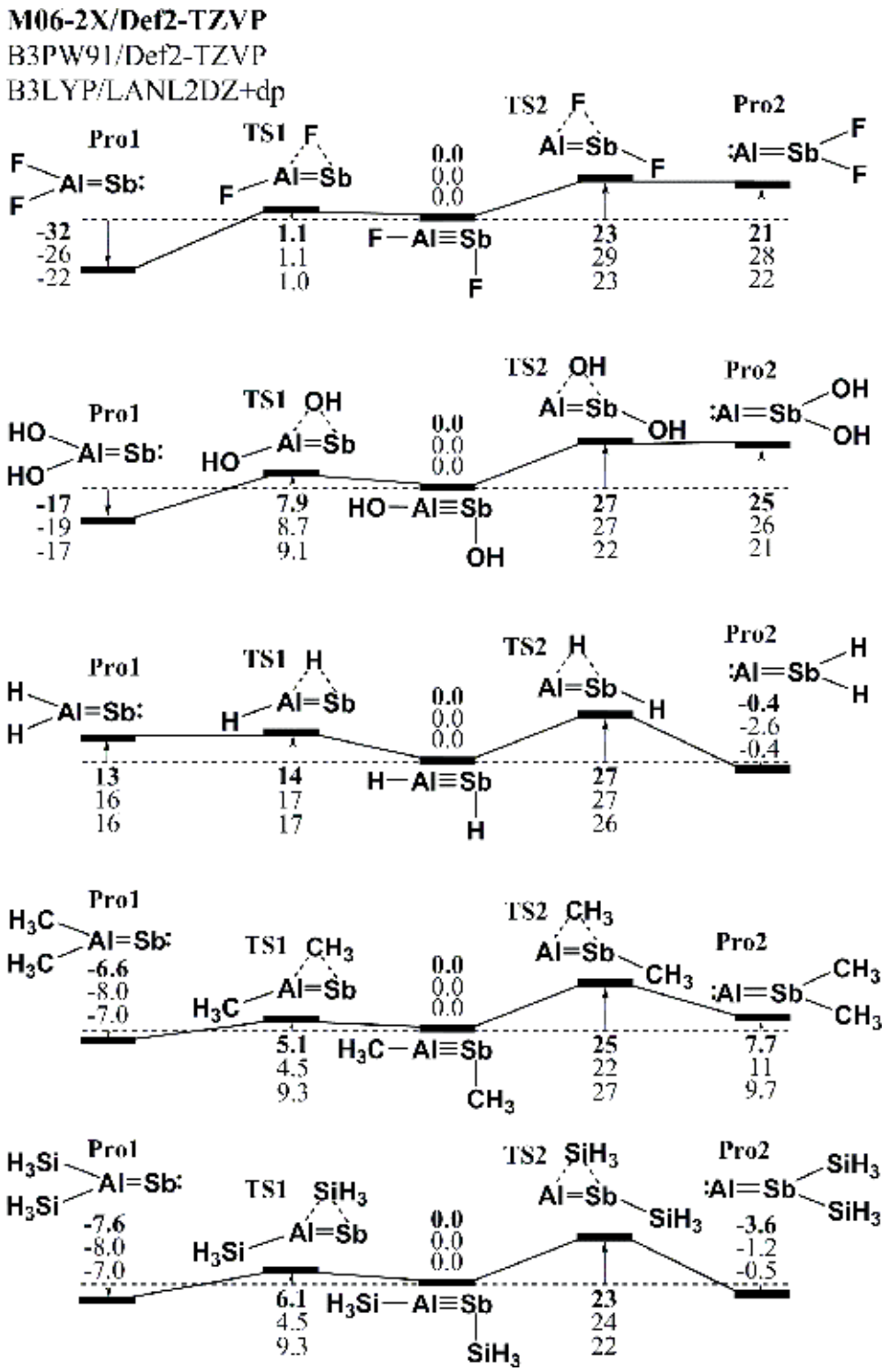

Figure 2. The 1,2-migration energy surfaces for RAl≡SbR (R = H, F, CH_3, OH, and SiH_3). These relative Gibbs free energies (kcal/mol) are computed at the M06-2X/Def2-TZVP, B3PW91/Def2-TZVP, and B3LYP/LANL2DZ + dp levels of theory.

R	F	OH	H	CH_3	SiH_3
AlαSb (Å)	2.528 (2.536) [2.556]	2.531 (2.518) [2.565]	2.388 (2.397) [2.436]	2.466 (2.462) [2.499]	2.539 (2.524) [2.560]
∠R-Al-Sb (°)	176.8 (176.2) [179.2]	173.4 (172.0) [176.5]	170.7 (167.6) [167.6]	177.7 (173.8) [173.2]	176.8 (176.2) [179.7]
∠Al-Sb-R (°)	88.86 (88.07) [88.53]	86.55 (86.13) [90.43]	82.25 (84.42) [86.43]	94.46 (96.42) [96.75]	88.86 (88.07) [88.53]
∠R-Sb-Al-R (°)	179.9 (179.9) [180.0]	179.7 (176.9) [178.6]	180.0 (180.0) [180.0]	179.6 (179.9) [178.2]	179.9 (179.9) [180.0]
Q_{Al}[1]	0.5201 (0.495) [0.715]	0.418 (0.401) [0.469]	0.164 (0.161) [0.414]	0.291 (0.262) [0.282]	0.208 (0.219) [0.193]
Q_{Sb}[2]	0.329 (0.277) [0.217]	0.196 (0.136) [0.119]	−0.134 (−0.107) [-0.032]	−0.054 (−0.018) [−0.134]	−0.198 (−0.100) [−0.179]
ΔE_{ST} for Al-R (kcal/mol)[3]	79.78 (71.44) [73.78]	72.05 (65.86) [67.75]	43.73 (40.25) [40.80]	48.75 (42.38) [45.00]	32.87 (29.08) [31.97]
ΔE_{ST} for Sb-R (kcal/mol)[4]	−32.40 (−28.88) [−27.52]	−25.88 (−21.16) [−20.04]	−33.35 (−29.42) [−27.91]	−31.52 (−27.31) [−26.00]	−30.78 (−25.61) [−25.21]
HOMO-LUMO (kcal/mol)	165.5 (168.4) [167.2]	159.8 (140.1) [145.2]	257.6 (205.2) [277.6]	146.4 (123.3) [129.2]	172.2 (179.5) [177.9]
BE (kcal/mol)[5]	25.82 (32.05) [27.43]	22.77 (27.32) [21.96]	55.28 (64.05) [56.79]	42.23 (51.72) [46.41]	61.00 (67.80) [57.43]
WBI[6]	1.483 (1.556) [1.560]	1.474 (1.550) [1.555]	1.754 (1.799) [1.779]	1.659 (1.714) [1.733]	1.581 (1.596) [1.637]

[1]The charge density on the Al element.
[2]The charge density on the Sb element.
[3]ΔE_{ST} = E(triplet state for R—Al) − E(singlet state for R—Sb).
[4]ΔE_{ST} = E(triplet state for R—Al) − E(singlet state for R—Sb).
[5]BE = E(singlet state for R—Al) + E(triplet state for R—Sb) − E(singlet state for RAl≡SbR).
[6]The Wiberg bond index (WBI) for the Al≡Sb bond: see Ref. [22].

Table 1. The key geometrical parameters, the singlet-triplet energy splitting (ΔE_{ST}), the natural charge densities (QAl and QSb), the binding energies (BE), the HOMO-LUMO energy gaps, and the Wiberg bond index (WBI) for RAl≡SbR using the M06-2X/Def2-TZVP, B3PW91/Def2-TZVP (in round brackets) and B3LYP/LANL2DZ + dp (in square brackets) levels of theory.

As seen in **Table 1**, the three DFT computational results predict that the Al≡Sb triple bond distance (Å) is in the ranges 2.388–2.539 (M06-2X/Def2-TZVP), 2.397–2.536 (B3PW91/Def2-TZVP) and 2.436–2.565 (B3LYP/LANL2DZ + dp). **Table 1** also shows that all of the geometrical

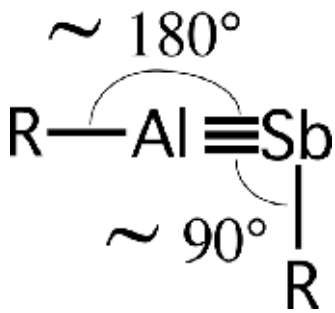

Scheme 2. The geometrical structure of RAl≡SbR with the small substituent, R.

structures of RAl≡SbR adopt the bent form, as demonstrated in **Scheme 2**. That is, ∠R—Al—Sb ≈ 180.0° and ∠Al—Sb—R ≈ 90.0°. The reason for this vertical angle at the Sb center can be ascribed to the relativistic effect, as discussed previously [21]. The three DFT calculations shown in **Table 1** all indicate that the electronic ground states for R—Al and the R—Sb fragments are singlet and triplet, respectively. In particular, all of the DFT results shown in **Table 1** show that most of the singlet-triplet energy splitting (ΔE_{ST}) of R-Al is larger than that of the corresponding R—Sb. This strongly implies that the bonding characters of the triply bonded RAl≡SbR species that feature small substituents are better described by model [1], as shown in **Figure 1**. In other words, the triple bond consists of one donor-acceptor σ bond and two donor-acceptor π bonds, which are schematically represented as R—Al⇆Sb—R. As previously mentioned, since the lone pair orbitals of both the R-Al and the R-Sb fragments feature the valence s character, their overlapping populations between the lone orbital and the valence p orbital should be smaller. Indeed, the supporting evidence from **Table 1** shows that all bond orders for the RAl≡SbR species are estimated to be less than 2.0 (WBI = 1.474–1.799), which is less than the bond order for the C≡C triple bond in acetylene (WBI = 2.99).

In brief, the three DFT calculations shown in this work show that irrespective of their electronegativity, the triply bonded RAl≡SbR molecules that feature small ligands are highly unlikely to exist, even in the low-temperature matrices. In particular, the bond orders of these Al≡Sb triple bonds are theoretically predicted to be a weak double bond, rather than a triple bond.

3.2. Large ligands on substituted R′Al≡SbR′

Three bulky groups were then used to search for kinetically stable triple-bonded R′Al≡SbR′ molecules: R′(=SiMe(Si*t*Bu3)2, Si*i*PrDis2, Tbt, and Ar*) [19]. These are shown in **Scheme 1**. It is known that London dispersion (nonvalent interactions) plays a prominent role in both chemical and physical properties of inorganic molecules [23]. As a result, the dispersion-corrected M06-2X/Def2-TZVP method is used in the present study to investigate the behaviors of the triply bonded R′Al≡SbR′ compounds bearing bulky substituents. Similarly to the cases for small ligands on substituted RAl≡SbR, the dispersion-corrected M06-2X/Def2-TZVP level of theory is used to determine the potential energy surfaces for the intra-molecular 1,2-migration

reactions of R′Al≡SbR′, as shown in **Scheme 3**. The computed relative energies are listed in **Table 2**. The reaction enthalpies for both the 1,2-shift reactions (R′Al≡SbR′ → R2′Al=Sb and R′Al≡SbR′ → R2′Sb=Al) are apparently too high. They are estimated to be at least 80 kcal/mol. The reason that both doubly bonded R2′Al=Sb and R2′Sb=Al isomers occupy such high energy points is simply because two bulky groups can cause steric overcrowding. As a consequence, the theoretical findings strongly suggest that the triply bonded R′Al≡SbR′, which is attached by two bulkier substituents, is kinetically stabilized.

Table 2 shows that the Al≡Sb triple bond distance is predicted to be 2.422–2.477 Å. Since no experimental results for the Al≡Sb triple bond length have been reported, these values are estimates. These theoretical calculations also show that the geometrical structures of R′Al≡SbR′ molecules that feature bulky groups adopt a bent structure; i.e., ∠R′—Al—Sb ≈ 160.0° and ∠Al—Sb—R′ ≈ 120.0°. As stated previously, the triply bonded R′Al≡SbR′ species feature this bent geometry because of the relativistic effect [23].

In addition, the bonding energy (BE) that is shown in **Table 2** shows that the central aluminum and antimony atoms in the substituted R′Al≡SbR′ compounds are strongly bonded, since the

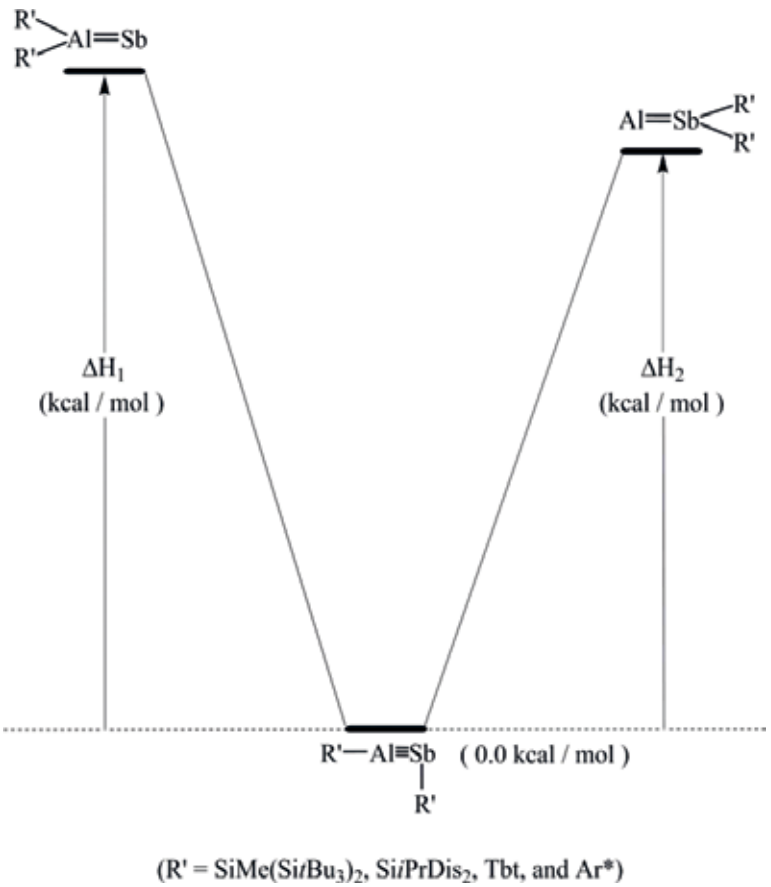

Scheme 3. The qualitative potential energy surface of the R′Al≡SbR′ isomers with the bulky substituent, R′.

R′	SiMe(Si*t*Bu$_3$)$_2$	Si*i*PrDis$_2$	Tbt	Ar*
Al≡Sb (Å)	2.463	2.422	2.477	2.447
∠R′—Al—Sb (°)	157.6	152.0	161.3	165.0
∠Al—Sb—R′ (°)	126.5	123.6	122.2	124.6
∠R′—Al—Sb—R′ (°)	173.5	172.9	167.2	166.0
Q_{Al}[1]	0.619	0.637	1.008	1.027
Q_{Sb}[2]	−0.387	−0.492	−0.025	−0.114
ΔE_{ST} for Al—R′ (kcal/mol)[3]	28.89	27.30	42.50	40.21
ΔE_{ST} for Sb—R′ (kcal/mol)[4]	−16.89	−24.80	−30.51	−15.92
HOMO-LUMO (kcal/mol)	53.56	60.07	56.08	56.68
BE (kcal/mol)[5]	71.29	72.97	87.43	74.33
ΔH_1 (kcal/mol)[6]	94.23	84.67	92.12	82.68
ΔH_2 (kcal/mol)[6]	83.15	84.08	80.01	88.19
WBI[7]	2.174	2.181	2.072	2.016

[1]The charge density on the Al element.
[2]The charge density on the Sb element.
[3]ΔE_{ST} (kcal mol^{-1}) = E(triplet state for R′—Al) − E(singlet state for R′—Al).
[4]ΔE_{ST} (kcal mol^{-1}) = E(triplet state for R′—Sb) − E(singlet state for R′—Sb).
[5]BE (kcal mol^{-1}) = E(triplet state for R′—Al) + E(triplet state for R′—Sb) − E(singlet for R′Al≡SbR′).
[6]See **Scheme 3**.
[7]The Wiberg bond index (WBI) for the AlαSb bond: see Ref. [22].
See also **Scheme 3**.

Table 2. The key geometrical parameters, the singlet-triplet energy splitting (ΔE_{ST}), the natural charge densities (QAl and QSb), the binding energies (BE), the HOMO-LUMO energy gaps, reaction enthalpies, and the Wiberg bond index (WBI) for R′Al≡SbR′ at the dispersion-corrected M06-2X/Def2-TZVP level of theory.

BE values are in the range 71–97 kcal/mol for R′ = SiMe(Si*t*Bu3)2, Si*i*PrDis2, Tbt, and Ar*. **Table 2** also shows that the modulus ΔE_{ST} (kcal/mol) for Al—R′ and Sb—R′ fragments are predicted to be 43–27 and 31–16. These theoretical values allow two interpretations. Firstly, even when attached by bulkier groups, it is theoretically verified that both the Al—R′ and the Sb—R′ units occupy the ground singlet state and the ground triplet state, respectively. Since the ΔE_{ST} values for Al—R′ are so small (compared with those for Al—R, as shown in **Table 1**), model [2] in **Figure 1** is most suitable to interpret the triple bonding characters in the R′Al≡SbR′ species that feature bulky substituents. As schematically shown in **Figure 1**, the nature of the Al≡Sb triple bond can be considered as one conventional σ bond, one conventional π bond and one donor-acceptor π bond. That is, R′—Al⇇Sb—R′. It is worthy of note that two factors affect the overlapping populations between the central Al and Sb elements. The first is that the lone pair orbital of the Sb—R′ moiety features the valence s character. This, in turn, renders the overlap population between the pure p orbital of Al and the lone pair orbital of Sb very small. The other is that the sizes of the valence p orbitals for Al and Sb are quite different, since they belong to different rows of the periodic table having different principal quantum numbers. As a result, the triple bond in R′Al≡SbR′ molecules that feature

bulky substituents is predicted to be quite weak. Indeed, the theoretical evidences given in **Table 2** shows that the bond order is a little bit higher than 2.0 (WBI ≈ 2.17, 2.18, 2.07 and 2.02 for R′ = SiMe(Si*t*Bu3)2, Si*i*PrDis2, Tbt, and Ar*, respectively). The bond order for the conventional C≡C bond in acetylene is estimated to be 2.99.

Besides these, Dapprich and Frenking developed a useful method [24], which is called the introduced charge decomposition analysis (CDA), from which one may analyze donor-acceptor interactions of a A-B molecule. From CDA, one may obtain three parts. The first part is the number of electrons donated from the R′—Al unit to the R′—Sb monomer, which can be considered as (R′—Al) → (R′—Sb). The second part is the number of electrons back donated from the R′—Sb component to the R′—Al moiety, which can be represented as (R′—Al) ← (R′—Sb). The third part is the repulsive interactions between (R′—Al) and (R′—Sb), which can be described as (R′—Al) ↔ (R′—Sb). The CDA results about the (SiMe(Si*t*Bu$_3$)$_2$)Al≡Sb(SiMe(Si*t*Bu$_3$)$_2$) molecule based on the dispersion-corrected M06-2X/Def2-TZVP method are given in **Table 3**. As seen in **Table 3**, for the (R′—Sb) fragment, its largest contribution is No. 267 (HOMO) orbital, displaying that a R′—Sb component donates electrons to a R′—Ga unit mainly through the HOMO orbital. In consequence, the net amount of electron transfer is estimated to be −0.207, implying that the R′—Sb part donates more electrons to the R′—Al moiety. This theoretical finding agrees well with the valence-electron bonding model shown in **Figure 1** (i.e., model [2]). Namely, the bonding character of R′Al≡SbR′ can be recognized as R′Al⇇SbR′.

	Orbital	Occupancy	A	B	A-B	W
	257	2.000000	0.000897	0.000398	0.000499	0.000052
	258	2.000000	−0.000691	−0.000223	−0.000469	−0.003158
	259	2.000000	0.000003	0.000212	−0.000209	−0.000135
	260	2.000000	−0.000574	0.001495	−0.002069	−0.003430
	261	2.000000	0.000322	0.000997	−0.000676	−0.003797
	262	2.000000	0.000333	0.000068	−0.002466	−0.012549
	263	2.000000	0.000927	0.007097	0.000859	0.000836
	264	2.000000	0.001417	0.031682	−0.003680	−0.003811
	265	2.000000	0.005618	0.033540	−0.057513	−0.129159
	266	2.000000	0.016174	0.031540	−0.017366	0.011841
HOMO	267	2.000000	−0.000521	0.063131	−0.032203	−0.047961
LUMO	268	0.000000	0.000000	0.000000	0.000000	0.000000
	269	0.000000	0.000000	0.000000	0.000000	0.000000
Sum[a]		534.000000	0.043071	0.250110	−0.207039	−0.099090

For clearness, only list the X, Y, and W terms for HOMO(no.267)-11 ∼ LUMO+2.
[a]Summation of contributions from all unoccupied and occupied orbitals.

Table 3. The charge decomposition analysis (CDA) for R′Al≡SbR′ (R′ = SiMe(Si*t*Bu$_3$)$_2$) system based on M06-2X orbitals, where a is the number of electrons donating from R′—Al unit to R′—Sb unit, B is the number of electrons donating from R′-Sb moiety to R′-Al moiety and W is the number of electrons involved in repulsive polarization.

The bonding characters of the Al≡Sb triple bond in R′Al≡SbR′ molecules were examined using the natural bond orbital (NBO) [22] and the natural resonance theory (NRT) [25] analysis, whose results are given in **Table 4**, are used to determine the bonding properties. For instance, **Table 4** shows that for (SiMe(Si*t*Bu3)2)Al≡Sb(SiMe(Si*t*Bu3)2), the NBO model shows that the Al-Sb σ bonding orbital contains about 23% natural Al orbitals and 77% natural Sb orbitals. Also, the Al≡Sb π bonding orbital contains averagely about 25% natural Al orbitals and 75% natural Sb orbitals (**Figure 3**). These values give strong evidence that the Al≡Sb π bond is polarized. **Table 4** also shows that the Al≡Sb π bonding interaction: $\pi_{\perp}$(Al≡Sb) = 0.529 (3s3p$^{1.98}$)Al + 0.849(5s5p$^{12.43}$)Sb and $\pi_{\parallel}$(Al≡Sb) = 0.475(3s3p$^{99.99}$)Al + 0.880(5s5p$^{99.99}$)Sb, which again implies that the predominant bonding interaction between the Al—R and the Sb—R moieties originates from 3p(Al) ← 5p(Sb) donation. In other words, the electron deficiency on Al and the π bond polarity are partially balanced by the donation of the Sb lone pair to the empty Al p orbital (**Figure 3**). **Table 4** also shows that, on the basis of the NRT analyses of the electron density for (SiMe(Si*t*Bu3)2)Al≡Sb(SiMe(Si*t*Bu3)2), its Al≡Sb triple bond has a greater

R′Al≡SbR′	WBI	NBO analysis			NRT analysis	
		Occupancy	Hybridization	Polarization	Total/covalent/ionic	Resonance weight
R′ = SiMe (Si*t*Bu$_3$)$_2$	2.17	σ: 1.91	σ: 0.4799 Al (sp$^{3.23}$) + 0.8773 Sb (sp$^{0.60}$)	23.03% (Al) 76.97% (Sb)	2.06/1.25/0.81	Al—Sb: 10.84% Al⊜Sb: 71.95% Al≡Sb: 17.21%
		$\pi_{\perp}$: 1.81	$\pi_{\perp}$: 0.5288 Al (sp$^{1.98}$) + 0.8487 Sb (sp$^{12.43}$)	27.96% (Al) 72.04% (Sb)		
		$\pi_{\parallel}$: 1.89	$\pi_{\parallel}$: 0.4753 Al (sp$^{99.99}$) + 0.8798 Sb (sp$^{99.99}$)	22.59% (Al) 77.41% (Sb)		
R′ = Si*i*PrDis$_2$	2.18	σ: 1.91	σ: 0.5525 Al (sp$^{1.71}$) + 0.8335 Sb (sp$^{1.15}$)	30.53% (Al) 69.47% (Sb)	2.48/1.29/1.19	Al—Sb: 10.63% Al⊜Sb: 75.53% Al≡Sb: 13.84%
		$\pi_{\perp}$: 1.86	$\pi_{\perp}$: 0.4723 Al (sp$^{3.67}$) + 0.8815 Sb (sp$^{3.68}$)	22.30% (Al) 77.70% (Sb)		
		$\pi_{\parallel}$: 1.89	$\pi_{\parallel}$: 0.4476 Al (sp$^{99.99}$) + 0.8943 Sb (sp$^{99.99}$)	20.03% (Al) 79.97% (Sb)		
R′ = Tbt	2.07	σ: 1.95	σ: 0.6923 Al (sp$^{0.18}$) + 0.7216 Sb (sp$^{12.38}$)	47.93% (Al) 52.07% (Sb)	2.22/1.41/0.82	Al—Sb: 5.89% Al⊜Sb: 65.89% Al≡Sb: 28.22%
		$\pi_{\perp}$: 1.88	$\pi_{\perp}$: 0.4488 Al (sp$^{47.14}$) + 0.8936 Sb (sp$^{99.99}$)	20.14% (Al) 79.86% (Sb)		
		$\pi_{\parallel}$: 1.91	$\pi_{\parallel}$: 0.4772 Al (sp$^{99.99}$) + 0.8788 Sb (sp$^{99.99}$)	22.78% (Al) 77.22% (Sb)		
R′ = Ar*	2.02	σ: 1.96	σ: 0.6946 Al (sp$^{0.16}$) + 0.7194 Sb (sp$^{18.14}$)	48.25% (Al) 51.75% (Sb)	2.01/1.44/0.57	Al—Sb: 11.37% Al⊜Sb: 76.76% Al≡Sb: 11.87%
		$\pi_{\perp}$: 1.83	$\pi_{\perp}$: 0.4543 Al (sp$^{99.99}$) + 0.8908 Sb (sp$^{40.30}$)	20.64% (Al) 79.36% (Sb)		
		$\pi_{\parallel}$: 1.92	$\pi_{\parallel}$: 0.4266 Al (sp$^{99.99}$) + 0.9044 Sb (sp$^{99.99}$)	18.20% (Al) 81.80% (Sb)		

Table 4. The natural bond orbital (NBO), the natural resonance theory (NRT) analysis, and Wiberg bond index (WBI) for R′Al≡SbR′ molecules that feature ligands (R′ = SiMe(Si*t*Bu$_3$)$_2$, Si*i*PrDis$_2$, and NHC) at the dispersion-corrected M06-2X/Def2-TZVP level of theory.

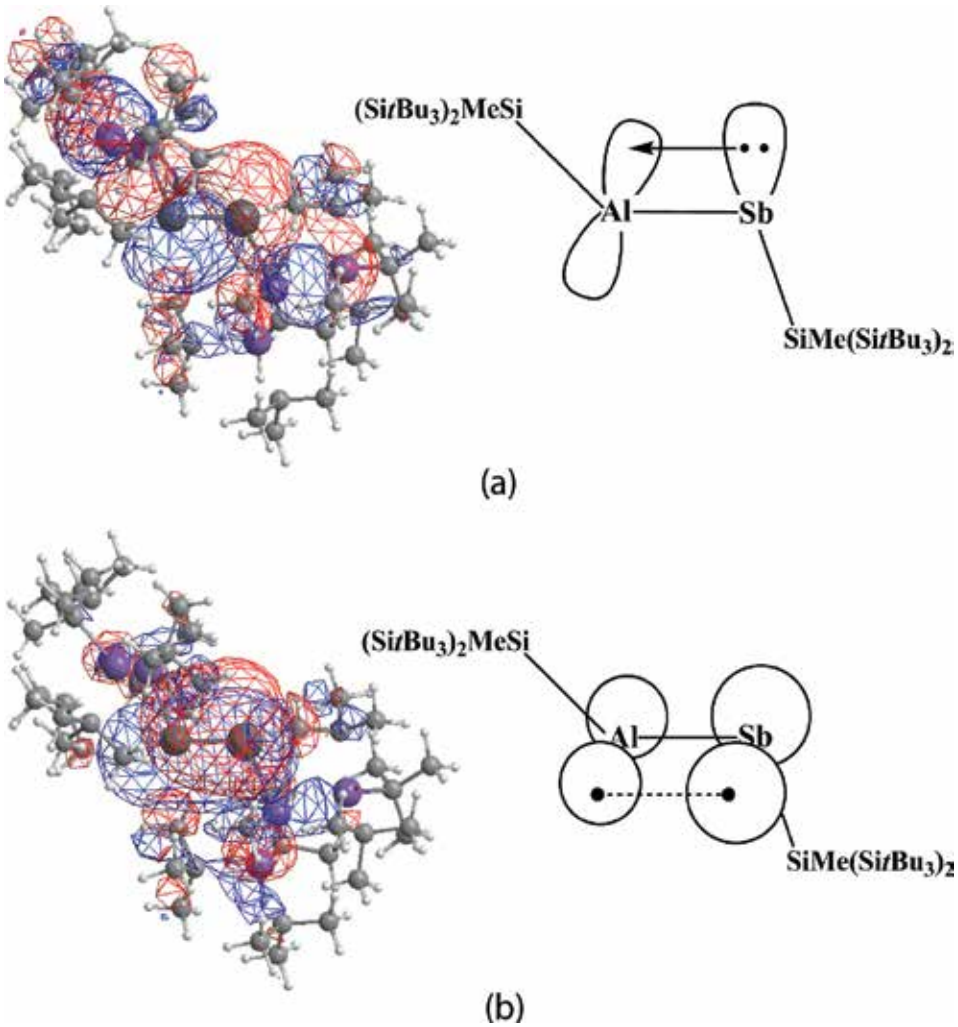

Figure 3. The natural Al≡Sb π bonding orbitals ((i) and (ii)) for (SiMe(Si*t*Bu$_3$)$_2$)Al≡Sb(SiMe(Si*t*Bu$_3$)$_2$). Also, see **Figure 1**. (i) $\pi_{\perp}$, (ii) $\pi_{\parallel}$.

covalent character, as shown by the greater covalent part of the NRT bond order (1.25), compared to its ionic part (0.81). The reason for this may be due to the fact that the difference between the electronegativity values for the Al and Sb elements is small (Al: 1.5 and Sb: 1.8) [26].

4. Conclusion

This study uses DFT computations to theoretically design substituted RAl≡SbR molecules that feature the Al≡Sb triple bond, that are stable from the kinetic viewpoint. The theoretical observations show that only bulky substituents (R′) can significantly stabilize the triply

bonded R′Al≡SbR′ compounds, and not small substituents. The theoretical findings also show that the bonding characters of the R′Al≡SbR′ species that feature bulky groups can be represented as R′—Al⇐Sb—R′. That is to say, the R′Al≡SbR′ species contains a conventional σ bond, a conventional π bond and a donor-acceptor π bond. However, due to the poor overlapping populations between the Al and Sb elements, which is due to the different atomic sizes of the two elements and the nature of overlapping bonding orbitals, the Al≡Sb triple bond is very weak. The theoretical results also give strong evidence that the geometrical structures of the R′Al≡SbR′ species adopt a bent conformation with a nearly perpendicular angle at the antimony center.

Acknowledgements

The authors are grateful to the National Center for High-Performance Computing of Taiwan for generous amounts of computing time, and the Ministry of Science and Technology of Taiwan for the financial support.

Author details

Jia-Syun Lu[1], Ming-Chung Yang[1] and Ming-Der Su[1,2]*

*Address all correspondence to: midesu@mail.ncyu.edu.tw

1 Department of Applied Chemistry, National Chiayi University, Chiayi, Taiwan

2 Department of Medicinal and Applied Chemistry, Kaohsiung Medical University, Kaohsiung, Taiwan

References

[1] Fischer RC, Power PP. π-Bonding and the lone pair effect in multiple bonds involving heavier main group elements: Developments in the new millennium. Chemical Reviews. 2010;**110**:3877-3923. DOI: 10.1021/cr100133q

[2] Danovich D, Bino A, Shaik S. Formation of carbon–carbon triply bonded molecules from two free carbyne radicals via a conical intersection. Journal of Physical Chemistry Letters. 2013;**4**:58-64. DOI: 10.1021/jz3016765

[3] Sasamori T, Hironaka K, Sugiyama T, Takagi N, Nagase S, Hosoi Y, Furukawa Y, Tokitoh N. Synthesis and reactions of a stable 1,2-diaryl-1,2-dibromodisilene: A precursor for substituted disilenes and a 1,2-diaryldisilyne. Journal of the American Chemical Society. 2008;**130**:13856-13857. DOI: 10.1021/ja8061002.

[4] Spikes GH, Power PP. Lewis base induced tuning of the Ge–Ge bond order in a "digermyne". Chemical Communications. 2007;**1**:85-87. DOI: 10.1039/B612202G

[5] Phillips AD, Wright RJ, Olmstead MM, Synthesis PPP. Characterization of 2,6-$Dipp_2$-$H_3C_6SnSnC_6H_3$-2,6-$Dipp_2$ (Dipp = C_6H_3-2,6-Pr^i_2): A tin analogue of an alkyne. Journal of the American Chemical Society. 2002;**124**:5930-5931. DOI: 10.1021/ja0257164

[6] Pu L, Twamley B, Power PP. Synthesis and characterization of 2,6-$Trip_2H_3C_6PbPbC_6H_3$-2,6-$Trip_2$ (trip=C_6H_2-2,4,6-i-Pr_3): A stable heavier group 14 element analogue of an alkyne. Journal of the American Chemical Society. 2000;**122**:3524-3525. DOI: 10.1021/ja993346m

[7] Lühmann N, Müller T. A compound with a Si–C triple bond. Angewandte Chemie, International Edition. 2010;**49**:10042-10044. DOI: 10.1002/anie.201005149

[8] Wu P-C, Su M-D. Theoretical designs for germaacetylene (RC≡GeR'): A new target for synthesis. Dalton Transactions. 2011;**40**:4253-4259. DOI: 10.1039/C0DT00800A

[9] Wu P-C, Su M-D. Triply bonded stannaacetylene (RC≡SnR): Theoretical designs and characterization. Inorganic Chemistry. 2011;**50**:6814-6822. DOI: 10.1021/ic200930v

[10] Wu P-C, Su M-D. A new target for synthesis of triply bonded plumbacetylene (RC≡PbR): A theoretical design. Organometallics. 2011;**30**:3293-3301. DOI: 10.1021/om2000234

[11] Paetzold P. Boron-nitrogen analogues of cyclobutadiene, benzene and cyclooctatetraene. Phosphorus, Sulfur, and Silicon. 1994;**93-94**:39-50. DOI: 10.1080/10426509408021797

[12] Wright RJ, Phillips AD, Allen TL, Fink WH, Power PP. Synthesis and characterization of the monomeric imides Ar′MNAr′′ (M = Ga or in; Ar′ or Ar′′ = terphenyl ligands) with two-coordinate gallium and indium. Journal of the American Chemical Society. 2003;**125**:1694-1695. DOI: 10.1021/ja029422u

[13] Gardiner MG, Raston CL. Advances in the chemistry of Lewis base adducts of alane and gallane. Coordination Chemistry Reviews. 1997;**166**:1-34. DOI: 10.1016/S0010-8545(97)00002-7

[14] Grovenor CRM. Microelectronic Materials. Philadelphia, PA: Adam Hilger; 1989

[15] Park HY, Wessels A, Roesky HW, Schulz S. First approach to an AlSb layer from the single source precursors $[Et_2AlSb(SiMe_3)_2]_2$ and $[^iBu_2AlSb(SiMe_3)_2]_2$. Chemical Vapor Deposition. 1999;**5**:179-184. DOI: 10.1002/(SICI)1521-3862(199908)5:4<179::AID CVDE179>3.0.CO;2-6

[16] Schulz S, Kuczkowski A, Nieger M. Synthesis and X-ray structures of all-alkyl-substituted AlSb ring compounds. Organometallics. 2000;**19**:699-702. DOI: 10.1021/om990795m

[17] Kuczkowski A, Schulz S, Nieger M, Schreiner PR. Experimental and Computational Studies of R_3Al-ER'_3 (E = P, As, Sb, Bi; R = Et, *t*-Bu; R′ = $SiMe_3$, *i*-Pr) Donor-Acceptor Complexes: Role of the Central Pnictine and the Substituents on the Structure and Stability of Alane Adducts. Organometallics. 2002;**21**:1408-1419. DOI: 10.1021/om0200205

[18] Zhao Y, Truhlar DG. Density functionals with broad applicability in chemistry. Accounts of Chemical Research. 2008;**41**:157-167. DOI: 10.1021/ar700111a

[19] Takagi N, Nagase S. Substituent effects on germanium−germanium and tin−tin triple bonds. Organometallics. 2001;**20**:5498-5500. DOI: 10.1021/om010669u

[20] Ebbing DD, Gammon SD. General Chemistry. New York: Brooks/Cole; 2015. Chap. 9

[21] Reed AE, Curtiss LA, Weinhold F. Intermolecular interactions from a natural bond orbital, donor-acceptor viewpoint. Chemical Reviews. 1998;**88**:899-926. DOI: 10.1021/cr00088a005

[22] Pyykkö P. Strong closed-shell interactions in inorganic chemistry. Chemical Reviews. 1997;**97**:597-636. DOI: 10.1021/cr940396v

[23] Liptrot DJ, Power PP. London dispersion forces in sterically crowded inorganic and organometallic molecules. Nature Reviews Chemistry. 2017;**1**:4-16. DOI: 10.1038/s41570-016-0004

[24] Dapprich S, Frenking G. Investigation of donor-acceptor interactions: A charge decomposition analysis using fragment molecular orbitals. The Journal of Physical Chemistry. 1995; **99**:9352-9362. DOI: 10.1021/j100023a009

[25] Glendening ED, Badenhoop JK, Weinhold F. Natural resonance theory. III. Chemical applications. Journal of Computational Chemistry. 1998;**19**:628-646. DOI: 10.1002/(SICI)1096-987X(19980430)19:6<628::AID-JCC5>3.0.CO;2-T

[26] Huheey JE, Keiter EA, Keiter RL. Inorganic Chemistry: Principles of Structure and Reactivity. 4th ed. New York, USA: Harper Collins; 1993. p. 246

Chapter 6

Periodic Trends among Interstellar Molecular Species: The Case of Oxygen- and Sulfur-Containing Species

Etim Emmanuel, Lawal Usman, Khanal Govinda and Mbakara Idaresit

Additional information is available at the end of the chapter

http://dx.doi.org/10.5772/intechopen.80884

Abstract

Out of the 19 known S-containing interstellar molecules, 16 have the corresponding O-compound analogues marks out of the interstellar chemistry of sulfur and oxygen as a unique one among other observed interstellar periodic trends. However, the rule that the ratio of an interstellar sulfur molecule to its oxygen analogue is close to the cosmic S/O ratio is far from reality in many cases even when both species are observed from the same source. In this chapter, the effect of interstellar hydrogen bonding on the variation of the S/O abundance ratio with respect to the cosmic S/O ratio is investigated using high-level quantum chemical simulations. The detectability of the yet to be observed analogues of both S and O molecules is also examined. From the results, the deviation from the cosmic S/O ratio is largely due to hydrogen bonding on the surface of the dust grains. As the ratio of the binding energy of S- and O-species (binding energy of S/O) with water approaches unity, the S/O abundance ratio approaches cosmic S/O ratio. The more this ratio deviates from unity, the more the S/O abundance deviates from the cosmic S/O ratio. Regarding the detectability of the unknown analogues, it suffices to say that every known O-species is an indication of the presence and detectability of the S-analogue, while for every known S-species, the O-analogue is not only present in detectable abundance, it can be said to have even been overdue for astronomical detection.

Keywords: astrochemistry, interstellar medium, hydrogen bonding, abundance ratio, spectroscopy

1. Introduction

Astrophysicists and astronomers are largely concerned with discovering new molecules in the Interstellar medium (ISM) and not so much with the understanding of the chemistry and

physics of these molecules just like the early chemists were interested in discovering new chemical substances without much concern about their chemical behavior, thus leading to the emergence of the field of chemical kinetics. Understanding the chemistry of these molecules discovered by astrophysicists and astronomers has given birth to astrochemistry, a young interdisciplinary field that blends chemistry into astronomy and astrophysics. Inasmuch, we are still trying to understand the chemistry and physics of these molecules, and some of the features are very glaring to be observed by all and sundry. The dominance of organic molecules, isomerism, successive hydrogen addition, periodic trends, etc., are some of the notable features among these interstellar and circumstellar molecules. The dominance of organic molecules these molecular species is very obvious with a greater percentage of these molecules found to contain the four most important biogenic elements; C, H, N, and O. Slightly above 200 different molecular species have been detected from different astronomical sources [1]. About 132 of these species contain at least an atom of H, same number also contain at least an atom of C, 64 of these molecular species contain at least an atom of N, while not fewer than 59 contain an atom of O. The high abundances of these elements among the interstellar and circumstellar species can be seen as a direct reflection of their cosmic abundances. With the exceptions of the noble gases and the unusual abundance of Fe, these four elements (H, O, C, and N) have the highest cosmic abundances.

Isomerism among these molecular species has emerged as one of the important tools in exploring the basic chemistry of these species. This can be understood from the fact that about 40% of all interstellar and circumstellar species have isomeric counterparts, and these isomers are believed to have a common precursor for their formation routes; thus, the detection of one isomer gives an insight about the presence and the detectability of others. That most of these isomers are easily observed from the same astronomical sources strongly supports the fact that they have a common precursor for their formation process. In the C_2H_3N isomeric group, methyl cyanide, methyl isocyanide, and ketenimine have all been observed from the same astronomical source [2–4]. In the $C_2H_4O_2$ isomeric group, acetic acid, methyl formate, and glycolaldehyde have also been observed from the same molecular cloud [5–7]. This trend is common among isomers: HCN and HNC, MgCN and MgNC, SiCN, SiNC, etc. [8–13]. Successive hydrogen addition is considered as a possible route for the formation of alcohol from their corresponding aldehydes; methanol from formaldehyde, ethanol from acetaldehyde, and ethylene glycol from glycolaldehyde. Also, these molecules are commonly detected from the same spectral region. Laboratory experiments under interstellar medium conditions have demonstrated how small molecules grow into larger ones via successive hydrogen addition [14].

Periodic trends are another observable features of interstellar and circumstellar molecules. Elements from the same group are found to have corresponding molecules as known interstellar and circumstellar molecules as seen in the cases of C and Si, N and P, O and S, F and Cl, among others. Among these trends, those of O and S are very conspicuous. Of the 19 known S-containing molecules, 16 have the corresponding O-analogues as known interstellar and circumstellar molecules. Interestingly, 12 of the S- and their corresponding O-analogues were

first detected from the same astronomical sources, suggesting a common link in their formation processes [95–97]. The abundance ratio of these molecules with respect to their cosmic or elemental abundance is also an interesting feature. According to Linke [15], "*Methyl mercaptan is apparently a fairly good example of the rule that the ratio of an interstellar sulfur molecule to its oxygen analogue is close to the cosmic S/O ratio*." This "rule" of course is far from being true in many cases even for molecules observed from the same source. It thus requires an in-depth investigation. Reactions that occur on the surfaces of the interstellar dust grains are the dominant processes for the formation of interstellar molecules. The composition of the interstellar dust grains, which create the surface for these reactions also serve as a platform for hydrogen bonding between the water molecule (the most abundant component of the interstellar dust grains) and the molecules that are formed on these surfaces. This interstellar hydrogen bonding, thus, reduces the abundance of molecules that are firmed on the surface of the dust grains since a greater portion of these molecules are attached to surface of the interstellar dust grains [16]. This poses a serious exception to interstellar formation processes that have been shown to be largely thermodynamically controlled [17–19].

In the present work, the effect interstellar hydrogen bonding on the variation of the S/O abundance ratio with respect to the cosmic S/O ratio is examined using high-level quantum chemical simulations. The binding energy between water molecule on the surface of the dust grains and the O- or S-containing molecule gives inside about the level to which the interstellar abundance of such molecule is affected. There are 59 O-containing and 19 S-containing interstellar species; for 16 that are S and O analogues, there is no order regarding their astronomical observations, i.e., in some cases, the O-containing species was observed before the S-containing and vice versa. Thus, the observation of one always gives information about the presence and the possible detectability of the order. In the light of this, the known molecules from this S/O group whose corresponding analogues are not yet observed are examined for their possible detectability. These species are subjected to the effect of interstellar hydrogen bonding. Their binding energies with water on the surface of the interstellar dust grains are determined. From the ratio of the binding energies of these systems, the S/O abundance ratio is predicted for the unknown systems. For the O-containing molecules where two or more isomers are observed, standard enthalpies of formation are computed for both the O and corresponding S-analogues to guide the preference for astronomical searches for the S-analogues since the most stable isomer is more probably the most abundant in the interstellar medium except where the effect of hydrogen is well pronounced as in the case of methyl formate and acetic acid. After describing the methodology employed in this work, the results obtained are presented and discussed before the concluding remarks.

2. Computational details

The quantum chemical calculations reported in this work are carried out using the Gaussian 09 suite of programs [20]. The binding energy (B. E.) between the water molecule on the

surface of the interstellar dust grains and molecule of interest (O- or S-containing) is determined using the method as described in our recent paper [94], which is expressed as Eq. (1):

$$\text{B. E. (complex)} = \text{E (complex)} - [\text{E(water molecule)} + \text{E(heterocycle molecule)}] \quad (1)$$

To obtain high accurate values for the binding energy, the MP2(full) with the 6-311++G** basis set is used in examining the effect of interstellar hydrogen bonding. By definition, the standard enthalpy of formation ($\Delta_f H^0$) of any molecule is the enthalpy change of the reaction by which it is formed from its constituent's elements. Among the different composite quantum chemical methods that are now used to accurately predict thermochemistry data, the G4 method has been found to be very effective in predicting enthalpy of formation values to chemical accuracy in many molecules as reported in literatures [17–19, 21–24]. Details regarding the steps in calculating zero-point-corrected standard enthalpy of formation have been well described in our previous studies [17–19]. The values reported in this work are calculated from the optimized geometries of the systems at the levels of theory mentioned above. The structures are found to be stationary with no imaginary frequency through harmonic vibrational frequency calculations.

3. Results and discussion

The known S-containing molecules and their corresponding O-analogues are discussed with respect to the observed S/O abundance ratio followed by the detectability of the unknown analogues of these species. **Table 1** shows all the known S-containing interstellar species in a chronological order with their corresponding O-analogues (where available); the binding energies (B. E.) of these species with water on the surface of the interstellar dust grains computed at the MP2(full)/6-311++G** level discussed above are presented in columns 2 and 4, respectively; for S- and O-species, the S/O ratio is from the observed abundances of these species taken from the references in the column 6. The magnitude of the binding energy shows the extent to which the molecule (S- or O-containing) is bonded to the surface of the interstellar dust grains. The higher the magnitude of the B. E., the more strongly bonded is the molecule and vice versa. This also implies that as molecule is strongly bonded to the surface of the interstellar dust grains, a greater portion of it is attached to the surface of the dust grains, thus reducing its overall abundance. When the S-containing species is more strongly bonded as compared to the O-analogue, the S/O abundance ratio becomes much more smaller than the S/O cosmic ratio of 0.024 (1/42) [15, 25] and the reverse becomes the case when O-analogue is more strongly bonded as compared to the S-analogue. When the ratio of the binding energy of an S-containing species and their O-analogue approach unity, the observed S/O ratio also approaches the cosmic S/O ratio. Because in this case, there is little or no much pronounced effect of interstellar hydrogen bonding, which affects the interstellar abundance of these species. The major exception to this trend is observed with the components of the interstellar ices: H_2O, CH_3OH, and H_2CO.

which are thus more abundant than their corresponding S-analogues irrespective of the effect of interstellar hydrogen bonding. **Figure 1** and **Table 2** summarize the observed trends

S-containing molecule	B. E (kcal/mol) with water	O-analogue	B. E (kcal/mol) with water	S/O ratio	References
CS (1971)	−1.967	CO (1970)	−0.913	0.013	[39, 52]
OCS (1971)	−1.521	CO_2 (1989)	−2.898	0.032	[50, 51]
H_2S (1972)	−2.292	H_2O (1969)	−4.672	<<0.001	[48, 49]
H_2CS (1973)	−2.614	H_2CO (1969)	−4.104	≈0.025	[47]
SO (1973)	−3.063	O_2 (2011)	−0.324	0.015	[45, 46]
SO2 (1975)	**−2.123**	**O3 (not observed)**	**−0.512**	**NA**	
SiS (1975)	−3.688	SiO (1971)	−6.785	≈1	[43, 44]
NS (1975)	0.272	NO (1978)	−0.097	0.005	[41, 42]
CH_3SH (1979)	−2.048	CH_3OH (1970)	−4.417	≈0.023	[15, 40]
HNCS (1979)	−7.532	HNCO (1972)	−9.146	0.025	[25, 31]
HCS^+ (1981)	−12.490	HCO^+ (1970)	−39.779	≈0.191	[38, 39]
C_2S (1987)	−2.602	C_2O (1991)	−2.493	0.01	[26, 27]
C_3S (1987)	−2.584	C_3O (1985)	−2.584	0.028	[28, 29]
SO+ (1992)	**−18.589**	**O2+ (not observed)**	**−50.272**	**NA**	
HSCN (2009)	−98.722	HOCN (2009)	−37.227	4.5E-3	[30, 31]
SH^+ (2011)	−73.314	OH^+ (2010)	−69.343	0.029	[32, 33]
SH (2012)	−1.394	OH (1963)	−2.927	0.023	[34, 35]
CH_3CH_2SH (2014)	−1.678	CH3CH2OH (1975)	−4.343	0.286	[36, 37]
C5S (2014)	**−1.908**	**C5O (not observed)**	**−2.969**	**NA**	

Ref. [15, 25–52].

Table 1. S- and O-containing species, their B. E with water, and S/O ratio.

in **Table 1**. With the few exceptions observed above, S/O abundance ratio of all the known S-containing species and their corresponding O-analogues follows the same trend as displayed in **Table 2**. As the B. E. S/O ratio approaches unity, the observed S/O ratio approaches the cosmic S/O ratio as in the cases of HNCS/HNCO and C_3S/C_3O. When this ratio is above unity, the observed S/O ratio becomes much less than the cosmic S/O ratio, e.g., CS/CO, SO/O_2, NS/NO, C_2S/C_2O, and HSCN/HOCN and the reverse is observed when the ratio is less than unity, e.g., OCS/CO_2, SiS/SiO, HCS^+/HCO^+, CH_3CH_2SH/CH_3CH_2OH. In summary, the B. E. O/S ratio is inversely proportional to the observed variation of S/O abundance ratio with the cosmic S/O ratio.

Known O-containing species and detectable S-analogues: as previously mentioned, there are at least 59 known O-containing interstellar and circumstellar molecules of which 16 have the corresponding S-analogues as known astromolecules leaving us with over 40 O-containing species without the corresponding S-analogues. In assessing the detectability of these S-analogues of known O-containing molecules, the binding energies of these species (both S- and O-containing

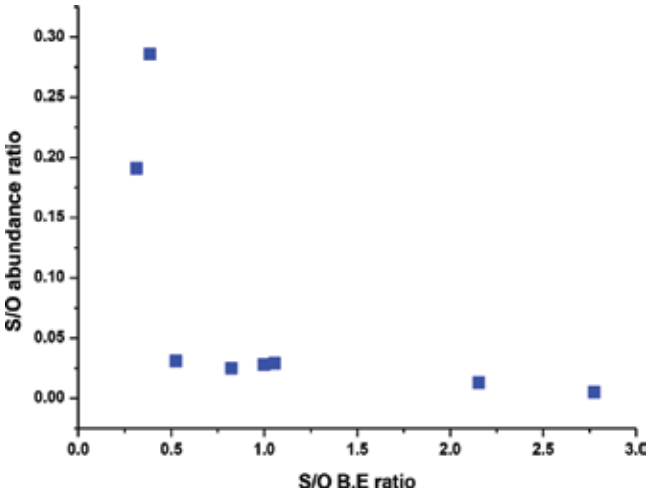

Figure 1. Correlation between B. E. and S/O abundance ratio.

S/O B. E.	S/O B. E.	S/O B. E.
>1	≈1	<1
S/O ratio	S/O ratio	S/O ratio
<Cosmic S/O ratio	≈Cosmic S/O ratio	>Cosmic S/O ratio

Table 2. Deviation from cosmic S/O ratio as a function of binding energy (B. E.).

species) with water on the surface of the interstellar dust grains have been computed. These values are presented in **Table 3**. The reported column densities for the known O-containing molecules are shown in the column 2 with the source of the data in the column 3 of the same table (refs). The column 7 shows the ratio of the binding energy of the S- and O-containing species, from this ratio, the S/O abundance ratio is predicted (column 8) following the observations made in the preceding section (see **Table 2**). That the S-containing molecular species are less bonded to the surface of the interstellar dust grains compared to their respective O-analogues as it is observed in over 80% of the systems here (**Table 3**) is a good omen with respect to the detectability of these species because their overall interstellar abundance will be less affected by the effect of interstellar hydrogen bond unlike their O-analogues. However, with respective to the role that the ratio of an interstellar sulfur molecule to its oxygen analogue is close to the cosmic S/O ratio, there will be much deviation from this role since the degree to which the S-containing species is affected by the effect of hydrogen bonding on the surface of the dust grains is much different from those of the corresponding O-analogues. As a result of this, S/O abundance ratio would be expected to be much higher than the cosmic S/O ratio as shown in the column 8 of **Table 1** for majority of the cases and in very few cases the ratio will tend toward the cosmic S/O ratio except where other processes play a role.

Interstellar formation processes have been shown to be largely thermodynamically controlled in many cases. Except with a pronounced effect of interstellar hydrogen bonding, the most

O-containing molecule	Column density (cm^{-2})	Refs.	B. E. (kcal/mol) with water	S-analogue	B. E. (kcal/mol) with water	B. E. S/O ratio	Estimated S/O abundance ratio
CO^+	≈E12	[53]	−58.540	CS^+	−13.562	0.232	>S/O*
FeO	9E11	[54]	10.299	FeS	−3.637	0.353	>S/O*
PO	≈2.8E15	[55]	−10.236	PS	−1.228	0.120	>S/O*
OH^+	2.4E15	[56]	−69.343	SH^+	−73.314	1.057	≈S/O*
TiO	6.99E14	[57]	−3.874	TiS	−2.413	0.623	>S/O*
NO^+	2.2E12	[58]	−20.719	NS^+	−21.547	1.040	≈S/O*
AlO	≈2E15	[59]	−0.027	AlS	−15.032	556.741	<S/O*
N_2O	≈E15	[60]	−2.225	N_2S	−1.862	0.837	≈S/O*
HCO	≈E11	[61]	−27.168	HCS	−7.477	0.275	>S/O*
HNO	6E11–3.2E14	[62]	−72.436	HNS	−35.794	0.494	>S/O*
HOC^+	≈3E12	[63]	−72.861	HSC^+	−127.024	1.743	<S/O*
OCN^-	—	[64]	−11.887	SCN^-	−9.036	0.760	>S/O*
H_2O^+	7.2E12, 2.3E13, 1.1E15	[65]	−45.608	H_2S^+	−19.086	0.418	>S/O*
TiO_2	7.5E14	[57]	−32.491	TiOS	−15.607	0.480	>S/O*
HO_2	2.8E12	[66]	−2.066	HSO	−2.675	1.295	≈S/O*
AlOH	≈E17	[67]	−4.043	AlSH	−21.869	5.409	<S/O*
H_3O^+	3E14	[68]	−30.591	H_3S^+	−17.753	0.580	>S/O*
$HOCO^+$	—	[69]	−33.959	$HOCS^+$	−45.806	1.349	≈S/O*
HCNO	≈8.9E12	[56]	−1.948	HCNS	−1.148	0.589	>S/O*
HOOH	8E12	[70]	−5.894	HOSH	−2.747	0.466	>S/O*
HCOOH	≈5E13	[71]	−4.353	HSCHO	−0.436	0.100	>S/O*
H_2C_2O	≈E14	[72]	−2.191	H_2C_2S	−0.486	0.222	>S/O*
H_2COH^+	E12-E14	[73]	−25.388	H_2CSH^+	−15.103	0.595	>S/O*
CNCHO	1-17E14	[74]	−4.743	CNCHS	−4.201	0.887	≈S/O*
CH_3O	7E11	[75]	−3.180	CH_3S	−2.175	0.684	>S/O*
H_2NCO^+	6-14E11	[76]	−21.372	H_2NCS^+	−17.922	0.838	≈S/O*
H_2NCHO	2.2E16	[77]	−5.457	H_2NCHS	−4.171	0.764	>S/O*
HC_2CHO	1.5E12	[78]	−4.079	HC_2CHS	−2.908	0.713	>S/O*
c-H_2C_3O	≈E13	[79]	−6.081	c-H_2C_3S	−5.628	0.925	≈S/O*
CH_3CHO	≈1.5E14	[80]	−4.675	CH_3CHS	−2.544	0.544	>S/O*
c-C_2H_4O	3.3E14	[81]	−4.457	c-C_2H_4S	−2.892	0.689	>S/O*

O-containing molecule	Column density (cm^{-2})	Refs.	B. E. (kcal/mol) with water	S-analogue	B. E. (kcal/mol) with water	B. E. S/O ratio	Estimated S/O abundance ratio
CH_2CHOH	2.4E13	[82]	−6.103	CH_2CHSH	−2.585	0.423	
CH_3COOH	7.3E15	[6]	−7.863	CH_3CSOH	−7.001	0.890	≈S/O*
$HCOOCH_3$	≈1.9E17	[7]	−4.975	$HCSOCH_3$	−2.418	0.486	>S/O*
$HOCH_2CHO$	2.8E16	[7]	−5.414	$HSCH_2CHO$	−4.337	0.801	>S/O*
CH_2CHCHO	—	[83]	−5.215	CH_2CHCHS	−2.843	0.545	>S/O*
$(NH_2)_2CO$	≈E15	[84]	−7.422	$(NH_2)_2CS$	−6.676	0.899	≈S/O*
CH_3OCH_3	<18E14	[85]	−4.411	CH_3SCH_3	−2.548	0.578	>S/O*
CH_3CONH_2	1.8E14	[86]	−5.922	CH_3CSNH_2	−3.914	0.661	>S/O*
$(CH_3)_2CO$	2.9E16	[87]	−5.051	$(CH_3)_2CS$	−6.711	1.329	≈S/O*
$HOCH_2CH_2OH$	3.2E14	[14]	−4.064	$HOCH_2CH_2SH$	−2.073	0.510	>S/O*
CH_3CH_2CHO	—	[83]	−4.560	CH_3CH_2CHS	−3.296	0.723	>S/O*
C_2H_5OCHO	5.4E16	[88]	−4.896	C_2H_5OCHO	−14.803	3.023	<S/O*
CH_3COOCH_3	4.2E15	[88]	−4.815	CH_3COOCH_3	−4.006	0.831	>S/O*
$C_2H_5OCH_3$	2E14	[89]	−4.250	$C_2H_5OCH_3$	−2.519	0.593	>S/O*

Where S/O* is the cosmic abundance ratio.
Refs. [7, 17, 53–89].

Table 3. Parameters for known O- and detectable S-containing molecules.

stable isomer has always been observed to be the most abundant isomer in the interstellar space. Thus, the most stable isomer is easily observed as compared to other isomers of the group. **Figure 2** pictures this concept. It shows how the interstellar abundance (column density) of two isomers each from the CHNO and CHNS groups varies with the stability (enthalpy of formation) where the most stable isomer (with lower enthalpy of formation) is found to be the most abundant in both cases. Searching for the most stable isomer is, thus, a step toward successful observation, and the successful detection of an isomer reaffirms the presences of other isomers since they are believed to have a common precursor for their formation routes. In view of this, for known O-containing molecules with at least two isomers, the standard enthalpies of formation for these isomers and their S-analogues have been determined as a guide for preference in the astronomical searches for these isomers. **Table 4** presents the enthalpy of formation for O-containing isomers and their detectable S-analogues. As would be expected, the trend of the stability for O and S-species is the same. From the parameters presented in **Table 2** coupled with the advancements in astronomical and spectroscopic equipment, that all the S-analogues of known O-containing interstellar molecular species would not be considered as exaggeration. They are detectable.

Known S-species and overdue detectable O-analogue: without any exception, an interstellar O-containing molecular species is more abundant than its S-analogue (**Table 1**). So for every

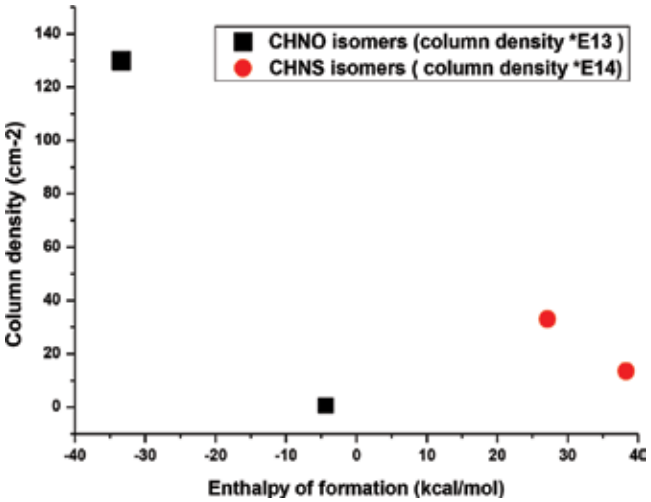

Figure 2. Dependence of column density on enthalpy of formation for CHNO and CHNS systems.

Molecule	Enthalpy of formation (kcal/mol)	
	X = O	**X = S**
	3-atoms	
HXC^+	234.419	340.747
HCX^+	198.564	246.625
	4-atoms	
HCNX	34.084	61.162
HXCN	−4.387	38.312
HNCX	−33.357	27.126
	7-atoms	
c-H_2CH_2CX	−14.596	19.146
H_2CCHXH (anti)	−28.519	19.386
H_2CCHXH (syn)	−30.236	19.439
H_3CCHX	−42.405	16.453
	8-atoms	
HXH_2CCHX	−70.542	31.962
H_3CXCHX	−89.381	20.743
$H_3C(X)XH$	−103.746	18.612
	9-atoms	
$(CH_3)_2X$	−48.956	−10.697
C_2H_5XH	−56.718	−11.943
	11 atoms	

Molecule	Enthalpy of formation (kcal/mol)	
	X = O	X = S
$H_3COC(O)CH_3$	−95.098	12.071
H_3CH_2CXCHX	−97.515	12.489

Table 4. Enthalpy of formation for O-containing isomers and their detectable S-analogues.

S-containing molecule	Column density (cm^{-2})	References	B. E. (kcal/mol) with water	O-analogue	B. E. (kcal/mol) with water	B. E. S/O ratio	Estimated S/O abundance ratio
SO_2	<3.5E16	93	−2.123	O_3	−0.512	4.146	<S/O*
SO^+	5E12	94	−18.589	O_2^+	−50.272	0.370	>S/O*
C_5S	2-14E12	95	−1.908	C_5O	−2.969	0.643	>S/O*

Where S/O* is the cosmic abundance ratio.
Refs. [90–93].

Table 5. Parameters for known S- and detectable O-containing molecules.

known S-species, the O-analogue is not only present in detectable abundance, it can be said to have even been overdue for astronomical detection because for sure the O-species are more abundant than their S-analogue and as such could be detected with less difficulty as compared to its S-analogue. **Table 5** lists the parameters for known S-containing interstellar species and their detectable O-analogues. The high abundances reported for these S-containing species (column 2) strongly support the detectability of their O-analogues.

4. Basic inorganic chemistry of oxygen, sulfur, and hydrogen

4.1. Hydrogen

The first element in the periodic table is hydrogen. Although hydrogen is very abundant in nature, the air contains almost no free hydrogen. On the other hand, hydrogen is found in water, which is about 70% of the earth. Additionally, hydrogen compounds combined with carbon are found in space and it plays important roles in such as the nuclear fission reaction in the sun. Molecules of associated hydrogen element are the basis of astrochemical space research.

Physical properties of hydrogen

Relative atomic mass	1.008
Electron structure	$1s^1$
Ionization energy	1312 $KJmol^{-1}$
Electron affinity	−72 $KJmol^{-1}$

Molecular formula	H_2
Melting point	14 K
Boiling point	20 K
Density at s.t.p	0.09 $KJmol^{-1}$
Bond energy, H–H	436 $KJmol^{-1}$
Bond length, H–H	74 pm
Colorless, odorless, and tasteless gas.	

^1_1H,Protium (H), ^2_1H,deuterium (D), and ^3_1H,tritium (T) are the three known isotopes of hydrogen. The naturally occurring isotope is deuterium, while tritium is made during nuclear reaction.

$$^2_1H + ^2_1H \rightarrow ^3_1H + ^1_1H \tag{2}$$

Tritium is radioactive, decaying by beta emission.

4.2. Large-scale production of hydrogen

Natural gas (methane) is an important source of hydrogen. Methane is reacted with steam at high pressure of about 35 atmosphere pressure and 800°C in the presence of a nickel catalyst. The result is a mixture of carbon dioxide, carbon monoxide, and hydrogen.

$$CH_{4(g)} + H_2O_{(g)} \rightarrow CO_{(g)} + 3H_{2(g)} \tag{3}$$

$$CO_{(g)} + H_2O_{(g)} \rightarrow CO_{(g)} + H_{2(g)} \tag{4}$$

In the refining industry, hydrogen is obtained in many reactions that involve cracking long-chain hydrocarbons into smaller molecules.

$$C_6H_{12(g)} \rightarrow C_6H_{6(g)} + 3H_{2(g)} \tag{5}$$

Bosch reaction is another method of making hydrogen; here, steam is passed over white hot coke.

Uses of hydrogen:

Majority of hydrogen produced are used in making ammonia in the Haber process. Production of margarines from vegetable oils, welding, and fuels cells are some of its other uses.

Chemical properties of oxygen:

Hydrogen gas is made up of hydrogen molecule, H_2. Hydrogen atoms are too reactive to exist on their own. The explosive mixture of hydrogen and oxygen is its commonest reaction. The possibility of explosion exists in the laboratory when hydrogen is made in large scale, and the experiment mostly goes on with caution. The normal method is to react dilute sulfuric acid with zinc.

$$Zn_{(s)} + 2H^{+}_{(aq)} \rightarrow Zn^{2+} + H_{2(g)} \tag{6}$$

Hydrogen forms hydride with many elements. Hydrides of metals are ionic, example NaH and CaH_2. Hydrides of nonmetals are covalent in nature, example CH_4 and NH_4. Hydrogen forms hydrogen bonding with highly electronegative atoms, for example HF and H_2O. Hydrogen gas explodes with oxygen when ignited.

$$2H_{2(g)} + O_{2(g)} \rightarrow 2H_2O_{(g)} \tag{7}$$

As a reducing agent, hydrogen will remove oxygen from many oxides.

$$CuO_{(s)} + H_{2(g)} \rightarrow Cu_{(s)} + H_2O_{(g)} \tag{8}$$

Hydrogen is liberated from acids by metals.

$$Zn_{(S)} + 2H^{+} \rightarrow Zn^{2+}_{(aq)} + H_{2(g)} \tag{9}$$

Hydrogen is prepared in the laboratory this way.

Hydrogen can exist both as $H^{+}_{(aq)}$ and $H_3O_{(aq)}$ in water. Hydrogen ions form the active ions in aqueous aids.

4.3. Unusual hydrides of hydrogen

Chemical bonding theories were unable to explain chemical bonding in boron hydrides when they were first examined. They are several boron hydrides some of which are shown below.

Name	Formula	Comment
Diborane	B_2H_6	Highly flammable and hydrolyzed easily
Tetraborane	B_4H_{10}	Less reactive than diborane
Hexaborane-10	B_6H_{10}	Same reactivity like tetraborane
Decaborane	$B_{10}H_{14}$	Does not easily reacts with air or water
Icosaborane-10	$B_{20}H_{16}$	Does not easily reacts with air or water

The simplest member of the group is diborane. The six hydrogen atoms provide six electrons for bonding, and there are three valence electrons in the shell of each work, with 12 electrons in all. However, X-ray structure of diborane reveals that each boron atom has two hydrogen atoms attached to it and another two hydrogen atoms shared between the two boron atoms. Expectedly, there will be sixteen (16) electrons participating in eight (8) bonds. Conversely, this is not the case as there appear to be too few electrons accounting for the number of bonds. Such molecules are now known as the electron-deficient molecules or compounds.

Furthermore, molecular orbital theory clarifies situations like this. Here, bridging hydrogen atoms are believed to be bonded to the boron atoms by a bond stretching across all three atoms. This type of bond is called a three center bond. Each one contains two electrons, which together with the four pairs of electrons in the bonds to the four terminal hydrogen atoms, bringing the total to the twelve (12) electrons observed. The bonding in other members of the borane group is explained in similar fashion, although bigger members show more complexity in their bonding.

Lithium tetrahydridoaluminate (III), $LiAlH_4$ (lithium aluminum hydride), is another hydride rather being unusual.

4.4. Oxygen

A diatomic molecule, O_2, oxygen alone constitutes about 20.8% of air. Three isotopes of oxygen are known; ${}^{16}_{8}O$ is the main isotope with an abundance of 99.8%. The others are ${}^{17}_{8}O$ and ${}^{18}_{8}O$ with the abundance of 0.04 and 0.2%, respectively. Oxygen is very important to life of animals and plants including human being on earth. Oxygen is slightly soluble in water, which is essential for fish and other aquatic life survival.

Moreover, oxygen is an essential component of combustion reaction, especially of organic materials such as wood, oil, and coal. Our modern age is characterized by combustion of these fuels for our electricity, transportation, and heating needs.

Oxygen is located at upper layer of atmosphere where it absorbs harmful ultraviolet light from the sun. Ozone is an allotrope of oxygen, O_3. The importance of oxygen to plant and animal life cannot be overemphasized.

Oxygen compounds of all elements are known except for those of He, Ne, and Ar. Molecular oxygen O_2 (dioxygen) react with all elements in periodic table with the exception of the halogens, some noble metals, and the rare gases.

The chemistry of oxygen is representative of having the neon stable configuration in the following ways. Gaining of electron ad in the case of H_2O and sharing of electrons like in the case of OH^-, and finally formation three covalent bonds like in H_3O^+, R_3O^+, etc.

4.5. Oxides

The varieties of physical and chemical properties showed by oxides are functions of the bond types from primarily electrovalent to covalent. Formation of oxide ion is an energy consuming process.

In ionic metal oxide formation, energy is also expanded in vaporizing and ionization of metal atom. Many ionic oxides are possible as a result of the high lattice energy of oxides that have the lesser double bond charged O^{2-} ion. Where this lattice energy is not sufficient to give the needed energy for ionization, oxides with significant covalent attributes are formed. The following are some examples BeO, SiO_2, etc.

4.6. Sources of oxygen

Fractional distillation of air is the main source of obtaining oxygen. Air is forced under pressure through nozzles. The compressed air is allowed to expand into a region of lower pressure, which cools the air. The air is cooled further in expansion tubes until it condenses into liquid. The liquid air is a mixture of nitrogen, oxygen, and rare gases and is separated by allowing an increase in temperature of the medium. The other gases boil more easily than oxygen, so they evaporate leaving oxygen. Liquid oxygen, which is pale blue in color and strongly paramagnetic, is stored under pressure or in insulated containers.

Oxygen extracted this way is used to aid respiration medically, for breathing by divers and astronauts, in oxy-acetylene welding and rocket fuels, etc.

4.7. Ozone

An allotrope of oxygen after dioxygen (O_2). Ozone (O_3) is formed by the action of electric current on oxygen, concentration of about 10% realized this way. Ozone is blue in color like oxygen but diamagnetic. Pure ozone is a deep blue explosive liquid, which is obtained by fractional liquefaction of O_2–O_3 mixture. In the atmosphere, ozone comes about by the action of ultraviolet light radiation on oxygen. Ozone located at about the altitude of 25 km is responsible for preventing excess ultraviolet light from reaching on the earth.

Ozone is chemically found to be very endothermic and decomposes only slowly at 250°C in the presence of catalyst or ultraviolet (UV) light.

$$O_3 \rightleftharpoons \frac{3}{2}O, \Delta H = -142\ \text{kJmol}^{-1} \tag{10}$$

Ozone is triangular in shape with equal bond length of about 128 nm. The degree of single and double bonds formed by ozone is same. Each oxygen atom of the ozone has six valence electrons. Describing this with valence bond theory, each bond will involve a set of resonance hybrid in which one of the bonds is a double bond and the other is a coordinate bond. Moreover, the real structure does not swap between the resonance frames; rather, each bond partly shows a nature of a double bond and partly that of a single bond.

In the laboratory, ozone is made by passing oxygen through an electric field. An equilibrium is set up.

$$3O_{2(g)} \rightleftharpoons 2O_{3(g)} \tag{11}$$

The metastable nature of ozone makes it transient, having the tendency of always converting to oxygen. It is a vigorous oxidizing agent, always reacting to give up oxygen gas

$$S^{2-} + 2O_{3(g)} \rightarrow SO_4^{2-}{}_{(aq)} + O_{2(g)} \tag{12}$$

At an altitude of about 25 km above the earth surface, dioxygen can be split apart by ultraviolet light radiation coming from the sun. Some of these atoms react with other oxygen molecules forming the ozone layer

$$O_{2(g)} + O_{(g)} \rightarrow O_{3(g)} \tag{13}$$

This reaction is of extreme importance to the maintenance of balance here on earth. This is because the ozone has the ability to absorb dangerous ultraviolet radiation from the sun, thus preventing it from reaching the earth surface. This radiation is of high energy, therefore, of short wavelength. If too much of this radiation reaches the earth, the energy balance will be upset leading to increase greenhouse effect and global atmospheric temperature.

Secondly, exposure to increase ultraviolet radiation will lead to cell mutation of living tissues. The consequences of this will increase in skin cancer incidence in particular.

4.8. Chemical properties of oxygen

4.8.1. Oxides

The ability of oxygen molecule to combine with both metals and nonmetals to form oxides is its most outstanding property. Oxides are of four different types: neutral, basic, acidic, and amphoteric. Oxides that show both basic and acidic behavior are called amphoteric oxides. Few oxides are neutral: nitrous oxide and carbon monoxide are examples. Group I and II oxides are examples of basic oxides. Oxides of nonmetals are mainly acidic in nature. Aluminum oxide is an example of amphoteric oxide.

It shows basic properties by reacting with hydrogen ions

$$Al_2O_{3(s)} + 6H^+_{(aq)} \rightarrow 2Al^{3+}_{(aq)} + 3H_2O_{(l)} \tag{14}$$

Additionally, it shows acidic property when dissolved in alkali

$$Al_2O_{3(s)} + 6OH^- + 3H_2O_{(l)} \rightarrow 2Al(OH)_6^{3-}{}_{(aq)} \tag{15}$$

Formulae of some oxides in the periodic table:

Group I	Group II	Group III	Group IV	Group V	Group VI	Group VII
Li_2O	BeO	B_2O3	CO_2	N_2O_5	O_2	F_2O
Na_2O	MgO	Al_2O3	SiO_2	P_4O_{10}	SO_2	Cl_2O
K_2O	CaO	Ga_2O3	GeO_2	As_2O_3	SeO_2	BrO
Rb_2O	SrO	In_2O3	SnO	Sb_2O_3	TeO_2	I_2O_5
Cs_2O	BaO	Tl_2O	PbO	Bi_2O_2	PoO_2	

Not all the oxides are shown.

4.8.2. Peroxides

The most important peroxide of oxygen is hydrogen peroxide, H_2O_2. Hydrogen peroxide is a colorless liquid with a boiling point of 152.1 °C. It is similar to water in many of its properties

and forms hydrogen bonding too, and it is 40% denser than water. It has high dielectric constant and so used as ionizing solvent, but its utility in this capacity is limited by its strong oxidizing nature, which makes it readily decompose in the presence of many heavy-metal ions as given in the equation below.

$$2H_2O_2 \rightarrow 2H_2O + O_2,\ \Delta H = -99\ KJmol^{-1} \tag{16}$$

4.9. Sulfur

Sulfur is the second member of the oxygen group in the periodic table. Sulfur has more allotropic forms than any other elements. These different forms of allotropes are to the extent to which sulfur is polymerized and the crystal structure adopted. The α or rhombic and β or monoclinic sulfur are the two most common ones. Sulfur is not a gas unlike oxygen and has a significantly lower electronegativity. They only react with group one element to form ionic compounds. In many sulfur compounds, the d-orbital is used in bonding and these bonds appear shorter than expected, which suggest a double bond character. Sulfur can make up to six covalent bonds making use of its s-, p-, and d-orbitals. Sulfates and hexafluorides are examples of this instance.

Physical property of sulfur:

Symbol	Sulfur
Electron structure	(Ne) $3S^2 3p^4$
Electronegativity	2.5
I.E. ($KJmol^{-1}$)	1000
Melting point (°C)	114.5
Boiling point (°C)	444.5
Atomic radius (pm)	104
Principal oxidation number	−2, +4, +6

Uses of sulfur:

Sulfur has several purposes of uses; it is mainly used as sulfuric acid. It is also used in fertilizer, explosives, dyes, detergents, polymers, and in processing of many other chemicals.

Extraction of sulfur:

Sulfur is found in many minerals, mostly in combination with copper, mercury, lead metals. Sulfur is obtained as the byproduct of the extraction of their ore. Sulfur is also directly extracted from the ground using a method called the *Frasch* process. Sulfur in the form of hydrogen sulfide is also obtained from oil and natural gas refineries.

Sulfuric acid:

This is used in the manufacturing of superphosphate fertilizer, ammonium sulfate fertilizer, detergents, paper, rayon, polymer, and processing of metal ores. It is also used in the

manufacture of paints and pigments, electrolytes for heavy duty batteries, and laboratory reagents. Sulfuric acid has a dynamic chemistry. In dilute solution, it behaves as a typically strong acid. When concentrated, it behaves both like an oxidizing and a dehydrating agent. It is also a sulfonating agent in organic chemistry.

Sulfuric acid as a strong acid:

In water, sulfuric acid behaves as a strong acid. It dissociates in to two stages

$$H_2SO_{4(aq)} + H_2O_{(l)} \rightarrow HSO_4^- + H_3O^+_{(aq)} \tag{17}$$

$$HSO_{4-(aq)} + H_2O_{(l)} \rightarrow SO_4^{2-}{}_{(aq)} \tag{18}$$

Only the first dissociation is complete; the second is partial. When it is diluted, it shows properties of an acid. It will evolve hydrogen when it reacts with metals

$$Zn_{(s)} + H_2SO_{4(aq)} \rightarrow ZnSO_{4(aq)} + H_{2(g)} \tag{19}$$

Sulfuric acid as oxidizing agent:

The acid shows oxidizing property in concentrated form. For example, sulfuric acid cannot be used to prepare hydrogen bromide from sodium bromide. This is because it can oxidize the hydrogen bromide produced.

$$2HBr_{(g)} + H_2SO_{4(l)} \rightarrow Br_{2(l)} + SO_2 + 2H_2O_{(l)} \tag{20}$$

This oxidizing property is a feature of sulfate ion. Since the ion has a high oxidation state of +6, it makes it to take electrons to revert to a lower oxidation state.

Sulfuric acid as a dehydrating agent:

Concentrated sulfuric acid will remove water from various organic compounds as can be noted when few drops of it are added to sugar (glucose). The sugar suddenly becomes very hot and frothy, leaving a black mass of carbon.

Sulfur hydrides:

Hydrogen sulfide is an important hydride of sulfur. It is a very poisonous gas, and when inhaled for some time, it can be fatal. The gas is made by mixing hydrochloric acid with a metal sulfide, often iron (II) sulfide.

Unlike water, hydrogen sulfide will burn in air with a pale blue flame.

$$2H_2S_{(g)} + 3O_2 \rightarrow 2H_2O_{(g)} + 2SO_{2(g)} \tag{21}$$

A useful property of hydrogen sulfide is that it releases sulfide ions when dissolved in water.

5. Summary

The first part (Sections 1 to 4) of this chapter, which is based on research, discusses the nonterrestrial chemistry of oxygen, sulfur, and their compounds in the interstellar medium, while the second part of the chapter (Section 5) discusses about the basic inorganic chemistry of oxygen, sulfur, and oxygen. Both parts of this chapter point out the importance of these elements and their compounds in both terrestrial and nonterrestrial environments. Also, the importance of chemistry in these environments cannot be overemphasized.

6. Conclusions

The deviation of the observed S/O abundance from the rule that the ratio of an interstellar sulfur molecule to its oxygen analogue is close to the cosmic S/O ratio and the possibility of detecting other analogues of the known S- and O-containing species have been examined in this study. The effect of hydrogen bonding on the surface of the interstellar dust grains where these molecules are believed to be formed plays a vital role in the observed S/O abundance ratio. From the binding energy of these species with the water molecule on the surface of the dust grains, the more the molecules are strongly bonded to the surface of the dust grains, the more their abundances are reduced. As the ratio of the binding energy of S- and O-species (B. E. of S/O) with water approaches unity, the S/O abundance ratio approaches cosmic S/O ratio. When this ratio is less than one, the observed S/O abundance ratio becomes much higher than the cosmic S/O ratio and vice versa except for the species that are major components of the interstellar ice. With respect to the detectability of the unknown analogues of these species, every known O-species is an indication of the presence and detectability of the S-analogue. This has been shown to be true in many cases where the S-analogues of known O-species are successfully observed, following the detection of the O-analogues. That these S-containing species are less bonded to the surface of the interstellar dust grains as compared to their O-analogues firmly support the high abundances and the detectability of these species. For the known S-species whose O-analogues are yet to be observed, the O-analogues are not only present in detectable abundance, it can be said to have even been overdue for astronomical detection since the O-species without any exception are more abundant than their S-analogues and as such they could be detected with less difficulty as compared to their S-analogues that are already known. The second part of this chapter discusses the basic inorganic chemistry of hydrogen, oxygen, and sulfur.

Author details

Etim Emmanuel[1]*, Lawal Usman[1], Khanal Govinda[2] and Mbakara Idaresit[3]

*Address all correspondence to: emmaetim@gmail.com

1 Department of Chemical Sciences, Federal University Wukari, Taraba State, Nigeria

2 Department of Inorganic and Physical Chemistry, Indian Institute of Science, Bangalore, India

3 Department of Chemistry, University of Ibadan, Oyo State, Nigeria

References

[1] Etim EE, Arunan E. Rotational spectroscopy and interstellar molecules. Planex Newsletter. 2015;**5**(2):16-21

[2] Solomon PM, Jefferts KB, Penzias AA, Wilson RW. Carbon monoxide in the interstellar spectrum of zeta Ophiuchi. The Astrophysical Journal. 1971;**168**:L107

[3] Cernicharo J, Kahane C, Guélin M, Gomez-Gonzalez J. The IRAM-30 m line survey of the horsehead PDR. III. High abundance of complex (iso-)nitrile molecules in UV-illuminated gas. Astronomy & Astrophysics. 1988;**189**:L1

[4] Lovas FJ, Hollis JM, Remijan AJ, Jewell PR. Detection of Ketenimine (CH2CNH) in Sagittarius B2(N) hot cores. The Astrophysical Journal. 2006;**645**:L137

[5] Brown RD, Crofts JG, Godfrey PD, et al. Discovery of interstellar methyl formate. The Astrophysical Journal. 1975;**197**:L29

[6] Mehringer DM, Snyder LE, Miao Y, Lovas F. Detection and confirmation of interstellar acetic acid. The Astrophysical Journal. 1997;**480**:L71

[7] Hollis JM, Lovas FJ, Jewell PR. Interstellar Glycolaldehyde: The first sugar. The Astrophysical Journal. 2000;**540**:L107

[8] Snyder LE, Buhl D. Observations of radio emission from interstellar hydrogen cyanide. The Astrophysical Journal. 1971;**163**:L47-L52

[9] Zuckerman B, Morris M, Palmer P, Turner BE. Observations of CS, HCN, U89.2, and U90.7 in NGC 2264. The Astrophysical Journal. 1972;**173**:L125. The Microwave Spectrum of HNC: Identification of U90.7

[10] Guélin M, Cernicharo J, Kahane C, Gomez-Gonzales J. A new free radical in IRC +10216. Astronomy & Astrophysics. 1986;**157**:17

[11] Guélin M, Muller S, Cernicharo J, et al. Astronomical detection of the free radical SiCN. Astronomy & Astrophysics. 2000;**369**:9

[12] Guélin M, Muller S, Cernicharo J, McCarthy MC, Thaddeus P. Detection of the SiNC radical in IRC +10216. Astronomy & Astrophysics. 2004;**426**:49

[13] Ziurys LM, Apponi AJ. Detection of MgCN in IRC +10216: A new metal-bearing free radical. The Astrophysical Journal. 1995;**455**:L73

[14] Hollis JM, Lovas FJ, Jewell PR, Coudert LH. Interstellar antifreeze: Ethylene glycol. The Astrophysical Journal. 2002;**571**:L59

[15] Linke RA, Frerking MA, Thaddeus P. Interstellar methyl mercaptan. The Astrophysical Journal. 1979;**234**:L139

[16] Etim EE, Gorai P, Das A, Arunan E. Interstellar protonated molecular species. Advances in Space Science. 2017;**60**:709-721. DOI: 10.1016/j.asr.2017.04.003

[17] Etim EE, Inyang EJ, Ushie OA, Mbakara IE, Andrew C, Lawal U. Is ESA relationship the tool for searching for interstellar heterocycles? FUW Trends in Science and Technology Journal. 2017;**2**(2):665-678

[18] Etim EE, Gorai P, Das A, Arunan E. Theoretical investigation of interstellar C–C–O and C–O–C bonding backbone molecules. Astrophysics and Space Science. 2018;**363**:6. DOI: 10.1007/s10509-017-3226-5

[19] Etim EE, Mbakara IE, Inyang EJ, Ushie OA, Lawal U, Andrew C. Spectroscopy of linear interstellar carbon chain isotopologues: Meeting experimental accuracy. Tropical Journal of Applied Natural Sciences. 2017;**2**(1):11-16

[20] Frisch MJ, Trucks GW, Schlegel HB, et al. G09:RevC.01. Wallingford CT: Gaussian, Inc.; 2009

[21] Møller C, Plesset MS. Note on an approximation treatment for many-electron systems. Physics Review. 1934;**46**(7):618-622

[22] Curtiss LA, Raghavachari K, Redfern PC, Rassolov V, Pople JA. Gaussian-3 (G3) theory for molecules containing first and second-row atoms. The Journal of Chemical Physics, The Journal of Chemical Physics. 1998;**109**:7764

[23] Curtiss LA, Redfern PC, Raghavachari K. Gaussian-4 theory. The Journal of Chemical Physics, The Journal of Chemical Physics. 2007;**126**:084108

[24] Curtiss LA, Redfern PC, Raghavachari K. Gaussian-4 theory using reduced order perturbation theory. The Journal of Chemical Physics. 2007;**127**:124105

[25] Frerking MA, Linke RA, Thaddeus P. Interstellar isothiocyanic acid. The Astrophysical Journal. 1979;**234**:L143-L145

[26] Ohishi M, Suzuki H, Ishikawa SI, et al. Detection of a new carbon-chain molecule, CCO. The Astrophysical Journal. 1991;**380**:L39-L42

[27] Saito S, Kawaguchi K, Yamamoto S, et al. Laboratory detection and astronomical identification of a new free radical, CCS 3Sigma-. The Astrophysical Journal. 1987;**317**:L115

[28] Yamamoto S, Saito S, Kawaguchi K, Kaifu N, Suzuki H. Laboratory detection of a new carbon-chain molecule C3S and its astronomical identification. The Astrophysical Journal. 1987;**317**:L119

[29] Brown RD, Godfrey PD, Cragg DM, et al. Tricarbon monoxide in TMC-1. The Astrophysical Journal. 1985;**297**:302

[30] Brünken S, Belloche A, Martín S, Verheyen L, Menten KL. Interstellar HOCN in the galactic center region. Astronomy & Astrophysics. 2010;**516**:A109

[31] Halfen DT, Ziurys LM, Brünken S, et al. Detection of a new interstellar molecule: Thiocyanic acid HSCN. The Astrophysical Journal. 2009;**702**:L124

[32] Wyrowski F, Menten KM, Güsten R, Belloche A. First interstellar detection of OH+. Astronomy & Astrophysics. 2010;**518**:A26

[33] Menten KM, Wyrowski F, Belloche A, et al. Submillimeter absorption from SH+, a new widespread interstellar radical, 13CH+ and HCl. Astronomy & Astrophysics. 2011;**525**:A77

[34] Neufeld DA, Falgarone E, Gerin M, et al. Discovery of interstellar mercapto radicals (SH) with the GREAT instrument on SOFIA. Astronomy & Astrophysics. 2012;**542**:L6

[35] Weinreb S, Barrett AH, Meeks ML, Henry JC. Radio observations of OH in the interstellar medium. Nature. 1963;**200**:829

[36] Kolesniková L, Tercero B, Cernicharo J, et al. Spectroscopic characterization and detection of ethyl mercaptan in orion. The Astrophysical Journal. 2014;**784**:L7

[37] Pearson JC, Sastry KVLN, Herbst E, De Lucia FC. Gauche ethyl alcohol: Laboratory assignments and interstellar identification. The Astrophysical Journal. 1997;**480**

[38] Thaddeus P, Guélin M, Linke RA. Three new "nonterrestrial" molecules. The Astrophysical Journal. 1981;**246**:L41

[39] Penzias AA, Solomon PM, Wilson RW, Jefferts KB. Interstellar carbon monosulfide. The Astrophysical Journal. 1971;**168**:L53

[40] Gottlieb CA, Ball JA, Gottlieb EW, Dickinson DF. Interstellar methyl alcohol. The Astrophysical Journal. 1979;**227**:422

[41] Gottlieb CA, Ball JA, Gottlieb EW, Lada CJ, Penfield H. Detection of interstellar nitrogen sulfide. The Astrophysical Journal. 1975;**200**:L147

[42] Liszt HS, Turner BE. Microwave detection of interstellar NO. The Astrophysical Journal. 1978;**224**:L73

[43] Morris M, Gilmore W, Palmer P, Turner BE, Zuckerman B. Detection of interstellar SiS and a study of the IRC +10216 molecular envelope. The Astrophysical Journal. 1975;**199**:L47

[44] Wilson RW, Penzias AA, Jefferts KB, Kutner N, Thaddeus P. Discovery of interstellar silicon monoxide. The Astrophysical Journal. 1971;**167**:L97

[45] Gottlieb CA, Ball J. Interstellar sulfur monoxide. The Astrophysical Journal. 1973;**184**:L59

[46] Goldsmith PF, Liseau R, Bell TA, et al. Herschel measurements of molecular oxygen in orion. The Astrophysical Journal. 2011;**737**:96

[47] Sinclair MW, Fourikis N, Ribes JC, et al. Detection of interstellar thioformaldehyde. Australian Journal of Physics. 1973;**26**:85

[48] Thaddeus P, Kutner ML, Penzias AA, Wilson WR, Jefferts KB. Interstellar hydrogen sulfide. The Astrophysical Journal. 1972;**176**:L73

[49] Coutens A, Vastel C, Caux E, et al. A study of deuterated water in the low-mass protostar IRAS 16293-2422. Astronomy & Astrophysics. 2012;**539**:132

[50] D'Hendecourt LB, de Muizon MJ. The discovery of interstellar carbon dioxide. Astronomy & Astrophysics. 1989;**223**:L5

[51] Jefferts KB, Penzias AA, Wilson RW, Solomon PM. Detection of interstellar carbonyl sulfide. The Astrophysical Journal. 1971;**168**:L111

[52] Smith AM, Stecher TP. Carbon monoxide in the interstellar spectrum of zeta Ophiuchi. The Astrophysical Journal. 1971;**164**:L43

[53] Latter WB, Walker CK, Maloney PR. Detection of the carbon monoxide ion (CO+) in the interstellar medium and a planetary nebula. The Astrophysical Journal. 1993;**419**:L97

[54] Walmsley CM, Bachiller R, Pineau des Forêts G, Schilke P. Detection of FeO toward Sagittarius B2. The Astrophysical Journal. 2002;**566**:L109

[55] Tenenbaum ED, Woolf NJ, Ziurys LM. Identification of phosphorus monoxide (X 2Pi_r) in VY Canis Majoris: Detection of the first P-O bond in space. The Astrophysical Journal. 2007;**666**:L29

[56] Marcelino N, Cernicharo J, Tercero B, Roueff E. Discovery of fulminic acid, HCNO, in dark clouds. The Astrophysical Journal. 2009;**690**:L27

[57] Kamiński T, Gottlieb CA, Menten KM, et al. Pure rotational spectra of TiO and TiO_2 in VY Canis Majoris. Astronomy & Astrophysics. 2013;**551**:A113

[58] Cernicharo J, Bailleux S, Alekseev E, et al. Tentative detection of the nitrosylium ion in space. The Astrophysical Journal. 2014;**795**:40

[59] Tenenbaum ED, Ziurys LM. Millimeter detection of AlO (X 2Sigma+): Metal oxide chemistry in the envelope of VY Canis Majoris. The Astrophysical Journal. 2009;**693**:L59

[60] Ziurys LM, Apponi AJ, Hollis JM, Snyder LE. Detection of interstellar N_2O: A new molecule containing an N-O bond. The Astrophysical Journal. 1994;**436**:L181

[61] Snyder LE, Hollis JM, Ulich BL. Radio detection of the interstellar formyl radical. The Astrophysical Journal. 1976;**208**:L91

[62] Snyder LE, Kuan Y-J, Ziurys LM, Hollis JM. New 3 millimeter observations of interstellar HNO—Reinstating a discredited identification. The Astrophysical Journal. 1993;**403**:L17

[63] Ziurys LM, Apponi AJ, Guélin M, Cernicharo J. Detection of MgCN in IRC +10216: A new metal-bearing free radical. The Astrophysical Journal. 1995;**445**:47

[64] Soifer BT, Puetter RC, Russell RW. The 4-8 micron spectrum of the infrared source W33A. The Astrophysical Journal. 1979;**232**:L53

[65] Ossenkopf V, Müller HSP, Lis DC, et al. Detection of interstellar oxidaniumyl: Abundant H_2O+ towards the star-forming regions DR21, Sgr B2, and NGC6334. Astronomy & Astrophysics. 2010;**518**:Llll

[66] Parise B, Bergman P, Du F. Detection of the hydroperoxyl radical HO2 toward ϱ Ophiuchi a. additional constraints on the water chemical network. Astronomy & Astrophysics. 2012;**541**:L11

[67] Tenenbaum ED, Ziurys LM. Exotic metal molecules in oxygen-rich envelopes: Detection of AlOH (X1Sigma+) in VY Canis Majoris. The Astrophysical Journal. 2010;**712**:L93

[68] Wootten A, Boulanger F, Bogey M, et al. A search for interstellar H_3O+. Astronomy & Astrophysics. 1986;**166**:L15

[69] Bogey M, Demuynck C, Destombes JL. Laboratory detection of the protonated carbon dioxide by submillimeter wave spectroscopy. Astronomy & Astrophysics. 1984;**138**:L11

[70] Bergman P, Parise B, Liseau R, et al. Detection of interstellar hydrogen peroxide. Astronomy & Astrophysics. 2011;**531**:L8

[71] Winnewisser G, Churchwell E. Detection of formic acid in Sagittarius B2 by its 2(11)-2(12) transition. The Astrophysical Journal. 1975;**200**:L33

[72] Turner BE. Microwave detection of interstellar ketene. The Astrophysical Journal. 1977;**213**:L75

[73] Ohishi M, Ishikawa S, Amano T, Oka H, Irvine WM, Dickens JE, et al. Detection of a new interstellar molecular ion, H2COH+ (protonated formaldehyde). The Astrophysical Journal. 1996;**471**:L61

[74] Remijan AJ, Hollis JM, Lovas FJ, et al. Detection of interstellar cyanoformaldehyde (CNCHO). The Astrophysical Journal. 2008;**675**:L85

[75] Cernicharo J, Marcelino N, Roueff E, et al. Discovery of the Methoxy radical, CH_3O, toward B1: Dust grain and gas-phase chemistry in cold dark clouds. The Astrophysical Journal. 2012;**759**:L43

[76] Gupta H, Gottlieb CA, Lattanzi V, Pearson JC, McCarthy MC. Laboratory measurements and tentative astronomical identification of H_2NCO+. The Astrophysical Journal. 2013;**778**:L1

[77] Rubin RH, Swenson GW Jr, Solomon RC, Flygare HL. Microwave detection of interstellar formamide. The Astrophysical Journal. 1971;**169**:L39

[78] Irvine WM, Brown RD, Craig DM, et al. A new interstellar polyatomic molecule: Detection of propynal in the cold cloud TMC-1. The Astrophysical Journal. 1988;**335**:L89

[79] Hollis JM, Remijan AJ, Jewell PR, Lovas FJ. Cyclopropenone (c-H_2C_3O): A new interstellar ring molecule. The Astrophysical Journal. 2006;**642**:933

[80] Gilmore W, Morris M, Palmer P, et al. Observation of the 6(16)-5(15) transitions of acetaldehyde in Sagittarius B2. The Astrophysical Journal. 1976;**204**:43

[81] Dickens JE, Irvine WM, Ohishi M, et al. Detection of interstellar ethylene oxide (c-C2H4O). The Astrophysical Journal. 1997;**489**:753

[82] Turner BE, Apponi AJ. Microwave detection of interstellar vinyl alcohol. CH_2CHOH. The Astrophysical Journal. 2001;**561**:L207

[83] Hollis JM, Jewell PR, Lovas FJ, Remijan A, Møllendal H. Green bank telescope detection of new interstellar aldehydes: Propenal and propanal. The Astrophysical Journal. 2004;**610**:L21

[84] Remijan AJ, Snyder LE, McGuire BA, et al. The Astrophysical Journal. 2014;**783**:77

[85] Snyder LE, Buhl D, Schwartz PR, et al. Radio detection of interstellar dimethyl ether. The Astrophysical Journal. 1974;**191**:L79

[86] Hollis JM, Lovas FJ, Remijan AJ, et al. Detection of acetamide (CH3CONH2): The largest interstellar molecule with a peptide bond. The Astrophysical Journal. 2006;**643**:L25

[87] Snyder LE, Lovas FJ, Mehnringer DM, et al. Confirmation of nterstellar acetone. The Astrophysical Journal. 2002;**578**:245

[88] Belloche A, Garrod RT, Müller HSP, et al. Increased complexity in interstellar chemistry: Detection and chemical modeling of ethyl formate and n-propyl cyanide in Sagittarius B2(N). Astronomy & Astrophysics. 2009;**499**:215

[89] Tercero B, Kleiner I, Cernicharo J, et al. Discovery of methyl acetate and gauche ethyl formate in orion*. The Astrophysical Journal. 2013;**770**:L13

[90] Fuchs GW, Fuchs U, Giesen TF, Wyrowski F. Trans-ethyl methyl ether in space a new look at a complex molecule in selected hot core regions. Astronomy & Astrophysics. 2005;**444**:521

[91] Snyder LE, Hollis JM, Ulich BL, et al. Radio detection of interstellar sulfur dioxide. The Astrophysical Journal. 1975;**198**:L81

[92] Turner BE. Detection of interstellar SO(+)—A diagnostic of dissociative shock chemistry. The Astrophysical Journal. 1992;**396**:L107

[93] Agúndez M, Cernicharo J, Guélin M. New molecules in IRC +10216: Confirmation of C_5S and tentative identification of MgCCH, NCCP, and SiH_3CN**. Astronomy & Astrophysics. 2014;**570**:A45

[94] Etim EE, Gorai P, Das A, Chakrabarti SK, Arunan E. Interstellar hydrogen bonding. Advances in Space Research. 2018;61(11):2870-2880. DOI: 10.1016/j.asr.2018.03.003

[95] Vidal THG, Wakelam V. A new look at Sulphur chemistry in hot cores and corinos. Monthly Notices of the Royal Astronomical Society. 2018;**474**:5575

[96] Fuente A, Goicoechea J-R, Pety J, et al. First detection of interstellar S2H. The Astrophysical Journal. 2017;**851**:L49

[97] Vidal THG, Loison J-C, Jaziri AY, et al. On the reservoir of Sulphur in dark clouds: Chemistry and elemental abundance reconciled. Monthly Notices of the Royal Astronomical Society. 2017;**469**:435

Chapter 7

Mechanism of Interactions of Zinc(II) and Copper(II) Complexes with Small Biomolecules

Tanja Soldatović

Additional information is available at the end of the chapter

http://dx.doi.org/10.5772/intechopen.79472

Abstract

Over the past few decades, transition metal complexes have attracted considerable attention in medicinal inorganic chemistry, especially as synthetic metallonucleases and metal-based anticancer drugs that are able to bind to DNA under physiological conditions. The use of metal-based drugs presents the most important strategy in the development of new anticancer and antimicrobial agents. Negative side effects during treatment (such as vomiting, resistance, nephrotoxicity, ototoxicity, neurotoxicity and cardiotoxicity) prompted researchers to design new classes of DNA and protein targeting metal-based anticancer agents with potential in vitro selectivity and less toxicity. Knowledge of mechanism of the interaction zinc(II) and copper (II) ions with biomolecules and other relevant ligands is essential for understanding the cellular biology of delivery complexes to DNA and proteins. Results obtained from investigations provide useful information for the future design of potential zinc- and copper-based anticancer drugs. Different mechanism of interactions with selected biomolecules compared to platinum-based drugs has been observed.

Keywords: transition metal complexes, kinetics, mechanism of interactions, metal-based drugs, biomolecules, antitumour activity

1. Introduction

The aim of this chapter is to present fundamental chemical properties and new investigations of coordination compounds of some transition metal ions with an overview of medicinal applications. Transition metals appear in almost every facet of our day-to-day life, from industrial uses such as the manufacture of construction and building materials, tools, vehicles, up to cosmetics, paints and fertilizers. Their reactions are in general important in many

technical processes such as catalysis, materials synthesis, photochemistry, as well as, in biology and medicine.

It is known that metal ions play an important role in the biological and biomedical processes. Namely, many processes such as breathing, metabolism, photosynthesis, growth, reproduction, muscle contraction cannot imagine without the presence of some metal ions. It is currently believed that about 24 elements are essential for the life of mammals, which are: H, C, N, O, F, Na, Mg, Si, P, S, Cl, K, Ca, V, Mn, Fe, Co, Ni, Cu, Zn, Se, Mo, Sn and I.

The field of inorganic coordination chemistry, among other thing, is concerned with the study of the use of compounds of essential and non-essential elements in medicine, as well as, of the interaction of given compounds with the present biomolecules within the organism. Now many inorganic coordination compounds are widely used in medicine for the treatment of many diseases, including various cancers, Alzheimer's disease, diabetes, rheumatoid arthritis and others. In this chapter, among other things, we are focused on coordination compounds zinc(II) and copper(II) and on investigation of the mechanism of interactions with biologically relevant molecules.

2. Transition metal ions chemistry

2.1. Lewis acid base theory

Although, in this chapter, we mainly discuss the coordination compounds of transition metal ions, it is very important to explain some of the basic characteristics of complex compounds such as are definition of Lewis acids and bases.

A Lewis acid is an electron acceptor and a Lewis base is an electron donor. In a coordination complex, the central metal ions act as a Lewis acid and are coordinated (bonded) by one or more molecules or ions (ligands) which act as Lewis bases. Formed coordinated bonds between central atom or ion with ligands have covalent character and are known under name *coordinate covalent bond* or simple *coordinate bond*. Atoms in the ligands that are directly bonded to the central atom or ion are donor atoms.

2.2. Hydration or hydrolysis of metal ions?

When a metal salt is dissolved in water, the ionic bond is interrupted, the cations and anions are hydrated. For example, when NaCl is dissolved in water, the inner hydration shell around Na^+ is formed. The $Na^+ \cdots O$ interaction can be described in terms of an ion-dipole interaction, while the solvation of the anion can be described in terms of the formation of hydrogen bonds between Cl^- and H atoms of surrounding H_2O molecules (**Figure 1**).

Hydration is solvation when the solvent is water. If the metal-oxygen bond possesses covalent character, there is also an ionic contribution to the bonding interaction. Each O atom donates a pair of electrons to the metal M^{z+} ion, and each H_2O molecule acts as a Lewis base while the metal ion acts as a Lewis acid. The M-O interaction is covalent, in contrast to the case for Na^+.

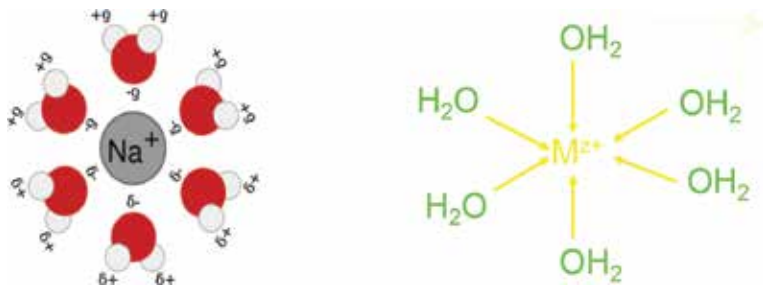

Figure 1. Left: the first hydration shell of an Na^+ ion; ion-dipole interactions between the Na^+ ion and the H_2O molecules; Right: bonding of metal ions and H_2O molecules.

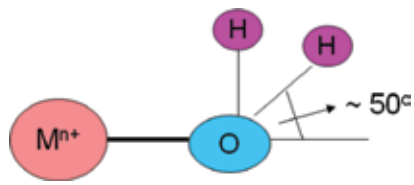

Figure 2. The plane of the water molecule in the direction M^{z+}·····O axis.

In practice, the character of the metal-·oxygen interaction varies with the nature of the metal ion and relevant to this is the electroneutrality principle (**Figure 1**).

In concentrated solutions, the plane of the water molecule makes an angle of up to 50° degree with the M^{z+}·····O axis (**Figure 2**) implying interaction of the cation with a lone pair of electrons rather than an ion-dipole interaction, it suggests that the metal-oxygen interaction involves the use of an oxygen lone pair. Metal cations are equated with the formula $[M(H_2O)_n]^{z+}$, where z is 1, 2 or 3, and they tend to hydrolyze [1].

2.3. Transition metal ions as Brønsted acids

Metal ions in aqueous solution behave as Lewis acids. The positive charge on the metal ion draws electron density from the O-H bond in the water. This increases the bond's polarity making it easier to break. When the O-H bond breaks, an aqueous proton is released producing an acidic solution. Hydrolysis refers to the reversible loss of H^+ from an aqua species.

Transition metal ions can act as Brønsted acids by loss of H^+ from a coordinated water molecule. Small cations such as Li^+, Mg^{2+}, Al^{3+}, Fe^{3+} and Ti^{3+} possess high charge densities, cannot be Brønsted acids by themselves. Water molecules covalently bound to one of these metal ions are more acidic than normal, the H atoms carry significant positive charge. Thus, reactions such as the following occur.

$$[Fe(H_2O)_5(OH)]^{2+} + H_2O \rightleftharpoons [Fe(H_2O)_4(OH)_2]^+ + H_3O^+$$
$$pK_{eq}([Fe(H_2O)_6]^{3+}) \sim pK_a(HNO_2)$$

The characteristic colour of the $[Fe(H_2O)_6]^{3+}$ ion is purple, but aqueous solutions appear yellow due to the formation of the hydroxo species $[Fe(H_2O)_5(OH)]^{2+}$ and $[Fe(H_2O)_4(OH)_2]^{+}$.

The equilibrium constant K_{eq} for the hydrolysis of a hydrated cation is analogous to the K_a for the ionization of a weak acid. Generally, hydrolysis constants for cations are signed as $-\log K_a$. These hydrolysis constants are averages of different experimental measurements. If we compare the value of constant for previous reaction with K_a of weak acids, it can be seen that pK_{eq} of $[Fe(H_2O_6)]^{3+}$ correspond to pK_a of weak nitrous acid.

2.4. Stability constants of coordination complexes

Metal ions in aqueous solution are hydrated; the aqua species may be accounted as $M^{z+}{}_{(aq)}$ where this often represents the hexaaqua ion $[M(H_2O)_6]^{n+}$. Addition of a neutral ligand L to the solution leads the formation of a series of complexes $[M(H_2O)_5L]^{n+}$, $[M(H_2O)_4L_2]^{n+}\ldots[ML_6]^{n+}$. The stepwise displacements of coordinated H_2O by L are represented by Eqs. (1) and (2).

$$[M(H_2O)_6]^{z+} + L \xrightleftharpoons{K_1} [M(H_2O)_5L]^{z+} + H_2O$$

$$K_1 = \frac{[M(H_2O)_5L]^{z+}}{[M(H_2O)_6]^{z+}\,[L]} \tag{1}$$

$$[M(H_2O)L_5]^{z+} + L \xrightleftharpoons{K_6} [ML_6]^{z+} + H_2O$$

$$K_6 = \frac{[ML_6]^{z+}}{[M(H_2O)L_5]^{z+}\,[L]} \tag{2}$$

In step-wise formation of complex $[ML_6]^{+}$ from $[M(H_2O)_6]^{z+}$, each displacement of a coordinated water molecule by ligand L has a characteristic *stepwise stability constant*, K_1, K_2, K_3, K_4, K_5 or K_6. Alternatively, we may consider the overall formation of $[ML_6]^{z+}$ (Eq. (3)).

$$[M(H_2O)_6]^{z+} + 6L \rightleftharpoons [ML_6]^{z+} + 6H_2O$$

$$\beta_6 = \frac{[ML_6]^{z+}}{[M(H_2O)_6]^{z+}\,[L]^6} \tag{3}$$

The constant β_6 we call as *cumulative stability constant.* The connection between values of stepwise formation stability constant and overall stability constant is given by expression: $\beta_6 = K_1K_2K_3K_4K_5K_6$ or $\log\beta_6 = \log K_1 + \log K_2 + \log K_3 + \log K_4 + \log K_5 + \log K_6$. Determinations of stability constants can be made by polarographic or potentiometric measurements (if a suitable reversible electrode exists), by pH measurements (if the ligand is the conjugate base of a weak acid) or by ion-exchange, spectrophotometric (i.e. observation of electronic spectra and use of the Beer–Lambert Law), NMR spectroscopic or distribution methods [1].

Hard (acids)	Intermediate (acids)	Soft (acids)
Li^+, Na^+, K^+, Rb^+, Be^{2+}, Mg^{2+}, Ca^{2+}, Sr^{2+}, Sn^{2+}, Mn^{2+}, Al^{3+}, Ga^{3+}, In^{3+}, Sc^{3+}, Cr^{3+}, Fe^{3+}, Co^{3+}, Y^{3+}, Th^{4+}, Pu^{4+}, Ti^{4+}, Zr^{4+}, $[VO]^{2+}$, $[VO_2]^+$	Pb^{2+}, Fe^{2+}, Co^{2+}, Ni^{2+}, Cu^{2+}, Zn^{2+}, Os^{2+}, Ru^{3+}, Rh^{3+}, Ir^{2+}	Zero oxidation state metal centres, Tl^+, Cu^+, Ag^+, Au^+, $[Hg_2]^{2+}$, Hg^{2+}, Cd^{2+}, Pd^{2+}, Pt^{2+}, Ru^{2+} Tl^{3+}
Hard (bases)	**Intermediate (bases)**	**Soft (bases)**
F^-, Cl^-, H_2O, ROH, R_2O, $[OH]^-$, $[RO]^-$, $[RCO_2]^-$, $[CO_3]^{2-}$, $[NO_3]^-$, $[PO_4]^{3-}$, $[SO_4]^{2-}$, $[ClO_4]^-$, $[ox]^{2-}$, NH_3, RNH_2	Br^-, $[N_3]^-$, py, $[SCN]^-$ (*N*-bound), $ArNH_2$, $[NO_2]^-$, $[SO_3]^{2-}$	I^-, H^-, R^-, $[CN]^-$ (*C*-bound), CO (*C*-bound), RNC, RSH, R_2S, $[RS]^-$, $[SCN]^-$ (*S*-bound), R_3P, R_3As, R_3Sb, alkenes, arene

Table 1. Selected hard and soft metal centres (Lewis acids) and ligands (Lewis bases) and those that exhibit intermediate behaviour.

2.5. Hard and soft acid base principle

Based on acceptor properties of metal ions towards ligands (i.e. Lewis acid-Lewis base interactions), two classes of metal ion can be identified, although the distinction between them is not clear-cut. The terms "hard" and "soft" acids arise from a polarizabilities of the metal ions. Hard acids are typically either small monocations with a relatively high charge density or are highly charged, again with a high charge density. These ions are not very polarizable and show a preference for donor atoms that are also not very polarizable, for example, F^-. Such ligands are called hard bases. Soft acids tend to be large monocations with a low charge density, for example, Au^+, and are very polarizable. They prefer to form coordinate bonds with donor atoms that are also highly polarizable, for example, I^-. Such ligands are called soft bases [1]. Hard acids (hard metal cations) form more stable complexes with hard bases (hard ligands), while soft acids (soft metal cations) show a preference for soft bases (soft ligands). The list of hard and soft acids and bases with included intermediates is shown in **Table 1**.

The hard and soft acid base (HSAB) principle is qualitatively useful, the hard-hard or soft-soft matching of acid and base represents a stabilization that is additional to other factors that contribute to the strength of the bonds between donor and acceptor. These factors include the sizes of the cation and donor atom, their charges, their electronegativities and the orbital overlap between them.

Complex formation usually involves ligand substitution. If we suppose that M^{z+} is a hard acid. It is already associated with hard H_2O ligands, and hard-hard interaction is a favourable. If L is a soft base, ligand substitution will not be favourable. If M^{z+} is a soft acid, ligand substitution will be favourable [1].

3. Medicinal application of inorganic complexes (metal-based drugs)

3.1. Medicinal inorganic chemistry

Medicinal inorganic chemistry is a part of bioinorganic chemistry that occupies a significant place in the field of therapeutic and diagnostic medicine. Inorganic coordination compounds are now used in medicine for the treatment of numerous diseases.

Today, it is well known that some metal ions are required for normal functions of organism. Lack of zinc, iron, copper, ions and so on can induce disease. Some metal ions such as arsenic, cadmium, chromium, lead and mercury can induce toxicity in humans. Even essential metal ions can be toxic when present in excess. An important aspect of medicinal bioinorganic chemistry is ability to understand all this in the molecular level and treat diseases caused by inadequate metal ion function constitutes.

Medicinal inorganic chemistry is a multidisciplinary field combining elements of chemistry (synthesis and reactivity), pharmacology (pharmacokinetics and toxicology), biochemistry (targets, structure and conformational changes) and medicinal chemistry (therapeutics, pharmacodynamics and structure-activity relationships). The main focus of this field is to design of novel therapeutic and diagnostic agents and to investigate the mechanism of medicinal action, as improvement of the action of many organic compounds used in medicine by activation or biotransformation by metal ions [2–4].

3.2. Metal complexes as drugs

In order for the coordination complexes to be approved as drugs, it is necessary to detailed examination of the fundamental aqueous chemistry of the proposed drug, including its pharmacokinetics, the metabolic processes in blood and intracellularly, and the effects of the drug on the target of choice. Inorganic coordination chemistry offers a wide variety of synthesis of coordination compounds with different coordination spheres, including ligand designs, oxidation states and redox potentials of transition metal ions, thus gives the ability to systematically alter the kinetic and thermodynamic properties of the complexes towards biological receptors. Well-known metal ions and their coordination complexes that have found usage in medicine can be divided into:

1. Platinum anticancer agents (e.g., cisplatin, *cis*-$[PtCl_2(NH_3)_2]$)
2. The gold(I)-containing antiarthritic drugs (e.g. auranofin)
3. Metal-mediated antibiotics like bleomycin, which requires iron or other metals for activity
4. Technetium-99 m and other short-lived isotopes (rhenium-186, rhenium-188 and gallium-68) used as radiopharmaceuticals in disease diagnosis and treatment
5. Magnetic resonance imaging (MRI)-enhancing gadolinium(III) compounds
6. Antibacterials, antivirals, antiparasitics and radiosensitizing agents

Platinum complexes are now among the most widely used drugs for the treatment of cancer. Thanks to the successful and widespread use of cisplatin a large number of analogous compounds were synthesized. All these compounds have several common characteristics:

1. bifunctional complex compounds with *cis*-geometry
2. the general formula of these compounds is *cis*-$[PtA_2X_2]$ where A_2 are two inert monodentate nitrogen donor ligands or one inert bidentate nitrogen donor ligand, while with X_2 are two labile monodentate or one labile bidentate ligand

3. the oxidation state of platinum in the complexes is +2 or +4
4. nitrogen-donor ligands have to contain at least one NH bond.

Figure 3 presents some of platinum complexes that are in the medicinal use worldwide.

The second-generation platinum(II) antitumour complexes are carboplatin, oxaliplatin, nonplatinum, zenithplatin, enloplatin, NK121, CI-973 and others. Instead of labile chloride ligands, they contain bidentate ligands such as 1,1-cyclobutanedicarboxylate, glycolate, and complexes with 1,2-diaminocyclohexane as an inert ligand, while the labile ligands are sulphates, malonates and other ligands [5]. The second-generation complexes based on the cisplatin structure were developed to improve toxicity and/or expand the range of useful anticancer activity. The third-generation platinum antitumour complexes are octahedral platinum(IV) coordination compounds with general formula *cis*-$[PtA_2X_2Y_2]$, where two labile monodentate or one labile bidentate ligand is labeled as Y_2. The platinum(IV) drugs are orally administrated to patients. In the presence of various biomolecules such as cysteine or ascorbic acid, the redaction to Pt(II) occurred by leaving the axial ligands Y_2. In addition, this group includes new complexes with a *trans*-geometric structure, polynuclear platinum complexes (BBR3464) and complexes containing a ligand with an asymmetric carbon atom [6].

The mechanism of the antitumour effects of platinum complexes consists in their binding to DNA molecules, thereby preventing replication and transcription of DNA, that is, preventing the process of uncontrolled cell growth [7–9]. From the moment of injection of the drugs in the body to their binding to DNA molecules, a large number of secondary processes happen that

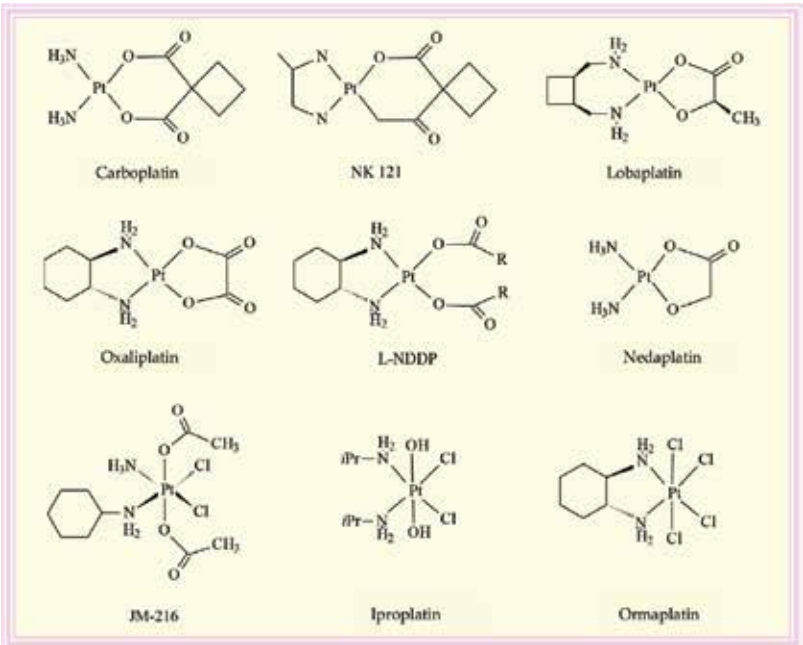

Figure 3. Platinum antitumour complexes with adopted commercial names.

are responsible for the occurrence of toxic effects [8, 9]. Hydrolysis of Pt(II) drugs in the body occurs as a result of a different concentration of chloride ions in and out of the cell. Namely, the high concentration of Cl^- ion in the extracellular fluid (104 mM) suppresses the hydrolysis process, while in the intracellular low concentration of about 4 mM, it is suitable for the hydrolytic reactions of platinum(II) antitumour drugs [10, 11]. The antitumour platinum(II) agents must not be either too reactive or too inert, since in both cases their toxicity is increasing [10]. On the other hand, the essential characteristic of these compounds must be selectivity towards certain biomolecules [12]. High affinities for the platinum complexes show the biomolecules that contain sulphur, as the thiols and the thioethers, as soft acid platinum(II) drugs form very stable compounds with sulphur donor biomolecules, for example, soft bases. The resulting compounds are responsible for negative side effects during treatment (such as vomiting, resistance, nephrotoxicity, ototoxicity, neurotoxicity and cardiotoxicity).

During the recent years, many ruthenium complexes with oxidation state +2 or +3 found to have anticancer activity. Antitumour activities of Ru(II) and Ru(III) complexes take place in a different manner in comparison with platinum(II) drugs, what is linked with geometrical structures and reversible redox potential of ruthenium. The real revolution among the ruthenium complexes was initiated by two isostructural complexes Ru(III): [ImH]*trans*-[$RuCl_4(Im)_2$] and [IndH]*trans*-[$RuCl_4(Ind)_2$], better known by the names ICR and KP1019, respectively (Im = imidazole and Ind = indazole) and [Na]*trans*-[$RuCl_4$(Im)(dmso-*S*)] or NAMI-A (dmso-*S* = dimethyl sulphoxide coordinated through sulphur), which is a structural analogue to the previously synthesized ICR complex (**Figure 4**). Apart from the fact that these complexes have shown activity to several different types of tumours, it is particularly interesting that they are active against tumours resistant to platinum complexes. The mechanism of action of this compound is not related to DNA binding; rather, it is an antimetastatic agent [13]. Metastasis (the process whereby tumour growth occurs distant from the original or primary tumour site)

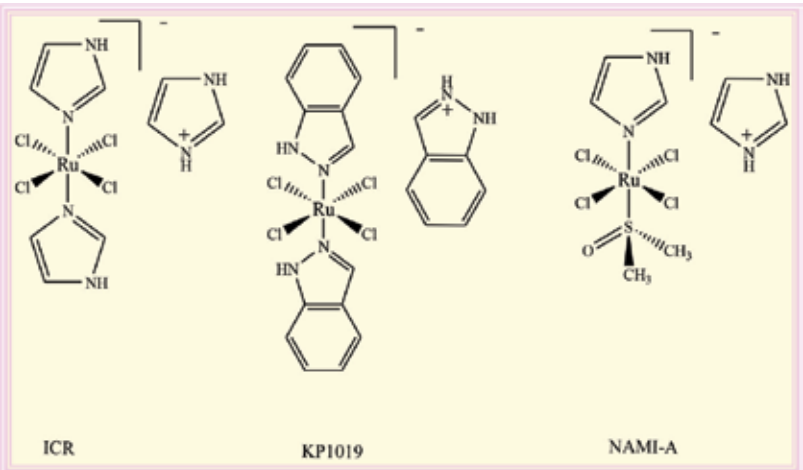

Figure 4. The structures of the ruthenium(III) complexes: [ImH]*trans*-[$RuCl_4(Im)_2$] or ICR; [IndH]*trans*[$RuCl_4(Ind)_2$] or KP1019 and ([ImH]*trans*-[$RuCl_4$(Im)(dmso-*S*) or NAMI-A.

is linked with angiogenesis, the dynamic process that involves new blood vessel formation. Antitumour activity of ruthenium complexes is related with interaction with proteins in cell membrane or collagen in extracellular fluid.

The ruthenium(II) complexes types $[Ru(II)(\eta^6\text{-arene})(en)X]^+$ ($X = Cl^-$ or I^-, arene = p-cumene or biphenyl, en = ethylenediamine) characterize higher stability to hydrolysis and get in cytoplasm in unchanged form. They are supposed to act as catalysts for glutathione oxidation, which contribute to the increase in cellular oxidative stress and programmed cell death, i.e. apoptosis. Ru(III) complexes tend to be more biologically inert than related Ru(II) complexes, like several other metal ions, can be delivered to cells *via* the iron transport protein transferrin.

The coordination compounds of other metal ions such as Au(I), Au(III), Ti(IV), Cu(II) or MnSOD (manganese-based superoxide dismutase mimics) are on clinical trial. The enzyme superoxide dismutase (SOD), either as the manganese containing MnSOD (present in the mitochondrion) or the dinuclear Cu/Zn-SOD (present in the cytosol and extracellular space), performs the role of superoxide detoxification in normal cells and tissue [14].

Polyoxometallates of the Keggin type such as $[NaW_{21}Sb_{29}O_{86}][NH_4]_{17}$ and $K_{12}H_2[P_2W_{12}O_{48}]\cdot 24H_2O$ have potential in the anti-HIV field, they bind to viral envelope sites on cell surfaces and interfere with virus adsorption [3]. Metal-chelating macrocyclic bicyclam ligands are among the most potent inhibitors of HIV ever described, and there is considerable interest in the role of Zn proteins in the viral life cycle. Metal ions are required for the activity of anti-HIV G-quartet oligonucleotides (antisense oligonucleotides) such as T30177, a potent inhibitor of the enzyme HIV-1 integrase [3].

Bismuth compounds have been used for their antacid and astringent properties in a variety of gastrointestinal disorders [15, 16]. The effectiveness of bismuth is due to its bacteriocidal action against the Gram-negative bacterium, *Helicobacter pylori*. Usually, the bismuth preparations are obtained by mixing an inorganic salt with a sugar-like carrier.

Injectable Au(I) thiolates and an oral Au(I) phosphine complex are widely used for the treatment of rheumatoid arthritis. Proteins appear to be the targets for gold therapy, including albumin in blood plasma and enzymes in joint tissues. The detection of $[Au(CN)_2]$ in the blood and urine of patients undergoing gold therapy (chrysotherapy) raises the possibility that this is an active metabolite. Cyanide could be involved in the metabolic pathways for other metal ions (both natural and therapeutic) in the body since it can be synthesized by some cells. The recent discovery that oxidation of administered Au(I) compounds to Au(III) may be responsible for some of the side effects of gold therapy has highlighted interests in the biological redox chemistry of gold, including possible stabilization of Au(III) complexes by peptides and proteins, which now is main target for developing antitumour Au(III) drugs [3, 4, 6].

Peroxovanadate complexes can inhibit insulin receptor-associated phosphotyrosine phosphatase and activate insulin receptor kinase, and both V(IV) and V(V) compounds offer promise as potential insulin mimics [4, 6]. Lithium compounds are kinetically labile and are used for the treatment of bipolardisorders, and Li(I) inhibition of Mg(II)-dependent inositol monophosphatase enzymes leads to interference with Ca(II) metabolism [4]. Newer uses have appeared in

the treatment of viral diseases including AIDS, alteration of the immune response and cancer. The lithium salt of linolenic acid (LiGLA) has a significant anticancer effect against certain cancers [6].

Less labile metal ions can be used to control the levels of biologically active ligands in the body. Thus, Fe(III) in sodium nitroprusside delivers NO to tissues and is used for the treatment of hypertension and control of blood pressure. The possibility arises of utilizing Ru(III) to scavenge NO in the treatment of septic shock. As is mentioned, the injection of gram quantities of Gd(III) complexes to provide contrast magnetic resonance images (MRI) of the body illustrates how the toxicity of metal ions and tissue targeting can be controlled by the appropriate choice of ligands [4]. The importance of metal complexes as imaging agents for various diseases including heart disease and brain disorders have also been recognized. They are able to determine specific aspects of disease such as tissue hypoxia, and can detect molecular phenomenon such as multidrug resistance [3]. Metal centres, being positively charged, favourably bind to negatively charged biomolecules (proteins and nucleic acids) and offer excellent tools for understanding of more specific biological processes including the formation of thrombi and the imaging of infection, and so on. By means of scanning techniques viz. gamma scintigraphy, positron emission tomography (PET) and magnetic resonance imaging (MRI), tissues and organs with radiolabelled compounds can be visualized and such visualization facilitates the detection of abnormalities in their function. Radionuclide complexes are used for diagnosis, as contrast media and as therapeutic agents. A ^{99m}Tc radiopharmaceutical (^{99m}Tc–SESTAMIBI), known as cardiolite, is an established radiopharmaceutical for myocardial perfusion imaging [3, 4]. A wide variety of coordinated spheres, oxidation states and redox potentials of metal ions in coordinated and organometallic compounds give possibility of design and synthesis of new metal complexes with selected kinetic and thermodynamic properties towards biological receptors [3, 4, 6].

Many Cu-complexes of anti-inflammatory drugs have been found more active in animal models than either their parent Cu(II) salt or NSAID (nonsteroidal anti-inflammatory drugs). Cu(II) complex of salicylate has been found about 30 times more effective than aspirin as an anti-inflammatory agent. The pharmacological activity of these complexes has been proposed to be due to its inherent physico-chemical properties of the complex itself rather than that of its constituents [17].

The amount of metals present in the human body is approximately 0.03% of the body weight. Low metal ion concentrations may be harmful for the body. It has been reported that in various cancers the concentrations of Cd, Cr, Ti, V, Cu, Se and Zn were found to be at a lower level than in normal conditions of body [18]. Ligands having electron donor atoms like N, O, S and P may form coordination bond with metal ion. Chelation causes drastic changes in biological properties of ligands as well as metal moiety and in many cases it causes synergistic effect of metal ion and ligand both [19]. On the other hand, the presence of metals such as lead, mercury, arsenic, uranium and plutonium induces metal poisoning. In order to remove these metals medical procedure, chelation therapy is performing. The medical procedure involves the administration of chelating agents to remove heavy metals from the body. Some common chelating agents are ethylenediaminetetraacetic acid (EDTA), 2,3-dimercaptopropanesulphonic acid (DMPS) and thiamine tetrahydrofurfuryl disulphide (TTFD).

4. Investigation of the interactions of zinc(II) and copper(II) complexes with small biomolecules

4.1. Substitution mechanisms in complex compounds

Complex compounds are involved in a number of substitution reactions such as ligand exchange, solvent exchange, complexation or anation reactions, solvolysis, acid and base hydrolysis, inter- and intramolecular isomerization, racemization and metal ion exchange [20]. Substitution reactions of complexes can be electrophilic (SE) or nucleophilic (SN) depending on the replacement of either central metal ion or ligand. If the metal ion is substituted during the reaction, that is, electrophile, the reactions are electrophilic substitution (Eq. (4)), otherwise if a ligand is replaced that is nucleophilic substitution reaction (Eq. (5)) [21, 22].

$$[ML_n] + M' \rightleftharpoons [M'L_n] + M \tag{4}$$

$$[ML_n] + X \rightleftharpoons [ML_{n-1}X] + L \tag{5}$$

Nucleophilic substitution reactions, according to Langford and Gray, are carried out in three different mechanisms: dissociative (D), associative (A) or interchange mechanism (I) [22]. In the dissociative mechanism (D), the first step of the reaction is dissociation of the one ligand L from the inner coordination sphere, whereby an intermediate with a decreased coordination number forms. In the next step, the entering ligand X binds to the central metal ion. Since the first step of the reaction is slower, it determines the overall rate of the substitution reaction. In the associative mechanism (A), in the first step, the entering ligand X binds to the central metal ion, forming an intermediate with an increased coordination number, and then, in the second step, the leaving ligand L leaves the coordination sphere of the complex. The formation of an intermediate with an increased coordination number is slower and it determines the rates of this substitution process. When an intermediate cannot be detected by kinetic, stereochemical or product distribution studies, the so-called interchange mechanisms (I) are invoked. Associative interchange mechanisms (I_A) have rates dependent on the nature of the entering group, whereas dissociative interchange (I_D) mechanisms do not. If the process of breaking the bond between the central metal ion and the outgoing ligand L has a greater impact on the rate of reaction, the mechanism is I_D, and if the forming a new bond between the central metal ion and the entering ligand X has a greater impact on the chemical reaction rate, the mechanism is marked with I_A [21, 22].

Factors affecting metal ion lability include size, charge, electron configuration and coordination number. The associative mechanism is well known and preferred for four-coordinated square-planar complexes. Dissociative mechanisms are more common for six-coordinated octahedral complexes. Five-coordinated complexes could react in both mechanisms [23]. The study of kinetics and mechanism of the reactions of transition metal complexes expanded with development of organometallic and bioinorganic chemistry, as well as, with the development of new experimental techniques (UV-Vis spectrophotometry, NMR spectroscopy, "stop-flow" spectrophotometry, HPLC, EPR spectroscopy, etc.). The main aims of study are determination of rates of substitution processes, investigation of the influence of different parameters (change

of reactant concentration, pH, temperature and pressure change, introduction catalyst, etc.), investigation of interactions between potential antitumour metal-based drugs and biologically relevant molecules [20–24].

4.2. The bioinorganic chemistry of zinc(II) and copper(II) complexes

Transition metal compounds play crucial roles as cofactors in metalloproteins; they act mainly as a Lewis acid. Two essential metal ions, namely zinc and copper ions, modulate enzymes activities, catalytic and regulatory functions, oxidative-reductive processes, etc. [4, 24]. Zinc has a specific role in bioinorganic processes because of the peculiar properties of the coordination compounds of the zinc(II) ion, easily can be four-, five- or six-coordinate, without a marked preference for six coordination [24]. The most studied metalloproteins in which zinc serves a structural role belong to the zinc-finger family, which is involved in control of nucleic acid replication, transcription and repair [25]. In zinc-finger proteins, zinc is tetrahedrally coordinate to histidines and/or cysteines, the coordination of aspartic acid and glutamic acid residues to the metal, also has been found in metalloenzymes [26].

Zinc is a good intermediate Lewis acid, especially in complexes with lower coordination numbers; it lowers the pK_a of coordinated water and is kinetically labile, and the inter conversion among its four-, five- and six-coordinate states is fast [27]. The theoretical studies have shown that zinc does not have a strong preference for a particular number of water molecules in its first coordination layer and can accommodate four, five or six water ligands; the calculated energy differences between isomeric $[Zn(H_2O)_6]^{2+}$, $\{[Zn(H_2O)_5],(H_2O)\}^{2+}$ and $\{[Zn(H_2O)_4],(H_2O)_2\}^{2+}$ complexes differ by only a few kilocalories per mole [28]. Moreover, dynamic conversion of structural zinc into a transient catalytic centre may be a mechanism for nucleic acid cleavage [29]. Recently, we determined the metal–ligand stoichiometry between $[ZnCl_2(en)]$ (where en = 1,2-diaminoethane or ethylenediamine) complex and chloride at pH 7.2. In the presence of an excess of chloride (0.010 M NaCl), the octahedral $[ZnCl_4(en)]^{2-}$ formed in solution at pH 7.2 [30] (Eq. (6)).

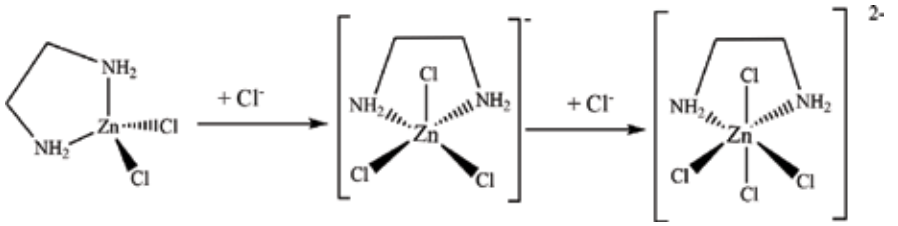

(6)

Also, we have investigated the mechanism of interaction between biologically relevant nucleophiles and $[ZnCl_2(terpy)]$ (where terpy = 2,2′:6′,2″- terpyridine) complex in the presence of NaCl [31, 32]. The excess of chloride did not affect coordination geometry of complex [32]. The result of the metal–ligand stoichiometry between $[ZnCl_2(terpy)]$ complex and imidazole implied formation of the five-coordinate specie $[Zn(terpy)(imidazole)_2]$ [31] (**Figure 5**).

Promising anticancer agents could be the zinc-based compounds, especially because zinc is implicated as an important cytotoxic/tumour suppressor agent in several cancers [33].

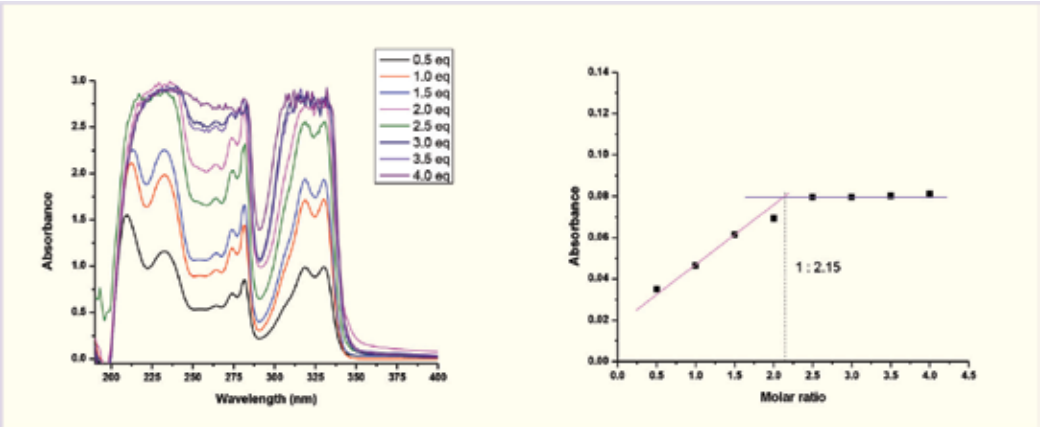

Figure 5. Titrations of $[ZnCl_2(terpy)]$ with imidiazole as monitored by UV-vis spectra. Left: $[ZnCl_2(terpy)]$-imidiazole, right: cross-section of UV-vis spectra at 350 nm in the presence of 0.001 M NaCl [31].

The mechanism of potential anticancer activity of zinc(II) complexes is assumed to be connected with: (i) fast inter conversion among its four-, five- and six-coordinate states; (ii) preference of the variable coordination geometries (tetrahedral, five-coordinate and octahedral) that zinc(II) is able to adopt, towards diverse donor site of relevant nucleophiles [27]. Knowledge of mechanism of the interaction zinc(II) ions with biomolecules and other relevant ligands is essential for understanding the processes in the cells during delivery of complexes to DNA and proteins.

On the other hand, copper(II) controls cancer development. It serves as a limiting factor for multiple aspects of tumour progression, growth, angiogenesis and metastasis [34–36]. Copper(II) complexes offer various potential advantages as antimicrobial, antiviral, anti-inflammatory, antitumour agents, enzyme inhibitor, chemical nucleases, and they are also beneficial against several diseases like copper rheumatoid and gastric ulcers [37, 38]. It has been shown recently that metal complexes of imidazole terpyridine (itpy) have potential applications in chemotherapy [39]. Changing the ligand environment towards the specific target is a possible way of tuning the selectivity of a drug molecule. The nature of the ligands plays an important role in the binding of a metal complex to a biomolecule such as DNA or protein [39, 40].

The chemistry of copper is dominated by the +2 oxidation state, for example, copper(II) complex ions. In comparison with other divalent first-row transition-metal aqua ions, the $[Cu(H_2O)_6]^{2+}$ ion is extremely labile [41, 42]. This effect is a consequence of Jahn-Teller distortion. As a result of the d^9 electronic configuration, an elongation of the axial-bound solvent molecules is weakly coordinated. Due to this distortion the axial water molecules are weaker bound to the central atom and therefore can be more easily substituted. The strong ligand field forces the metal ion into a different geometry, for example, 2,2′,2″-triaminotriethylamine ligands (tren) will restrict the degree and rapidity of distortion of the $[Cu(tren)H_2O]^{2+}$ complex and remove the dynamic Jahn-Teller effect as stabilizing effect [43]. The bulk of five-coordinate {Cu(terpy)(bipy)} and {Cu(terpy)(phen)} (terpy = 2,2′:6′,2″- terpyridine or derivative, bipy = 2,2′-bipyridine or derivative, phen = 1,10-phenanthroline or derivative) complexes

exhibiting ostensibly square-based pyramidal geometries also shows an additional interaction in the remaining axial site leading to a better description as their being six-coordinate [44].

4.3. Study on the kinetics and mechanism of the reactions of zinc(II) and copper(II) complex compounds with relevant biomolecules

Clear understanding of complex formation reactions between zinc(II) and copper(II) complexes and biorelevant nucleophiles is still largely missing. Substitution behaviour of Zn and Cu-complex compounds at physiological conditions is very complex due to the rather high molecular mobility, distortions of complex compound and facile interconversion of four- to five-, six-coordinate complexes. Adopted geometry of complex compounds conditionals different preferences towards bio-ligands. Thus, the square pyramidal structure of Zn(II) and Cu(II) in biological systems prefers *O*-carboxylate or carbonyl and *N*-imidazole donor bio-ligand, while tetrahedral prefers *S*-thiolate or thioether, *N*-imidazole [4]. Investigation of mechanism of the interaction between zinc(II) and copper(II) ions and biomolecules and other relevant ligands is essential for understanding the mechanism of action of the potential zinc- and copper-based antitumour drugs.

Recently, we have investigated by different methods (UV-Vis, EPR, HPLC-MS, density-functional calculations, mole-ratio, etc.) the kinetics and mechanism of the reactions between tetrahedral and square-pyramidal Zn(II) or Cu(II) complex compounds (i.e. [$ZnCl_2$(en)], [$CuCl_2$(en)], [$CuCl_2$(terpy)] and [$ZnCl_2$(terpy)]) with bio-nucleophiles as a function of entering nucleophile concentrations and temperature at pH 7.2–7.4 [30–32, 45]. The kinetics showed that the substitution reactions involve the consecutive displacement of both chloride ligands for every complex. Higher reactivity of [$CuCl_2$(terpy)] complex then [$ZnCl_2$(terpy)] was obtained. The order of reactivity of the investigated biomolecules for the first reaction step is: glutathione (GSH) >> DL-aspartic acid (DL-Asp) > guanosine-5′-monophosphate (5′-GMP) > inosine-5′-monophosphate (5′-IMP) > L-methionine (L-Met) (for [$CuCl_2$(terpy)]), while for [$ZnCl_2$(terpy)] order is: DL-Asp > GSH > 5′-GMP > 5′-IMP >> L-Met. Chelate formation and pre-equilibrium were obtained for the substitution process between [$ZnCl_2$(terpy)] complex and glutathione [32]. The π-acceptor properties of the tridentate N-donor chelate (terpy) predominantly control the overall reaction pattern [31, 32, 45]. Based on energetic stability of complexes, it can be concluded that both complexes make hydrates very easy, but the bond between water molecule and metal ion is pretty weak. In addition, there is a very good agreement between experimental and calculated spectra obtained for hydrated and non-hydrated complexes in aqueous solution. During formation of monohydrate, Zn(II) and Cu(II) complexes obtain little shaped octahedral geometry, with three nitrogen and chloride atom in the central plane, and with water molecule and the other chloride atom on the line almost normal to the plane [32]. The presence of various concentration of chlorides has significant impact on rate constants of substitution processes of the [$ZnCl_2$(terpy)] complex by nucleophiles [31].

As we mentioned in Section 4.2, the mole-ratio method was used for determining the metal-ligand stoichiometry between [$ZnCl_2$(en)] and chloride at pH 7.2. The results have shown stepwise formation of 1:1 and 1:2 complexes, and indicate additional coordination of chlorides in the first coordination sphere (Eq. (6)) [30]. The kinetics of ligand substitution reactions of this

complex and biological relevant nucleophiles such as 5′-IMP, 5′-GMP, L-Met, GSH and DL-Asp was followed under *pseudo*-first-order conditions by UV-Vis spectrophotometry. In the presence of an excess of chloride the octahedral complex anion $[ZnCl_4(en)]^{2-}$ has been formed. The first step of the substitution reactions could be interpreted as substitution of the axial chlorido ligands in *cis* position towards bidentate ethylenediamine by the biologically relevant nucleophiles, while the second step is substitution of the equatorial chlorido ligand. The order of reactivity of the investigated nucleophiles for the first reaction step is 5′-IMP > GSH > L-Met > DL-Asp > 5′-GMP, while for the second reaction step is GSH > L-Met > 5′-IMP > DL-Asp > 5′-GMP [30].

In the presence of an excess of chloride, the square-planar complex $[CuCl_2(en)]$ exists as a *pseudo* octahedral complex with two axially and weakly-bound solvent ligands, these ligands are rapidly replaced/substituted by chloride ions to form $[CuCl_4(en)]^{2-}$ as a pre-equilibrium intermediate, while equilibrium reaction was observed for $[CuCl_2(terpy)]$ [45]. The order of reactivity of the investigated bio-relevant nucleophiles towards $[CuCl_4(en)]^{2-}$ complex is: GSH > 5′-GMP > 5′-IMP > DL-Asp > L-Met, while towards $[CuCl_2(terpy)]$ the order of reactivity is: DL-Asp > L-Met > GSH > 5′-GMP > 5′-IMP, for the first reaction step. Different order of reactivity of biomolecules towards $[CuCl_2(en)]$ and $[CuCl_2(terpy)]$ complexes could be explained by different geometrical structures of complexes (octahedral and square-pyramidal, respectively) in the presence of chloride and their different preferences towards donor atoms of biomolecules. Mass spectrum of $[CuCl_2(terpy)]$ in Hepes buffer has shown two new signals at m/z = 477.150 and m/z = 521.00, assigned to $[CuCl(terpy)]^+$ − Hepes fragments of coordinated Hepes buffer. These signals also appear in mass spectra of ligand-substitution reactions between $[CuCl_2(terpy)]$ and biomolecules in molar ratio 1:1 and 1:2. According to EPR data, L-Met forms the most stable complex with $[CuCl_2(en)]$ among the ligands considered (**Figure 6**), while $[CuCl_2(terpy)]$ complex did not show significant changes in its square-pyramidal geometry in the presence of the buffer or bio-ligands [45].

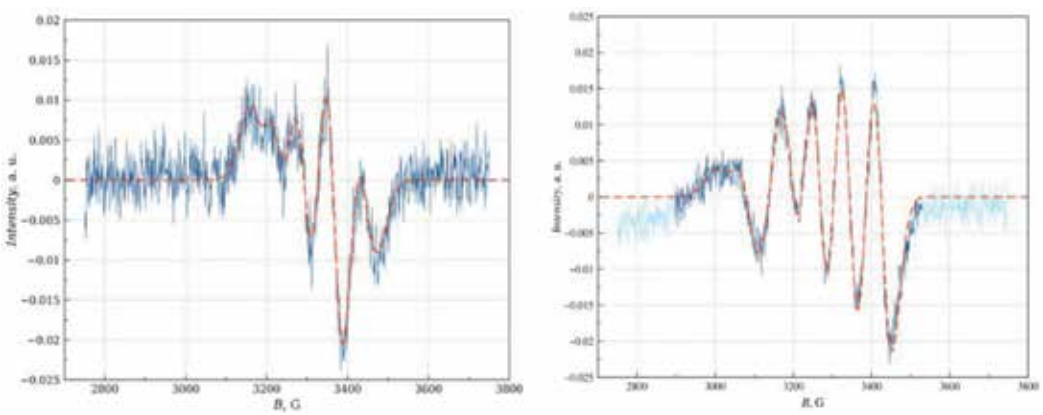

Figure 6. Left: EPR spectrum of 0.0001 M $[CuCl_2(en)]$ complex solution in 0.010 M NaCl 0.025 M Hepes buffer, pH 7.4, at 300 K. Right: EPR spectrum of 0.0001 M equimolar $[CuCl_2(en)]$ − L-Met solution in 0.0010 M NaCl 0.025 M Hepes buffer, pH 7.4, at 300 K [45].

5. Conclusions

Detailed knowledge of chemical properties of complex compounds could be very useful for the future investigations of new pharmacological agents. Although recent studies are trying to obtain more mechanistic information, and results provide very useful information for the future design of potential zinc- or copper-based anticancer drugs, it is evident that, up to now, this field is not investigated enough. In general, attempts to correlate the antitumour activity of zinc(II) and copper(II) compounds with coordination number and geometry could be very promising for discovery of the alternative tumour treatment.

Acknowledgements

The author gratefully acknowledges financial support from State University of Novi Pazar, and Ministry of Education, Science and Technological Development, Republic of Serbia (Projects No. 172011).

Conflict of interest

No potential conflict of interest was reported by the author.

Author details

Tanja Soldatović

Address all correspondence to: tsoldatovic@np.ac.rs

Department of Chemical-Technological Sciences, State University of Novi Pazar, Novi Pazar, Serbia

References

[1] Housecroft CE, Sharpe AG. Inorganic Chemistry. 4th ed. Harlow, England; New York: Pearson; 2012. 1213p. ISBN-13: 978-0273742753

[2] Lippard SJ. Metals in medicine. In: Bertini I, Gray HB, Lippard SJ, Valentine JS, editors. Bioinorganic Chemistry. Sausalito, USA: University Science Books; 1994. pp. 505-583. ISBN: 0-935702-57-1

[3] Guo Z, Salder PJ. Medicinal inorganic chemistry. In: Sykes AG, editor. Advances in Inorganic Chemistry. Vol. 49. London, UK: Academic Press; 1999. pp. 183-283. ISBN: 9780080524481

[4] Roat-Malone RM. Bioinorganic Chemistry: A Short Course. Hoboken, NJ: John Wiley & Sons Inc.; 2002. 348p. ISBN: 0-471-15976-X

[5] Jakupec MA, Galanski M, Keppler BK. Tumour-inhibiting platinum complexes state of the art and future perspectives. Reviews of Physiology, Biochemistry and Pharmacology. 2003;**146**:1-53. DOI: 10.1007/s10254-002-0001-x

[6] Farrell N. Metal complexes as drugs and chemotherapeutic agents. In: McCleverty JA, Meyer TJ, editors. Comprehensive Coordination Chemistry. 2nd ed. Vol. II. Oxford; New York: Elsevier Ltd.; 2003. pp. 809-840. ISBN: 9780080437484

[7] Lippert B editor. Cisplatin, chemistry and biochemistry of leading antitumor drugs. Zurich: Wiley-VCH; 1999. 563p. ISBN: 3906390209

[8] Reedijk J. Why does cisplatin reach guanine-N7 with competing S-donor ligands available in the cell? Chemical Reviews. 1999;**99**:2499-2510. DOI: 10.1021/cr980422f

[9] Fuertes MA, Alonso C, Pérez JM. Biochemical modulation of cisplatin mechanisms of action: Enhancement of antitumor activity and circumvention of drug resistance. Chemical Reviews. 2003;**103**(3):645-662. DOI: 10.1021/cr020010d

[10] Rau T, van Eldik R. Mechanistic insight from kinetic studies on the interaction of model palladium(II) complexes with nucleic acid components. In: Sigel A, Sigel H, editors. Metal Ions in Biological Systems. 31. Marcel Dekker Inc., New York; 1996. p. 339–378. ISBN: 0-8247-9688-8

[11] Martin RB. Platinum complexes: Hydrolysis and binding to N(7) and N(1) of purines. In: Lippert B, editor. Cisplatin, chemistry and biochemistry of leading antitumor drugs. Zurich: Wiley-VCH; 1999. pp. 183-206. ISBN: 3906390209

[12] Legendre F, Chottard JC. Kinetics and selectivity of DNA-platination. In: Lippert B, editor. Cisplatin, chemistry and biochemistry of leading antitumor drugs. Zurich: Wiley-VCH; 1999. pp. 223-245. ISBN: 3906390209

[13] Sanna B, Debidda M, Pintus G, Tadolini B, Posadino AM, Bennardini F, Sava G, Ventura C. The anti-metastatic agent imidazolium *trans*-imidazoledimethylsulfoxide-tetrachlororuthenate induces endothelial cell apoptosis by inhibiting the mitogen-activated protein kinase/extracellular signal-regulated kinase signaling pathway. Archives of Biochemistry and Biophysics. 2002;**403**:209-218. DOI: 10.1016/S0003-9861(02)00218-7

[14] McCord JM, Fridovich IJ. Superoxide dismutase. An enzymic function for erythrocuprein (hemocuprein). The Journal of Biological Chemistry. 1969;**244**:6049-6055. PMID: 5389100

[15] Clement JL, Jarrett PS. Antibacterial silver. Metal-Based Drugs. 1994;**1**:467-782. DOI: 10.1155/MBD.1994.467

[16] Briand GG, Burford N. Bismuth compounds and preparations with biological or medicinal relevance. Chemical Reviews. 1999;**99**:2601-2658. DOI: 10.1021/cr980425s

[17] Sorenson JR. Handbook of Metal-Ligand Interactions in Biological Fluids. 1st ed. Vol. 2. New York: Marcel Dekker Inc.; 1995. 1318p. ISBN: 9780824792961

[18] Kwiatek WM, Drewniak T, Gajda M, Galka M, Hanson AL, Cichocki TJ. Preliminary study on the distribution of selected elements in cancerous and non-cancerous kidney

tissues. Journal of Trace Elements in Medicine and Biology. 2002;**16**:155-160. DOI: 10.1016/S0946-672X(02)80018-9

[19] Sanchez-Delgado RA, Lazardi K, Rincon L, Urbina JA. Toward a novel metal-based chemotherapy against tropical diseases. 1. Enhancement of the efficacy of clotrimazole against *Trypanosoma cruzi* by complexation to ruthenium in $RuCl_2$(clotrimazole)$_2$. Journal of Medicinal Chemistry. 1993;**36**:2041-2043. DOI: 10.1021/jm00066a014

[20] Katakis D, Gordon G. Mechanism of Inorganic Reactions. New York: Wiley; 1987. 416p. ISBN-13: 978-0471842583

[21] Tobe ML, Burgess J, editors. Inorganic Reaction Mechanism. England: Longman; 1999. 688p. ISBN-13: 978-0582236776

[22] Langford CH, Gray HB. Ligand Substitution Processes. 2nd ed. New York: Benjamin; 1974. 103p

[23] Wilkins RG. Kinetics and Mechanism of Reactions of Transition Metal Complexes. 2nd thoroughly revised ed. New York; Weinheim: Wiley-VCH Verlag GmbH; 2002. 465p. ISBN: 3-527-28389-7

[24] Bertini I, Gray HB, Stiefel EI, Valentine JS. Biological Inorganic Chemistry. Structure and Reactivity. Sausalito, CA: University Science Books; 2007. 739p. ISBN-13: 978-1891389436

[25] Berg JM, Godwin HA. Lessons from zinc-binding peptides. Annual Review of Biophysics and Biomolecular Structure. 1997;**26**:57-371. DOI: 10.1146/annurev.biophys.26.1.357

[26] Jernigan R, Raghunathan G, Bahar I. Characterization of interactions and metal-ion binding sites in proteins. Current Opinion in Structural Biology. 1994;**4**:256-263. DOI: 10.1016/S0959-440X(94)90317-4

[27] Williams RJP. Bioinorganic chemistry: Its conceptual evolution. Coordination Chemistry Reviews. 1990;**100**:573-610. DOI: 10.1016/0010-8545(90)85020-S

[28] Pavlov M, Siegbahn PEM, Sandström MJ. Hydration of beryllium, magnesium, calcium, and zinc ions using density functional theory. The Journal of Physical Chemistry A. 1998; **102**:219-228. DOI: 10.1021/jp972072r

[29] Bose RN, Yang WW, Evanics F. Structural perturbation of a C4 zinc-finger module by *cis*-diamminedichloroplatinum(II): Insights into the inhibition of transcription processes by the antitumor drug. Inorganica Chimica Acta. 2005;**358**:2844-2854. DOI: 10.1016/j.ica.2004.06.052

[30] Soldatović T, Selimović E. Kinetic studies of the reactions between dichlorido[1,2-diaminoethane]zinc(II) and biologically relevant nucleophiles in the presence of chloride. Progress in Reaction Kinetics. 2018;**43**(1):53-61. DOI: 10.3184/146867818X15066862094897

[31] Selimović E, Soldatović T. Impact of the chloride concentration on ligand substitution reactions of zinc(II) complexes with relevant nitrogen nucleophiles. Progress in Reaction Kinetics. 2017 (accepted for publication)

[32] Selimović E, Jeremić S, Ličina B, Soldatović T, Kinetics DFT. study and antibacterial activity of zinc(II) and copper(II) terpyridine complexes. Journal of the Mexican Chemical Society. 2018;**62**(1):1-18. DOI: 10.29356/jmcs.v62i1.576

[33] Costello LC, Franklin RB. Cytotoxic/tumor suppressor role of zinc for the treatment of cancer: An enigma and an opportunity. Expert Review of Anticancer Therapy. 2012;**12**(1): 121-128. DOI: 10.1586/era.11.190

[34] Jany T, Moreth A, Gruschka C, Sischka A, Spiering A, Dieding M, Wang Y, Samo SH, Stammler A, Bogge H, von Mollard GF, Anselmetti D, Glaser T. Rational design of a cytotoxic dinuclear Cu_2 complex that binds by molecular recognition at two neighboring phosphates of the DNA backbone. Inorganic Chemistry. 2015;**54**:2679-2690. DOI: 10.1021/ic5028465

[35] Chen HH, Kuo MT. Overcoming platinum drug resistance with copper-lowering agents. Anticancer Research. 2013;**33**:4157-4161. PMID: 24122978

[36] Ohrvik H, Thiele DJJ. The role of Ctr1 and Ctr2 in mammalian copper homeostasis and platinum-based chemotherapy. Journal of Trace Elements in Medicine and Biology. 2014; **31**:178-182. DOI: 10.1016/j.jtemb.2014.03.006

[37] Sadler PJ. Inorganic chemistry and drug design. Advances in Inorganic Chemistry. 1991; **36**:1-48. DOI: 10.1016/S0898-8838(08)60035-5

[38] Fricker SP. Metal based drugs: From serendipity to design. Dalton Transactions. 2007;**43**: 4903-4917. DOI: 10.1039/b705551j

[39] Manikandamathavan VM, Weyhermüller T, Parameswari RP, Sathishkumar M, Subramaniana V, Nair BU. DNA/protein interaction and cytotoxic activity of imidazole terpyridine derived Cu(II)/Zn(II) metal complexes. Dalton Transactions. 2014;**43**:13018-13031. DOI: 10.1039/C4DT01378F

[40] Manikandamathavan VM, Rajapandian V, Freddy AJ, Weyhermuller T, Subramanian V, Nair BU. Effect of coordinated ligands on antiproliferative activity and DNA cleavage property of three mononuclear Cu(II)-terpyridine complexes. European Journal of Medicinal Chemistry. 2012;**57**:449-458. DOI: 10.1016/j.ejmech.2012.06.039

[41] Azuara LR, Bravo-Gómez ME. Copper compounds in cancer chemotherapy. Current Medicinal Chemistry. 2010;**17**(31):3606-3615. DOI: 10.2174/09298671079321375

[42] Santini C, Pellei M, Gandin V, Porchia M, Tisato F, M. Advances in copper complexes as anticancer agents. Chemical Reviews. 2014;**114**:815-862. DOI: 10.1021/cr400135x

[43] Powell DH, Merbach AE, Fabian I, Schindler S, Van Eldik R. Evidence for a chelate-induced changeover in the substitution mechanism of aquated copper(II). Volume profile analyses of water exchange and complex-formation reactions. Inorganic Chemistry. 1994; **33**(20):4468-4473. DOI: 10.1021/ic00098a011

[44] Constable EC, Housecroft CE, Price JR, Zampese JA. When five are six: The myth of five-coordinate copper(II) in supramolecular chemistry. CrystEngComm. 2010;**12**:3163-3171. DOI: 10.1039/C0CE00019A

[45] Selimović E, Komolkin AV, Egorov AV, Soldatović T. Substitution behavior of square-planar and square-pyramidal Cu(II) complexes with bio-relevant nucleophiles. Journal of Coordination Chemistry. 2018;**71**(7):1003-1019. DOI: 10.1080/00958972.2018.1456656

Edited by Takashiro Akitsu

This book is both a review of current research and an undergraduate textbook for inorganic chemistry at university level. In university undergraduate lectures, basic concepts are mainly explained and added examples of frontier research are optional. However, in many cases, frontier research is more interesting for students than basic studies. This book is aimed at undergraduates in inorganic chemistry. Each author introduces or reviews "frontier research topics" of inorganic coordination chemistry. Additionally, "basic concepts," as found in textbooks on this subject, indicate application examples of "frontier research topics."

Published in London, UK

IntechOpen

ISBN 978-1-83881-835-7
9 781838 818357